**Distribution Agreement**

In presenting this thesis or dissertation as a partial fulfillment of the requirements for an advanced degree from Emory University, I hereby grant to Emory University and its agents the non-exclusive license to archive, make accessible, and display my thesis or dissertation in whole or in part in all forms of media, now or hereafter known, including display on the world wide web. I understand that I may select some access restrictions as part of the online submission of this thesis or dissertation. I retain all ownership rights to the copyright of the thesis or dissertation. I also retain the right to use in future works (such as articles or books) all or part of this thesis or dissertation.

Signature:

_____ _____

Matthew Emerson Randolph, D.V.M. Date

The Role of Pharyngeal Satellite Cells in Pharyngeal Muscle Biology

By

Matthew Emerson Randolph, D.V.M.

Doctor of Philosophy

Graduate Division of Biological and Biomedical Science

Biochemistry, Cell and Developmental Biology

_____

Grace K. Pavlath, Ph.D.

Advisor

_____ _____

Tamara Caspary, Ph.D. Anita H. Corbett, Ph.D.

Committee Member Committee Member

_____ _____

Hans E. Grossniklaus, MD, MBA Winfield S. Sale, Ph.D.

Committee Member Committee Member

Accepted:

_____

Lisa A. Tedesco, Ph.D.

Dean of the James T. Laney School of Graduate Studies

_____

Date

# The Role of Pharyngeal Satellite Cells in Pharyngeal Muscle Biology

By

Matthew Emerson Randolph

D.V.M., University of Georgia, 2000

Advisor: Grace K. Pavlath, Ph.D.

An abstract of

A dissertation submitted to the Faculty of the

James T. Laney School of Graduate Studies of Emory University

in partial fulfillment of the requirements for the degree of

Doctor of Philosophy

in Biochemistry, Cell and Developmental Biology

Graduate Division of Biological and Biomedical Sciences

2015

## Abstract

The Role of Pharyngeal Satellite Cells in Pharyngeal Muscle Biology

By Matthew Emerson Randolph, D.V.M.

The inability to swallow, or dysphagia, is a debilitating and life-threatening condition that arises with aging or disease. The seven major pharyngeal muscles of the nasal, oral, and laryngeal pharynxes are required for swallowing. Interestingly, pharyngeal muscles are preferentially affected in some muscular dystrophies yet spared in others. Unique properties of pharyngeal muscles or their associated muscle stem cells, called satellite cells, may be critical factors in the development of pharyngeal muscle disorders; however, very little is known about the effects of disease and aging on pharyngeal muscles, nor the normal physiology of pharyngeal satellite cells (PSCs) and their role in pharyngeal muscles. We showed that aging affects pharyngeal muscle growth and atrophy in mice depending on the particular muscle analyzed. Wild-type mice also develop dysphagia with aging. Additionally, we studied pharyngeal muscles in a mouse model for oculopharyngeal muscular dystrophy, a dysphagic disease caused by a polyalanine expansion in the RNA binding protein, polyadenylate binding nuclear protein 1 (PABPN1). We examined pharyngeal muscles of mice overexpressing either wild-type or mutant PABPN1 and found overexpression of mutant PABPN1 differentially affected growth dependent on the anatomic location of muscles within the pharynx. Overexpression of wild-type PABPN1 was protective against age-related muscle atrophy in the laryngopharynx and prevented the development of age-related dysphagia. These results demonstrate that pharyngeal muscles are differentially affected by both aging and muscular dystrophy in a region-dependent manner. Our examination of PSCs revealed both transcriptional and biological differences from the commonly studied limb satellite cells. Under basal conditions PSCs proliferated, progressed through myogenesis, and fused with pharyngeal myofibers. Furthermore, PSC also exhibited biologic differences dependent on anatomic location in the pharynx. Importantly, PSCs were required to maintain myofiber size and myonuclear number in pharyngeal myofibers. These results demonstrate that PSCs are critical for pharyngeal muscle maintenance and suggest that satellite cell impairment could contribute to pharyngeal muscle pathology associated with various muscular dystrophies and aging. These studies lay important groundwork for understanding the molecular and cellular mechanisms that regulate pharyngeal muscle maintenance, growth and atrophy, which could lead to novel therapies for individuals afflicted with dysphagia.

# The Role for Pharyngeal Satellite Cells in Pharyngeal Muscle Biology

By

Matthew Emerson Randolph

D.V.M., University of Georgia, 2000

Advisor: Grace K. Pavlath, Ph.D.

A dissertation submitted to the Faculty of the

James T. Laney School of Graduate Studies of Emory University

in partial fulfillment of the requirements for the degree of

Doctor of Philosophy

in Biochemistry, Cell and Developmental Biology

Graduate Division of Biological and Biomedical Sciences

2015

**Acknowledgements**

I would like to thank my advisor, Dr. Grace K. Pavlath, for taking the time to mentor me as a scientist and a colleague. Your leadership and guidance have helped to mold me into the experimental scientist that I am. I have been blessed to work with you, brainstorm with you, receive correction from you, and call you my friend. I would also like to thank all the wonderful colleagues and friends of the Pavlath lab. I take with me many fond Pavlathian memories and friendships.

I also want to thank my dissertation committee members, Anita Corbett, Tamara Caspary, Hans Grossniklaus, and Win Sale for their continuous support throughout the years. I appreciated your willingness to sit with me and troubleshoot, brainstorm, or just vent. The faculty of Emory's Biochemistry, Cell, and Developmental Biology program are also deserving of recognition. Their passion for training, teaching, and striving for excellence has inspired me to do the same.

I want to thank all of my friends at Emory and Gateway Believers Fellowship for providing me with love, support, and the occasional distraction to keep me sane and focused. When my house burned and I lost everything, your love and support during that time was a priceless gift that I can never repay. I will forever cherish the memories of my times with you.

I also thank God for my amazing family. You have always given me your support despite your questions and concerns. I would not be where I am if it were not for all of you. And most of all, I want to thank my new bride, Casey, for her extreme patience and understanding during these last few months. Words cannot express how thankful I am to have you in my life. I thank you for believing in me and loving me.

**Table of Contents**

## List of Figures

## List of Tables

## List of Abbreviations

β-gal - beta-galactosidase

A10, wild-type - A10.1 PABPN1 overexpression transgenic mouse

A17, mutant - A17.1 PABPN1 overexpression transgenic mouse

Alpha7 - alpha-7 integrin

APS - ammonium persulfate

bHLP - basic-helix-loop-helix class of transcription factors

BrdU - 5-bromo-2'-deoxyuridine

Cre - cre recombinase

CreERTM - fusion protein of cre recombinase with tamoxifen-inducible estrogen receptor

CSA - cross-sectional area

DM1, DM2 – Dystrophic myopathy 1, dystrophic myopathy 2

DMD – Duchenne muscular dystrophy

DTA - mice containing a floxed truncated diptheria toxin A-176 allele in the Rosa26 locus

DAPI - 4',6-diamidino-2-phenylindole

ECM - extracellular matrix

EOM - extraocular muscle

FACS - fluorescence-activated cell sorting

FSHD - Facioscapulohumeral muscular dystrophy

FVB - Friend leukemia virus B

H&E - hematoxylin and eosin

HMGB1 - high-mobility group box 1

IL-6 – interleukin-6

LGMD – limb-girdle muscular dystrophy

LIF – leukemia inhibitory factor

$Lin^-$ - CD31/CD45/Sca1 negative cells

LSC - limb satellite cells

MD – muscular dystrophy

MHC - myosin heavy chains

MCP-1 (CCL2) - monocyte chemoattractant protein-1

Mrf4 - myogenic regulatory factor 4

Myf5 - myogenic factor 5

Myf5-nls-LacZ - fusion protein of Myf5 and beta-galactosidase containing a nuclear localization sequence

MyoD – myogenic differntiation protein

OE – overexpression

OPMD - oculopharyngeal muscular dystrophy

PABPN1 - polyadenylate binding nuclear protein 1

Pax7 - paired box protein 7

PD - Parkinson's disease

PSC - pharyngeal satellite cells

PI - propidium iodide

qRT-PCR - quantitative real-time polymerase chain reaction

RAGE - receptor for advanced glycation end-products

SC - satellite cells

Sca1 - stem cell antigen-1 (Ly-6A/E)

tdTom - tandem-dimer Tomato fluorescent protein

TUNEL - terminal deoxynucleotidyl transferase dUTP nick-end labeling

Type I - slow-twitch oxidative myofiber

Type II - fast-twitch glycolytic myofiber

VFSS - videofluoroscopic studies

X-gal - 5-bromo-4-chloro-3-indolyl-b

# Chapter 1: Introduction

# Chapter 1: Introduction

Muscular dystrophies are a group of degenerative muscle diseases that impair different subsets of skeletal muscles (Emery, 2002). One muscle group differentially affected in muscular dystrophies is found in the pharynx. Muscles arising from the cranial mesoderm comprise the pharyngeal muscles of the nasal, oral, and laryngeal pharynxes. These muscles contract in a coordinated manner to ensure proper swallowing and prevent the aspiration of food or liquid into the lungs. Pharyngeal muscles are preferentially affected in diseased conditions such as oculopharyngeal muscular dystrophy (OPMD) yet spared in other muscular dystrophies. Little is known about the effects of age or disease on pharyngeal muscles as a collective group or what factors predispose them to the effects of pathologic conditions. Furthermore, muscle stem cells, called satellite cells, may also contribute to the development of pharyngeal myopathies; however, very little is known about pharyngeal satellite cells and their role in pharyngeal muscles.

**The central goal of this dissertation was to elucidate biological properties of both pharyngeal muscles and their associated satellite cells that may contribute to the pathologic sensitivity of these muscles to various disease-causing conditions.** Seven major muscles are responsible for pharyngeal contraction when swallowing (Donner et al., 1985; Ekberg et al., 2009a; Rubesin et al., 1987). Impairment of the swallow function, dysphagia, is a debilitating condition that affects millions of individuals (Robbins et al., 2002), yet little is known about basic pharyngeal muscle biology. Additionally, pharyngeal muscles are pathologically affected in oculopharyngeal muscular dystrophy (OPMD), an autosomal dominant disease caused by an aberrant

expansion of 2-7 additional alanines in the N-terminus of poly-adenosine binding protein-nuclear one (PABPN1) (Abu-Baker and Rouleau, 2007; Brais et al., 1998; Messaed and Rouleau, 2009). Therefore, **our first goal was to characterize pharyngeal muscles in a region-dependent manner using mouse models, and test whether these muscles were differentially affected with age or muscle-specific overexpression of mutant PABPN1 using a mouse model of OPMD.** Our data provide insight into the types of myofibers present in pharyngeal muscles and also reveal region-dependent variation of growth and atrophic changes associated with aging or muscular dystrophy (Randolph et al., 2014). Additionally, we show that swallowing behavior in mice is altered with both aging and overexpression of mutant PABPN1, while swallow function was protected throughout life in mice overexpressing wild-type PABPN1 (Randolph et al., 2014). **Chapter 4 of this dissertation outlines the region-dependent variability of pharyngeal muscles under basal, aged, and dystrophic conditions.**

During our pharyngeal muscle studies, we observed a preponderance of centrally localized myonuclei within myofibers, suggestive of recently fused satellite cells during muscle regeneration. The primary cell type involved in post-natal muscle regeneration is the satellite cell (Murphy et al., 2011). In limb skeletal muscle under basal conditions, satellite cells are mitotically quiescent. When muscle tissue is injured, satellite cells proliferate, differentiate, and fuse to each other and existing myofibers to form new multi-nucleated myofibers. However, the central myonuclei observed in pharyngeal muscle sections were not associated with any gross histologic evidence of myofiber degeneration that would incite a regenerative response in pharyngeal muscles. Thus, **our next goal was to examine pharyngeal satellite cells (PSCs) and what role they play in**

**pharyngeal muscle biology.** We demonstrated that PSCs contribute new myonuclei to pharyngeal myofibers through constitutive myogenesis in the absence of injury. Additionally, our data demonstrate that PSCs are transcriptionally distinct satellite cells compared to limb satellite cells and are required to maintain both pharyngeal myofiber size and myonuclear numbers in a region-dependent manner. **Therefore, Chapter 5 outlines the basal biology of PSCs and their role in maintaining pharyngeal muscles in the absence of induced injury.**

The findings presented in this dissertation provide fundamental insights into the unique biology of pharyngeal muscles and PSCs, and the biological importance of regional localization of muscles within the pharynx. We propose that PSCs are required for maintenance of pharyngeal myofiber size and myonuclear numbers. We also suggest that mutations or conditions that adversely affect PSC function or enhance myonuclear turnover could have pathological consequences in pharyngeal muscle. Overall, these studies provide novel insights into mechanisms that could contribute to the differential sensitivity of pharyngeal muscles in diseased or aged states. Future studies on pharyngeal muscles, PSCs, and pharyngeal myonuclear loss could lead to new therapeutics for individuals suffering from pharyngeal myopathies or life-threatening dysphagia.

# Chapter 2: Background and Significance

**Portions of this chapter are submitted as:**

**Randolph, M. E.** and Pavlath, G. K. (2015). A muscle stem cell for every muscle: variability of stem cell biology among different muscle groups. *Manuscript in preparation.*

# Chapter 2: Background and Significance

## 2.1 Skeletal Muscle

Skeletal muscle is a highly organized tissue that comprises up to 40% of a human's body mass and is required for essential functions such as metabolism, locomotion and breathing (Janssen et al., 2000; MacIntosh et al., 2006). Proper muscle function is known to be impaired in multiple disease processes including metabolic disorders, traumatic injury, muscular dystrophies, inflammatory myopathies, various genetic disorders, and aging (Chang and Rudnicki, 2014; Dimachkie and Barohn, 2014; Doherty, 2003; Emery, 2002; Rolfe and Brown, 1997). Such loss of function can have life-threatening implications. In response to damage or injury, skeletal muscle has an impressive ability to regenerate and repair itself through a complex cascade of cellular mechanisms (Chang and Rudnicki, 2014). Understanding of the cellular mechanisms involved in maintaining and repairing muscle function is critical to the development of life-saving therapies for individuals suffering from diseased or dystrophic muscle.

### 2.1.1 Skeletal Muscle Structure and Function

The structure and function of skeletal muscle has been thoroughly studied in vertebrates (MacIntosh et al., 2006). Skeletal muscles are attached to bony or cartilaginous origins of insertions through specialized connective tissues called tendons, and are composed of large cylindrical syncytial cells called myofibers that contain hundreds of post-mitotic myonuclei per myofiber (Figure 2.6.1A). Myofiber size varies between 10-100 μm diameters in human limb muscles and can range in length from 2-30 cm. Externally, myofibers are bundled together into structural units called fascicles by

sheets of connective tissue, i.e. fascia, that allows for transference of force from contracting myofibers to the tendons, translating the force into movement. However, contained within a single myofiber are hundreds of striated structures called myofibrils that are formed from interlocking sarcomeres. The sarcomere is the functional contractile apparatus of muscle that contains alternating bands of actin and myosin proteins. Sarcomere contraction is regulated by neural innervation of myofibers by motor neurons at neuromuscular junctions. Using ATP as an energy source, actin and myosin filaments slide against each other to generate tensile force, which in turn moves both the muscle and adjacent structures.

Myofibers are heterogeneous cells that demonstrate variable metabolic and contractile properties dependent on the types of metabolic enzymes and myosin heavy chains that are expressed (Schiaffino and Reggiani, 2011). Each myofiber type is composed of distinct isoforms of contractile proteins including myosin heavy chains (MHCs). Slow-twitch oxidative myofibers (Type I) are typically observed in muscles utilized for endurance that are resistant to fatigue and rely heavily on mitochondrial oxidative respiration for energy production. In contrast, there are three types of the fast-twitch glycolytic myofibers (Type II) based on their metabolic and contractile properties. Type IIA myofibers are fast-twitch oxidative glycolytic myofibers that contain high levels of both glycoloytic enzymes and mitochondria. Type IIB myofibers have faster contraction rates but are more prone to fatigue and are thus called fast-twitch glycolytic myofibers. A third Type II myofiber, Type IIX myofibers, has similar twitch reactions as Type IIA and IIB but demonstrate an intermediate level of fatigue resistance. During muscle development or regeneration, myofibers can also express developmental myosin

heavy chains such as embryonic and neonatal MHCs, both of which can be used to identify recently regenerated myofibers (Reiser et al., 1985a; Reiser et al., 1985b; Schiaffino and Reggiani, 2011).

Myofibers are encased by the basal lamina, an extracellular matrix containing mainly laminin, collagen, and proteoglycans, which acts both as a structural scaffold and a component of the myofiber niche (Kuang et al., 2008). Juxtaposed between the basal lamina and the myofiber cell membrane, adult muscle stem cells called satellite cells reside at the periphery of skeletal myofibers (Katz, 1961; Mauro, 1961). Satellite cells are a heterogeneous stem cell population (Alfaro et al., 2011; Ono et al., 2010; Rocheteau et al., 2012; Tanaka et al., 2009) that are responsible for repair and regeneration of muscle tissue. In limb skeletal muscle under basal conditions, satellite cells are mitotically quiescent. When skeletal muscle is injured, satellite cells proliferate, differentiate, migrate, adhere and fuse to each other and existing myofibers to form new post-mitotic, multi-nucleated myofibers (Abmayr and Pavlath, 2012). A subset of satellite cells will also undergo self-renewal to maintain a quiescent stem cell population for future use (Figure 2.6.1B) (Kuang et al., 2007; Shinin et al., 2006). In adult skeletal muscle, quiescent satellite cells express *paired box protein 7* (*Pax7),* a myogenic transcript commonly used to identify satellite cells. *Pax7* expression has recently been shown to affect satellite cell biology where cells containing high levels of Pax7 demonstrate slower proliferation rates, lower metabolism, and resistance towards differentiation, indicating a more “stem-like” phenotype compared to satellite cells with lower levels of Pax7 protein (Rocheteau et al., 2012). Other myogenic transcription factors are involved in satellite cell activation/proliferation such as myogenic differentiation protein (MyoD) and

myogenic factor 5 (Myf5), while *Myogenin* and *myogenic regulatory factor 4* (*Mrf4)* are expressed during terminal differentiation of satellite cells. Satellite cells and their role in muscle regeneration will be discussed later in greater detail.

The ability of satellite cells to proliferate, differentiate, and self-renew can be affected by cells and factors in the microenvironment, termed the niche. The regulatory role of the niche in mammalian stem cell biology of intestines, hair follicles, neurons, and hematopoietic bone marrow has been well established (Kuang et al., 2008; Sambasivan and Tajbakhsh, 2007). Similarly, components of the satellite cell niche have also been elucidated (Figure 2.6.2). The basal lamina and sarcolemma of muscle fibers are both niche components shown to affect satellite cell function (Bentzinger et al., 2013). Under homeostatic conditions, the basal lamina and myofiber are believed to contribute to Notch signaling and interactions with adhesion molecules that are critical for maintaining satellite cell quiescence as well as self-renewal (Bentzinger et al., 2013; Pisconti et al., 2010). However, regulatory signals, such as growth factors, cytokines, and adhesion molecules, from the extracellular matrix, basal lamina, myofiber, microvasculature, nerves, connective tissue and immune cells (Bentzinger et al., 2013; Chazaud et al., 2003a; Gopinath and Rando, 2008; Kuang et al., 2008; Sambasivan and Tajbakhsh, 2007) can also influence satellite cell behavior. For example, when the niche is altered, such as in inflammation, the myogenic abilites of satellite cells are also affected. Chazaud *et al*. demonstrated that macrophages in the niche contribute to both: 1) increased satellite cell proliferation via paracrine signaling; and 2) increased satellite cell survival via direct cell contact interactions (2003).

Multiple non-muscle cell types residing in skeletal muscle tissue contribute to the maintenance and repair of the skeletal muscles (Tedesco et al., 2010). Blood vessels carry essential oxygen and nutrients to muscles. Hematopoietic cells, such as macrophages and regulatory T cells, play critical roles in muscle regeneration (Chazaud et al., 2003b; Zhang et al., 2014). Endothelial cells, pericytes, interstitial cells, fibroadipogenic progenitors, and fibroblasts also play roles in muscle regeneration, regulation of satellite cell biology, and they can enter into the myogenic pathway (Bentzinger et al., 2013; Fry et al., 2014; Fry et al., 2015; Murphy et al., 2011; Pannerec et al., 2012). However, recent studies have demonstrated that satellite cells are the primary stem cell required for muscle regeneration (Lepper et al., 2011; Murphy et al., 2011).

### 2.1.2 Skeletal Muscle Regeneration

Skeletal muscle has a remarkable ability to regenerate damaged or injured myofibers through a process called myogenesis. In response to molecular and cellular signals induced by injury or disease, skeletal muscle has the capacity to regenerate and repair back to full power within 21 days (Bintliff and Walker, 1960; Clark, 1946; Rosenblatt and Woods, 1992). Upon muscle injury, several molecular signals are released which activate satellite cells both locally and systemically (Rodgers et al., 2014). Once activated, satellite cells exit cellular quiescence, enter the cell cycle, and begin progression through the myogenic lineage through a process controlled by myogenic regulatory factors (MRFs), muscle-specific transcription factors of the basic-helix-loop-helix (bHLH) class, including MyoD, Myf-5, Mrf4, and myogenin (Chang and Rudnicki, 2014; Olson and Klein, 1994; Weintraub et al., 1991). *MyoD* and *Myf5* are expressed

during the proliferation phase and regulate myogenic differentiation at a transcriptional level (Cooper et al., 1999; Valdez et al., 2000), while *Mrf4* and *myogenin* are expressed upon terminal differentiation and exit from the cell cycle (Chang and Rudnicki, 2014).

Regeneration of skeletal muscle occurs in two distinct phases: a degenerative phase and a regenerative phase (Rai et al., 2014). The main characteristics of the degenerative phase involve myofiber sarcolemmal damage or myofiber necrosis, followed by an influx of mononucleated inflammatory cells (Rai et al., 2014). Factors released from damaged myofibers initiate an inflammatory response. Neutrophils and macrophages enter the damaged region and engage in both the removal of cellular debris as well as regulation of muscle repair (Lescaudron et al., 1999; McLennan, 1996; Pallafacchina et al., 2013). The basal lamina remains intact acting as a scaffold for the next phase, muscle regeneration (Schmalbruch, 1976). Local and systemic factors, such as growth factors, chemokines, and cytokines, activate satellite cells to proliferate as myoblasts within the first 24-48 hours following injury (Chang and Rudnicki, 2014). Myoblasts then terminally differentiate becoming post-mitotic myocytes, which then fuse with other myocytes or myofibers to regenerate or repair damaged myofibers. Thus, new myonuclei are added to damaged or nascent myofibers (Abmayr and Pavlath, 2012). A subset of myogenic cells repopulate the satellite cell niche, thus maintaining and replenishing the quiescent satellite cell pool for subsequent rounds of regeneration (Collins et al., 2005; Shinin et al., 2006). Thus, muscle regeneration restores injured muscle to a state that is morphologically and functionally similar to that of uninjured muscle (Chang and Rudnicki, 2014).

### 2.1.3 Skeletal Muscle Growth

Skeletal muscle growth is a highly dynamic process that can be influenced by many factors. For example, exercise can result in myofiber hypertrophy while disuse or age-related conditions can result in atrophy. In humans, myofiber size increases during the first two decades of life until adult myofiber size is achieved. However with aging, a loss of muscle size, referred to as atrophy, is observed in limb skeletal muscles (Aherne et al., 1971; Lexell et al., 1988; Wada et al., 2003). Myofiber growth occurs when levels of cytoplasmic protein are increased resulting in increased myofiber size. Postnatal myofiber growth occurs via two main mechanisms: cytoplasmic increase either with or without myonuclear accretion. In mice, the first three weeks of neonatal growth results in a three-fold increase in muscle mass where the satellite cell population undergoes a significant reduction from ~30% of myonuclei per myofiber down to 5%, following fusion with neonatal muscles. Parallel increases in myonuclear numbers and cytoplasmic proteins occur up to post-natal day 21 (White et al., 2010). However, after day 21, a level of homeostasis is achieved where satellite cells enter into a quiescent cellular state under the regulation of Notch signaling (Fukada et al., 2011), but myofiber size continues to increase without the addition of new myonuclei (White et al., 2010).

Experiments with adult limb muscle support these models of muscle growth. Myonuclear addition from satellite cells occurs in regeneration (Bayliss and Sloper, 1971), growth recovery following atrophy (Mitchell and Pavlath, 2001), and hypertrophy (Schiaffino et al., 1976; Seiden, 1976). Recent satellite cell ablation studies have also shown that myonuclear addition from limb satellite cells is dispensable for hypertrophic growth (McCarthy et al., 2011). Additionally, satellite cells are not required for

maintenance of adult limb muscle. A recent *in vivo* satellite cell ablation study found that loss of >90% of adult limb satellite cells failed to alter muscle size or myofiber type with aging (Fry et al., 2015). Thus, adult muscle growth can occur either with or without the addition of myonuclei from satellite cells, but maintenance of adult limb muscle size is not dependent on satellite cells.

## 2.2 Craniofacial Skeletal Muscle and Satellite Cell Biology

The majority of knowledge concerning skeletal muscle biology, as described in Chapter 2.1.1-2.1.3, arises from studies of somite-derived limb muscles such as the quadriceps, gastrocnemius, tibialis anterior, soleus, extensor digitorum longus, plantaris, biceps, and deltoid muscles, which collectively represent less than 2% of all skeletal muscles. However, muscles of the head, representing over 20% of all skeletal muscles (Esteve-Altava et al., 2015), remain severely understudied. Importantly, skeletal muscle and satellite cell biology of select head muscles deviate from the canonical biology of their limb counterparts (Kelly, 2010) as outlined below.

### 2.2.1 Embryological Origins

Craniofacial muscles of the head arise from different non-somitic mesoderms: the extraocular muscles (EOMs) from prechordal mesoderm and first brachial arch; the masseter muscle from the first and second brachial arches of the cranial paraxial mesoderm, and the pharynx from the third and fourth brachial arches of the caudal paraxial mesoderm (Figure 2.6.3) (Kelly et al., 2004; McLoon et al., 2007; Mootoosamy and Dietrich, 2002; Noden and Francis-West, 2006; Shuler and Dalrymple, 2001). In

contrast, skeletal muscles and satellite cells of the trunk and limb arise from segmented paraxial mesoderm, called somites, as specified by expression of *paired-box protein 3* (*Pax3), c-met,* and *Myf5* (Tajbakhsh, 2003).

Craniofacial muscles also have distinct myogenic genetic programs when compared to somitic muscles (Harel et al., 2009). The somite-derived myogenic genetic network involves *Pax3* and *Pax7,* which are upstream regulators of *MyoD* and *Myf5* (Bajard et al., 2006; Hu et al., 2008), which in turn are upstream of *Mrf4* and *myogenin* (Rudnicki et al., 2008). However, craniofacial muscles utilize alternate transcription factors which act upstream of *Myf5* and *MyoD* in craniofacial development as *Pax3* is not expressed in the cranial mesoderm. These factors include the bHLH transcriptional repressors *capsulin* (*Tcf21*) and *MyoR*, as well as the homeobox transcription factor *Pitx2* and the T-box containing transcriptional activator *Tbx1*; and thus play critical roles in the formation of extraocular, facial, masseter, tongue, and pharyngeal muscles (Kelly, 2010).

### 2.2.2 Satellite Cells of Extraocular Muscles

Extraocular muscles (EOMs) and satellite cells arise from the prechordal and cranial paraxial mesoderm during development (Couly et al., 1992; Noden and Francis-West, 2006). Satellite cells of EOMs also demonstrate unique gene expression profiles in comparison to quiescent limb muscles (Pacheco-Pinedo et al., 2009; Porter and Baker, 1996). Extraocular satellite cells, in several species, chronically proliferate *in vivo* and *in vitro* (Christiansen and McLoon, 2006; McLoon and Wirtschafter, 2002a; McLoon and Wirtschafter, 2003; Stuelsatz et al., 2015; Wirtschafter et al., 2004b), which may in part be due to a specific highly proliferative subpopulation (Kallestad et al., 2011).

Additionally, global and orbital EOM satellite cells undergo myonuclear addition in the absence of injury, contributing new myonuclei to EOM myofibers (McLoon and Wirtschafter, 2002a; McLoon and Wirtschafter, 2003; McLoon and Wirtschafter, 2002b; Wirtschafter et al., 2004a). These studies highlight satellite cell biology that is distinct from limb satellite cells.

### 2.2.3 Satellite Cells of Masseter Muscles

Adult masseter satellite cells arise from the first and second brachial arch of the cranial paraxial mesoderm and express a unique transcription profile compared to limb satellite cells (Mouly et al., 1993; Noden and Francis-West, 2006; Ono et al., 2010; Sambasivan et al., 2009). Early *in vivo* studies demonstrated an impaired regenerative ability in masseter muscles compared to limb that was associated with a lower incidence of satellite cells during regeneration (Pavlath et al., 1998). Masseter satellite cells undergo prolonged periods of proliferation *in vitro* with a concurrent delay of differentiation onset (Ono et al., 2010). This delay in differentiation potentially contributes to the impaired regenerative response to acute injury in masseter muscles (Ono et al., 2010).

### 2.2.4 Satellite Cells of Tongue Muscles

Tongue muscles arise from mixed mesodermal origins. The intrinsic and extrinsic muscles arise from the first occipital somite with cranial paraxial mesoderm contributions also occurring in the exterior tongue muscles (Czajkowski et al., 2014). However, the connective tissue, blood supply, and lymphatics arise from the cranial paraxial mesoderm

(Couly et al., 1992; Noden and Francis-West, 2006; Shuler and Dalrymple, 2001). To date, knowledge of adult tongue muscle satellite cell biology is severely limited. A denervation study of the tongue muscle revealed increased myonuclear addition *in vivo*, which the authors speculated arose from mitotic contributions of resident satellite cells (McGeachie and Allbrook, 1978). Tongue-derived myoblasts have been isolated, cultured and successfully differentiated into nascent myotubes *in vitro*, but the myogenic characteristics of these cells remain to be directly studied (LaFramboise et al., 2003; Ternaux and Portalier, 1993).

### 2.3 Variable Susceptibility of Skeletal Muscles to Aging and Disease

The human body contains over 640 unique skeletal muscles, each having distinct functions and roles in human physiology (Relaix and Zammit, 2012). Multiple factors contribute to skeletal muscle diversity including embryologic origin, myogenic regulatory pathways, and functional/metabolic requirements, as previously discussed. Additionally, skeletal muscles also demonstrate varying susceptibility to age-related changes. Muscle heterogeneity is further underscored by the variable sensitivity of specific subsets of skeletal muscles to over 35 unique genetic mutations that result in muscular dystrophies (Bione et al., 1994; Bonne et al., 1999; Brais et al., 1998; Emery, 2002; Godfrey et al., 2007; Hoffman et al., 1987; Monaco et al., 1988; Nonaka, 1999; Robinson et al., 2005; Vieira et al., 2014). Studies elucidating the biological diversity of skeletal muscles and their satellite cells are critical for providing mechanistic insights into the differential sensitivities of individual skeletal muscles to aging and disease.

### 2.3.1 Variable Effects of Aging on Skeletal Muscle

Several studies have reported a decrease of both limb satellite cell number and regenerative abilities with age in normal skeletal muscle (Brack et al., 2007; Brack and Rando, 2007; Conboy et al., 2005; Gopinath and Rando, 2008). Age-related impairments of satellite cell biology can involve factors from the satellite cell niche (Chang and Rudnicki, 2014). Parabiosis studies, connecting the circulatory systems of paired old and young mice, revealed a restoration of regenerative capabilities *in vivo* upon exposure of 'old' satellite cells to 'young' systemic factors (Conboy et al., 2005). Interestingly, skeletal muscles and satellite cells of craniofacial muscles demonstrate different phenotypes with aging. Extraocular muscles are preferentially spared with aging (Kaminski et al., 1992; Porter et al., 1998; Schoser and Pongratz, 2006) and aged EOM satellite cells maintain proliferative and self-renewal abilities out to 24 months of age in mice (Stuelsatz et al., 2015). In contrast, masseter satellite cell numbers increase in number while their proliferative capabilities decline (Ono et al., 2010). The mechanisms underlying the muscle-specific variability of age-related effects on satellite cell biology still remain to be discovered.

### 2.3.2 Variation in Myogenic Networks and Skeletal Muscle Disease

The unique myogenic regulatory networks of skeletal muscles can affect the sensitivity of a muscle to certain pathological mutations. Examples are best described in genetic studies manipulating expression of craniofacial myogenic transcription factors. Human patients suffering from DiGeorge or velo-cardio-facial syndrome are heterozygous for the del22q11.2 mutation, a multi-gene chromosomal deletion in 22q11.2

chromosome, which results in *Tbx1* haploinsufficiency. Symptoms include craniofacial defects, cardiovascular anomalies, velopharyngeal insufficiency and skeletal muscle hypotonia resulting in swallowing deficits and cardiovascular impairment (Kelly et al., 2004). In fact, when homozygous deletion of *Tbx1* is performed, *Tbx1*$^{-/-}$ mouse embryos fail to develop muscles arising from the second and caudal brachial arches, including pharyngeal and laryngeal muscles (Kelly et al., 2004). Another example of embryologic origins influencing craniofacial muscle disease is found in mice lacking *Tcf21* and *MyoR* expression, which fail to transcribe *Myf5* in the first brachial arch, resulting in agenesis of a subset of mandibular muscles (Lu et al., 2002). These studies provide evidence that variation in myogenic genetic networks can contribute to the pathological susceptibility of skeletal muscles.

### 2.3.3 Variable Skeletal Muscle Susceptibility to Dystrophic Mutations

Muscular dystrophies (MD) are a group of degenerative muscle diseases caused by mutations in genes that encode proteins ranging in function from sarcolemma structure (Hoffman et al., 1987) to nuclear envelope structure (Bione et al., 1994; Bonne et al., 1999; Mittelbronn et al., 2008) to post-translational glycosylation (Godfrey et al., 2007) to RNA binding (Brais et al., 1998; Kühn et al., 2009). Over 30 known mutations have been characterized in both skeletal muscle-specific and ubiquitously expressed alleles, yet both manifest in muscular pathology. Intriguingly, each dystrophy affects a specific subset of skeletal muscles within the human body (Emery, 2002), suggesting that biological differences exist between individual muscles that predispose them to specific pathological etiologies.

Satellite cells have been implicated in the pathology of some muscular dystrophies (Morgan and Zammit, 2010) and may contribute to the variable muscle sensitivity observed in some dystrophies. In response to chronic myofiber degeneration, satellite cells are subjected to multiple rounds of regeneration, which can "exhaust" the regenerative abilities of the satellite cell population over time (Decary et al., 2000; Morgan and Zammit, 2010; Sacco et al., 2010; Webster and Blau, 1990). Satellite cells are thought to indirectly contribute to muscular dystrophies involving the dystrophin-associated protein complex, such as Duchenne's MD and limb girdle MD (Decary et al., 2000; Morgan and Zammit, 2010; Sacco et al., 2010; Webster and Blau, 1990). In other muscular dystrophies, satellite cell impairment may occur early in the disease process as satellite cells express the mutant alleles (Morgan and Zammit, 2010). Several studies have demonstrated functional defects in satellite cells with dystrophic mutations associated with Duchenne MD (Blau et al., 1983; Sacco et al., 2010; Webster and Blau, 1990), Emery-Dreifuss muscular dystrophy (Favreau et al., 2004; Frock et al., 2006), facioscapulohumeral muscular dystrophy (Barro et al., 2010; Winokur et al., 2003), myotonic dystrophy type 1 (Furling et al., 2001; Thornell et al., 2009), and oculopharyngeal muscular dystrophy (Apponi et al., 2010). Therefore, etiologies and pathologic mechanisms of dystrophies associated with satellite cell involvement will be described individually.

**A. Duchenne Muscular Dystrophy**

Duchenne muscular dystrophy (DMD) is an early onset childhood X-linked disease associated with the absence of dystrophin (Hoffman et al., 1987), a muscle-

specific sarcolemma-associated cytoplasmic protein critical for maintaining sarcolemmal integrity of myofibers (Durbeej and Campbell, 2002). Minimal levels of mechanical stress are needed to damage sarcolemmal integrity in the absence of dystrophin, resulting in recurrent rounds of myofiber damage and repair (Petrof et al., 1993). Patients suffering from DMD experience progressive muscle function loss, eventually leading to paralysis and death often before the age of 30. The main skeletal muscles affected in DMD are found in the shoulder, upper limbs, hips, thighs, and calves (Emery, 2002). Life-threatening symptoms for many patients involve cardiac and respiratory failure from impairment of the heart and diaphragm muscles, respectively (Nigro et al., 1990; Stedman et al., 1991). Of note, craniofacial muscles, such as the extraocular and internal laryngeal muscles, are mostly spared in DMD with the exception of pharyngeal muscles in advanced stages of the disease (Emery, 2002; Kaminski et al., 1992; Marques et al., 2007; Shinonaga et al., 2008). Satellite cell impairment in DMD is thought to play a role in the pathology of the disease as myoblasts cultured from DMD patients demonstrate impaired proliferative abilities in vitro (Blau et al., 1983). Additionally, premature satellite cell senescence due to telomeric shortening following repeated regenerative cycles is another mechanism thought to contribute to late-stage disease (Blau et al., 1983; Sacco et al., 2010).

**B. Limb-Girdle Muscular Dystrophy**

Limb-girdle muscular dystrophies (LGMD) are associated with genetic mutations of more than 20 different alleles in both muscle-specific and ubiquitously expressed genes that range in molecular functions (Vieira et al., 2014). These include sarcomere

proteins (titin), sarcolemmal proteins (sarcoglycan), glycosyltransferases (fukutin), nuclear envelope proteins (lamin A/C), and RNA-processing proteins (HNRPDL) to name a few. Intriguingly, despite the vast etiological variation, all 22 mutations elicit dystrophic changes in muscles of the upper limb, shoulder, chest, hip, and upper leg (Broglio et al., 2010; Mitsuhashi and Kang, 2012). Satellite cell exhaustion from repetitive bouts of regeneration is thought to indirectly contribute to LGMD with α-, β-, γ-, or δ-sarcoglycan involvement (Morgan and Zammit, 2010). However, satellite cell transplant experiments as well as phamaceutical induction of follistatin expression in endogenous satellite cells have proved beneficial in restoring myofiber size in α-sarcoglycan LGMD (Minetti et al., 2006; Wallace et al., 2008).

**C. Emery-Dreifuss Muscular Dystrophy**

Emery-Dreifuss muscular dystrophy results in progressive weakness of the shoulder, upper limb, and calf muscles of patients. This dystrophy is caused by genetic mutations of ubiquitously expressed nuclear envelope proteins emerin, lamin A and lamin C (Helbling-Leclerc et al., 2002). Emery-Dreifuss patients can have severe cardiac pathology occurring as early as 30 years of age (Broglio et al., 2010; Emery, 2002; Vohanka et al., 2001). *In vitro* studies using primary muscle cultures from *Lmna*$^{-/-}$ knockout mice or RNAi knockdown of emerin protein levels demonstrated defects in myoblast differentiation (Frock et al., 2006).

**D. Facioscapulohumeral Muscular Dystrophy**

Facioscapulohumeral muscular dystrophy (FSHD) is named for the muscles mainly affected in the disease, facial, shoulder and upper arm muscles, but foot and pelvic-girdle muscles can also be affected (Tawil and Van Der Maarel, 2006). Of the dystrophies affecting craniofacial muscles, FSHD carries the best prognosis for long-term survival, as it is a slowly progressive disease that rarely affects the heart or the ability to breathe (Tawil and Van Der Maarel, 2006). The causative deletion occurs in the subtelomeric region of chromosome 4, which induces pathologic expression of *DUX4c,* a homeobox transcription factor expressed in the testes and pluripotent stem cells but not somitic cells (Bosnakovski et al., 2008a; Bosnakovski et al., 2008b). *DUX4c* expression in cultured myoblasts inhibited myogenic differentiation by repression of *Myf5* and *MyoD*, indicating that satellite cells could play a direct role in FSHD pathology (Bosnakovski et al., 2008a; Bosnakovski et al., 2008b).

**E. Myotonic Dystrophy**

Myotonic dystrophy (DM) is a complex, multisystemic group of dystrophies that genetically arise from untranslated repeat nucleotide expansions of two separate genes, *dystophia myotonic protein kinase* (*DMPK*) and *zinc finger protein 9* (*ZNF9*) (Day and Ranum, 2005). A $(CTG)_{80\text{-}4000}$ repeat in the 3' untranslated region of DMPK is present in patients with myotonic dystrophy type 1 (DM1). The expanded regions of DMPK transcripts result in altered RNA biogenesis and processing of multiple transcripts, in part, by the sequestration of the splicing factor muscle blind (MBNL1) and stabilization of CUG-binding protein 1 (CUGBP1) (Apponi et al., 2011). In myotonic dystrophy type

2, up to 75-11,000 repeat expansions of $(TG)_n(TCTG)_n(CCTG)_n$ reside in intron 1 of *ZNF9* (Day and Ranum, 2005), dysregulating alternative slicing as well as protein production by sequestration of the 20S proteasome (Salisbury et al., 2009).

While DM1and DM2 result from distinct genetic pathologies, the biological consequences are similar as myotonia, muscular dystrophy, muscle pain, cataracts, cardiac arrhythmias, insulin insensitivity and diabetes, hypogammaglobulinemia, and testicular failure occur in both (Schoser and Timchenko, 2010). DM affects muscles of the eyelid, face, neck, lower arms and legs, diaphragm and intercostal muscles (Batten, 1909; Zifko et al., 1996). However, DM1 is associated with muscle weakness and atrophy in the lower limb muscles, while in DM2 the dystrophy is more predominant in the upper limbs (Tieleman et al., 2012). Life-threatening conditions involving cardiac disease, respiratory failure, and difficulties in swallowing can occur (Tieleman et al., 2009; Tieleman et al., 2012; Zifko et al., 1996). Satellite cell proliferation and numbers are differentially altered in DM1 patients. Cultured myoblasts, obtained from affected lower limb muscles, have reduced proliferative capacity *in vitro* verses unaffected upper limb muscle cultures derived from the same patients (Thornell et al., 2009).

**F. Oculopharyngeal Muscular Dystrophy**

Oculopharyngeal muscular dystrophy (OPMD) is an autosomal dominant disease, which typically affects people older than 50 years of age (Abu-Baker and Rouleau, 2007; Messaed and Rouleau, 2009). An aberrant expansion of alanines in the N-terminus of poly-adenosine binding protein-nuclear one (PABPN1) is the underlying cause of this presently incurable disease (Abu-Baker and Rouleau, 2007; Brais et al., 1998; Messaed

and Rouleau, 2009). PABPN1 is a ubiquitously expressed protein that plays key roles in RNA biogenesis including regulation of poly-adenosine tail length in mRNA transcripts, poly(A) RNA export, 3' end cleavage site selection, regulation of long non-coding RNAs, translation, and mRNA stability (Banerjee et al., 2013). The endogenous protein contains a 10-alanine repeat at its N-terminus, but expansions resulting in 12-17 alanines are reported in OPMD patients (Abu-Baker and Rouleau, 2007; Brais et al., 1998; Messaed and Rouleau, 2009). A hallmark of OPMD is the presence of nuclear aggregates in myonuclei of affected patients that contain PABPN1, RNA, and other nuclear proteins (Banerjee et al., 2013; Tome and Fardeau, 1980). Evidence exists for both loss-of function and toxic gain-of-function mechanisms underlying OPMD pathology (Banerjee et al., 2013). However, the exact mechanism(s) by which mutant PABPN1 induces a muscular dystrophy remains unclear.

The main muscles affected in OPMD are craniofacial skeletal muscles and include the upper eye-lid, pharyngeal, extraocular, and tongue muscles. However, muscles of the upper limbs can also develop progressive muscle weakness later in the disease (Abu-Baker and Rouleau, 2007; Emery, 2002; Messaed and Rouleau, 2009). Interestingly, the major life-threatening difficulty for OPMD patients is the resultant dysphagia, the inability to swallow (Périé et al., 2006a). Pharyngeal muscles of the nasal, oral, and laryngeal pharynxes are essential components of the swallow reflex (Ertekin and Aydogdu, 2003; Miller, 2002; Miller, 2008), which prevents aspiration of food and water into the trachea and lungs and the formation of life-threatening pneumonia (Martin et al., 1994; Prasse and Kikano, 2009). Of note, when satellite cells of pharyngeal muscles were isolated from OPMD patients, the cell cultures demonstrated decreased

proliferative abilities (Périé et al., 2006a). Additionally, *in vitro* studies show defects in pharyngeal myoblast proliferation and differentiation when PABPN1 levels are knocked down with siRNA (Apponi et al., 2010). Together, the above studies suggest that *PABPN1* expression plays a critical role in pharyngeal satellite cell myogenesis and may contribute to satellite cell impairment in OPMD patients.

### 2.4 Pharyngeal Skeletal Muscles and Satellite Cells: The Unknown

Dysphagia is a debilitating and potentially deadly disease involving the impairment of neurological and muscular functions of the swallow reflex (Ertekin and Aydogdu, 2003; Logemann, 2007; Miller, 2008) that afflicts almost 16 million Americans (Robbins et al., 2002). Individuals fifty to sixty years of age or older have an 11-16% chance of being affected with dysphagia (Holland et al., 2011; Kawashima et al., 2004; Logemann, 2007; Prasse and Kikano, 2009). Besides aging, several diseases are also known to affect pharyngeal function including: stroke (Lindgren and Janzon, 1991; Miller, 2008); Parkinson's disease (Logemann, 2007); myasthenia gravis (Ertekin, 2002; Ertekin et al., 2002); pharyngeal myositis (Ertekin, 2002); DiGeorge syndrome (Aggarwal and Morrow, 2008; Jerome and Papaioannou, 2001; Kelly et al., 2004); advanced stage Duchenne muscular dystrophy (Aloysius et al., 2008; Attal et al., 2000; Nozaki et al., 2007); and OPMD (Abu-Baker and Rouleau, 2007; Bumm et al., 2009; Lu et al., 2008). Many studies have addressed the associated neuronal and neuromuscular components of pharyngeal dysfunction (Ekberg et al., 2009b; Ertekin and Aydogdu, 2003; Logemann, 2007; Miller, 2008), while the primary role of the affected pharyngeal

muscles and their associated satellite cells in dysphagia and pharyngeal myopathies remains largely unknown and is the focus of this dissertation.

### 2.4.1 Pharyngeal Skeletal Muscles

Swallowing depends on the synchronous contraction of seven major muscles lining the nasal, oral, and laryngeal pharynxes to ensure propulsion of food and liquid from the oral cavity into the esophagus (Donner et al., 1985; Ekberg et al., 2009b; Rubesin et al., 1987). Pharyngeal muscles arise from the third and fourth pharyngeal arches (Mootoosamy and Dietrich, 2002; Noden and Francis-West, 2006) and include the stylopharyngeus, palatopharyngeus, salpingopharyngeus, and the superior, middle and inferior pharyngeal constrictor muscles (Donner et al., 1985; Dutta and Basmajian, 1960; Ekberg et al., 2009b; Himmelreich, 1973; Rubesin et al., 1987). The inferior pharyngeal constrictor can be subdivided into the cricopharyngeus and the thyropharyngeus muscles (Donner et al., 1985; Ekberg et al., 2009b; Rubesin et al., 1987). As depicted in Figure 4.4.1 of this dissertation, the muscles forming the nasopharynx include the superior pharyngeal constrictor and the palatopharyngeal fold comprised of the palatopharyngeus and salpingopharyngeus (Nakano and Muto, 1985; Rubesin et al., 1987). Muscles of the oropharynx include the middle pharyngeal constrictor and the continuation of the palatopharyngeus. The laryngopharynx contains the inferior constrictor muscles, thyropharyngeus and cricopharyngeus.

Myofiber compostions of human pharyngeal muscles have also been characterized. Edström *et al.* (1992) found similar distributions of Type I and Type II myofibers between palatopharyngeus and quadriceps muscles of the limb. However,

pharyngeal myofibers are approximately 25% smaller in diameter (Edström et al., 1992). Meanwhile, human cricopharyngeal muscle contains a layer of Type I myofibers closest to the mucosal epithelium and an outer layer of Type II myofibers (Mu and Sanders, 2002; Mu et al., 2007). This myofiber distribution of a slow-twitch inner layer and a fast-twitch outer layer may be critical for inferior constrictor function (Mu and Sanders, 2002).

Despite the critical nature of these muscles, few studies have analyzed the effects of age and disease on pharyngeal muscles as a group. Only one report has linked abnormalities in the palatopharyngeus muscle with dysphagia (Kirberger, 2006). However, muscles of the inferior pharyngeal constrictor muscles are detrimentally affected with either aging or disease (Bachmann et al., 2001; Davis et al., 2007; Gidaro et al., 2013; Hyodo et al., 1999; Leese and Hopwood, 1986; Mu and Sanders, 1998; Périé et al., 2006a). Studies addressing the effects of aging and disease on pharyngeal muscle biology as a collective group are still needed to provide further insight into mechanisms underlying dysphagia and pharyngeal myopathies.

### 2.4.2 Pharyngeal Satellite Cells

As previously discussed, craniofacial muscles differ from limb muscles in many ways, including embryologic origins (Grenier et al., 2009; McLoon et al., 2007; Mootoosamy and Dietrich, 2002; Noden and Francis-West, 2006; Pavlath et al., 1998; Sambasivan et al., 2009) and satellite cell number (McLoon et al., 2007; McLoon and Wirtschafter, 2002a; Ono et al., 2010; Pavlath et al., 1998). Craniofacial satellite cells of extraocular and masseter muscles also differ in myogenic capabilities and gene

expression from limb muscle satellite cells (McLoon et al., 2007; Mootoosamy and Dietrich, 2002; Noden and Francis-West, 2006; Ono et al., 2010; Pacheco-Pinedo et al., 2009; Pavlath et al., 1998; Sambasivan et al., 2009). Therefore, pharyngeal satellite cells, being of craniofacial origins, may also have unique myogenic biology.

Currently, the basal biology of pharyngeal satellite cells is unknown. If maintenance of normal pharyngeal physiology depends on the myogenic properties of pharyngeal satellite cells, alterations in pharyngeal satellite cell function could result in pharyngeal pathology or even dysphagia. Several groups have demonstrated that aging can impair satellite cell number and myogenesis, leading to muscle pathology (Brack et al., 2005; Brack et al., 2007; Conboy et al., 2005; Dreyer et al., 2006; Verdijk et al., 2007). If pharyngeal satellite cells are also impaired with aging, any resultant muscle pathology could contribute to the dysphagia observed in up to 20% of the elderly population (Logemann, 2007; Prasse and Kikano, 2009).

As discussed, satellite cell impairment occurs in some muscular dystrophies. Limb satellite cells from mouse models of Duchenne muscular dystrophy (DMD) demonstrate a premature exhaustion of the satellite cell pool (Webster and Blau, 1990), while myogenic cells cultured from cricopharyngeal muscles of oculopharyngeal muscular dystrophy (OPMD) patients demonstrate decreased proliferative abilities (Périé et al., 2006a). Interestingly, dysphagia afflicts both OPMD and advanced stage DMD patients. Could pharyngeal satellite cell impairment in these muscular dystrophies contribute to the observed dysphagia? Data from these aging and muscular dystrophy studies are merely suggestive of a role for satellite cells in dysphagia; yet direct involvement of satellite cells in swallowing remains to be determined. Despite the critical

importance of proper swallow function, much still remains to be elucidated concerning the basal biology of pharyngeal muscle and their satellite cells, as well as their implications in dysphagic and myopathic disease.

**2.5 Summary**

Skeletal muscles are a highly diverse and dynamic group of tissues. Many factors contribute to skeletal muscle diversity including embryologic origin, gene expression, functional/metabolic requirements, and environmental niche. Such diversity likely contributes to the pathologic sensitivities of different skeletal muscles to aging and disease. Pharyngeal muscles are a unique subset of skeletal muscles that line the nasal, oral, and laryngeal cavities. Intriguingly, pharyngeal muscles are preferentially affected in diseased conditions such as OPMD yet spared in other muscular dystrophies. Little is known about the effects of age or disease on pharyngeal muscles as a collective group or what factors predispose them to the effects of pathologic conditions. Additionally, satellite cells could serve as pathological determinants in pharyngeal myopathies; however, very little is known about pharyngeal satellite cells and their role in pharyngeal muscle biology. Studies examining pharyngeal muscle and pharyngeal satellite cell biology are critically needed to further elucidate their roles in pharyngeal function and disease.

## 2.6 Figures

**Figure 2.6.1: Myofiber structure and cellular progression of myogenesis**

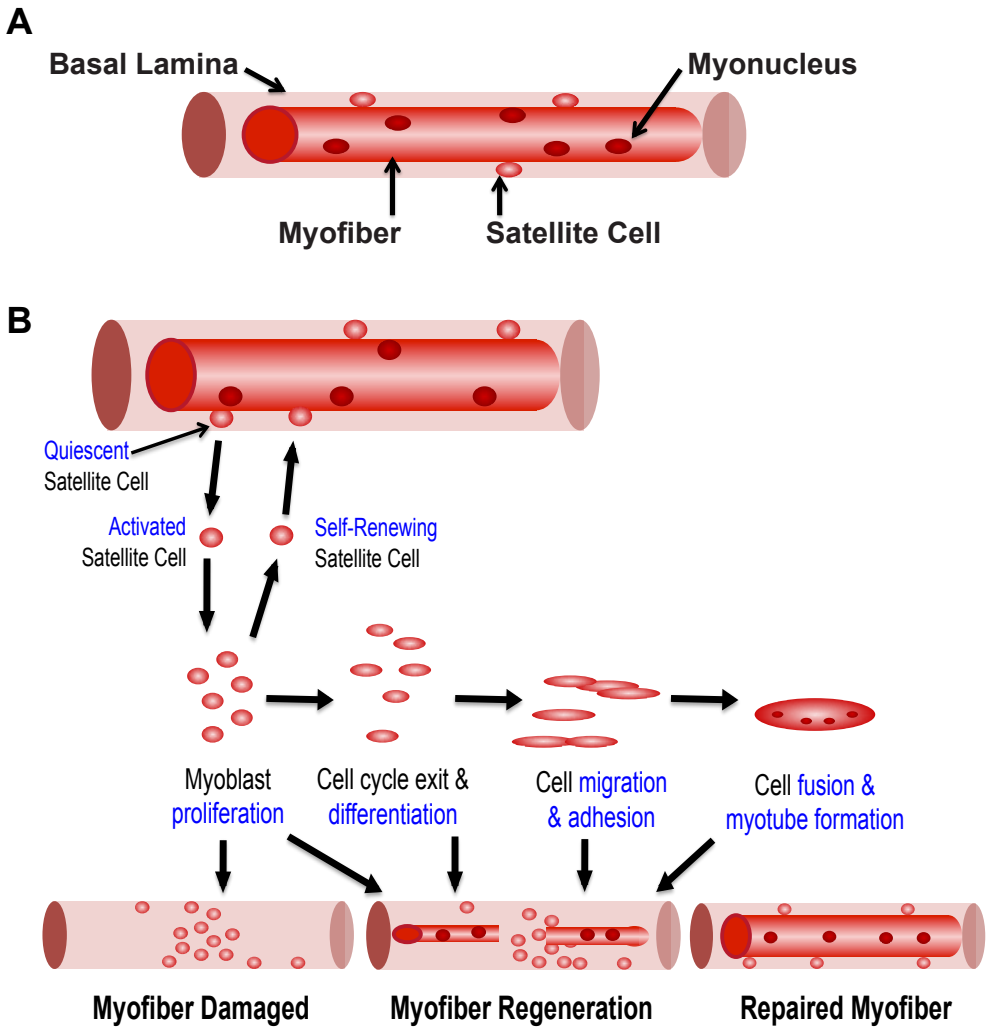

**Figure 2.6.1: Myofiber structure and cellular progression of myogenesis**

(**A**) Schematic figure of a single skeletal myofiber (red cylinder) containing multiple post-mitotic myonuclei (dark red circles). Satellite cells (red circles) are juxtaposed between the myofiber sarcolemma and the surrounding basal lamina (pink cylinder). (**B**) Schematic representation of the cellular stages of myogenesis and the corresponding stages of myofiber repair. Following injury or damage, quiescent satellite cells activate and give rise to proliferating myoblasts or undergo self-renewal. Myoblasts then differentiate, exit the cell cycle, migrate, adhere and fuse to each other and existing myofibers to form new post-mitotic, multi-nucleated myofibers. The basal lamina provides a scaffold for new myofiber formation.

**Figure 2.6.2: Schematic of the satellite cell niche and associated paracrine and secretory regulators**

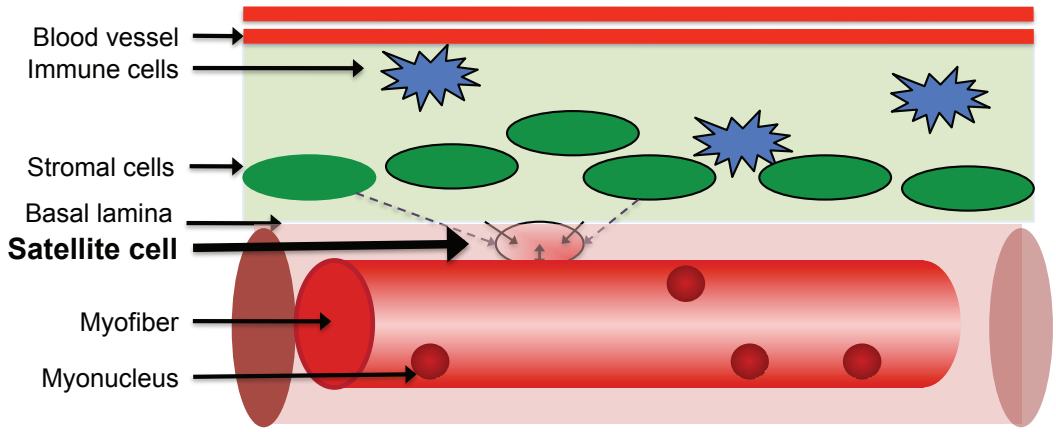

**Figure 2.6.2: Schematic of the satellite cell niche and associated paracrine and secretory regulators**

The satellite cell (pink oval) is shown confined between the basal lamina (light pink cylinder) and plasma membrane of the myofiber (red cylinder). Solid black arrows indicate direct cellular and/or paracrine interactions of the satellite cell with the myofiber and basal lamina. Dashed black arrows represent paracrine signaling from the stromal (grey ovals) and immune cells (stars) of the niche on satellite cells.

**Figure 2.6.3: Schematic of skeletal muscle embryonic origins**

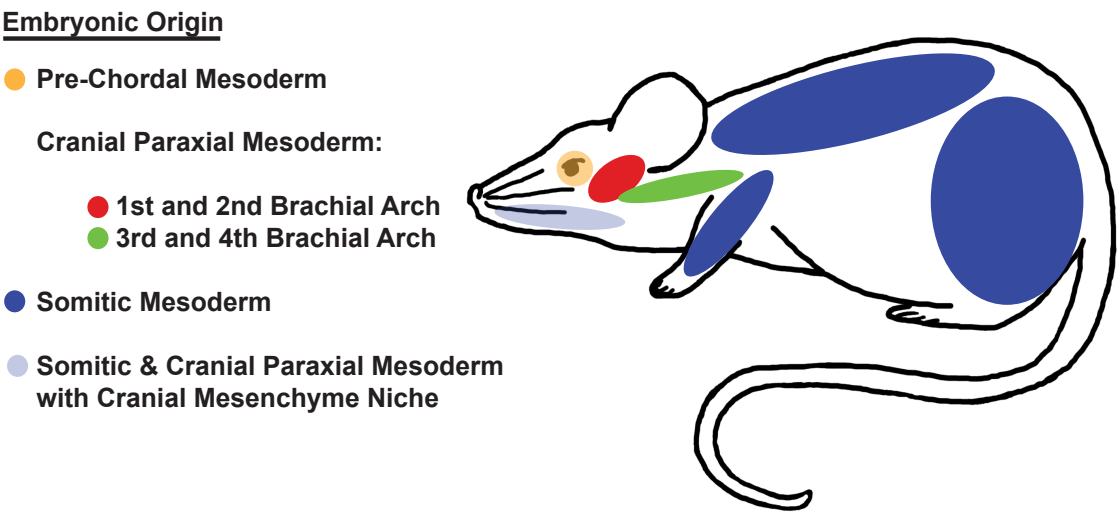

**Figure 2.6.3: Schematic of skeletal muscle embryonic origins**

Skeletal muscles of the trunk, limb (dark blue) and tongue (light blue) arise from somitic mesoderm. In contrast, the extraocular muscles arise from prechordal mesoderm and first brachial arch; the masseter muscle from the first and second brachial arches of the cranial paraxial mesoderm, and the pharynx from the third and fourth brachial arches of the caudal paraxial mesoderm. Tongue muscles arise from both somitic and cranial mesoderm while developing within the niche of the cranial mesenchyme, which is supplied by all four brachial arches.

## 2.7 Table

**Table 2.7.1: Table of Muscular Dystrophies That Effect Satellite Cells With Satellite Cell Involvement Highlighted in Blue**

| Muscular Dystrophy | Mutant Allele(s) | Mutant Protein(s) | Affected Muscles | Altered SC function |
|---|---|---|---|---|
| Duchenne | *DMD* | Dystrophin | shoulder, upper limb, diaphragm, and calf | Replicative exhaustion; Proliferation |
| Limb Girdle: | | | upper limb, shoulder, chest, hip, and upper leg | |
| LGMD1A | *MYOT* | Myotillin | | |
| LGMD1B | *LMNA* | Lamin A/C | | Differentiation |
| LGMD1C | *CAV3* | Caveolin 3 | | |
| LGMD1D | *DES* | Desmin | | |
| LGMD1E | *DNAJB6* | DNAJ/HSP 40 homolog, subfamily B, member 6 | | |
| LGMD2A | *CAPN3* | Calpain 3 | | |
| LGMD2B | *DYSF* | Dysferlin | | |
| LGMD2C | *SGCG* | γ-Sarcoglycan | | Replicative |
| LGMD2D | *SGCA* | α-Sarcoglycan | | exhaustion? |
| LGMD2E | *SGCB* | β-Sarcoglycan | | |
| LGMD2F | *SGCD* | δ-Sarcoglycan | | |
| LGMD2G | *TCAP* | Telethonin | | |
| LGMD2H | *TRIM32* | Tripartite motif-containing protein 32 | | |
| LGMD2I | *FKRP* | Fukutin related protein | | |

| | | | | |
|---|---|---|---|---|
| LGMD2J<br>LGMD2K<br>LGMD2L<br>LGMD2M<br>LGMD2N<br><br><br>LGMD2O<br><br><br><br>LGMD2P<br>LGMD2Q | *TTN*<br>*POMT1*<br>*ANO5*<br>*FKTN*<br>*POMT2*<br><br><br>*POMGNT1*<br><br><br><br>*DAG1*<br>*PLEC1* | Titin Protein<br>O-mannosyltransferase1<br>Anoctamin 5<br>Fukutin<br>Protein O-<br>mannosyltransferase 2<br>Protein O-mannose beta-<br>1,2-N-acetylglucos-<br>aminyltranserase<br>Dystroglycan<br>Plectin 1f | | Proliferation |
| Emery-Dreifuss (A) | *LMNA* | Lamin A/C | shoulder, upper limb, and calf | Differentiation |
| Emery-Dreifuss (X) | *EMD* | Emerin | shoulder, upper limb, and calf | Differentiation |
| FSHD | *Chrom.4q3 5 D4Z4* contraction | *DUX4* expression<br>FSHD-related gene? | facial, shoulder, upper arm, foot, and pelvic-girdle | Differentiation |
| DM1 | 3' UTR of *DMPK* | Dystophia myotonic protein kinase | eyelid, face, neck, lower arms/legs, diaphragm, intercostal m. | Replicative senescence; Differentiation |
| OPMD | *PABPN1* | Poly-adenosine binding protein-nuclear one | upper eye-lid, pharynx, tongue, extraocular m., upper arms/legs | Proliferation; Differentiation |

# Chapter 3: Methods and Materials

**A portion of this chapter is published as:**

**Randolph, M. E.**, Luo, Q., Ho, J., Vest, K. E., Sokoloff, A. J., & Pavlath, G. K. (2014). Ageing and muscular dystrophy differentially affect murine pharyngeal muscles in a region-dependent manner. *The Journal of Physiology*, *592*(Pt 23), 5301–5315.

**A portion of this chapter is submitted as:**

**Randolph, M. E.**, Phillips, B. L., Vest, K. E., Vera, Y., & Pavlath, G. K. (2015). Pharyngeal satellite cells undergo basal myogenesis and are required for pharyngeal muscle maintenance. *Manuscript under review.*

# Chapter 3: Methods and Materials

## Animals

Both male and female mice at various ages, as indicated for individual experiments, were utilized in the pharyngeal muscle studies. Adult male C57BL/6 mice, between 2-4 months of age, were used unless noted otherwise in the pharyngeal satellite cell studies. C57BL/6 and FVB were purchased from Charles River Laboratories. A10.1 and A17.1 PABPN1 transgenic mice (Davies et al., 2005), a mouse model for OPMD, were acquired from Dr. David Rubensztein. PCR was utilized to distinguish mice expressing the A10.1 or A17.1 PABPN1 allele from wild-type littermates using the following primer sequences (F: 5'- GAGCGACATCATGGTATTCCC -3'; R: 5'-AGGACTGACACGTGCTACGA -3') (Davies et al., 2005). *Myf5*$^{nLacZ/+}$ (Myf5 nLacZ) and *Pax7*$^{CreERTM/CreERTM}$ (Pax7$^{CreERTM}$) mice were obtained from S. Tajbakhsh (Tajbakhsh et al., 1996) and C. Keller (Nishijo et al., 2009), respectively. Duchenne muscular dystrophy model mice containing a dystrophin-deficient allele with a splice site mutation in exon 23, C57BL/10ScSn-Dmd$^{mdx}$/J (Mdx) (Bulfield et al., 1984), were purchased from Jackson Laboratories. Rosa26-CAG-tdTomato (Madisen et al., 2010) and Rosa26-DTA176 mice (Wu et al., 2006) were also purchased from Jackson Laboratories. Homozygous *Pax7*$^{CreERTM/CreERTM}$ male mice were crossed with either homozygous *Rosa*$^{DTA176/DTA176}$ (DTA) females to obtain *Pax7*$^{CreERTM/+}$; *Rosa*$^{DTA176/+}$ (DTA-Pax7$^{CreERTM}$) mice for satellite cell ablation experiments, or with homozygous *Rosa*$^{tdTomato/tdTomato}$ (tdTom) to obtain *Pax7*$^{CreERTM/+}$; *Rosa*$^{tdTomato/+}$ (tdTom-Pax7$^{CreERTM}$) mice to fluorescently label myogenic cells after tamoxifen treatment. Genomic recombination and removal of floxed stop sequences were induced in male DTA-

Pax7$^{CreERTM}$ and tdTom-Pax7$^{CreERTM}$ mice at 8 weeks-of-age. Tamoxifen, 1 mg (Sigma) per 10 grams body weight, was injected intraperitoneally once daily for five days. Flow cytometry was utilized to determine the recombination efficiency in both DTA-Pax7$^{CreERTM}$ and tdTom-Pax7$^{CreERTM}$ mice. Experiments were performed in accordance with approved guidelines and ethical approval from Emory University's Institutional Animal Care and Use Committee and in compliance with the National Institutes of Health.

**Dissection of Pharyngeal Tissue**

Mice were euthanized via $CO_2$ asphyxiation immediately prior to tissue collection. The mandible and lower jaw were removed, exposing the pharyngeal tissues. For histological analyses, the middle-cervical region of the trachea and esophagus were transected and pharyngeal tissue collected via blunt dissection rostrally toward the hard palate. Histological samples included the nasal, oral and laryngeal pharynxes, soft palate, larynx, cranial trachea, and cranial esophagus. The larynx and trachea were excluded from pharyngeal samples collected for isolation of myogenic cells.

**Histology/Immunohistochemistry**

All muscle tissues were frozen in Tissue Freezing Medium (Triangle Biomedical Sciences) and 10 mm cross sections were obtained using a Leica CM1850 cryostat. H&E images of pharyngeal muscle regions were obtained using a BX51 microscope with a 0.16 NA 4x UPlanApo objective (Olympus) and a MicroFire digital microscope camera using Neurolucida software (MBF Bioscience). All other images were acquired using an

Axioplan microscope with a 0.5 NA 20x Plan-Neofluar objective (Carl Zeiss MicroImaging, Inc.) and charge-coupled device camera (Carl Zeiss MicroImaging, Inc.) with Scion Image 1.63 (Scion Corp.). All images were globally processed for contrast, size, and brightness using Photoshop CS4 (Adobe).

For analysis of myofiber cross-sectional areas (CSA), sections were collected every 80 μm representing the entirety of the pharynx. Myofiber CSA of hematoxylin and eosin (H&E) stained sections of palatopharyngeus (naso- and oropharyngeal regions), thyropharyngeus, and cricopharyngeus (laryngopharyngeal region) were quantified using ImageJ 1.43u. Four, five, or six representative 200X sections were analyzed for myofiber CSA from the nasal, oral, and laryngeal pharynx. Male and female FVB mice ages 2, 12, or 24 months-of-age were used to assess effects of aging and disease on CSA. The total number of myofibers analyzed for each genotype averaged 1900 for the nasal and oral pharyngeal sections, and 700 for the laryngeal pharynx. Quantification of centrally localized nuclei was also performed on the aforementioned sections of 2-month-old male and female mice using ImageJ 1.43u. Myofiber cross-sectional areas of 929-1505 myofibers from pharyngeal and tibialis anterior muscles of DTA-Pax7$^{CreERTM}$ male mice 4-months post-tamoxifen treatment were analyzed. All images were acquired using an Axioplan microscope with a 0.5 NA 20x Plan-Neofluar objective (Carl Zeiss MicroImaging, Inc.) and charge-coupled device camera (Carl Zeiss MicroImaging, Inc.) with Scion Image 1.63 (Scion Corp.). Photoshop CS4 (Adobe) was used to globally process all images for contrast, size, and brightness. Data were blinded for analysis.

For immunostaining of myosin heavy chains, sections of pharyngeal and gastrocnemius/soleus muscles were blocked for endogenous peroxidases using 0.3% $H_2O_2$ in 0.1 M potassium phosphate buffer (pH 7.3) (PBS) for 10 minutes and then successively washed with PBS. TNB blocking buffer (0.1 M Tris–HCl, pH 7.5, 0.15 M NaCl and 0.5% blocking reagent) (PerkinElmer) was then applied to the sections for 30 minutes at room temperature, followed by blocking of endogenous binding sites using the M.O.M. Kit (Vector Laboratories Inc.). Subsequently, tissue sections were incubated for 1 hour at room temperature with either primary antibodies or appropriate isotype controls. The following antibody supernatants (Developmental Studies Hybridoma Bank) were used: BA-D5 (MHC I), N2.261 (MHC I/IIa/Neonatal), SC-71 (MHC IIa), BF-B6 (Embryonic/Neonatal), 6H1 (MHC IIx), and BF-F3 (MHC IIb). Successive washes in 0.05% Tween 20 in PBS (PBS-T) were followed by another 30 min incubation in TNB. Horseradish peroxidase (HRP) conjugated anti-mouse IgG or IgM (Jackson ImmunoResearch) at 4μg/ml in TNB buffer was applied for 60 min at room temperature. After washes with PBS-T, sections were incubated with DAB Fast 3,3′-Diaminobenzidine (Sigma).

For additional immunostaining of tissue sections, the M.O.M. Kit (Vector Laboratories Inc.) was used to block endogenous Fc receptor binding sites followed by a 1 hour incubation with 5% goat serum, 5% donkey serum, 0.5% BSA, 0.20% Triton-X 100 in PBS (blocking buffer). Sections were then labeled with blocking buffer containing primary antibodies or appropriate isotype controls overnight at 4°C. Successive washes in 0.25% Tween 20 in PBS (PBS-T) were followed by another 60 minute incubation with appropriate secondary antibodies at room temperature. Sections were then washed with

PBS-T and nuclei labeled with 4',6-diamidino-2-phenylindole (DAPI) in PBS. Primary antibodies included rat anti-BrdU (2 μg/ml, clone BU1/75 (ICR1), Accurate Chemical and Scientific), mouse anti-dystrophin (13.5 μg/ml, clone MANDYS8, Sigma), and mouse anti-Pax7 (7.5 μg/ml, Developmental Studies Hybridoma Bank). Immunostaining for BrdU was performed on post-dystrophin immunostained sections as follows. Sections were fixed with 2% paraformaldehyde in PBS for 10 minutes, followed by a PBS wash, 2 minute chilled acetone treatment, and another PBS wash. Subsequently, sections were treated with 1 N HCl in PBS at 45°C for 20 minutes and immediately neutralized with a 0.1 M sodium tetraborate/boric acid buffer, pH 8.5, for 8 minutes at room temperature. Additional tissue blocking was performed with 0.3 M glycine in PBS for 30 minutes and 24 μg/ml AffiniPure goat α-mouse IgG $F(ab')_2$ (Jackson Immuno-Research)/ml PBS-T at room temperature for 1 hour. Sections were then immunostained for BrdU following the standard immunostaining protocol described above.

Histochemical staining was utilized to identify satellite cells *in vivo*. Tissue sections from Myf5-nLacZ mice were fixed in 4% paraformaldehyde, 0.1 M $NaP_i$ (pH 7.2), 0.5% glutaraldehyde, followed by a PBS wash, and then incubated at 37°C with 1 mg/ml X-gal in dimethylformamide for 12-18 hours to identify β-galactosidase activity. Peripheral and centrally localized β-gal positive nuclei were quantified using ImageJ 1.43u on histologic sections.

**Single myofiber isolation and imaging**

Single myofibers were isolated, as previously described (Mitchell and Pavlath, 2004) from pharyngeal or extensor digitorum longus (EDL) muscles of mice 2-5, 12, or

18 months-of-age. Briefly, muscles were dissected and digested with gentle agitation in 4.5 mg/ml glucose, 100 U/ml penicillin G, 100 μg/ml streptomycin, 25 mM HEPES in DMEM containing either 400 or 800 U/ml collagenase type I (Worthington), respectively, at 37°C for 90 minutes. Single myofibers were washed 3 times with collagenase-free DMEM prior to manual extraction onto clean 100-mm plates. Myofibers were then individually transferred onto 10% growth factor-reduced Matrigel (BD Biosciences) coated 24-well plates, and centrifuged at 1100x *g* to enhance myofiber adherence. Myofibers were then fixed with 2% formaldehyde in PBS and stained with DAPI. Pharyngeal muscles from 18-month-old mice required digestion with 1600 U collagenase type I/ml DMEM media. Histochemical X-gal staining, as described above, was also performed on myofibers isolated from Myf5-nLacZ mice. Single myofiber images were visualized using an Axiovert 200M microscope with a 0.3 NA 10X Plan-Neofluar objective (Carl Zeiss MicroImaging, Inc.). Images were captured with a QImaging camera and OpenLab 5.5.2 (Improvision) software. Myofiber diameter, length, and nuclear number were quantified using ImageJ 1.43u. β-gal positive nuclei were quantified manually. Photoshop CS4 (Adobe) was used to globally process all images for contrast and brightness. Between 929-1505 myofibers were pooled and analyzed from 5 mice per age group for each muscle.

**Biochemical Analysis of Myosin Heavy Chain Isoforms**

Extraocular, gastrocnemius/soleus, heart and pharyngeal muscles (i.e. the entire pharynx with larynx/trachea removed) were dissected from 2 or 6 month-old male or female C57BL/6 mice. Tongues were collected from day-old post-natal C57BL/6 pups.

From each sample, 40-50 mg of tissue was homogenized in 200 µl of PBS containing 5% protease inhibitor cocktail (Sigma, Aldrich). Homogenates were centrifuged at 10,000 x g (4°C) for 10 minutes and the pellets re-suspended in PBS with proteinase inhibitors for isolation of the myosin heavy chain (MHC) fraction. Total protein content was determined by bicinchoninic acid assay (Pierce BCA protein assay, Thermo Fisher Scientific Inc).

The gel electrophoresis protocol was modified from Talmadge and Roy (1993). Briefly, we used stacking gels of 4% acrylamide (wt/vol; acrylamide:N,N'-methylene-bis-acrylamide, 37.5:1), 30% glycerol, 70 mM Tris, 4 mM EDTA, 0.05% N, N, N', N'-tetramethylethylenediamine (TEMED), 0.4% sodium dodecyl sulfate (SDS), and 0.1% ammonium persulfate (APS); and separating gels of 8% acrylamide (wt/vol; acrylamide:N,N'-methylene-bis-acrylamide, 50:1), 30% glycerol, 0.2 M Tris, 0.1 M glycine, 0.05% TEMED, 0.4% SDS, and 0.1% APS. Two electrode buffers were utilized: 50 mM Tris, 75 mM glycine, and 0.05% SDS buffer was used for the lower electrode while a 6X concentrate of the aforementioned solution with 0.12% 2-mercaptoethanol was used for the upper electrode. Laemmli sample buffer (Bio-Rad Laboratories) at a 1:1 dilution was used to solubilize proteins. Electrophoresis was performed at 140 V for 22 hours at 4°C. One set of gels were stained with Imperial Protein Stain (Thermo Fisher Scientific Inc.), destained with water, and visualized using an Epson Perfection V33 imager.

For MHC immunoblotting, proteins were transferred from SDS-PAGE gels onto Immuno-Blot PVDF membranes (Bio-Rad Laboratories). After incubation in 0.5X blocking buffer (USB Corporation), membranes were incubated overnight with A4.84

(MHC 1) (Developmental Studies Hybridoma Bank) in 0.5X blocking buffer with 0.1% Triton X-100 at 4°C. Membranes were then washed, incubated with IRDye 800CW goat anti-mouse IgM (Rockland, Gilbertsville, PA), and visualized by Odyssey Infrared Imaging System (LI-COR).

**PABPN1 Immunoblotting**

Whole pharynxes from 2-month-old male mice, with larynx/trachea removed, were homogenized in RIPA-2 buffer (50 mM Tris–HCl, pH 8.0, 150 mM NaCl, 1% NP-40, 0.5% deoxycholic acid, 0.1% SDS) containing protease inhibitors (Mini Complete; Roche). The homogenate was centrifuged at 3000 x g for 30 minutes, and the supernatant utilized for SDS-PAGE and immunoblotting. Tissue lysates containing 100 μg of protein were loaded onto 12% Mini-PROTEAN TGX gels (Bio-Rad Laboratories) and subsequently transferred to 0.45 μm nitrocellulose membranes (Bio-Rad Laboratories). The membranes were blocked for non-specific binding with 5% non-fat dry milk in Tris-buffered saline (TBS) and then incubated with primary antibodies against PABPN1 (Apponi et al., 2010) and Hsp90 (Santa Cruz) overnight at 4°C. Secondary antibody labeling was performed using species appropriate horseradish peroxidase (HRP)-conjugated IgGs (Jackson ImmunoResearch) for 1 hour at room temperature. Enhanced chemiluminescence was utilized to detect antibody binding and densitometry analysis performed using ImageJ 1.43u.

**Flow Cytometry and Fluorescence Activated Cell Sorting**

For analysis via flow cytometry, mononucleated cells were isolated from pharyngeal and limb (gastrocnemius and quadriceps) muscles as previously described (Bondesen et al., 2004; Mitchell and Pavlath, 2001). Briefly, pharyngeal and limb muscles were minced and digested in Dulbecco's Modified Eagle's Medium (DMEM) (Mediatech) containing 1 mg/ml pronase (Calbiochem), 25 mM HEPES at 37°C for 45 minutes or 1 hour, respectively. Digested muscles were washed with DMEM and mononucleated cells collected using 100 μm Steriflip filtration systems (Milipore). Red blood cells were removed using Percoll (GE Healthcare) gradients prior to antibody labeling.

For analysis and collection via Fluorescence Activated Cell Sorting (FACS), pharyngeal and limb (gastrocnemius and quadriceps) muscles were minced and digested in Ham's F10 media (Hyclone) containing 500 units/ml collagenase II (Gibco) and 10% fetal bovine serum (FBS) at 37°C while shaken at 65 rpm for 90 minutes. Digested muscles were then rinsed with Ham's F10 media containing 10% FBS, 100 U/ml penicillin G, and 100 μg/ml streptomycin (P/S), followed by a second digestion using 100 units/ml collagenase II, 1 unit/ml dispase (Gibco) in Ham's F10 media containing 10% FBS, P/S under the same conditions for 30 minutes. Digested muscles were washed with 0.1 M Dulbecco's phosphate-buffered saline, pH 7.3 (PBS) (Gibco) and mononucleated cells collected using 100 μm Steri-Flip filtration systems (Milipore).

Isolated cells were resuspended in PBS containing 1% bovine serum albumin (BSA) for antibody labeling. Dead cells were identified using 5 μg/ml propidium iodide (PI). Myogenic cells, identified as $PI^-/Sca1^-/CD31^-/CD45^-/\alpha7\text{-integrin}^+$ (Kafadar et al., 2009)

were isolated and collected using a FACSAria II (Becton-Dickinson) at the Emory University School of Medicine Core Facility for Flow Cytometry. Analyses of flow cytometry data were performed using FlowJo (version 9.5.2). Isolated myogenic cells were then processed for *in vitro* cultures, immunofluorescent staining, or RNA extraction. Primary antibodies included rat anti-CD31-Phycoerythrin (PE) (0.5 μg/ml; eBioscience) and rat CD45-PE (0.5 μg/ml; BD Pharmingen), rat Sca-1-PE-Cy7 (0.05 μg/ml; BD Pharmingen), rat α7-integrin-AlexaFluor649 (1 μg/ml; AbLabs) and appropriate rat isotype control antibodies (BD Pharmingen).

**Evans Blue Assay**

C57BL/6 and Mdx mice received an intraperitoneal injection of 1% Evans Blue Dye (Sigma) suspended in sterile PBS at a volume of 10 μl/gram body weight. Mice were euthanized via $CO_2$ asphyxiation 24 hours post-injection and immediately prior to dissection and collection of tibialis anterior and pharyngeal muscles for cryosectioning. Tissues were sectioned at a thickness of 10 μm and analyzed for the presence of Evans Blue fluorescence within myofibers. Images were acquired using an Axioplan microscope with a 0.8 NA 25x Plan-Neofluar objective (Carl Zeiss MicroImaging, Inc.) and charge-coupled device camera (Carl Zeiss MicroImaging, Inc.) with Scion Image 1.63 (Scion Corp.). Photoshop CS4 (Adobe) was used to globally process all images for contrast, size, and brightness.

### *In Vivo* BrdU Assays

To compare the proliferative and fusogenic abilities of pharyngeal and limb satellite cells *in vivo*, 5-bromo-2'-deoxyuridine (BrdU) assays were performed. Three-month-old male C57BL/6 mice were injected with 10 μg BrdU (Sigma)/gram body weight intraperitoneally every 12 hours. To assess proliferation, mice were injected over a 48-hour period. To assess fusion, injections were given for 7 days followed by 7 days of 0.8% BrdU in 2% sucrose water. *Proliferation assay*: Pharyngeal and gastrocnemius muscles of 3-5 mice were collected forty-eight hours post-initial BrdU injection. Mononucleated cells were isolated from pooled muscles, immunostained and analyzed using flow cytometry, as described above. Proliferating myogenic cells were identified as $BrdU^+$, $Sca1^-/CD31^-/CD45^-/\alpha7\text{-integrin}^+$. BrdU immunostaining was performed using the FITC BrdU Flow Kit (1:200, BD PharmingenTM). As a positive control for proliferating cells, muscle injuries were performed in anesthetized mice by injecting 40 μl of 1.2% $BaCl_2$ into gastrocnemius muscles as previously described (O'Connor et al., 2007) two days prior to collection. *Fusion assay*: Pharyngeal and tibialis anterior muscles were collected 14 days post-initial BrdU injection as described for tissue sectioning. Representative tissue sections were immunostained to detect dystrophin and BrdU as described above. The number of intrafiber $BrdU^+$ myonuclei/100 myofibers was quantified using ImageJ 1.43u. Samples were blinded for analysis.

### Microarray

Myogenic cells from pharyngeal and limb (gastrocnemius and quadriceps) muscles were isolated, sorted using FACS, and collected from 10-30 mice per

experiment. The Emory University Integrated Genomics Core facility processed samples for total RNA isolation using Qiagen miRNEAsy kit with on-column DNAse treatment followed by one round of amplification using NuGEN's WT-Ovation Pico amplification kit. Analysis of genomic gene expression was performed using an Illumina Mouse WG-6 v2.0 Expression BeadChip. Data was extracted using the Illumina HiScan Scanner and iScan control software. Illumina Genome Studio 2011.1 software suite was used to normalize probe level intensity data with background correction using manifest MouseWG-6_V2_0_R1_11278593_A.txt. Detection p-values were calculated as the proportion of negative control probes with expression greater than the regular probe in question using Partek Genome Studio. Data were further analyzed using both MetaCore Genego (https://portal.genego.com; Thomas Reuters) and Gene Set Enrichment Analysis (www.broadinstitute.org/gsea/index.jsp; Broad Institue).

**Real-time PCR**

Myogenic cells from pharyngeal and limb (gastrocnemius and quadriceps) muscles were isolated, sorted using FACS, and collected from 10-30 mice per experiment. Total RNA was isolated using the PicoPure RNA Isolation Kit (Applied Biosystems) from samples of 150,000-200,000 pooled cells each. cDNA was generated from total RNA via a reverse transcriptase reaction using M-MLV reverse transcriptase (Invitrogen) and random hexamer primers. cDNA was then amplified using the SYBR Select Master Mix reagent (Applied Biosystems) and 2.5 μM of each primer. All RNA samples were tested for DNA contamination by PCR. Primer sequences were: MyoD (F: 5′- GCCCGCGCTCCAACTGCTCTGAT-3′ and R: 5′-

CCTACGGTGGTGCGCCCTCTGC-3′); Pax7 (F: 5′-CACCCCGGGGACAGAGGAAGAT-3′ and R: 5′-GAGAGGGCGGGGTACAAGGAAGAC-3’). All other primers were purchased from Qiagen’s $RT^2$ qPCR Primer Assay library. Real-time PCR reactions were performed and analyzed with a Step**One**Plus Real Time PCR System (Applied Biosystems), using GAPDH or 18S as an internal control. Fold change of gene expression was determined using the ΔΔCt method (Livak and Schmittgen, 2001). Three to four independent experiments were performed and analyzed in duplicate.

**Clonal Expansion Assay**

Conditioned media (CM), collected from either primary limb or pharyngeal muscle cell cultures, contained 20% FBS, 100 U/ml penicillin, 100 μg/ml streptomycin, 5 ng/ml basic fibroblast growth factor (bFGF) in Ham’s F10 media. Any contaminating cells were removed through sterile syringe filtration with a 0.20 μm filter (Corning). Mononucleated cell suspensions obtained from pharyngeal and limb (gastrocnemius and quadriceps) muscles of C57BL/6 mice were then subjected to FACS, as previously described. Sorted myogenic cells were plated at clonal densities of 100-250 cells/100 mm collagen-coated plates and grown in CM diluted 1:1 with Ham’s F10 media containg 20% FBS, 100 U/ml penicillin, 100 μg/ml streptomycin and 5 ng/ml bFGF at 37°C for 8 days prior to 2% paraformaldehyde fixation. Cells were then counterstained with hematoxylin (Thermo Scientific). Analyses of cell number per colony and number of clonal colonies were performed manually on 105-159 clones.

**Lick Assays**

Pharyngeal function was assessed indirectly using lick assays as described by Lever et al. (2009). Briefly, food and water were removed from female mice for 14-16 hours overnight. Afterwards, room temperature water and one pellet of food were reintroduced. Water was delivered via a sipper tube bottle with a ball-bearing spout. Mice were digitally videoed to capture lick episodes when drinking. Video was captured using a Panasonic HC-V10 Digital Video Camera, recorded as MP4 files at 60 frames per second, and analyzed by two blinded independent reviewers using AVIDEMUX 2.5.4 software (Mean). Lick rates were determined by counting five independent, continuous lick episodes that spanned 60 frames of video per animal. Data were averaged per mouse and reported in licks per second.

**Statistical Analyses**

Data were analyzed for statistical significance using GraphPad Prism version 5 for Macintosh (GraphPad Software). For all statistical tests, a 0.05 level of confidence was considered statistically significant. When comparing two groups, data were analyzed by unpaired Students *t* test. To determine significance among multiple groups, data were analyzed using one-way ANOVA with Bonferroni's posttest. Nonparametric data were analyzed using Mood's median test to identify statistical differences between sample distributions using Microsoft Excel 2008 for Mac Software.

# Chapter 4: Aging and muscular dystrophy differentially affect murine pharyngeal muscles in a region-dependent manner

**A portion of this chapter is published as:**

**Randolph, M. E.**, Luo, Q., Ho, J., Vest, K. E., Sokoloff, A. J., & Pavlath, G. K. (2014). Ageing and muscular dystrophy differentially affect murine pharyngeal muscles in a region-dependent manner. *The Journal of Physiology*, *592*(Pt 23), 5301–5315.

**Contributions:**

Elizabeth P. Andreas (Figures 4.4.1 illustration, 4.4.6 data), Justin Ho (Figure 4.4.2 data), Qingwei Luo (Figure 4.4.2 data), Katherine E. Vest (Figures 4.4.3 data, 4.4.4 data, 4.4.5 data)

# Chapter 4: Aging and muscular dystrophy differentially affect murine pharyngeal muscles in a region-dependent manner

## 4.1 Introduction

Swallowing is a highly complex and coordinated reflex regulated through the central nervous system to elicit a synchronized contraction of muscle tissues surrounding the oral, pharyngeal, and esophageal cavities (Donner et al., 1985; Ertekin and Aydogdu, 2003; Miller, 2008; Rubesin et al., 1987). The swallow reflex prevents the aspiration of food and liquid into the trachea/lungs and the subsequent development of life-threatening pneumonia (Martin et al., 1994; Prasse and Kikano, 2009). Almost 16 million people in the United States are affected with dysphagia (Robbins et al., 2002), a debilitating and potentially deadly condition involving impairment of the swallow reflex (Logemann, 2007). Swallow impairment is associated with several diseases including stroke (Lindgren and Janzon, 1991; Miller, 2008), Parkinson's disease (Logemann, 2007), myasthenia gravis (Ertekin et al., 1998), pharyngeal myositis (Ertekin and Aydogdu, 2003), DiGeorge syndrome (Eicher et al., 2000), advanced stage Duchenne muscular dystrophy (Aloysius et al., 2008; Nozaki et al., 2007), and oculopharyngeal muscular dystrophy (OPMD) (Taylor, 1915; Victor et al., 1962). Additionally, dysphagia is also associated with aging (Kawashima et al., 2004; Logemann, 2007; Prasse and Kikano, 2009). Studies from Japan, the Netherlands, and the United Kingdom suggest that 11-16% of the elderly suffer from dysphagia (Bloem et al., 1990; Eslick and Talley, 2008; Holland et al., 2011; Kawashima et al., 2004). One study found that almost 45% of

dysphagic elderly individuals reported no history of stroke or overt disease (Kawashima et al., 2004), suggesting a high incidence of age-related dysphagia.

Pharyngeal muscles are an essential component of the swallow reflex (Ertekin and Aydogdu, 2003; Miller, 2008). Seven major muscles are responsible for pharyngeal contraction when swallowing (Donner et al., 1985; Ekberg et al., 2009b; Rubesin et al., 1987). These muscles arise during vertebrate development from the third and fourth pharyngeal arches (Mootoosamy and Dietrich, 2002; Noden and Francis-West, 2006) and are comprised of the stylopharyngeus, palatopharyngeus, salpingopharyngeus, and the superior, middle and inferior pharyngeal constrictor muscles (Donner et al., 1985; Dutta and Basmajian, 1960; Himmelreich, 1973; Rubesin et al., 1987). The inferior pharyngeal constrictor can be subdivided into the cricopharyngeus and the thyropharyngeus muscles (Donner et al., 1985; Rubesin et al., 1987). Despite the critical nature of these muscles, few studies have analyzed the effects of age and disease on pharyngeal muscles as a group.

Only a few individual pharyngeal muscles have been studied in the context of aging and dysphagia. To our knowledge, only one report has linked abnormalities in the palatopharyngeus muscle with dysphagia (Kirberger et al., 2006). In contrast, the effects of aging or disease on the inferior pharyngeal constrictor muscles, particularly the cricopharyngeus muscle, have been well studied (Bachmann et al., 2001; Davis et al., 2007; Gidaro et al., 2013; Hyodo et al., 1999; Leese and Hopwood, 1986; Mu et al., 2012; Périé et al., 2006a).

One dysphagic disease that directly affects the cricopharyngeus is the autosomal dominant disease, oculopharyngeal muscular dystrophy (OPMD) (Brais et al., 1998;

Victor et al., 1962). OPMD is caused by a polyalanine expansion in the N-terminus of polyadenylate-binding nuclear protein 1 (PABPN1) (Brais et al., 1998; Robinson et al., 2005), which plays key roles in RNA biogenesis (Banerjee et al., 2013). Despite the ubiquitous expression of PABPN1, only a subset of muscles is primarily affected in OPMD: pharyngeal muscles, tongue, levator palpebrae, extraocular muscles, and proximal limb muscles (Little and Perl, 1982; Victor et al., 1962). The main prognostic factor for OPMD patients is the dysphagia associated with cricopharyngeal muscle pathology and dysfunction (Blakeley et al., 1968; Little and Perl, 1982; Montgomery and Lynch, 1971; Victor et al., 1962). Little is known concerning the effects of mutant PABPN1 expression in the other pharyngeal muscles and their potential contribution to pathology.

To gain an integrated view of pharyngeal muscle physiology, we characterized multiple pharyngeal muscles in mice, and tested whether these muscles are differentially affected with age or muscle-specific overexpression of mutant A17 PABPN1 using a mouse model of OPMD. Our studies provide insight into the myofiber composition of murine pharyngeal muscles and also reveal variable sensitivity of individual pharyngeal muscles to growth and atrophic changes associated with aging or muscular dystrophy. Furthermore, we show that both aging and overexpression of mutant A17 PABPN1 alter swallowing behavior in mice, while overexpression of wild-type A10 PABPN1 protects swallow function throughout life. These studies provide a critical foundation for advancing our understanding of molecular mechanisms underlying changes in pharyngeal muscles that occur with age and/or a disease state.

## 4.2 Results

### Identification of murine pharyngeal muscles

The swallow reflex occurs in three phases termed oral, pharyngeal, and esophageal (Donner et al., 1985; Rubesin et al., 1987). Each phase involves a unique set of muscles. The pharyngeal phase of the swallow reflex relies on coordinated neuromuscular contractions within the oral cavity paired with muscles located in the nasal, oral and laryngeal regions of the pharynx (Donner et al., 1985; Rubesin et al., 1987). To study the muscles of each pharyngeal region in mice (Fig. 4.4.1A), we first identified the various pharyngeal muscles histologically. Pharyngeal tissues extending from the rostral soft palate caudally to the mid-cervical trachea/esophagus were collected for transverse tissue sectioning and histologic examination via hemotoxylin and eosin (H&E) staining.

The nasopharynx was defined as beginning at the closure of the pharyngeal epithelial mucosa where both the superior pharyngeal constrictor muscles dorsolaterally (Fig. 4.4.1B, yellow diamond) and the palatopharyngeal fold comprised of the palatopharyngeus and salpingopharyngeus ventrolaterally form the pharyngeal cavity (Fig. 4.4.1B, yellow asterisks) (Nakano and Muto, 1985; Rubesin et al., 1987). The velopharyngeal opening marked the end of the nasopharynx and beginning of the oropharynx. The oropharynx extended caudally to the pharyngeal aponeurosis of the palatopharyngeal muscle (Rubesin et al., 1987). Muscles identified in the oropharynx included the middle pharyngeal constrictor (Fig. 1*B*, green triangle) and palatopharyngeus (Fig. 4.4.1B, green asterisks). The laryngopharynx began at the pharyngeal aponeurosis and extended caudally to the first tracheal ring. Muscles

identified in the laryngopharynx were the inferior constrictor muscles, thyropharyngeus (Fig. 4.4.1B, blue circle) and cricopharyngeus (Fig. 4.4.1B, blue square). These studies demonstrate that pharyngeal muscles are easily identified in mice using histologic sections, allowing for subsequent comparative analyses among the muscles required for the pharyngeal phase of swallowing.

**Variability in myofiber types between pharyngeal muscles**

To examine differences among muscles throughout the pharynx, we began by analyzing myofiber types as the myofiber composition of a muscle affects its function. Slow-twitch oxidative myofibers (Type I) are typically observed in muscles utilized for endurance, whereas the fast-twitch glycolytic myofibers (Type II) are overrepresented in muscles used for rapid contractions (Reiser et al., 1985a; Reiser et al., 1985b). Each myofiber type is composed of distinct isoforms of contractile proteins including myosin heavy chains (MHCs). Initially, to determine the myofiber types present in murine pharyngeal muscles as a whole, we isolated MHC proteins and performed separation SDS-PAGE and Coomassie to discriminate myosin isoforms. Mouse pharyngeal muscles predominantly contained Type IIb, IIx, and neonatal MHCs, with trace amounts of Type IIa MHC (Fig. 4.4.2A). Type I MHC was not detected by either Coomassie stain or immunoblot (Fig. 4.4.2A). Additionally, neonatal myosin heavy chain was present in pharyngeal muscles of both young and mature mice (Fig. 4.4.2A).

To analyze the myofiber composition of individual muscles of the pharynx, we used immunohistochemistry to visualize myofiber types *in vivo*. Type IIb MHC was predominantly expressed in the palatopharyngeus as well as in the superior, middle, and

inferior pharyngeal constrictor muscles, with lesser amounts of Type IIa and IIx. Type I MHC was not observed in any pharyngeal muscle. Immunostaining of representative muscles is shown in Fig. 2*B*. The expression of neonatal MHC was strictly confined to muscles of the inferior constrictor adjacent to the mucosal epithelium of the laryngopharynx (Fig. 4.4.2C). Thus, murine pharyngeal muscles are mainly composed of fast glycolytic myofibers with neonatal MHC expression confined to the laryngopharynx.

**Regional effects of aging on pharyngeal myofiber size**

To study the effects of aging on the muscles of each pharyngeal region, we performed a histologic study utilizing wild-type FVB mice at 2, 12 and 24 months of age. Myofiber size was determined by analyzing cross-sectional areas (CSA) from the palatopharyngeus (naso- and oropharyngeal regions), thyropharyngeus, and cricopharyngeus (laryngopharyngeal region) as these muscles were transected transversely versus longitudinally in sections. From 2 to 12 months of age, significant increases in myofiber size were observed in both the naso- and oropharynx, while myofiber size decreased in the laryngopharynx (Fig. 4.4.3A). However, by 24 months of age, myofiber size significantly decreased in all three pharyngeal regions (Fig. 4.4.3B). These results provide evidence that muscles in every pharyngeal region undergo age-related atrophy while muscles of the laryngopharynx undergo atrophy at an earlier age than those in the naso- and oropharynxes.

**Overexpression of wild-type A10 and mutant A17 PABPN1 have differential effects on pharyngeal muscle growth**

We used an OPMD mouse model to test if regional differences in pharyngeal muscle growth or atrophy also occur with muscular dystrophy. This OPMD model overexpresses a 17-alanine-expanded mutant PABPN1 (A17-MUT) specifically in skeletal muscle (Davies et al., 2005). Mice overexpressing wild-type PABPN1 (A10-WT), which contains ten alanines in the N-terminus of the protein, were simultaneously created to control for any effects of overexpressing PABPN1 (Davies et al., 2005). The A17-MUT mice develop symptoms of muscle weakness and atrophy with minimal signs of degeneration in limb muscles as early as six months of age compared to both wild-type and A10-WT control mice (Davies et al., 2005; Trollet et al., 2010). As pharyngeal muscles of these mice have never been studied, we first confirmed PABPN1 overexpression in the pharyngeal muscles of both A10-WT and A17-MUT mice relative to wild-type littermates using immunoblots (Fig. 4.4.4A). A17-MUT mice demonstrated a two-fold increase in PABPN1 overexpression when compared to A10-WT mice (data not shown). The apparent absence of PABPN1 protein in the wild-type pharyngeal muscle is consistent with the findings reported by Apponi *et al.* (2013) that pharyngeal muscles express very low levels of PABPN1 protein compared to limb muscles and other tissues.

Initially, we compared myofiber cross-sectional area of wild-type and A10-WT mice for each region of the pharynx to investigate whether overexpression of wild-type A10 PABPN1 alters pharyngeal muscle growth (Fig. 4.4.4B). Again, regional differences in pharyngeal myofiber size were observed. At 2 months of age, myofiber size was

significantly increased in each pharyngeal region in A10-WT mice (Fig. 4.4.4B). However, only laryngopharyngeal muscles consistently exhibited increased myofiber size throughout the time course of the experiment (Fig. 4.4.4B), indicating that overexpression of wild-type A10 PABPN1 both enhances muscle growth and provides resistance to age-related atrophy in laryngopharyngeal muscles.

When analyzing the pharyngeal muscle sections from the A10-WT mice, we observed an unusual preponderance of myonuclei with a more central localization within the myofibers, as opposed to the typical sub-sarcolemmal position. The presence of such centrally located nuclei within myofibers is consistent with myogenesis, the fusion of muscle stem cells with myofibers, resulting in the addition of new myonuclei to myofibers, which contributes to muscle growth (Schmalbruch, 1976). Therefore, we analyzed H&E stained pharyngeal sections of wild-type and A10-WT 2-month-old mice for centrally located myonuclei (Fig. 4.4.4C). In the naso- and oropharynx, no significant difference in frequency of central nuclei was observed (Fig. 4.4.4D). However, wild-type A10 PABPN1 overexpression in the laryngopharynx resulted in a significant increase in the incidence of centrally localized nuclei, which was not observed in A17-MUT sections (Fig. 4.4.4D). These findings suggest that increased levels of wild-type A10 PABPN1 enhance myogenesis in laryngopharyngeal muscles, consistent with the enhanced myofiber size observed in these muscles of A10-WT mice.

Subsequently, we analyzed selected pharyngeal muscles (Fig. 4.4.3) of A17-MUT mice and compared them to A10-WT mice to control for the variable of PABPN1 overexpression. No signs of myofiber degeneration, immune infiltration, or increased interstitial fibrosis were observed in H&E sections (data not shown); however, when

myofiber size was quantified for sections from A17-MUT and A10-WT mice at 2, 12 and 24 months of age, overexpression of mutant A17 PABPN1 differentially affected muscle growth and atrophy of specific muscles in each pharyngeal region (Fig. 4.4.5). In 2-month-old A17-MUT mice, myofiber size was significantly smaller in the laryngopharynx while minimal changes occurred in the naso- and oropharynx. In 12-month-old A17-MUT mice, major decreases in myofiber size occurred in the oro- and laryngopharynx relative to myofibers from A10-WT mice. Furthermore, when we compared the region of the palatopharyngeus located in the oropharynx at 2 and 12 months, we observed a pronounced impairment of muscle growth demonstrated by failure of A17-MUT myofibers to shift towards a larger size as observed with A10-WT mice between these timepoints (Fig. 4.4.5). This growth impairment between 2 and 12 months was not observed in the nasopharyngeal region of the palatopharyngeus (Fig. 4.4.5). By 24 months, no major size differences were observed between A10-WT and A17-MUT myofibers (Fig. 4.4.5). Muscles of the oropharynx were more susceptible to the effects of mutant A17 PABPN1 than those in the nasopharynx. Within the muscles of the laryngopharynx, the observed decrease in size with mutant A17 PABPN1 overexpression may be related to pathology caused by the mutant protein. Alternatively, overexpression of the mutant A17 protein may fail to protect against age-related atrophy, as does overexpression of the wild-type A10 protein in laryngopharyngeal muscles. Taken together, these data indicate that variable effects of both age and disease occur in the different regions of the pharynx.

**Differential effects of age and overexpression of either wild-type A10 or mutant A17 PABPN1 on swallowing**

Considering the presence of pharyngeal muscle atrophy with aging in wild-type mice (Fig. 4.4.3), we next hypothesized that swallowing may be impacted by aging. Currently, no assays exist for directly measuring the pharyngeal phase of swallowing in mice. Therefore, as an indirect test of pharyngeal function, we utilized an assay that analyzes the oral phase of swallowing (Lever et al., 2009; Lever et al., 2010). In this assay, food and water were withdrawn from mice for 14-16 hours. Upon reintroduction of food and water, mice were digitally recorded to visualize individual lick episodes (Fig. 4.4.6A). Lick rates, defined as the number of licks/second, were quantified for wild-type FVB mice at 6, 18, and 24 months of age (Fig. 4.4.6B). At 24 months of age, a 9.5% decrease in lick rate occurred in wild-type mice (Fig. 4.4.6B). We then tested whether age also affects swallowing in A10-WT or A17-MUT mice. Surprisingly, A10-WT mice demonstrated no significant change in lick rates either at 18 or 24 months of age (Fig. 4.4.6C, D). However, at 18 and 24 months of age, A17-MUT mice exhibited decreases in lick rates of 5.9% and 7.2%, respectively, when compared to the A17-MUT 6-month baseline (Fig. 4.4.6D).

We then tested whether wild-type A10 PABPN1 overexpression provides a protective effect for lick function as was observed in laryngopharyngeal muscle growth (Fig. 4.4.4). Therefore, we compared lick rates of A10-WT mice to wild-type mice to determine if increased levels of wild-type A10 PABPN1 significantly altered the ability to swallow. No difference was observed between wild-type and A10-WT lick rates at 6

months of age (Fig. 4.4.6C). However, A10-WT lick rates were increased, relative to wild-type mice, at both 18 and 24 months of age by 6.2% and 7.3%, respectively.

Finally, we compared the lick rates of A17-MUT mice to the A10-WT overexpression control mice at each time point to determine if mutant A17 PABPN1 expression alters swallow function. No difference in lick rate was observed at 6 months of age (Fig. 4.4.6D). However, A17-MUT lick rates were impaired, relative to A10-WT mice, at both 18 and 24 months of age by 8.8% and 6.5%, respectively (Fig. 4.4.6D). No significant differences in lick rates were observed in A17-MUT mice at any age when compared to wild-type mice (data not shown). The decrease in lick rates observed in A17-MUT mice relative to A10-WT mice could be due to a failure of mutant A17 PABPN1 to rescue age-related dysphagia. Together these data demonstrate that mice develop impaired swallow function both with age and mutant A17 PABPN1 overexpression, while overexpression of wild-type A10 PABPN1 provides a protective effect against age-related dysphagia in mice.

**4.3 Discussion**

Dysphagia is a debilitating condition that affects millions of individuals (Robbins et al., 2002), yet little is known about basic pharyngeal muscle biology. Here we utilized a mouse model system to investigate pharyngeal muscles. With age, both pharyngeal muscle atrophy and oral dysphagia developed in wild-type mice. Interestingly, overexpression of wild-type A10 PABPN1 provided protection against the development of age-related dysphagia. Furthermore, we observed differential susceptibility of various pharyngeal muscles to overexpression of either wild-type or mutant A17 PABPN1 in age-related muscle growth and atrophy.

In all murine pharyngeal muscles examined, the predominant myofiber types were fast-twitch Type II myofibers with no evidence of slow-twitch Type I myofibers. In contrast, human cricopharyngeal muscle contains a layer of Type I myofibers closest to the mucosal epithelium and an outer layer of Type II myofibers (Mu and Sanders, 2002; Mu et al., 2007). The Type I myofibers provide the tonic force for maintaining closure of the upper esophageal sphincter (Davis et al., 2007). Interestingly in murine cricopharyngeal muscle, we observed an inner layer of myofibers expressing neonatal MHC, instead of Type I MHC. Other adult craniofacial muscles in mice also express neonatal MHC, such as extraocular muscles (Wieczorek et al., 1985), inner ear muscles (Scapolo et al., 1991), sternocleidomastoid muscles (McLoon, 1998) and masseter muscles (Bredman et al., 1992; Butler-Browne et al., 1988). Myofibers expressing neonatal MHC have decreased shortening velocities and strength (Johnson et al., 1994), hence they are more similar to slow-twitch myofibers than to fast-twitch. Thus the

neonatal MHC myofiber layer in murine cricopharyngeal muscle is likely functionally analogous to the slow-twitch inner myofiber layer of humans.

In wild-type mice, post-natal muscle growth occurred in muscles of the naso- and oropharynxes followed by late-life muscle atrophy, consistent with age-related muscle growth and atrophy of limb muscles in humans (Aherne et al., 1971; Lexell et al., 1988; Wada et al., 2003). However, muscles of the laryngopharynx reached maximum size in this study by 2 months of age and exhibited muscle atrophy by 12 months of age. These findings point to unique regulatory mechanisms underlying growth of murine laryngopharyngeal muscles in their role as pharyngeal constrictors. To date, post-natal muscle growth in the human laryngopharynx has not been assessed, therefore, whether early onset of laryngopharyngeal muscle atrophy also occurs in humans is unknown. Further studies examining the cellular and molecular mechanisms regulating the differential growth of pharyngeal muscles could provide valuable insights into region-specific differences underlying age-related muscle atrophy of the pharynx.

Davies *et al*. previously demonstrated that wild-type A10 PABPN1 overexpression in limb muscles protected against OPMD-related apoptosis and strength loss in A17-MUT mice (2008). We observed that overexpression of wild-type A10 PABPN1 alone provided a protective effect on myofiber growth of pharyngeal muscles in a region-dependent manner. Wild-type A10 PABPN1 overexpression enhanced myofiber size in all pharyngeal muscles at 2 months of age, but surprisingly, protected against age-related muscle atrophy only in laryngopharyngeal muscles. These data show that wild-type A10 PABPN1 overexpression differentially affects mechanisms underlying myofiber growth of pharyngeal muscles *in vivo*. Interestingly, recent studies of the Vastus

lateralis muscle indicate decreased levels of PABPN1 mRNA in the contexts of both muscle aging and OPMD in humans (Anvar et al., 2013; Raz and Raz, 2014), suggesting a connection between disease and diminished PABPN1 levels in certain muscles. Our studies suggest that alleviating age- or OPMD-related PABPN1 loss with overexpression of wild-type A10 PABPN1 could potentially prevent muscle loss in the human laryngopharynx and ameliorate one of the most devastating symptoms of OPMD.

Myofiber size in the muscles of the laryngopharynx in the A10-WT was associated with an increased number of centrally located nuclei in myofibers. Neither the enhanced size phenotype nor the corresponding increase in the number of central myonuclei was observed in any other pharyngeal region of A10-WT mice. Two mechanisms could account for the presence of the centrally located nuclei: 1) ongoing basal myogenesis; or 2) regeneration due to focal myofiber injury. Other craniofacial muscles, such as the extraocular muscles, undergo continuous myofiber remodeling and contain a population of proliferative myogenic precursor cells (McLoon et al., 2004; McLoon and Wirtschafter, 2002a; McLoon and Wirtschafter, 2003; McLoon and Wirtschafter, 2002b; Wirtschafter et al., 2004a). If pharyngeal muscles have a similar myogenic precursor population and undergo myofiber remodeling, wild-type A10 overexpression in the laryngopharynx may selectively enhance the myogenic potential of these cells, thereby increasing the incidence of central myonuclei present in the A10-WT laryngopharynx. Alternately, the continuous tonic demand of the inferior pharyngeal constrictor may result in focal myofiber damage not detected in sections leading to local muscle regeneration and an increase of centrally located myonuclei. Further studies are needed to distinguish between these two possibilities.

Using the A17-MUT OPMD mouse model (Davies et al., 2008), we analyzed the effects of mutant A17 PABPN1 overexpression on pharyngeal muscle growth. Mutant A17 PABPN1 overexpression adversely affected myofiber size in both the oro- and laryngopharynx at both 2 and 12 months of age relative to overexpression of wild-type A10 PABPN1. However, by 24 months of age, A10-WT oro- and laryngopharyngeal myofibers underwent atrophy and demonstrated a similar myofiber distribution as the A17-MUT animals, suggesting that age-related changes eventually nullified the positive growth effect of wild-type A10 PABPN1 overexpression in the oropharynx. Meanwhile, minimal to no effect of mutant A17 PABPN1 on myofiber size was observed in the palatopharyngeus of the nasopharynx regardless of age. Despite the fact that the palatopharyngeal muscle spans both the nasal and oral pharynxes, impairment of muscle growth was only observed in the oropharyngeal region of the palatopharyngeal muscle in 12-month-old A17-MUT mice. The regional differences in the effect of mutant A17 PABPN1 on myofiber size within the palatopharyngeal muscle are likely related to the unique functional demands of the oral versus the nasal pharynx. In the nasal pharynx, the palatopharyngeus merges with the stylopharyngeus and salpingopharyngeus to elevate the soft palate cranially and caudally as one collective unit. However, in the oral pharynx, the palatopharyngeal muscle splits into two separate heads that are no longer associated with the soft palate. This anatomical division of the palatopharyngeus within the oropharynx could exert unique physiological demands on these muscles and contribute to the region-dependent sensitivity of the palatopharyngeus to mutant A17 PABPN1 overexpression. Interestingly, overexpression of mutant A17 PABPN1 affected the muscles of the laryngopharynx in a different manner. While overexpression of wild-type

A10 PABPN1 increased myofiber size at all observed ages, no increase was observed upon overexpression of mutant A17 PABPN1, which could indicate that the alanine expansion in mutant A17 PABPN1 disrupts its ability to enhance growth. Muscles of the laryngopharynx are adversely affected in OPMD patients (Blakeley et al., 1968; Dayal and Freeman, 1976; Little and Perl, 1982; Montgomery and Lynch, 1971; Périé et al., 2006a), yet it is unknown whether oropharyngeal muscle growth is adversely affected with mutant PABPN1 expression in humans. Studies assessing oropharyngeal muscle growth in OPMD patients are needed to assess whether oropharyngeal muscles would also be viable therapeutic targets for treating OPMD-related dysphagia.

Because no direct assays for measuring pharyngeal swallow function were available, we utilized an established oral dysphagia model that analyzes lick rates (Lever et al., 2009; Lever et al., 2010) to indirectly assess the effects of aging and muscular dystrophy on pharyngeal function. We observed that both wild-type and A17-MUT mice developed dysphagia with age, however, muscle-specific overexpression of wild-type A10 PABPN1 protected against age-associated impairments in swallowing. Given that wild-type A10 PABPN1 overexpression protects against both age- and OPMD-dependent decreases in swallow function, as well as myofiber size, the development of therapies directed at modulating region-specific PABPN1 expression in dysphagic patients might be indicated.

We demonstrate that murine pharyngeal muscles exhibit unique phenotypes in response to aging and muscular dystrophy related to their location within the pharynx. The pronounced protective effects from muscle-specific wild-type A10 PABPN1 overexpression on pharyngeal muscle growth and swallow function emphasize the

integral role of pharyngeal muscles in swallow physiology. Additionally, our studies suggest mice are an excellent model organism in which to study molecular mechanisms underlying the changes in pharyngeal muscle physiology that occur with aging and disease. Given the availability of numerous mutant and transgenic mice, future studies addressing the molecular and cellular biology of pharyngeal muscle could lead to new therapeutic options for individuals suffering with dysphagia.

## 4.4 Figures

**Figure 4.4.1: Pharyngeal muscles of mice**

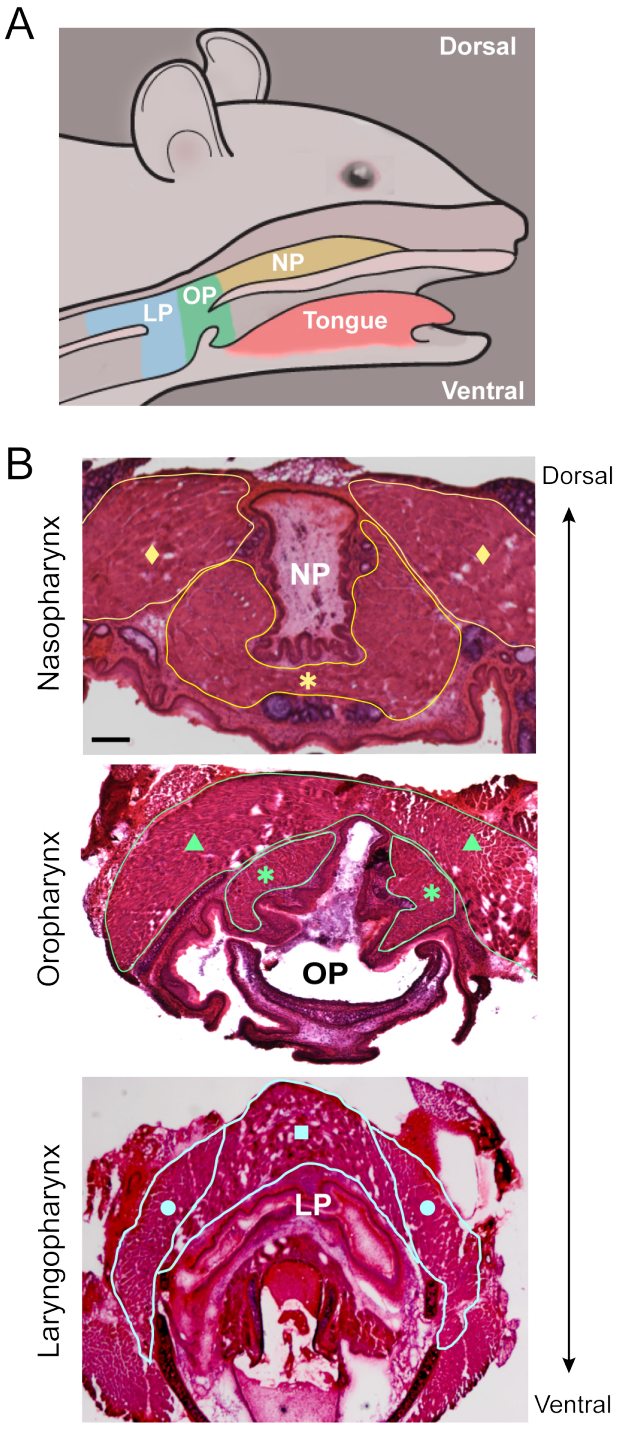

**Figure 4.4.1: Pharyngeal muscles of mice**

**(A)** Illustration of murine pharyngeal regions depicting the nasopharynx (NP) in yellow, the oropharynx (OP) in green, and the laryngopharynx (LP) in blue. **(B)** Representative histologic sections of murine pharyngeal tissue stained with hematoxylin and eosin (H&E). Pharyngeal muscles are outlined for identification. Representative images of the nasopharynx containing the superior pharyngeal constrictor (diamond) and palatopharyngeus (asterisk); the oropharynx containing the middle pharyngeal constrictor (triangle) and palatopharyngeus (asterisk); and the laryngopharynx containing the thyropharyngeus (circle) and cricopharyngeus (square) are shown. Bar: 250 μm.

**Figure 4.4.2: Pharyngeal muscles are composed of fast glycolytic myofibers but lack slow oxidative myofibers**

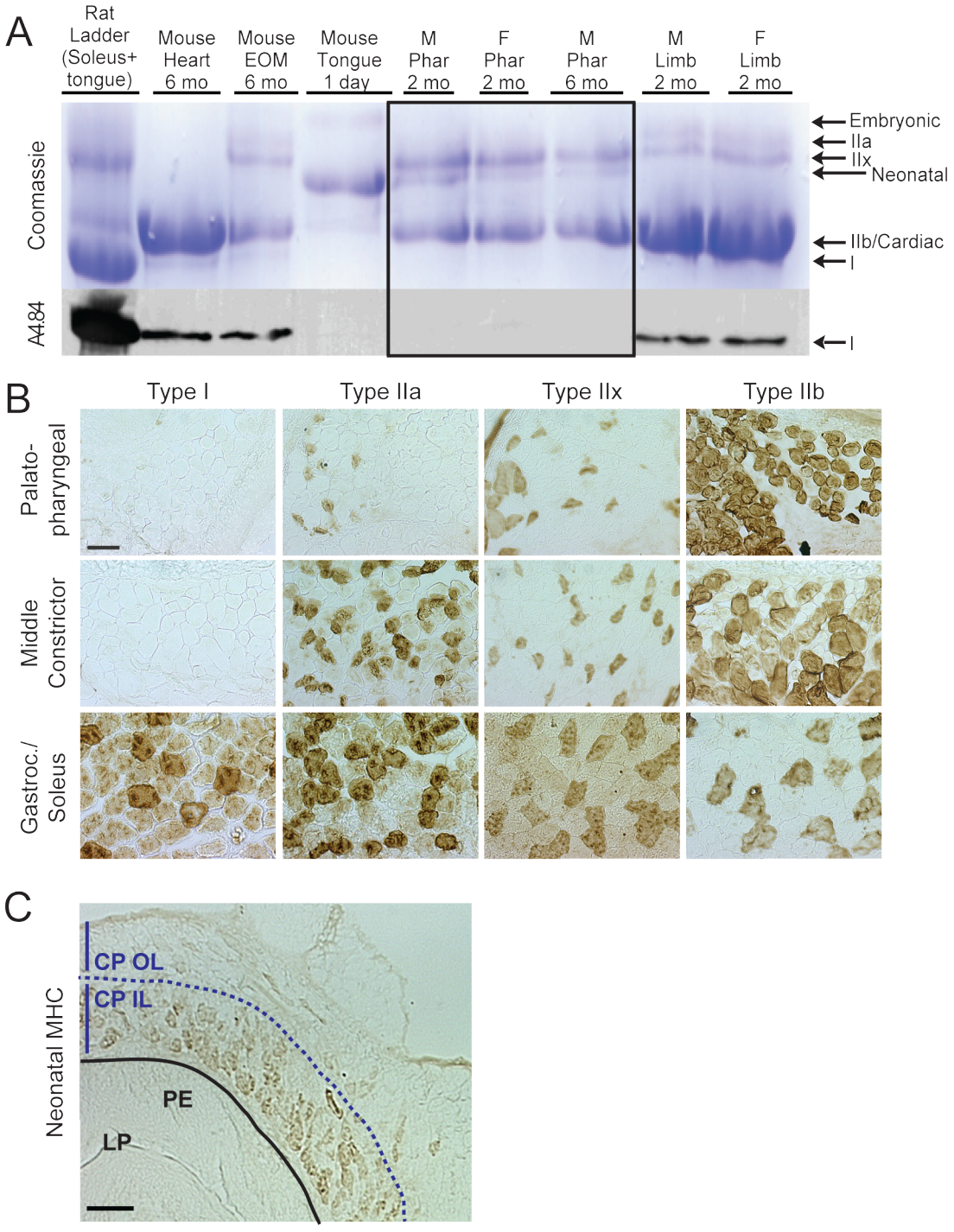

**Figure 4.4.2: Pharyngeal muscles are composed of fast glycolytic myofibers but lack slow oxidative myofibers**

**(A)** Myosin heavy chains (MHCs) were isolated from the indicated muscles, separated by gel electrophoresis and visualized with coomassie blue (top panel). The main MHCs present in pharyngeal muscles (Phar) (delineated within the black box) were Type IIb, IIx, and neonatal based on comigration with MHC standards from other muscles. No Type I MHC was observed in pharyngeal samples, which was confirmed by immunoblot analysis using the Type I MHC-specific antibody, A4.84 (bottom panel). EOM = extraocular muscle. M = male. F = female. n = 4 mice pooled per sample. **(B)** Pharyngeal muscle sections were immunostained with antibodies against Type I, IIa, IIx, and IIb MHCs. Representative sections from the palatopharyngeus and middle pharyngeal constrictor muscle are shown. Gastrocnemius (gastroc) and soleus muscles were used as positive controls. Bar: 50 $\mu$m. *n* = 3 mice, 2-3 months of age. **(C)** Representative image of neonatal MHC immunostaining of the cricopharyngeal muscle in the laryngopharynx marked with a dashed line to delineate the outer (CP OL) and inner (CP IL) layers of the muscle. PE = pharyngeal epithelium. LP = laryngopharynx. Bar: 100 μm. *n* = 3 male mice, 2-3 months of age.

**Figure 4.4.3: Regional differences in myofiber size occur with aging in pharyngeal muscles**

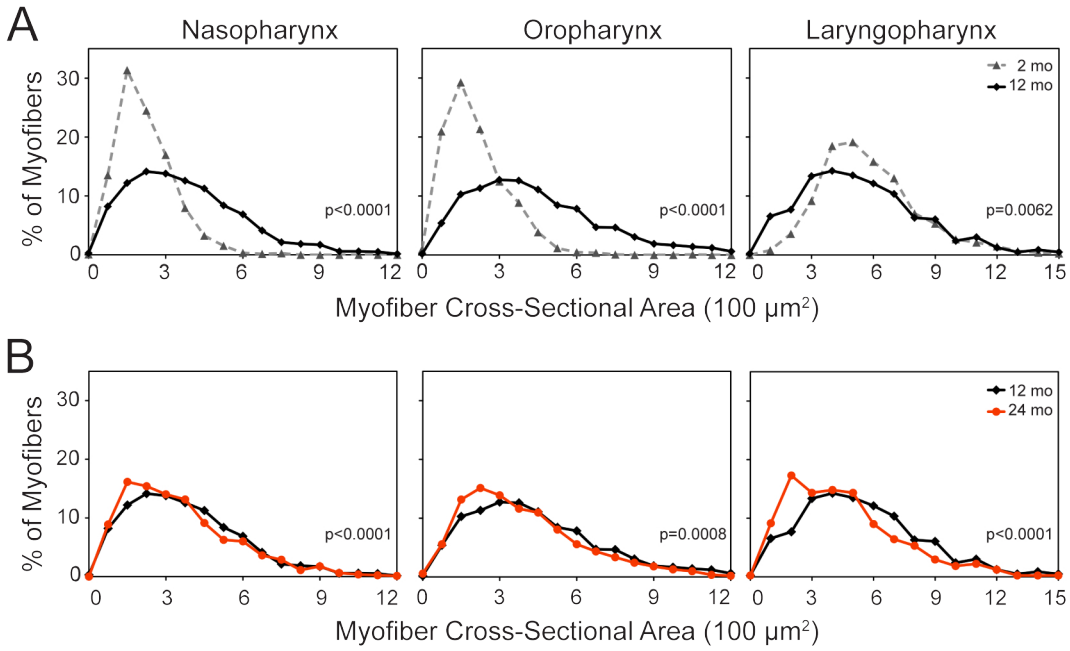

**Figure 4.4.3: Regional differences in myofiber size occur with aging in pharyngeal muscles**

Frequency distribution plots are shown for myofiber cross-sectional areas (CSA) from the naso-, oro-, and laryngopharyngeal regions of wild type FVB mice at 2, 12, or 24 months of age. **(A)** Myofiber CSA significantly increased from 2 to 12 months of age in the naso- and oropharynx but decreased in the laryngopharynx. *n* = 752-1943 myofibers, 3-4 mice per timepoint. **(B)** Myofiber CSA decreased from 12 to 24 months of age in all pharyngeal regions. Data from 12 months of age are shown again for comparison. *n* = 792-1943 myofibers, 4 mice per timepoint.

**Figure 4.4.4: Overexpression of wild-type A10 PABPN1 enhances muscle growth in only one region of the pharynx**

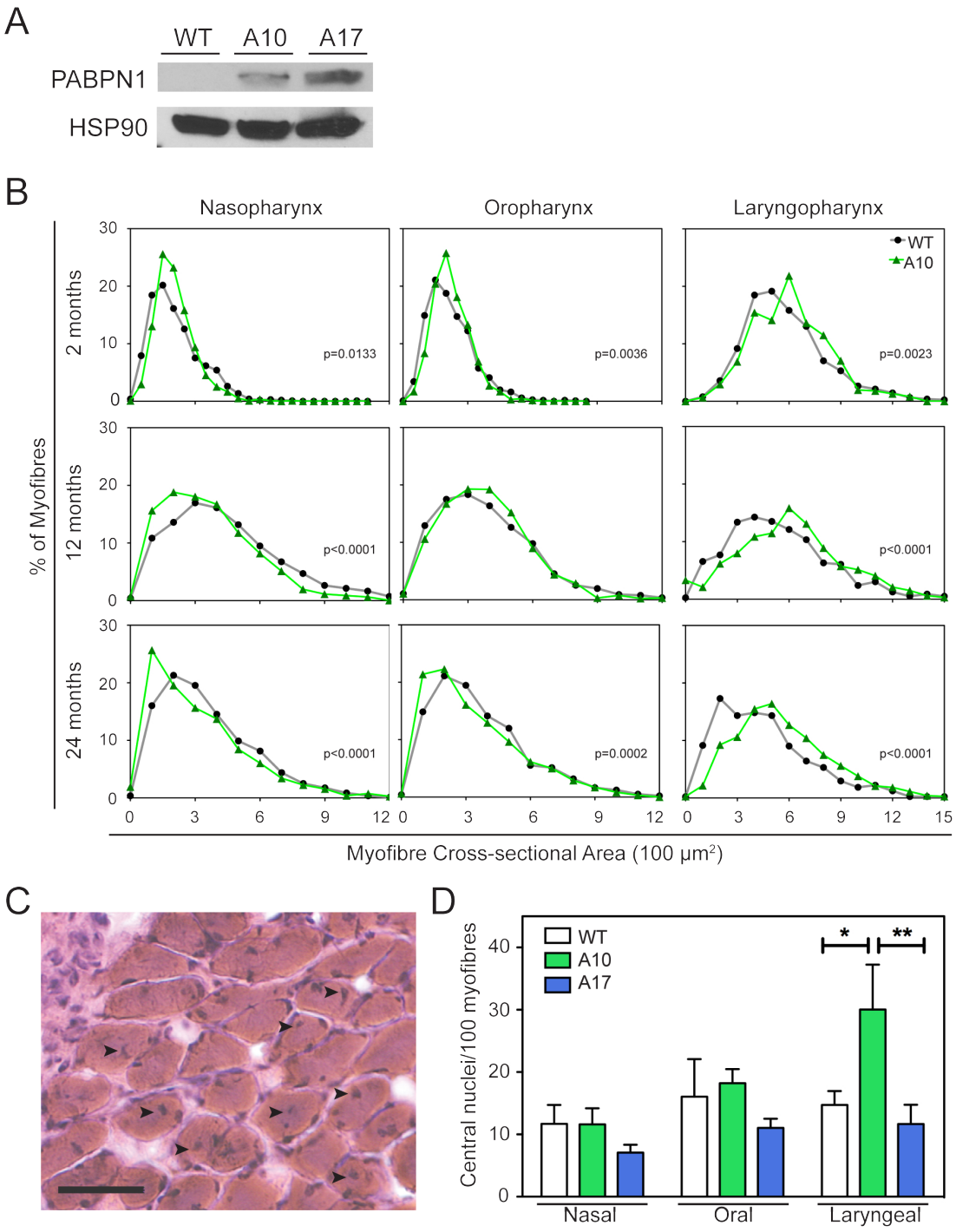

**Figure 4.4.4: Overexpression of wild-type A10 PABPN1 enhances muscle growth in only one region of the pharynx**

**(A)** Representative immunoblot of PABPN1 from pharyngeal muscle lysates of 2 month-old A10-WT, A17-MUT, and wild-type littermates. Lanes were loaded with 100 μg total protein. Heat shock protein 90 (HSP90) was used as a loading control. Data are representative of three independent experiments. (**B)** Frequency distribution plots are shown for myofiber cross-sectional areas (CSA) from the naso-, oro-, and laryngopharyngeal regions of wild-type (WT) and A10-WT mice at 2, 12, or 24 months of age. Data from wild-type mice in Figure 3 are shown again for comparison. At 2 months of age, overexpression of wild-type A10 PABPN1 significantly increased myofiber CSA in all three pharyngeal regions. At both 12 and 24 months of age, wild-type A10 PABPN1 overexpression only increased myofiber size in the laryngopharynx. *P* values are indicated in plots with significant differences in myofiber CSA. $n$ = 609-1943 myofibers; 3-5 mice per genotype and timepoint. **(C)** Representative H&E stained section of the inferior constrictor muscle located in the laryngopharyx of a wild-type 2-month-old mouse. Centrally located myonuclei (black arrowheads) are present in multiple myofibers. Bar: 50 μm. (**D)** Quantification of centrally located myonuclei within the nasal, oral, and laryngeal pharynxes of 2-month-old WT, A10-WT and A17-MUT mice. Centrally located myonuclei within A10-WT myofibers were significantly increased compared to wild-type (*P<0.05) or A17-MUT (**P<0.01) mice, but only in the laryngopharynx. Data are means ± S.E.M. from 752-1214 myofibers from 3 mice per genotype.

**Figure 4.4.5: Overexpression of 17-alanine-expanded PABPN1 is deleterious to myofiber size only in specific regions of the pharynx**

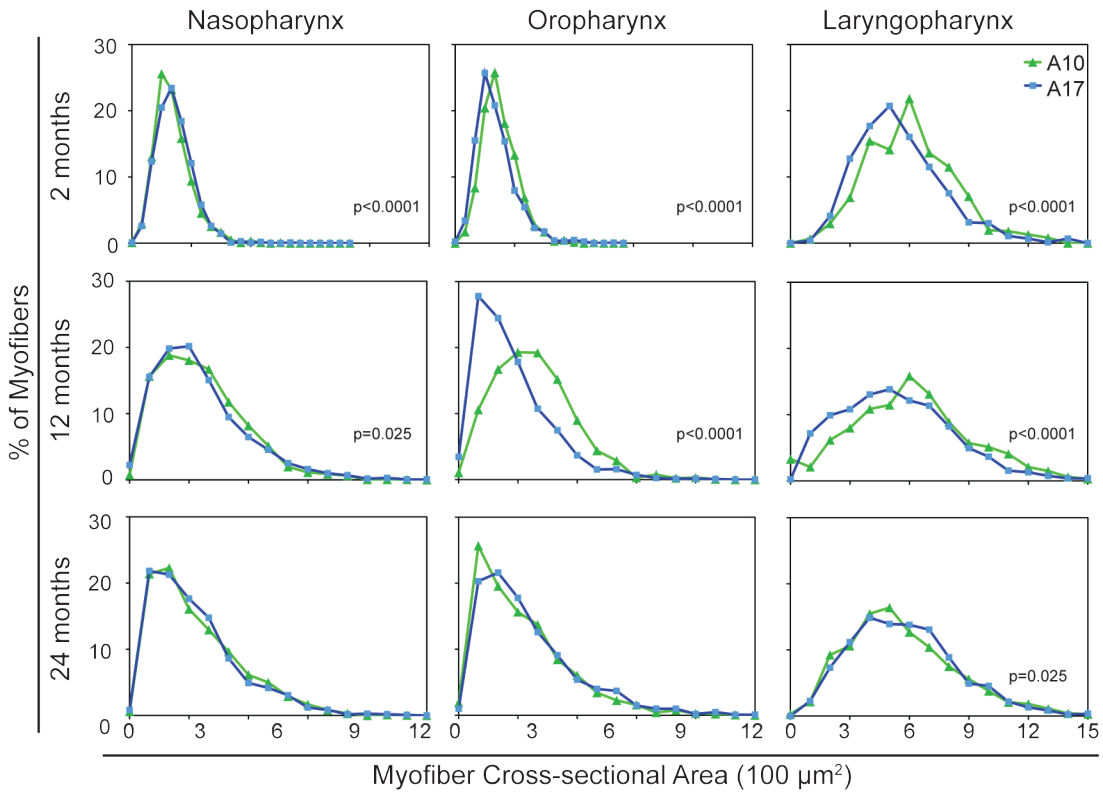

**Figure 4.4.5: Overexpression of 17-alanine-expanded PABPN1 is deleterious to myofiber size only in specific regions of the pharynx**

Frequency distribution plots are shown for myofiber cross-sectional areas (CSA) from the naso-, oro-, and laryngopharyngeal regions of A10-WT and A17-MUT mice at 2, 12, or 24 months of age. Data from A10-WT mice in Figure 4 are shown again for comparison. At 2 months of age, myofiber CSA majorly decreased in the laryngopharynx of A17-MUT mice while CSA minimally changed in the naso- and oropharynx. At 12 months of age, major decreases in A17-MUT myofiber CSA occurred in the oro- and laryngopharynx. A pronounced lack of growth occurred in the A17-MUT oropharynx from 2 to 12 months. At 24 months of age, no major differences in myofiber CSA were observed in any pharyngeal region. *P* values are indicated in plots with significant differences in myofiber CSA. $n$ = 609-2591 myofibers; 3-5 mice per genotype and timepoint.

**Figure 4.4.6: Overexpression of wild-type A10 PABPN1 protects against age and muscular dystrophy related dysphagia**

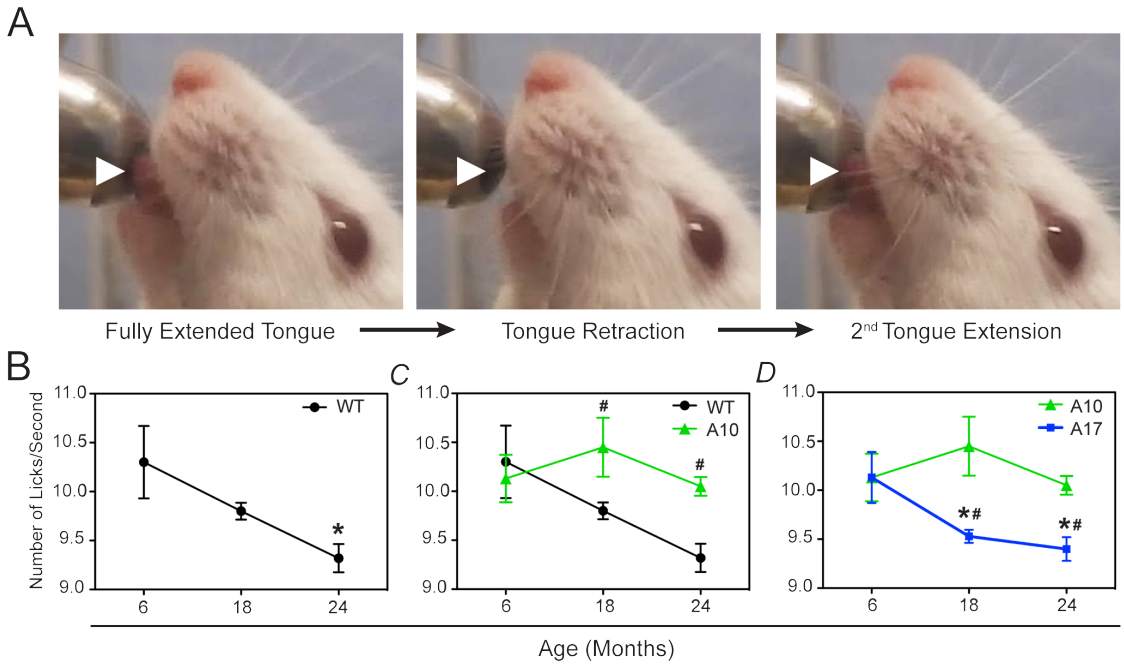

**Figure 4.4.6: Overexpression of wild-type A10 PABPN1 protects against age and muscular dystrophy related dysphagia**

**(A)** A single lick episode is depicted using still-frames from a representative lick assay video. White arrowheads highlight the extension and retraction of the tongue. **(B, C, D)** Quantification of lick rates of wild-type (WT), A10-WT, or A17-MUT mice at 6, 18, and 24 months of age. Data are means ± S.E.M. from 3-13 mice. **(B)** WT lick rates significantly decreased at 24 months of age (*P<0.05). **(C)** Overexpression of wild-type A10 PABPN1 provided a protective effect on lick rates at both 18 and 24 months of age ($^{\#}$P<0.05) when compared to wild-type mice at these timepoints. Data from wild-type and A10-WT mice. **(D)** Lick rates of A17-MUT mice significantly decreased at 18 and 24 months of age (*P<0.05) and were significantly impaired at these timepoints compared to A10-WT mice ($^{\#}$P<0.05).

# Chapter 5: Pharyngeal satellite cells undergo basal myogenesis and are required for pharyngeal muscle maintenance

**A portion of this chapter is submitted as:**

**Randolph, M. E.**, Phillips, B. L., Vest, K. E., Vera, Y., & Pavlath, G. K. (2015). Pharyngeal satellite cells undergo basal myogenesis and are required for pharyngeal muscle maintenance. *Manuscript under review.*

**Contributions:**

Elizabeth P. Andreas (Figure 5.4.1 illustration), Brittany L. Phillips (Figure 5.4.5 data, Table 5.5.1 data), Katherine E. Vest (Figures 5.4.6 data, 5.4.9 data).

# Chapter 5: Pharyngeal satellite cells undergo basal myogenesis and are required for pharyngeal muscle maintenance

## 5.1 Introduction

Muscular dystrophies are a group of degenerative muscle diseases that impair different subsets of skeletal muscles depending on the specific type of muscular dystrophy (Bione et al., 1994; Bonne et al., 1999; Brais et al., 1998; Godfrey et al., 2007; Hoffman et al., 1987; Monaco et al., 1988; Nonaka, 1999; Robinson et al., 2005). One muscle group differentially affected in muscular dystrophies is found in the pharynx. Pharyngeal muscles are a vital group of seven muscles involved in swallowing. They are non-somitic in origin, arising from the cranial mesoderm of the third and fourth pharyngeal arches in vertebrates (Mootoosamy and Dietrich, 2002; Noden and Francis-West, 2006). These muscles surround the nasal, oral, and laryngeal pharynxes and include the palatopharyngeus, stylopharyngeus, salpingopharyngeus, superior and middle pharyngeal constrictors, cricopharyngeus, and thyropharyngeus muscles (Donner et al., 1985; Dutta and Basmajian, 1960; Himmelreich, 1973; Miller, 2008; Randolph et al., 2014; Rubesin et al., 1987). One type of muscular dystrophy in which pharyngeal muscles are pathologically affected is oculopharyngeal muscular dystrophy (OPMD), a late onset autosomal dominant disease caused by a polyalanine expansion in the N-terminal domain of the ubiquitously expressed polyadenylate-binding protein nuclear 1 (PABPN1) protein (Brais et al., 1998; Little and Perl, 1982; Victor et al., 1962). Interestingly, the associated muscle stem cells of pharyngeal muscles are also pathologically affected in OPMD patients (Périé et al., 2006b).

Muscle stem cells, called satellite cells, are a heterogeneous cell population that are responsible for repair of muscle tissue (Relaix and Zammit, 2012). In limb skeletal muscle, satellite cells are mitotically quiescent under basal conditions (Relaix and Zammit, 2012). When muscle tissue is damaged or injured, satellite cells proliferate, differentiate, migrate, adhere and fuse to each other or existing myofibers to form multi-nucleated myofibers while a subset of satellite cells undergo self-renewal to maintain a quiescent stem cell population (Relaix and Zammit, 2012). Considering that pharyngeal satellite cells are altered in OPMD and that satellite cells in other skeletal muscles are thought to play a role in the pathology of muscle diseases such as Duchenne muscular dystrophy (Sacco et al., 2010), congenital muscular dystrophy 1A (Girgenrath et al., 2005), Emery-Dreifuss muscular dystrophy (Frock et al., 2006), and facioscapulohumeral muscular dystrophy (Barro et al., 2010; Winokur et al., 2003), we addressed whether pharyngeal satellite cells have unique biological properties that make them susceptible to disease-inducing conditions.

In this study, we analyzed the biologic properties of PSCs and their contribution to pharyngeal muscle maintenance. We characterized PSCs *in vivo* in a region-dependent manner: analyzing PSCs of the palatophayrngeus muscle (nasal and oral pharynx) along with the cricopharyngeal and thyropharyngeal muscles (laryngopharynx). Somite-derived satellite cells from limb muscles were used for comparison. We found that PSCs are distinct from limb satellite cells both transcriptionally and biologically. PSCs undergo constitutive myogenesis and, unlike limb satellite cells (Fry et al., 2015; Jackson et al., 2012; Lee et al., 2012; Lepper et al., 2009; McCarthy et al., 2011), are required to maintain myofiber size and myonuclear number in pharyngeal myofibers. Our findings

provide new insights into the biology of PSCs and pharyngeal muscles that may be important in understanding why certain muscular dystrophies target muscles of the pharynx.

## 5.2 Results

### Pharyngeal muscles contain larger numbers of satellite cells than limb in the absence of overt injury

To date, satellite cells of adult mouse pharyngeal muscles, which arise from the third and fourth pharyngeal arches during development, have not been studied, unlike satellite cells of muscles arising from the first and second pharyngeal arches (Ono et al., 2010; Pavlath et al., 1998; Sambasivan et al., 2009). Therefore, to gain insights into PSCs we initially analyzed their numbers in pharyngeal muscles. The pharynx can be subdivided into three distinct regions (nasal, oral, and laryngeal)(Fig. 5.4.1A). Each region and their associated muscles vary in both location and function. We recently reported that muscles within the nasal, oral, and laryngeal regions of the pharynx are differentially affected by aging and disease (Randolph et al., 2014). Therefore, all histologic studies were analyzed based on pharyngeal localization. To analyze satellite cell numbers throughout each region of the pharynx, we used a mouse model that expresses nuclear-localized β-galactosidase (β-gal) under the promoter of the endogenous myogenic transcription factor Myf5 (Myf5-nls-LacZ), which is commonly used to mark satellite cells within muscle tissues (Beauchamp et al., 2000; Cooper et al., 1999; Tajbakhsh et al., 1996). X-gal staining of limb and pharyngeal muscle sections from 3-5 month old mice (Fig. 5.4.1B) revealed significantly increased numbers of β-gal$^{+}$ cells (Fig. 5.4.1C), located at the periphery of myofibers throughout the oral and laryngeal pharynxes compared to limb muscle. When compared to limb, these data indicate that murine pharyngeal muscles possess increased satellite cell numbers and are consistent

with recent immunohistologic studies of human cricopharyngeal muscles (Gidaro et al., 2013).

We hypothesized that this increase in satellite cell number could be attributed to myofiber type or myofiber damage. Type 1, slow-twitch myofibers are associated with larger numbers of satellite cells than Type 2, fast-twitch myofibers (Ontell et al., 1984; Reimann et al., 2000). However, we recently reported that murine pharyngeal muscles are devoid of Type 1 myofibers (Randolph et al., 2014), thus, myofiber type likely does not account for the increased number of satellite cells in pharyngeal muscles. We then analyzed whether muscle damage was present in pharyngeal muscles, which would induce a regenerative response with increased satellite cell numbers. We observed no signs of myofiber degeneration in sections despite the fact that Myf5-nls-LacZ pharyngeal myofibers contained a high incidence of centrally located β-gal$^{+}$ myonuclei compared to limb muscles (Fig. 5.4.1D), suggestive of recent satellite cell fusion with myofibers (Cooper et al., 1999). To confirm that no overt myofiber damage was present, we injected mice with Evans Blue and muscle sections were analyzed for fluorescence. Damaged myofibers were identified by the presence of Evans Blue dye within the myofiber, as seen in mdx mice, which are characterized by damaged myofiber membranes due to the loss of dystrophin (Fig. 5.4.2). However, no Evans Blue positive myofibers were observed in any of the wild-type pharyngeal muscles examined (Fig. 5.4.2). Therefore, the increase in satellite cell number in pharyngeal muscles could not be attributed to myofiber damage, suggesting that alternative mechanisms are responsible for the increased satellite cell numbers and centrally located myonuclei present in pharyngeal muscles.

**Identification of pharyngeal satellite cells**

To gain further insights into the biology of pharyngeal satellite cells, we initially confirmed specific molecular markers that reliably identify these cells *in vivo*. Satellite cells in different muscles can be identified using multiple molecular markers (Asakura et al., 2002; Blanco-Bose et al., 2001; Cornelison et al., 2001; Fukada et al., 2007; Ikemoto et al., 2007; Kafadar et al., 2009; Sherwood et al., 2004; Tamaki et al., 2002), but such markers have not been validated for PSCs. Limb satellite cells (LSC) have previously been identified as cells expressing α7-integrin that are not of endothelial ($CD31^-$), hematopoietic ($CD45^-$), or fibro-adipogenic ($Sca1^-$) progenitor lineages ($CD31^-CD45^-Sca1^-$) (Kafadar et al., 2009). To validate whether these markers also identified PSCs, pharyngeal muscles were enzymatically dissociated to yield mononucleated cells. Analysis by flow cytometry revealed a distinct sub-population of lineage-negative ($CD31^-CD45^-Sca1^-$), α7-integrin expressing ($Lin^-$α7-$integrin^+$) cells present within pharyngeal tissue (Fig. 5.4.3A). To confirm the myogenic identity of pharyngeal $Lin^-$α7-$integrin^+$ cells, two different methods were used to confirm expression of Pax7, a transcription factor expressed by satellite cells (Seale et al., 2000)(Fig. 5.4.3B,C). First we stained FACS-sorted pharyngeal $Lin^-$α7-$integrin^+$ cells for Pax7 (Fig. 5.4.3B). Second, a tamoxifen-inducible Cre/LoxP system was utilized. Mice expressing a tamoxifen-inducible Cre recombinase under the endogenous *Pax7* promoter ($Pax7^{CreERTM}$) (Nishijo et al., 2009), were crossed with mice containing the floxed fluorescent reporter *Rosa26-tdTomato* allele (tdTom) (Madisen et al., 2010) to visualize satellite cells *in vivo*. Over 90% of pharyngeal $Lin^-$α7-$integrin^+$ cells from tamoxifen treated tdTom-$Pax7^{CreERTM}$ heterozygotes expressed tdTomato (Fig. 5.4.3C), further

confirming that Lin$^-$α7-integrin$^+$ labeling identifies Pax7$^+$ satellite cells from pharyngeal muscles.

**Pharyngeal satellite cells proliferate in the absence of induced injury**

Satellite cells of some craniofacial muscles, such as extraocular muscles, proliferate at a basal level in the absence of injury, in contrast to the quiescent phenotype of LSC (McLoon et al., 2007; McLoon and Wirtschafter, 2002a; McLoon and Wirtschafter, 2003; Stuelsatz et al., 2015). Considering that myofiber type and overt muscle injury did not explain the large number of PSCs or the centrally located myonuclei throughout the pharynx, we tested whether PSCs proliferate in the absence of induced injury. Bromodeoxyuridine (BrdU) assays were performed in both young and mature C57BL/6 mice to label proliferating cells. Mice received BrdU injections every twelve hours for two days (Fig. 5.4.4A). On day three, limb and pharyngeal muscles were collected, mononucleated cells isolated, and myogenic (Lin$^-$α7-integrin$^+$) cells analyzed via flow cytometry for evidence of BrdU labeling (Fig. 5.4.4B). At 2-5 months of age, we observed a trend towards increased satellite cell proliferation in the pharynx (Fig. 5.4.4C) and by 12 months of age the percentage of proliferating satellite cells was significantly increased by ~30-fold in pharyngeal muscle compared to limb (Fig. 5.4.4C). In sharp contrast to quiescent limb satellite cells, myogenic cells from pharyngeal muscle demonstrated robust proliferation in the absence of induced injury suggesting that basal satellite cell proliferation is a characteristic of pharyngeal muscles.

The basal proliferation of pharyngeal satellite cells could be in response to signals from the pharyngeal niche and/or an intrinsic property of PSCs. To examine whether the

proliferative SC phenotype in pharyngeal muscles was intrinsic to PSCs, satellite cells were isolated and sorted using Fluorescence Activated Cell Sorting (FACS) from both limb and pharyngeal muscles. Sorted myogenic cells were plated at clonal densities and grown for 8 days in the absence of the pharyngeal muscle niche. Cultures were then fixed and stained with hematoxylin to identify nuclei. We identified highly proliferative cells as clones that produced colonies numbering more than 300 cells. While the majority of pharyngeal clones were similar in size to those of the limb, 17% of pharyngeal colonies contained more than 300 cells, compared to only 6% of limb colonies (Fig. 5.4.4D). These data suggest that a highly proliferative subpopulation of PSCs exists in pharyngeal muscles under basal conditions, thus indicating that proliferation is an intrinsic property of some PSCs.

**Proliferating pharyngeal satellite cells progress through the myogenic lineage**

Following activation and proliferation, satellite cells typically progress through the myogenic lineage, contributing new myonuclei to muscle fibers (Relaix and Zammit, 2012). However, impaired differentiation (Ono et al., 2010) or cell death (Dupont-Versteegden et al., 1999) can prevent myogenic lineage progression. The increased incidence of centrally localized myonuclei in pharyngeal muscles (Fig. 5.4.4D) suggested that satellite cell fusion with myofibers does occur. To definitively test whether proliferating PSCs progressed through the myogenic lineage *in vivo*, proliferating cells were labeled with BrdU over a two-week period to allow for fusion of $BrdU^+$ cells into myofbers (Fig. 5.4.4E). During myogenic differentiation, satellite cells exit the cell cycle and are post-mitotic. Therefore, any $BrdU^+$ myonucleus located within a myofiber would

indicate recent fusion of a proliferating satellite cell. We analyzed pharyngeal muscle sections for the presence of $BrdU^{+}$ myonuclei within dystrophin immunostained myofibers (Fig. 5.4.4F). The number of intra-fiber $BrdU^{+}$ nuclei was significantly elevated in myofibers of the oral and laryngeal pharynxes relative to those within limb muscle (Fig. 5.4.4G). This result indicates that the proliferative satellite cells of pharyngeal muscles progress through the myogenic lineage and contribute new myonuclei to pharyngeal myofibers.

**Pharyngeal and limb satellite cells are transcriptionally distinct**

To address potential molecular mechanisms involved in the constitutive myogenesis of PSCs, we analyzed steady-state RNA levels of sorted $Lin^{-}\alpha7\text{-integrin}^{+}$ cells using both quantitative real-time PCR (qRT-PCR) and microarray. qRT-PCR was utilized to analyze transcript levels of several transcription factors involved in craniofacial muscle development and myogenesis. *Pax7, Myf5, MyoD, Myogenin, and Pitx2* transcripts were all decreased in PSCs (Fig. 5.4.5A) relative to LSCs, *Pax3* was not detected in PSCs, while *Tcf21* was expressed only in PSC (data not shown). These data demonstrate a unique transcription profile of myogenic regulatory factors in PSCs. Principal component analysis of microarray data revealed distinct expression profiles in pharyngeal versus limb satellite cells (Fig. 5.4.5B). Furthermore, the steady-state levels of 964 pharyngeal transcripts were differentially expressed by ≥1.5 fold. These included 478 up-regulated and 486 down-regulated transcripts (Appendix Table 1 and Fig. 5.4.5C). Consistent with our *in vivo* data, analysis of PSC transcripts revealed an enrichment of genes involved in regulation of cell proliferation (GO process: 0042127;

Fig. 5.4.5D). Interestingly, we found increased expression of several cytokine and chemokine transcripts in PSCs relative to limb, including *Lif*, *Ccl2*, *Ccl7*, *IL6*, and *IL6Ra*, all of which are involved in satellite cell proliferation and/or differentiation (Appendix Table 1) (Broholm et al., 2011; Griffin et al., 2010; Henningsen et al., 2011; Serrano et al., 2008; Spangenburg and Booth, 2002; Toth et al., 2011; Yahiaoui et al., 2008). qRT-PCR analysis confirmed increased expression of *Lif*, *Ccl2*, and *IL6* in PSCs relative to LSCs (Fig. 5.4.5E). Together, these data demonstrate that PSCs have a distinct molecular signature from those of limb muscles, which could contribute to their increased proliferation and myogenic lineage progression.

**Pharyngeal satellite cells are required to maintain myonuclear number in pharyngeal muscles**

Our data show that PSCs are transcriptionally distinct from LSCs, highly proliferative, and undergo myogenesis under basal conditions. Considering the continuous myonuclear addition occurring in pharyngeal muscles, myonuclear numbers within pharyngeal myofibers would be predicted to increase over time. To test this hypothesis, we isolated individual myofibers from both limb and pharyngeal muscles, stained myofibers with DAPI to visualize nuclei (Fig. 5.4.6A), and compared myonuclear numbers using three independent metrics (myofiber length, volume, and surface area) from mice at various ages. No increase of myonuclear number was observed across the studied age range (Fig. 5.4.6B-D). These data, in conjunction with the presence of a proliferative satellite cell population, suggest that pharyngeal muscles undergo active myonuclear turnover in the absence of induced injury. To directly test whether

myonuclear loss was occurring in pharyngeal myofibers, we crossed the Pax7$^{CreERTM}$ mouse with mice containing the floxed truncated diptheria toxin A-176 allele in the Rosa26 locus (DTA-Pax7$^{CreERTM}$) (Wu et al., 2006) to induce ablation of Pax7$^{+}$ satellite cells *in vivo* (Fig. 5.4.6E). When Pax7$^{+}$ cells were ablated following tamoxifen-induced expression of DTA, a 93% loss of Lin$^{-}$α7-integrin$^{+}$ cells was observed (Fig. 5.4.6F, Fig. 5.4.7). We hypothesized that removing ~93% of all satellite cells from pharyngeal muscles would severely impair myonuclear addition and, if myonuclear turnover were occurring in pharyngeal muscle, loss of myonuclei would be evident over time. Therefore, we collected pharyngeal muscles from DTA-Pax7$^{CreERTM}$ mice 4 months following treatment with either vehicle or tamoxifen (Fig. 5.4.6E). Muscle sections were labeled for dystrophin to identify pharyngeal myofibers and counterstained with DAPI to visualize myonuclei contained within myofibers. Myonuclear numbers were significantly decreased, compared to vehicle, in myofibers of the nasal pharynx but not the oral or laryngeal pharynxes (Fig. 5.4.6G). Myonuclear loss following satellite cell ablation suggests that Pax7$^{+}$ satellite cells are required to maintain myonuclear numbers in nasal pharyngeal muscles.

**Loss of pharyngeal satellite cells results in muscle atrophy but not fibrosis**

Muscle fibrosis can occur when satellite cells are impaired, such as in aged muscles or in satellite cell-ablated limb muscles following overload stress (Brack et al., 2007; Fry et al., 2014). Therefore, we tested whether fibrosis also occurred in the nasopharyngeal muscles of our satellite cell-ablated mice. Hematoxylin and eosin staining of nasal pharyngeal muscle sections revealed no obvious increase in extracellular

matrix (ECM) deposition in tamoxifen-treated mice compared to vehicle (Fig. 5.4.8A). These data were confirmed using fluorescently labeled wheat germ agglutinin to visualize *N*-acetyl-D-glucosamine glycosylated ECM proteins (Fig. 5.4.8B). No significant difference in wheat germ agglutin staining was observed between corresponding regions of the nasal pharynx of vehicle versus tamoxifen treated mice (Fig. 5.4.8C). These data demonstrate that satellite cell ablation does not cause fibrosis in pharyngeal muscles.

Interestingly, myonuclear loss has been associated with muscle atrophy resulting from various stimuli (Brack et al., 2005; Dupont-Versteegden et al., 1999; Hikida et al., 1997; Mitchell and Pavlath, 2004). Therefore, we tested whether satellite cell ablation, which resulted in myonuclear loss, also led to pharyngeal muscle atrophy. Pharyngeal muscle sections from tamoxifen treated DTA-Pax7$^{\mathbf{CreERTM}}$ mice (Fig. 5.4.6E) were stained with hematoxylin/eosin and myofiber cross-sectional areas from each pharyngeal region were measured. Myofiber size was significantly decreased in satellite cell-ablated muscles of the nasal pharynx versus DTA-Pax7$^{\mathrm{CreERTM}}$ mice injected with vehicle (Fig. 5.4.9). No change in myofiber size was observed in the oral pharynx while only a slight decrease in myofiber size occurred in laryngopharyngeal muscles (Fig. 5.4.9). Importantly, muscle atrophy correlated with myonuclear loss in the nasal pharynx. These data suggest that pharyngeal satellite cells are required to maintain myofiber size in pharyngeal muscles of both the nasal and laryngeal pharynx.

**5.3 Discussion**

Here we propose a novel role for satellite cells in the maintenance of pharyngeal muscles (Fig. 5.4.10). PSCs are transcriptionally distinct satellite cells that contribute new myonuclei to pharyngeal myofibers through constitutive myogenesis in the absence of injury. PSCs are required to maintain both pharyngeal myonuclear numbers and myofiber size, counteracting the results of active myonuclear turnover within pharyngeal muscles. As discussed below, these results give new insights into why pharyngeal muscles are affected in some muscular dystophies yet spared in others.

Our finding that PSCs proliferate under basal conditions in the absence of overt injury is in sharp contrast to the basal quiescence of satellite cells in adult limb skeletal muscles (Relaix and Zammit, 2012). Although previous groups have identified proliferative satellite cells in adult extraocular muscles (EOMs), only ~1% or less of EOM satellite cells proliferate under basal conditions compared to the ~30% of PSCs that proliferate in adult pharyngeal muscle (McLoon and Wirtschafter, 2002a; McLoon and Wirtschafter, 2003; Stuelsatz et al., 2015). However, a recent *in vivo* study of EOM satellite cells proposed that the proliferative phenotype observed was, in part, due to a specific highly proliferative subpopulation (Kallestad et al., 2011). Our *in vitro* clonal expansion data also suggest that a subpopulation of PSCs contributes to the robust proliferative phenotype observed in pharyngeal muscle. These results are in agreement with the fact that satellite cells are a heterogenous population with differences among cells in myogenic phenotypes (Alfaro et al., 2011; Ono et al., 2010; Rocheteau et al., 2012; Tanaka et al., 2009). PSCs are also distinct from limb satellite cells at the transcriptional level. Besides expressing a unique profile of myogenic regulatory factors,

PSCs also express unique chemokine/cytokines compared to LSCs. Interleukin-6, LIF, and monocyte chemoattractant protein-1 (MCP-1; CCL2), which were highly expressed in PSCs, all stimulate myoblast proliferation through autocrine and paracrine signaling (Broholm et al., 2011; Henningsen et al., 2011; Serrano et al., 2008; Spangenburg and Booth, 2002; Toth et al., 2011; Yahiaoui et al., 2008). This cytokine expression may drive the proliferative phenotype of PSCs. Potentially, myonuclear loss may also contribute to the proliferative phenotype of PSCs by directly or indirectly activating proliferative signaling pathways. For example, if nuclear material were expelled into the extracellular milleu during myonuclear turnover, nuclear molecules could induce signaling pathways, like the high-mobility group box 1 (HMGB1) and receptor for advanced glycation end-products (RAGE) pathway, that activate satellite cell proliferation (Riuzzi et al., 2012; Sims et al., 2010). The potential relationship between myonuclear turnover and pharyngeal satellite cell activation is an intriguing hypothesis that warrants investigation. Further studies are needed to determine the signaling pathways and mechanisms involved in PSC proliferation *in vivo*.

Proliferating PSCs also progress through the myogenic lineage and contribute new myonuclei to pharyngeal muscle fibers under basal conditions. To date, only one other group of muscles, the global and orbital regions of EOMs, exhibit a similar basal state of myonuclear addition (McLoon and Wirtschafter, 2002a; McLoon and Wirtschafter, 2003; McLoon and Wirtschafter, 2002b; Stuelsatz et al., 2015; Wirtschafter et al., 2004a). Of note, we found a correlation between satellite cell number and the incidence of satellite cell fusion with myofibers in a region-dependent manner in pharyngeal muscles. These results suggest that the increased levels of cell fusion in

specific pharyngeal regions are likely due to the presence of the large resident satellite cell population rather than an increased cellular propensity for fusion. Interestingly, fusion of PSCs into myofibers over a period of 16 months did not result in myonuclear accretion within pharyngeal myofibers. These findings suggested that a basal level of myonuclear loss or turnover occurs in pharyngeal muscles. To examine myonuclear turnover more directly, we ablated satellite cells *in vivo* and examined myonuclear numbers using pharyngeal muscle sections. In contrast to recent studies where satellite cell ablation did not alter myonuclear numbers in non-injured limb muscles (Jackson et al., 2012; Lee et al., 2012), decreased numbers of myonuclei were observed in satellite cell-ablated muscles of the nasal pharynx. Together these data suggest that maintenance of myonuclear numbers is dependent on basal satellite cell myogenesis in pharyngeal muscles, and for the first time demonstrate myonuclear loss occurring in the absence of associated injury, disease or aging in skeletal muscle.

We also analyzed the functional outcomes of PSC ablation. A decrease in myofiber size was associated with myonuclear loss in nasopharyngeal muscles, suggesting that constitutive myonuclear addition is required to maintain nasopharyngeal muscle size. However, a slight decrease in myofiber size was also found in laryngopharyngeal muscles but in the absence of significant changes in myonuclear number. Interestingly, the muscles of the laryngopharynx possess the largest numbers of satellite cells of all the pharyngeal muscles examined. Despite loss of over 90% of PSCs from these muscles, satellite cell numbers may have remained above a critical threshold leading to maintenance of myonuclear numbers in this region. The decrease in myofiber size in this region may have resulted from altered paracrine signaling between PSC and

laryngopharyngeal myofibers. Another functional role of satellite cells in limb muscles involves maintenance of the extracellular mileu (Fry et al., 2014). Interestingly, we found no fibrotic changes associated with satellite cell ablation in pharyngeal muscles, suggesting that PSCs may play less of a role in extracellular matrix maintenance than recently proposed for LSCs. In limb skeletal muscles, satellite cells are not required for maintenance of muscle size or myonuclear number in sedentary mice (Fry et al., 2015; Jackson et al., 2012; Lee et al., 2012; Lepper et al., 2009; McCarthy et al., 2011). However, our data provide evidence that satellite cells are required for maintenance of myofiber size in pharyngeal muscles and suggest that the rate of myonuclear turnover within a muscle determines whether or not the associated satellite cells are required for muscle maintenance.

To date, aging (Brack et al., 2005), muscle atrophy (Hikida et al., 1997), and muscular dystrophy (Mittelbronn et al., 2008) are the major processes associated with decreases in myonuclear number, yet the molecular mechanisms that regulate myonuclear turnover remain unclear. Several groups have suggested myonuclear loss occurs in limb and extraocular muscles by apoptosis as assessed using terminal deoxynucleotidyl transferase dUTP nick-end labeling (TUNEL) assays or caspase staining (Adhihetty et al., 2007; Dupont-Versteegden et al., 1999; McLoon et al., 2004). However TUNEL staining identifies DNA damage in the context of apoptosis but also necrosis and autolytic cell death pathways (Grasl-Kraupp et al., 1995). Alternate mechanisms such as nuclear autophagy (Mijaljica et al., 2010; Park et al., 2009) or even myonuclear extrusion (Runge et al., 2000) could also contribute to myonuclear turnover. Further studies are

needed to elucidate the mechanisms by which myonuclear loss occurs in pharyngeal muscles as well as why myonuclear loss occurs in these muscles.

We recently reported that both aging and disease differentially affect pharyngeal muscles dependent on their regional location within the pharynx (Randolph et al., 2014). Here we show PSCs also display differential phenotypes depending on the associated muscle and its location within the pharynx. For example, the palatopharyngeus muscle extends between the nasal and oral pharynxes, yet differs in both structure and function depending on its regional location within the pharynx (Randolph et al., 2014). Interestingly, in the nasal pharynx, the palatopharyngeus consistently demonstrated the lowest number of both satellite cells and fusion of all the pharyngeal regions examined. Additionally, the nasal palatopharyngeus was sensitive to satellite cell ablation as both myonuclear loss and decreased myofiber size occurred. This was in contrast to the palatopharyngeus of the oral pharynx, which had larger numbers of PSCs and fusion yet demonstrated a resistance to functional changes associated with satellite cell ablation. Additionally, PSC number and fusion were greatly increased in the cricopharyngeal and thyropharyngeal muscles of the laryngeal pharynx compared to other regions of the pharynx. Together, these data suggest that differences in regional location and physiological function of pharyngeal muscles also contribute to the unique properties of PSCs.

Our results may provide insights into why pharyngeal muscles are affected in some muscular dystrophies yet spared in others. Considering the requirement of PSCs in maintenance of pharyngeal myofiber size, mutations or conditions that adversely affect PSC numbers, proliferation, differentiation, or fusion could negatively impact pharyngeal

muscle function. We recently observed a significant decrease in lick rates, indicative of swallowing difficulties, in a mouse model of OPMD that correlated with decreases in central myonuclear localization in pharyngeal muscles, suggesting myonuclear addition was negatively affected (Randolph et al., 2014). Additionally, some disease-causing mutations could enhance myonuclear turnover in pharyngeal muscles to such an extent that PSCs could no longer adequately supply enough myonuclei to maintain homeostasis. Aging also adversely affects pharyngeal function, resulting in impaired swallowing in 11-16% of the elderly population (Holland et al., 2011; Kawashima et al., 2004). Impairment of satellite cell function with aging (Brack and Rando, 2007) could contribute to this age-related increase in swallowing disorders. Further studies addressing the effects of disease and aging on both pharyngeal satellite cells and pharyngeal myonuclear turnover are warranted and could lead to new therapeutics for individuals suffering from pharyngeal myopathies.

## 5.4 Figures

**Figure 5.4.1: Pharyngeal muscles contain a larger number of satellite cells than limb muscle**

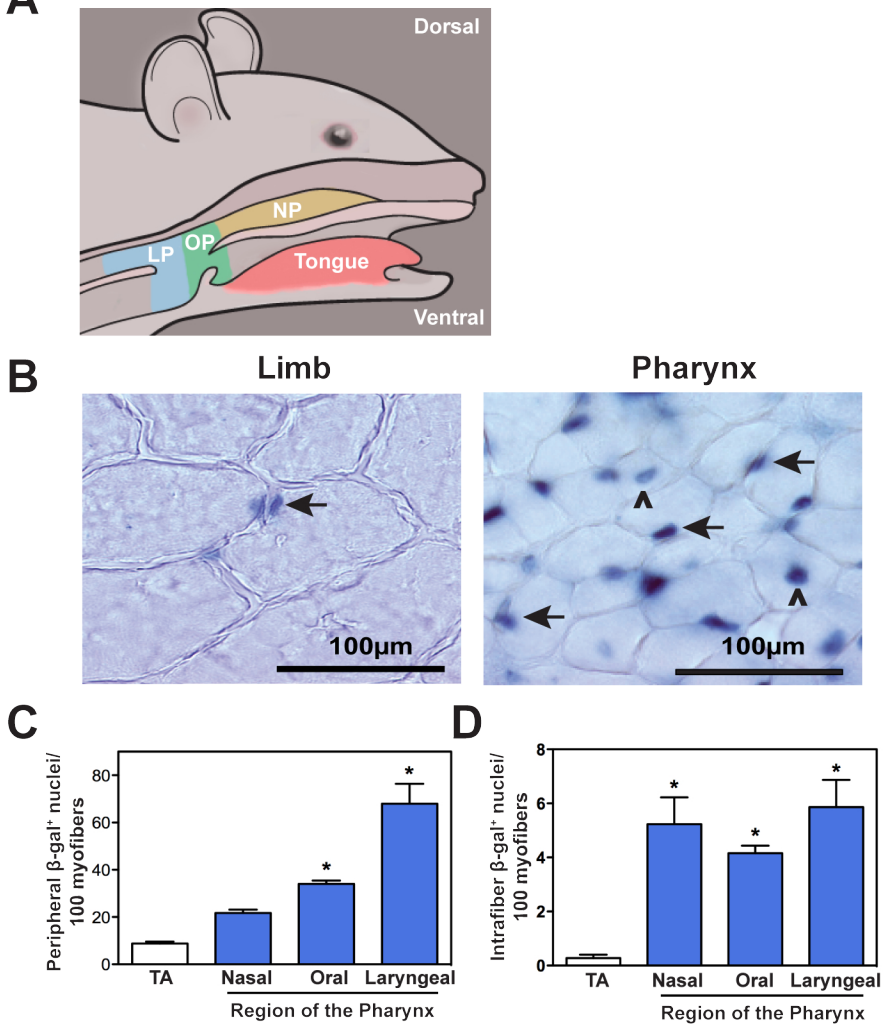

**Figure 5.4.1: Pharyngeal muscles contain a larger number of satellite cells than limb muscle**

**(A)** Schematic of murine pharyngeal regions: NP = nasal pharynx; OP = oral pharynx; LP = laryngopharynx. (Modified from Randolph *et al.*, 2014.) **(B)** Limb (tibialis anterior) and pharyngeal muscles were collected at nine weeks of age from Myf5-nlacZ mice, sectioned, and incubated with X-gal to identify β-gal$^{+}$ nuclei (blue). Representative muscle sections from limb and oral pharynx (palatopharyngeus) are shown. Two types of β-gal$^{+}$ nuclei were observed: peripherally located to myofibers (arrows) or centrally located within myofibers (∧). **(C)** Each pharyngeal region contained increased numbers of peripherally located β-gal$^{+}$ nuclei (satellite cells) versus limb muscle. **(D)** Increased numbers of centrally localized β-gal$^{+}$ myonuclei in myofibers were also observed in each pharyngeal region relative to limb muscle. Data represent the mean ± SEM. *$P < 0.05$. n=4 mice. TA= tibialis anterior muscle.

**Figure 5.4.2: No overt myofiber damage is present in pharyngeal muscle**

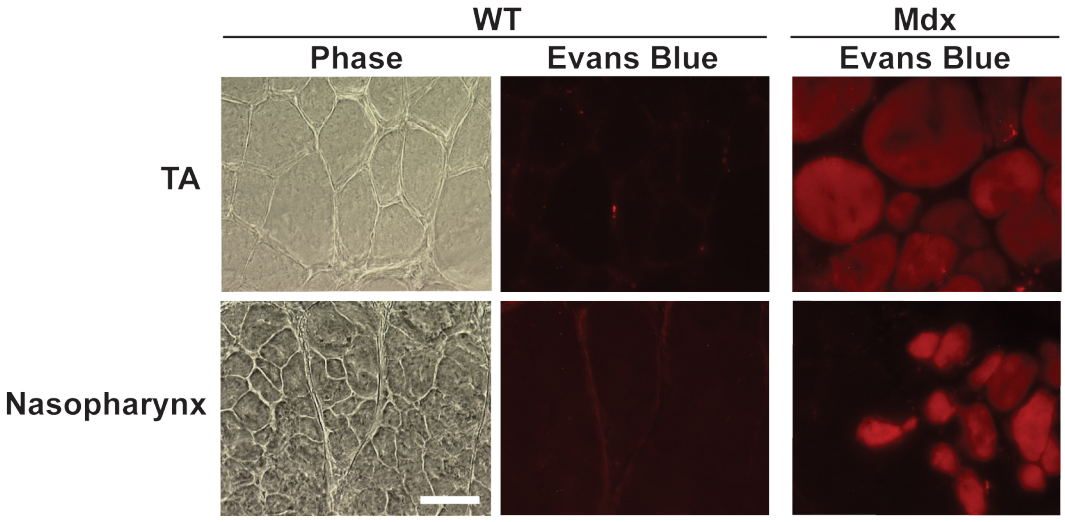

**Figure 5.4.2: No overt myofiber damage is present in pharyngeal muscle**

Mice were injected with Evans Blue solution to identify overt myofiber damage. Limb (tibialis anterior) and pharyngeal muscles were collected 24 hours post-injection. Immunofluorescence of Evans Blue dye (red) was not observed in pharyngeal myofibers, regardless of region. Dystrophin-deficient *mdx* mice were used as positive controls for Evans Blue fluorescence. n=5 wild-type mice, 3 *mdx* mice.

**Figure 5.4.3: Identification of pharyngeal satellite cells using established cellular markers for limb satellite cells**

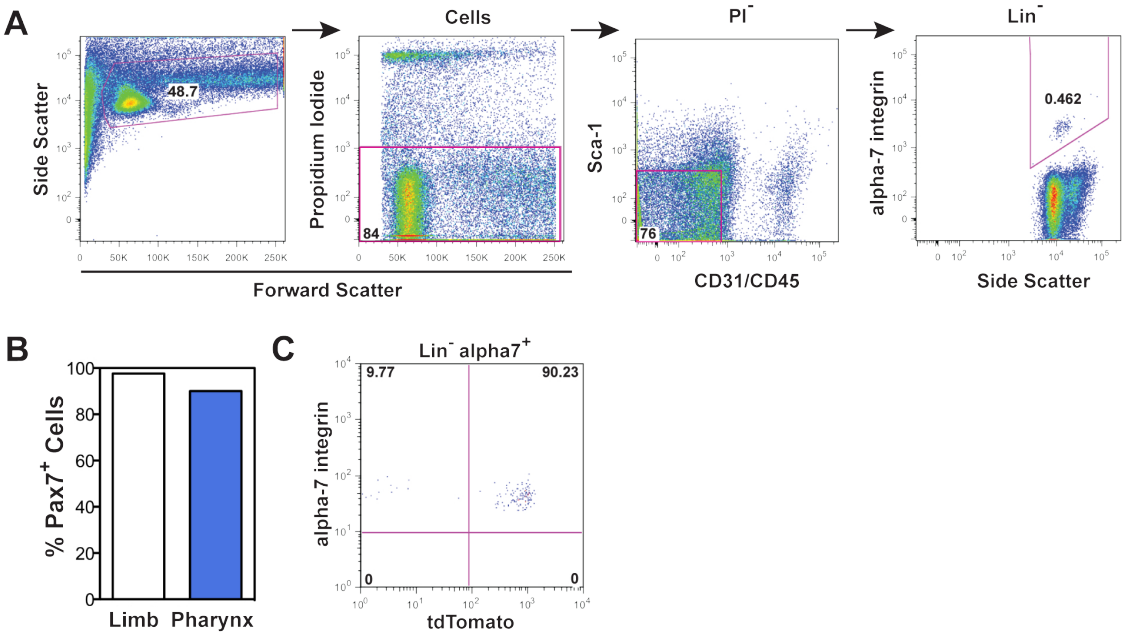

**Figure 5.4.3: Identification of pharyngeal satellite cells using established cellular markers for limb satellite cells**

**(A)** Flow cytometry gating to identify and sort satellite cells isolated from pharyngeal muscle. Pharyngeal satellite cells were identified as α7-integrin$^{+}$ cells not derived from endothelial (CD31), hematopoietic (CD45), or fibro-adipogenic progenitor (Sca1) lineages (Lin$^{-}$alpha7$^{+}$). **(B)** Lin$^{-}$alpha7$^{+}$ cells were sorted and Pax7 expression determined *in vitro* using immunofluorescence. n=10 mice pooled. **(C)** Approximately 90% of pharyngeal Lin$^{-}$α7-Integrin$^{+}$ cells were tdTomato$^{+}$ following tamoxifen-treatment of *Pax7*$^{CreERTM}$*/Rosa*$^{tdTomato}$ heterozyotes. n=2 experiments of 2-3 mice pooled. PI = propidium iodide.

**Figure 5.4.4: Pharyngeal satellite cells proliferate and fuse with pharyngeal myofibers in the absence of induced injury**

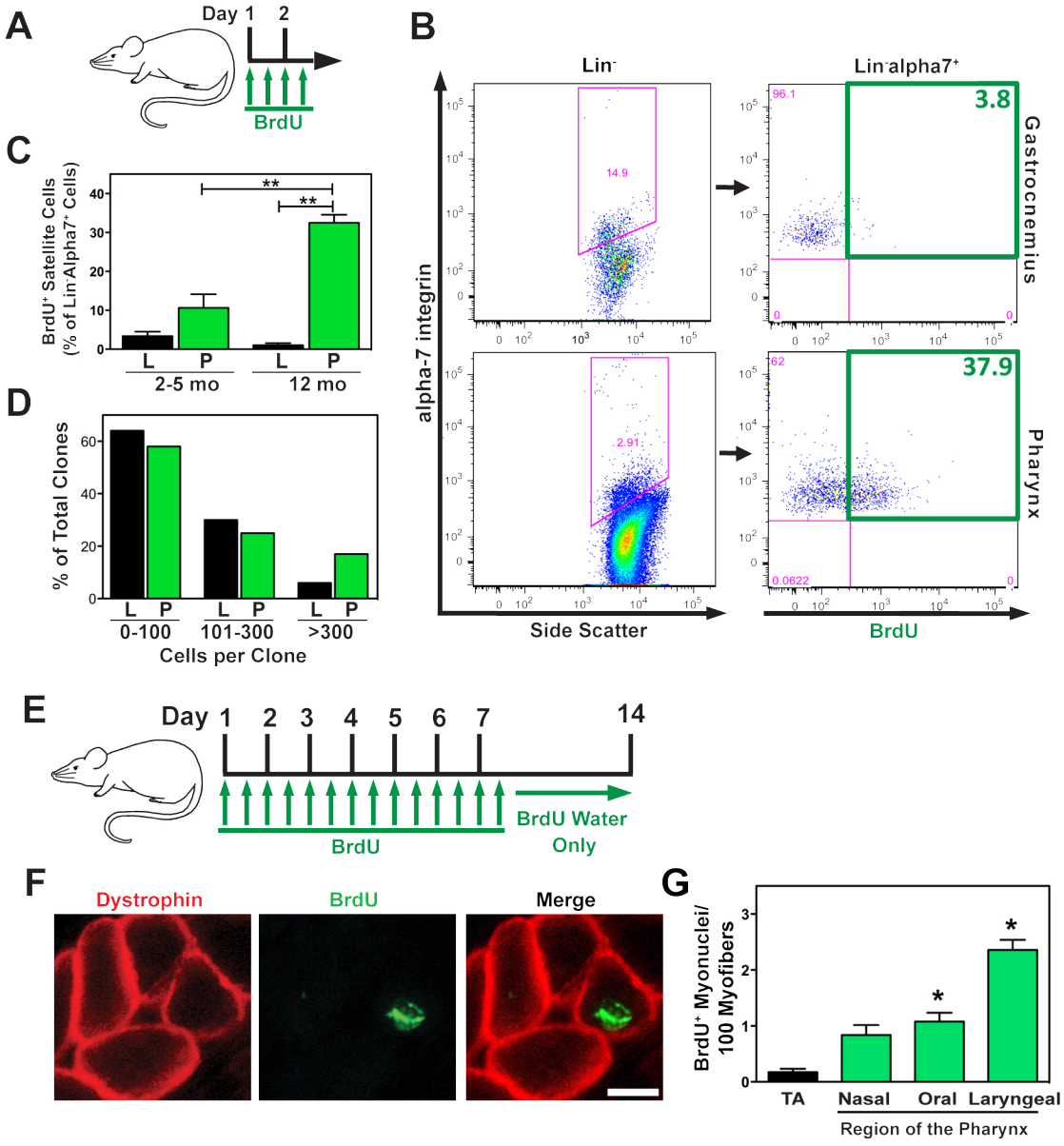

**Figure 5.4.4: Pharyngeal satellite cells proliferate and fuse with pharyngeal myofibers in the absence of induced injury**

**(A)** Schematic of BrdU treatment protocol. **(B)** $PI^-CD31^-CD45^-Sca1^-\alpha7\text{-}Integrin^+$ ($Lin^-$ $alpha7^+$) satellite cells were identified using flow cytometry (left column) and analyzed to determine the percentage of proliferating satellite cells ($BrdU^+$) in each tissue (right column). n=3 mice pooled. **(C)** Quantification of $BrdU^+$ $Lin^-alpha7^+$ cells demonstrated a significantly larger proliferating population of satellite cells in pharyngeal versus limb (gastrocnemius) muscles. Data represent the mean ± SEM. **P< 0.0001, n=3 experiments, 3-5 mice per experiment. **(D)** $Lin^-alpha7^+$ cells from either limb (gastrocnemius/quadriceps) or pharyngeal muscles were sorted, plated at clonal densities and cultured for 8 days. Cultures were then fixed and stained with hematoxylin for quantification of cell number per clone. The number of large clones (>300 cells) was increased three-fold in pharyngeal versus limb cultures. n=2 experiments, 105-159 clones. **(E)** Schematic of BrdU treatment protocol. **(F)** Muscle sections were immunostained for dystrophin (red) and BrdU (Bonne et al.). $BrdU^+$ nuclei contained within a $dystrophin^+$ myofiber outline represent satellite cells that recently proliferated and fused into myofibers. **(G)** Satellite cell fusion was quantified as the number of intrafiber $BrdU^+$ nuclei per 100 myofibers. Satellite cell fusion occurred with higher frequency in pharyngeal muscles compared to limb muscles. *P< 0.05, n=4 mice. L=limb. P=pharynx. TA=tibialis anterior.

**Figure 5.4.5: Comparative transcriptome analyses reveal pharyngeal and limb satellite cells are distinct**

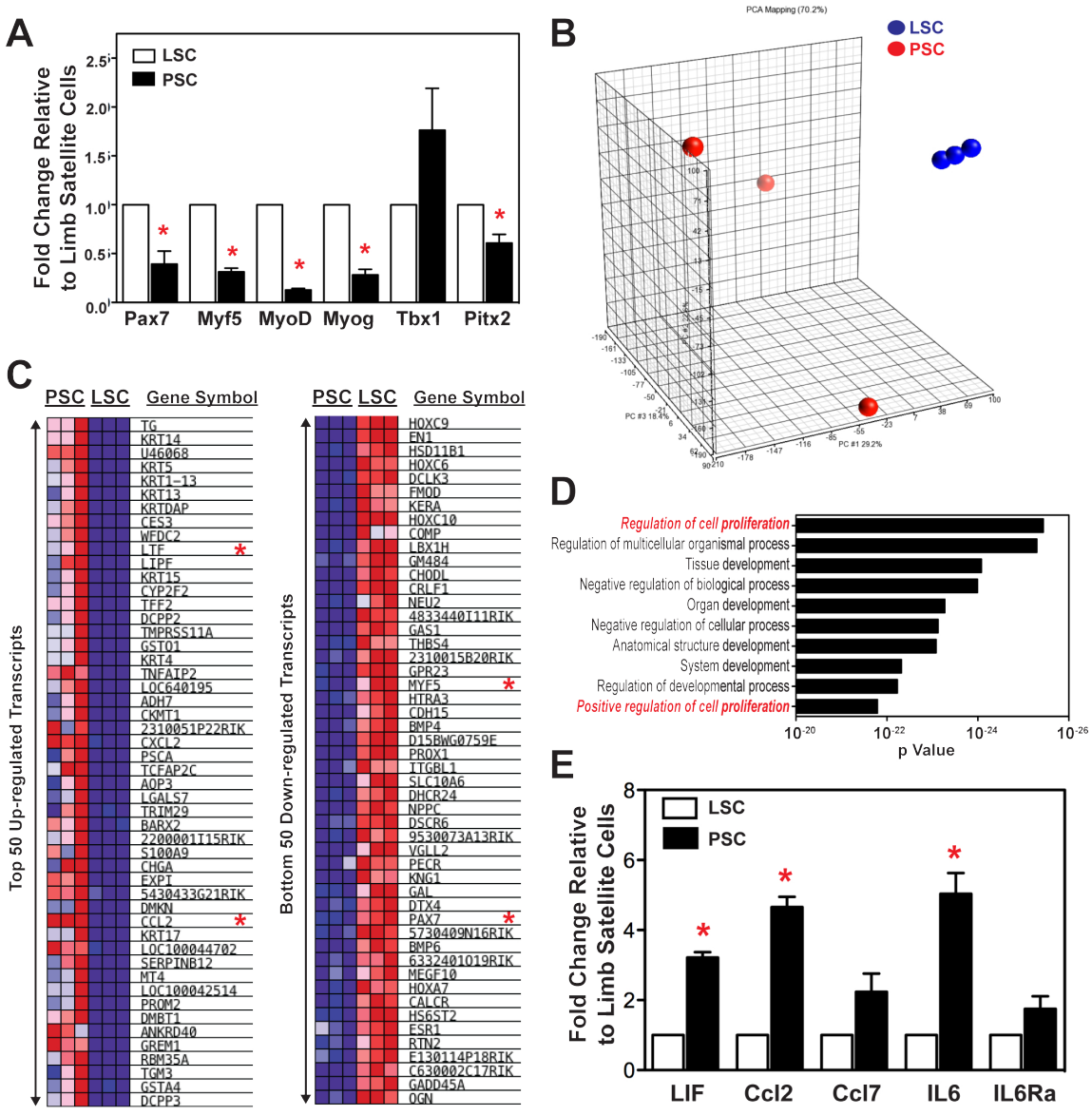

**Figure 5.4.5: Comparative transcriptome analyses reveal pharyngeal and limb satellite cells are distinct**

Gene-expression analyses of FACS sorted pharyngeal and limb satellite cells as determined by qRT-PCR **(A,E)** and microarray **(B-D)**. **(A)** Selected regulatory transcripts involved in myogenesis were analyzed via qRT-PCR using RNA isolated from FACS sorted PSCs and LSCs. Data represent the mean fold-change of transcript steady-state levels ± SEM. n=3 experiments each containing 150,000-200,000 satellite cells pooled from 10-30 mice. *P<0.05. **(B)** Principal component analysis (PCA) of pharyngeal satellite cells (PSC, red dots) versus limb (gastrocnemius/quadriceps) satellite cells (LSC, blue dots). PCA coordinates (PC1, 29.2%; PC2, 22.6%; and PC3, 18.4%) revealed a total data variation of 70.2%. n=3 experiments each containing 200,000 satellite cells pooled from 10-30 mice. **(C)** Heat maps comparing the levels of the top 50 transcripts either up- or down-regulated in PSCs relative to LSCs. Steady-state RNA levels are represented with a linear color scale ranging from dark red (enriched) to dark blue (depleted). Transcripts marked with red asterisks were validated by qRT-PCR. **(D)** Gene ontology (GO) process networks enriched in PSCs generated with MetaCore Genego software. GO networks related to cell proliferation are highlighted in red. **(E)** qRT-PCR was used to validate microarray data of selected cytokine/chemokine transcripts that were enriched in PSCs relative to LSCs. Data represent the mean fold-change of transcript steady-state levels ± SEM. n=3 limb and 4-5 pharyngeal experiments each containing 1500,000-200,000 satellite cells pooled from 10-30 mice. *P<0.05.

**Figure 5.4.6: Myonuclear turnover occurs in pharyngeal muscle under basal conditions**

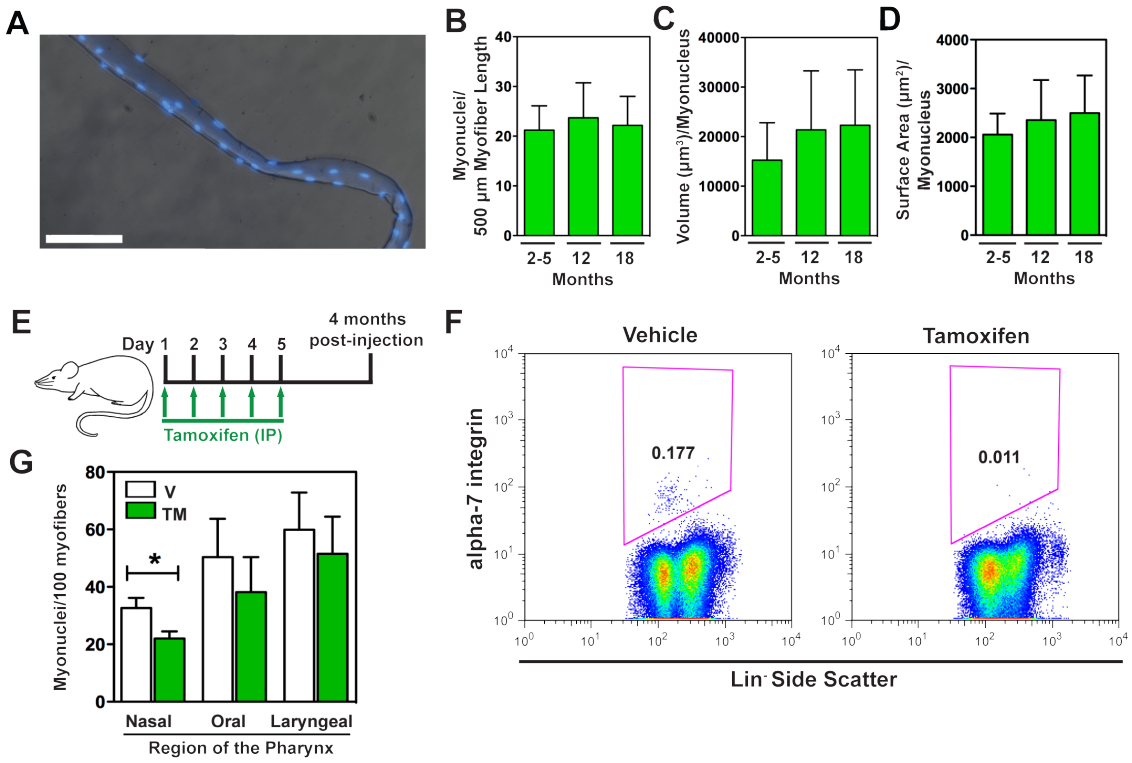

**Figure 5.4.6: Myonuclear turnover occurs in pharyngeal muscle under basal conditions**

**(A)** Merged DAPI and phase contrast images of a representative myofiber isolated from pharyngeal muscles. Bar=50μm. **(B-D)** Quantification of various pharyngeal myonuclear parameters indicated no change in myonuclear numbers with age. n=26-35 fibers per timepoint. **(E)** Schematic of satellite cell-specific ablation in *Pax7*$^{CreERTM}$/*Rosa*$^{DTA\text{-}176}$ heterozygous mice. **(F)** Pharyngeal Lin$^{-}$α7-Integrin$^{+}$ cells were ablated following tamoxifen-treatment of *Pax7*$^{CreERTM}$/*Rosa*$^{DTA\text{-}176}$ (DTA/Pax7$^{\text{CreERTM}}$) heterozygotes. Ablation efficiencies for pharyngeal Lin$^{-}$alpha7$^{+}$ cells ranged from 87-97%. n=8 experiments of 2-3 mice pooled. **(G)** Quantification of DAPI$^{+}$ nuclei contained within dystrophin$^{+}$ myofiber outlines revealed myonuclear loss within satellite cell-ablated muscles of the nasal pharynx. *P<0.05, n=3-4 mice per condition.

**Figure 5.4.7: Maintenance of satellite cell ablation in *Pax7*$^{CreERTM}$/*Rosa*$^{DTA-176}$ heterozygotes**

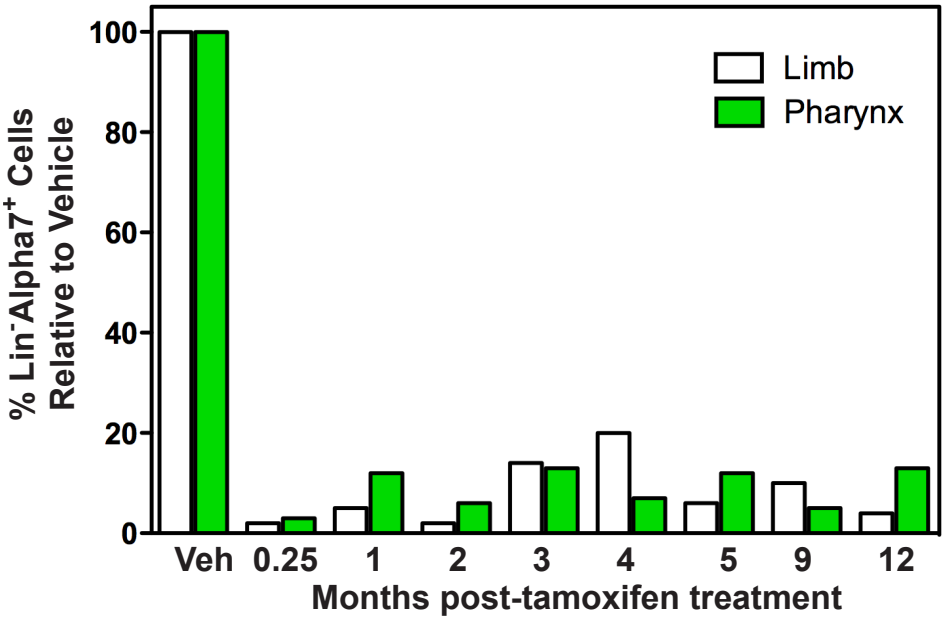

**Figure 5.4.7: Maintenance of satellite cell ablation in *Pax7$^{CreERTM}$/Rosa$^{DTA-176}$* heterozygotes**

DTA/Pax7$^{CreERTM}$ mice received either vehicle or tamoxifen injections as described in Fig. 5.4.6E. Pharyngeal muscles were digested and mononuclear cells analyzed via flow cytometry. The percentage of Lin$^-$alpha7$^+$ cells in tamxoifen versus vehicle treated mice is shown for various timepoints post-injection. On average 93% of PSCs were ablated in pharyngeal muscles with tamoxifen treatment. n= 50,000-100,000 cells pooled from 2-3 mice per condition per timepoint.

**Figure 5.4.8: No evidence of fibrosis in nasopharyngeal muscles 4 months post-satellite cell ablation**

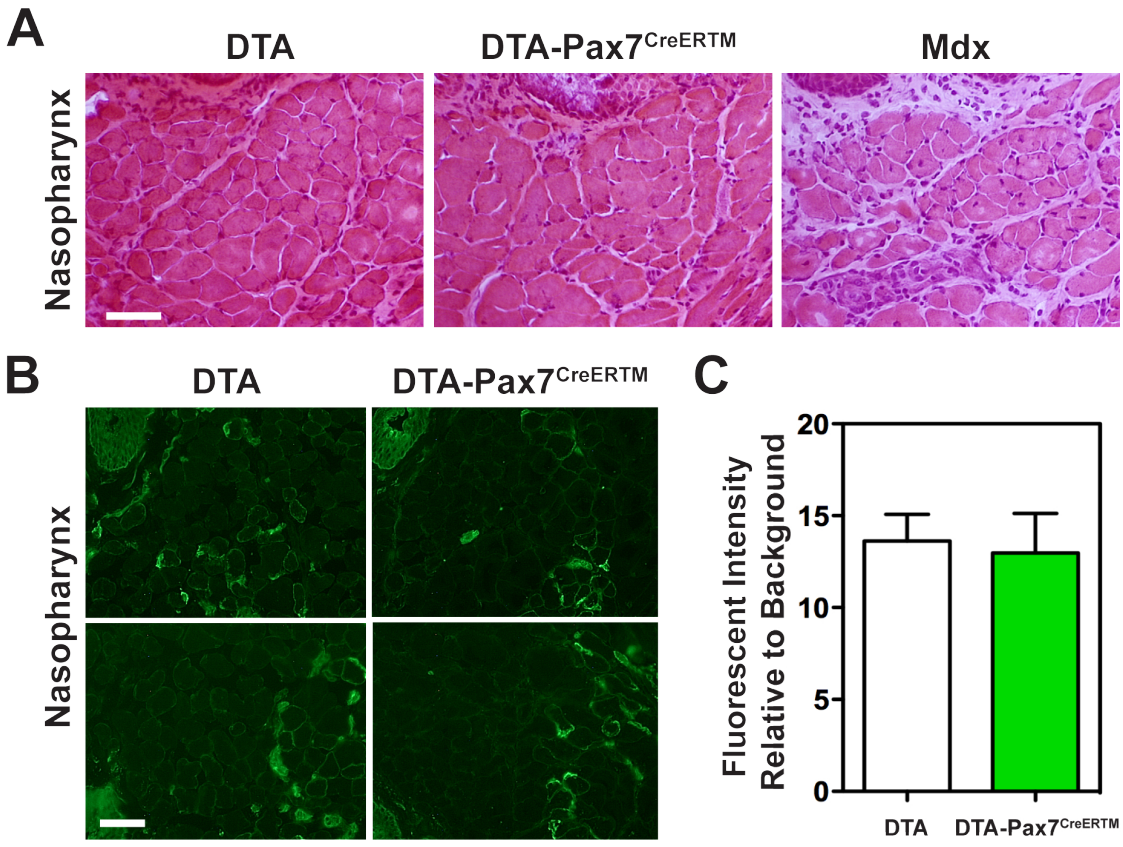

**Figure 5.4.8: No evidence of fibrosis in nasopharyngeal muscles 4 months post-satellite cell ablation**

**(A)** Representative images of hemotoxylin and eosin stained nasopharyngeal muscles sections are shown from either *Rosa*$^{DTA\text{-}176}$ homozygotes (DTA) or *Pax7*$^{CreERTM}$/*Rosa*$^{DTA\text{-}176}$ heterozyotes (DTA/Pax7$^{CreERTM}$) mice 4-months post-tamoxifen treatment. Fibrosis was not observed in satellite cell-ablated nasopharyngeal muscle (DTA/Pax7$^{CreERTM}$). Dystrophin-deficient *mdx* nasopharyngeal muscle is provided as a positive control for comparison. **(B)** Nasopharyngeal muscles were incubated with FITC-labeled wheat germ agglutinin (WGA) to analyze changes in extracellular protein deposition following satellite cell ablation. Representative images of pharyngeal muscles obtained from similar regions of the nasopharynx are shown (paired horizontally in both top and bottom panels). **(C)** Relative fluorescent intensity of FITC-WGA was analyzed from four paired regions of DTA and DTA/Pax7$^{CreERTM}$ nasopharyngeal muscle sections. No significant difference in WGA fluorescence was noted. n=4 mice per genotype.

**Figure 5.4.9: Pharyngeal satellite cells are required to prevent muscle atrophy in the nasal and laryngeal pharynxes**

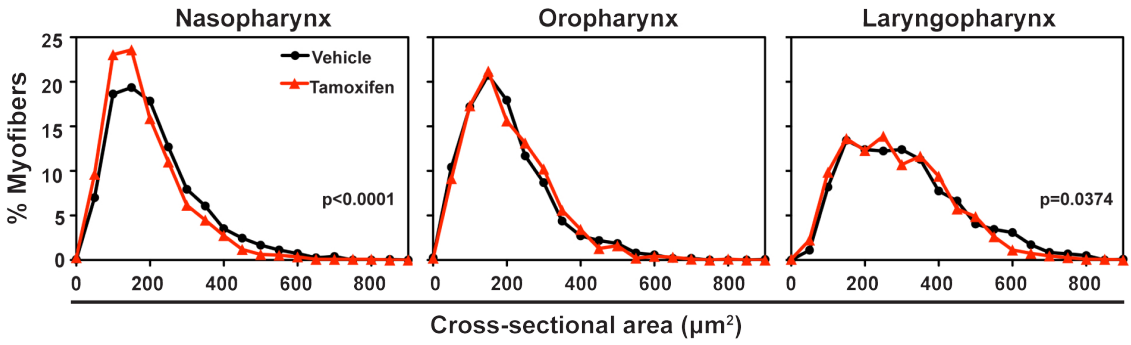

**Figure 5.4.9: Pharyngeal satellite cells are required to prevent muscle atrophy in the nasal and laryngeal pharynxes**

DTA/Pax7$^{CreERTM}$ mice received either vehicle or tamoxifen injections as described in Fig. 5.4.6E with pharyngeal muscles collected 4-months post-treatment. Frequency distribution plots of myofiber cross-sectional areas from the naso-, oro-, and laryngopharyngeal regions are shown. Myofiber size of nasal and laryngeal pharynx muscles decreased following tamoxifen-induced satellite cell ablation, as evidenced by a leftward shift of distribution plots. n=929-1505 myofibers, 3 mice per condition.

**Figure 5.4.10: Model of basal pharyngeal satellite cell biology and maintenance of myofiber size**

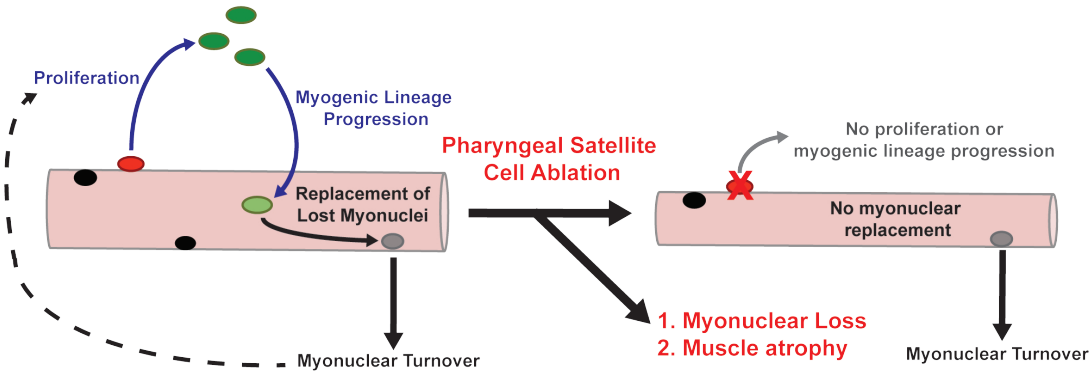

**Figure 5.4.10: Model of basal pharyngeal satellite cell biology and maintenance of myofiber size**

Pharyngeal satellite cells (red) proliferate, progress through myogenesis, and contribute myonuclei (black) to pharyngeal myofibers under basal conditions. The continual contribution of new myonuclei (light green) to pharyngeal myofibers counteracts the basal myonuclear loss (grey), preventing both loss of myonuclear numbers and myofiber size. Pharyngeal satellite cell impairment reduces myonuclear addition to pharyngeal myofibers resulting in both myonuclear loss and decreased myofiber size.

# Chapter 6: Discussion

**Contributions:**

Yandery Vera (Figure 6.11.1 data), Teresa E. Lever (Figure 6.11.3 data, Figure 6.11.4 data)

# Chapter 6: Discussion

## 6.1 Introduction

Pharyngeal muscles are a subset of skeletal muscles that line the nasal, oral, and laryngeal cavities that are preferentially affected in diseased conditions such as oculopharyngeal muscular dystrophy yet spared in other muscular dystrophies. Little is known about the effects of age or disease on pharyngeal muscles and their satellite cells nor what factors predispose them to the effects of pathologic conditions. The overall goal of this dissertation was to elucidate biological properties of both pharyngeal muscles and their associated satellite cells that may contribute to the pathologic sensitivity of these muscles to various disease-causing conditions.

The first section of this dissertation focused on pharyngeal muscle biology, specifically addressing the effects of aging and dystrophic disease on pharyngeal muscles in a region-dependent manner. In Chapter 4, we showed that with age, both pharyngeal muscle atrophy and oral dysphagia developed in wild-type mice. Using a mouse model of an age-associated dysphagic disease, oculopharyngeal muscular dystrophy, we showed that overexpression of wild-type A10 PABPN1 protein in muscle tissue prevented age-related dysphagia and age-related muscle atrophy of laryngopharyngeal muscles. Furthermore, we observed differential susceptibility of various pharyngeal muscles to overexpression of either wild-type or mutant A17 PABPN1 in age-related muscle growth and atrophy. These results demonstrate that pharyngeal muscles are differentially affected by both aging and muscular dystrophy in a region-dependent manner.

The second section of this dissertation analyzed the biologic properties of pharyngeal satellite cells (PSCs) and their contribution to pharyngeal muscle

maintenance. In Chapter 5, we characterized satellite cells of pharyngeal muscles demonstrating that pharyngeal satellite cells undergo myogenesis under basal conditions. Additionally, PSCs are required for maintenance of both pharyngeal myofiber size and myonuclear number, suggesting that satellite cell impairment could contribute to pharyngeal myopathies.

The findings presented in this dissertation provide fundamental insights into the unique biology of pharyngeal muscles and PSCs, and the biological importance of regional localization of muscles within the pharynx, as well as insights into the differential sensitivity of pharyngeal muscles in diseased or aged states. Further studies addressing the effects of disease and aging on pharyngeal muscles, pharyngeal satellite cells and pharyngeal myonuclear turnover are warranted and could lead to new therapeutics for individuals suffering from pharyngeal myopathies.

### 6.2 Implications of Pharyngeal Myofiber Composition and Structure in Disease Predisposition

We show that pharyngeal muscles predominantly contain Type II and neonatal MHCs but lack myofibers expressing Type I MHC. The preponderance of Type II myofibers in mice is consistent with human studies. Interestingly, Type II myofibers are preferentially affected in various pathologic conditions. In the context of aging, studies of elderly patients show that age-related decreases in satellite cell numbers are specifically associated with Type II myofibers of limb muscles (Verdijk et al., 2007). In cricopharyngeal muscles of human OPMD patients (Gidaro et al., 2013), atrophic changes preferentially occur in Type IIa myofibers, indicating a myofiber-specificity of

OPMD. Type II myofibers have also been implicated in the pathology of obstructive sleep apnea hypopnea syndrome (OSAHS). Diseased palatopharyngeal muscles demonstrate a loss of Type I myofibers with a concurrent increase in the proportion of Type II myofibers. The increase in Type II myofiber composition is hypothesized to impair the structural support of maintaining the airway of the nasal pharynx (Shi et al., 2014). In contrast, Parkinson's disease (PD) elicits an opposite effect on myofiber composition in laryngopharyngeal muscles. Mu *et al.* showed a loss of distinction between the inner and outer myofiber layers of Type I and Type II myofibers, respectively, in PD patients. However, instead of Type II myofibers, they found that Type I myofibers were preferentially susceptible to atrophic changes (2012). Future studies utilizing genetic model organisms are critically needed to study the mechanisms underlying both myosin heavy chain and myofiber biology in pharyngeal skeletal muscles. Specifically, therapeutic strategies aimed at locally altering the myofiber composition and function of diseased muscles could benefit patients suffering from multiple causes of pharyngeal muscle disease.

Pharyngeal myofibers also differed in their size and myonuclear composition compared to limb myofibers. Pharyngeal myofiber size was strikingly smaller than limb myofibers when examined both histologically and *ex vivo* (Fig. 6.11.1). In accordance with human histologic studies, most pharyngeal myofibers were visually smaller in histologic cross-sections when compared to tibialis anterior limb muscles (Fig. 5.4.1B). Therefore, to better characterize pharyngeal myofibers, we enzymatically isolated single myofibers from pharyngeal muscle and compared them to myofibers from the limb muscle extensor digitorum longus, which is also composed mainly of fast-twitch Type II

myofibers (Fig. 6.11.1A). We show that pharyngeal myofibers are shorter in length and contain fewer myonuclei per length of myofiber compared to limb myofibers (Fig. 6.11.1B-C). Interestingly, pharyngeal myofibers have a decreased cytoplasmic-volume-to-nucleus ratio, commonly referred to as a myonuclear domain (Fig. 6.11.1D). As skeletal muscle is multinucleated, it is hypothesized that each myonucleus is responsible for providing transcripts for a certain volume or region of cytoplasm within the myofiber (Van der Meer et al., 2011). The biological significance of the small myonuclear domain in pharyngeal myofibers remains to be determined, but could allow for increased sensitivity of pharyngeal skeletal muscle to pathological conditions affecting myonuclear number or function.

### 6.3 Implications of Pharyngeal Skeletal Muscle Growth and the Effects of Aging

Prior to these studies, murine pharyngeal muscle growth had not been studied. Human studies examining changes in limb myofiber size report a pattern of early postnatal growth followed by maintenance of adult myofiber size with regression of myofiber size occurring with late-life muscle atrophy (Aherne et al., 1971; Lexell et al., 1988; Wada et al., 2003). We report an unusual growth pattern associated with postnatal laryngeal muscle growth where adult muscle size is achieved by 2 months-of-age, with a progressive age-related atrophy following, while nasal and oral pharyngeal muscles demonstrated growth patterns similar to limb muscles. This finding suggests distinct regulatory mechanisms underlie pharyngeal constrictor muscle growth, which may make them more susceptible to pathologic atrophy associated with conditions such as aging, OPMD, and Parkinson's disease. Further studies examining the cellular and molecular

mechanisms regulating the differential growth of pharyngeal muscles could provide valuable insights into region-specific differences underlying age- and disease-related muscle atrophy of the pharynx. Specifically, comparative analyses of the transcriptomes and proteomes of pharyngeal muscles isolated from each region could provide invaluable insights into the differential mechanisms of pharyngeal muscle growth.

### 6.4 Implications of Region-Dependent Effects of Muscular Dystrophy on Pharyngeal Muscle

The regional differences observed with age-related pharyngeal muscle growth suggest that pathologic conditions could also differentially affect pharyngeal muscle biology in a region-dependent manner. In our OPMD mouse model, mutant A17 PABPN1 overexpression adversely affected myofiber size in the oro- and laryngopharynx at both 2 and 12 months of age relative to overexpression of wild-type A10 PABPN1. Meanwhile, minimal to no effect of mutant A17 PABPN1 on myofiber size was observed in the palatopharyngeus of the nasopharynx regardless of age. As discussed in Chapter 4.3, some of the regional differences may be accounted for by the distinct anatomical functions of pharyngeal muscles within each region. For example, the anatomical division of the palatopharyngeus within the oropharynx could exert unique physiological demands on these muscles and contribute to the region-dependent sensitivity of the palatopharyngeus to mutant A17 PABPN1 overexpression. Thus, the regional differences in the effect of mutant A17 PABPN1 on myofiber size within the palatopharyngeal muscle are likely, in part, related to the unique functional demands of the oral versus the nasal pharynx. Our data suggest that spatial and functional requirements can influence the

disease susceptibility of pharyngeal muscles, warranting further studies examining the unique physiological consequences of palatopharyngeal muscle's functional duality.

Interestingly, overexpression of mutant A17 PABPN1 affected the muscles of the laryngopharynx differently than in the palatopharyngeal muscle. While overexpression of wild-type A10 PABPN1 increased myofiber size at all observed ages, no increase was observed upon overexpression of mutant A17 PABPN1, which could indicate that the alanine expansion in mutant A17 PABPN1 disrupts its ability to enhance growth. Additionally, decreases in central myonuclear localization occurred in mutant A17 PABPN1 laryngopharyngeal muscles compared to wild-type A10 PABPN1 controls, suggesting myonuclear addition was also negatively affected. These regional differences raise interesting questions as to the molecular consequences of mutant PABPN1 within each region. Both wild-type and mutant PABPN1 have the capacity to polyadenylate RNAs both *in vitro* and in cultured cells (Banerjee et al., 2013; Calado et al., 2000; Kuhn and Wahle, 2004). However, whether mutant PABPN1 has the same functional abilities regarding 3' end cleavage site selection, nuclear export, or regulation of long non-coding RNAs has yet to be determined (Banerjee et al., 2013). Therefore, if the alanine expansion alters the various functions of PABPN1 *in vivo*, overexpression of mutant A17 PABPN1 could directly alter RNA biogenesis *in vivo*. If this is the case, differential misregulation of certain RNAs could be contributing to the variable pathologic sensitivities of pharyngeal muscles in OPMD. Another proposed pathological mechanism for mutant PABPN1 is the formation of nuclear aggregates and subsequent sequestration of wild-type PABPN1 (Banerjee et al., 2013). Are there differences in the levels of available wild-type PABPN1 between each region of the pharynx? If so, do these

differences differentially affect RNA biogenesis? What are the molecular and biological consequences of regional differences in wild-type PABPN1 protein levels? These questions need to be tested to further elucidate the molecular mechanisms underlying mutant A17 PABPN1's differential effects in pharyngeal muscle biology.

Our data provide further evidence that regional location within the pharynx contributes to the variable disease sensitivities of pharyngeal muscles. While current treatment for dysphagic patients involves myotomy of the inferior constrictor pharyngeal muscles (Perie et al., 2014), we are the first to provide evidence suggesting therapeutic treatments directed toward muscles of the oropharynx could also prove beneficial in alleviating OPMD-related disease. Collectively, these studies suggest that expression of mutant A17 PABPN1 affects pharyngeal muscles differentially based on regional-location and warrants the development of region-specific strategies for treating OPMD-related muscle disease.

### 6.5 Implications for PABPN1 Overexpression on Pharyngeal Muscle

Overexpression of wild-type A10 PABPN1 revealed new insights into mechanisms influencing pharyngeal muscle growth. Previous *in vitro* studies have shown that steady-state levels of both PABPN1 protein and mRNA levels were severely reduced in skeletal muscles, particularly craniofacial muscles, compared to other tissues of the body (Apponi et al., 2013). Additionally, recent studies of the vastus lateralis limb muscle indicated decreased levels of PABPN1 mRNA in the contexts of both muscle aging and OPMD in humans (Anvar et al., 2013; Raz and Raz, 2014), suggesting a connection between disease and diminished PABPN1 levels in certain muscles. Our

studies with A10-WT mice provide further evidence for PABPN1's role in pharyngeal muscle growth and function.

We found that overexpression of wild-type A10 PABPN1 alone provided a protective effect on myofiber growth of pharyngeal muscles in a region-dependent manner. Wild-type A10 PABPN1 overexpression enhanced myofiber size in all pharyngeal muscles at 2 months of age, but surprisingly, protected against age-related muscle atrophy only in laryngopharyngeal muscles. These data show that wild-type A10 PABPN1 overexpression differentially affects mechanisms underlying myofiber growth of pharyngeal muscles *in vivo*. Regional studies examining differential gene expression of pharyngeal muscles from wild type and A10-WT overexpression mice are needed to provide new insights into *PABPN1* overexpression on pharyngeal muscle growth.

To test whether wild-type A10 PABPN1 overexpression also affects swallow function in the contexts of aging and OPMD, we utilized an established oral dysphagia model that analyzes lick rates (Lever et al., 2009; Lever et al., 2010) to indirectly assess pharyngeal function. We observed that both wild-type and A17-MUT mice developed dysphagia with age, however, muscle-specific overexpression of wild-type A10 PABPN1 protected against age-associated impairments in swallowing. Transcriptome and proteome studies analyzing differential gene expression between control and wild-type A10 PABPN1 overexpression mice would provide useful insights into what pathways are involved in swallow function protection with aging. PABPN1 could play a critical role in the transcript biogenesis of these protective mechanisms through regulation of gene expression, post-transcriptional modifications, nuclear export, or transcript stability. Given that wild-type A10 PABPN1 overexpression protects against both age- and

OPMD-dependent decreases in swallow function and myofiber size, the development of therapies directed at modulating region-specific *PABPN1* expression could prove beneficial in treating the elderly population who suffer from age-related dysphagia as well as OPMD patients.

One final consideration pertaining to the therapeutic potential of *PABPN1* overexpression is in the context of acute pharyngeal muscle trauma or injury. Currently, *in vivo* studies examining manipulation of PABPN1 levels in regeneration of injured muscle are lacking. We know that *PABPN1* expression is required for normal pharyngeal myoblast proliferation and differentiation *in vitro* (Apponi et al., 2010). Our studies analyzing myofiber size in A10-WT mice found an association between increased myofiber size and incidence of centrally located nuclei in laryngopharyngeal myofibers, suggesting that myogenesis was associated with the growth phenotype. These results suggest that myofiber overexpression of wild-type A10 PABPN1 in the laryngopharynx may selectively enhance the myogenic potential of PSCs, thereby increasing the incidence of central myonuclei present in the A10-WT laryngopharynx. A potential mechanism by which PABPN1 overexpression could enhance PSC myogenesis is through positive regulation of growth factor, cytokine, and chemokine transcripts in the myofiber, which could act as paracrine signals to initiate satellite cell activation and myogenesis. If *PABPN1* overexpression has a similar role in laryngopharyngeal muscle regeneration as it does muscle growth, *PAPBN1* gene therapy could be a viable option for treating patients with laryngopharyngeal muscle trauma and injury.

### 6.6 Implications of Satellite Cells in Pharyngeal Muscle Maintenance

Our understanding of pharyngeal satellite cells in pharyngeal muscle biology has largely come from research delving into pathologic mechanisms of oculopharyngeal muscular dystrophy. Initial studies found that cultured myoblasts derived from cricopharyngeal muscles of oculopharyngeal muscular dystrophy (OPMD) patients demonstrate decreased proliferative abilities (Périé et al., 2006). These data suggested that altered function of pharyngeal satellite cells could contribute to dysphagic OPMD pathology. However, whether or not the myogenic defects observed in this study are a secondary result from chronic regeneration or a primary defect of the pharyngeal satellite cells remains to be determined. Another *in vitro* study demonstrated that knockdown of *PABPN1* expression in cultured wild-type pharyngeal myoblasts impairs both proliferation and differentiation, suggesting that *PABPN1* expression plays a critical role in pharyngeal satellite cell myogenesis (Apponi et al., 2010). Lastly, *in vivo* studies examining histologic biopsies of muscles from normal and OPMD-affected patients reveal an increased number of $Pax7^+$ satellite cells in normal cricopharyngeal muscles compared to other neck and limb muscles. Additionally, in OPMD-affected cricopharyngeal muscles, larger numbers of $Pax7^+$ cells were observed compared to limb and neck muscles (Gidaro et al., 2013). Results from recent clinical trials provide preliminary evidence for the use of satellite cell transplantation as a therapeutic treatment for dysphagic OPMD patients. Phase I/IIa clinical trials were performed with dysphagic OPMD patients where myoblasts obtained from unaffected skeletal muscles were amplified in culture and transplanted into cricopharyngeal muscles following surgical correction of the cricopharyngeal muscle. The report suggested that patients receiving

injections of larger numbers of unaffected myoblasts into the cricopharyngeal area demonstrated significant improvement in swallow ability over a two-year period (Perie et al., 2014), thus providing further evidence for a satellite cell involvement in OPMD pathology. Together, these studies suggested a unique role for satellite cells in both normal and OPMD-affected pharyngeal muscle.

We show that murine pharyngeal muscles possess increased numbers of satellite cells in pharyngeal muscles compared to limb skeletal muscle, consistent with the recent immunohistologic studies of human cricopharyngeal muscles (Gidaro et al., 2013). Four mechanisms could potentially account for the large satellite cell population: 1) myofiber composition of pharyngeal muscles; 2) regeneration due to focal myofiber injury; 3) ongoing basal myogenesis; or 4) remnant from postnatal development. We show that increased satellite cell numbers in pharyngeal muscles are not attributed to the presence of Type I myofibers, which are associated with increased numbers of satellite cells, nor the presence of gross myofiber damage or degeneration, indicating that alternative mechanisms are responsible for the increased satellite cell numbers, such as basal myogenesis or developmental remnants. While we did not address pharyngeal satellite cell numbers during postnatal development, we did find an increased incidence of centrally localized nuclei in all pharyngeal muscles examined compared to limb. The presence of central myonuclei suggests that myogenesis occurs in the absence of induced muscle injury in all regions of the pharynx, which is in agreement with our PSC proliferation studies. We show that pharyngeal muscle also contains a highly proliferative subpopulation of satellite cells that could contribute to the proliferative phenotype of PSCs. This PSC subpopulation could be unique to pharyngeal muscles or potentially

similar to the highly proliferative SC subpopulation of EOMs (Kallestad et al., 2011). The proliferative nature of EOM satellite cells has been proposed as a disease-sparing mechanism for those muscles. It remains to be seen whether this disease-resistant potential applies to pharyngeal skeletal muscle and PSCs. Molecular identification of the proliferative PSC subpopulation would assist in elucidating mechanisms contributing to the proliferative phenotype, and potential muscle-protectant properties.

Factors underlying this proliferative phenotype of PSCs are suggested by our PABPN1 overexpression experiments (discussed above), microarray analysis and myonuclear loss model. Interleukin-6, LIF, and CCL2 were highly expressed in PSCs compared to LSCs. All of these factors are known to stimulate myoblast proliferation through autocrine and paracrine signaling (Broholm et al., 2011; Henningsen et al., 2011; Serrano et al., 2008; Spangenburg and Booth, 2002; Toth et al., 2011; Yahiaoui et al., 2008). These cytokines may drive the proliferative phenotype of PSCs. If so, what cellular or molecular mechanisms are driving this cytokine expression in PSCs? Are regional differences in cytokine expression present? Are any or all of these cytokines sufficient or necessary for PSC proliferation and maintenance of pharyngeal myonuclear numbers? Is the expression or function of these cytokines adversely affected in pharyngeal myopathies? Further elucidation of the roles of Interleukin-6, LIF, and CCL2 play in both PSC and pharyngeal muscle biology could lead to therapeutic strategies in treating diseases where satellite cell proliferation is impaired.

Proliferating PSCs also progress through the myogenic lineage and contribute new myonuclei to pharyngeal muscle fibers under basal conditions. Additionally, we provide evidence that a decrease in myonuclear numbers does occur in satellite cell-

ablated muscles of the nasal pharynx. Mechanisms of myonuclear turnover, including apoptosis, necrosis, or nuclear extravasation, could serve as positive feedback between myonuclear loss and the need to initiate PSC proliferation to eventually replace the lost myonucleus. The potential relationship between myonuclear turnover and pharyngeal satellite cell activation is an intriguing hypothesis that warrants investigation.

Currently, isolated myonuclear apoptosis is generally accepted as the mechanism for myonuclear turnover (Adhihetty et al., 2007; Dupont-Versteegden et al., 1999; McLoon et al., 2004). While apoptosis is still a plausible mechanism, few studies have examained myonuclear turnover in-depth, leaving many questions unanswered. Alternate mechanisms such as nuclear autophagy (Mijaljica et al., 2010; Park et al., 2009) or even myonuclear extrusion (Runge et al., 2000) could contribute to myonuclear turnover. What are the mechanisms that signal a myonucleus for removal? Is myonuclear damage occurring with a high incidence? What contribution could pharyngeal myofiber metabolism have on myonuclear turnover? What mechanism(s) are involved in the removal process? Do any of these mechanisms include molecules or pathways that can be therapeutically targeted? Could mutations in pathways regulating myonuclear turnover contribute to pharyngeal muscle pathology? We reported that pharyngeal skeletal muscle does undergo basal myonuclear loss, making pharyngeal muscles the ideal model tissue for addressing biological mechanisms involved in myonuclear turnover. Furthermore, myonuclear turnover could contribute to pharyngeal skeletal muscle's variable sensitivity to pathologic mutations. Disease-causing mutations that enhance myonuclear turnover in pharyngeal muscles could prevent PSCs from adequately supplying enough myonuclei to maintain homeostasis, thus contributing to pharyngeal muscle pathology.

Although the effects of aging and disease on pharyngeal satellite cell biology were not directly tested in these studies, the unique biological properties of PSCs could certainly contribute to the pathologic sensitivities of pharyngeal skeletal muscle. As previously discussed, pharyngeal skeletal muscle is largely composed of Type II fast-twitch myofibers. The impact of aging on pharyngeal muscle biology could be significant as satellite cells associated with Type II myofibers decrease in number with age (Verdijk et al., 2007). The combined loss of PSCs as well as possible impairment of PSC function with age (Brack and Rando, 2007) could negatively impact pharyngeal muscle function and potentially contribute to the impaired swallowing observed in 11-16% of the elderly population (Holland et al., 2011; Kawashima et al., 2004). Taken together, these findings provide new provocative questions concerning pharyngeal satellite cells and pharyngeal muscle maintenance, which warrant future studies (Figure 6.11.2)

**6.7 Functional Outcomes of Pharyngeal Satellite Cell Impairment**

To address whether PSC are required for pharyngeal muscle maintenance, we analyzed the functional outcomes of PSC ablation. A >90% reduction of PSC numbers resulted in concurrent loss of both myonuclear number and myofiber size in the nasal region of the palatopharyngeus. These data suggest that constitutive myonuclear addition is required to maintain nasopharyngeal muscle size. While myonuclear loss was not present in the skeletal muscles of the oro- or laryngopharynxes, we suspect that myonuclear loss is also occurring in these regions. Both of these pharyngeal regions possess large numbers of PSCs. Thus, despite loss of over 90% of PSCs from these muscles, satellite cell numbers may have remained above a critical threshold leading to

maintenance of myonuclear numbers in these regions. Experimental models where the incidence of satellite cell impairment approaches 100% are needed to fully address myonuclear turnover in oro- and laryngopharyngeal muscles. These data provide evidence that satellite cells are required for maintenance of myofiber size in pharyngeal muscles and suggest that the rate of myonuclear turnover within a muscle determines whether or not the associated satellite cells are required for muscle maintenance.

Considering that satellite cell ablation affected pharyngeal muscle on a cellular level, we also wanted to test whether pharyngeal swallow function was altered with ablation of $Pax7^{+}$ satellite cells *in vivo.* Videofluoroscopy studies (VFSS) of the oral and pharyngeal cavities are routinely performed in human medicine to quantitatively measure functional metrics of swallowing (Altman, 2012). Therefore, in collaboration with the laboratory of Dr. Teresa Lever, a videofluoroscopic technique that quantitatively measures voluntary swallow function in mice was developed (Lever et al., 2015). In short, real-time x-ray imaging was performed on mice as they consumed chocolate flavored water containing 175 mg iodine/ml. Videofluoroscopy allowed for visualization of the radiopaque iodine solution as it traversed from the oral cavity, through the pharynx, into the esophagus, and was ultimately deposited into the stomach (Figure 6.11.3). To test the hypothesis that satellite cells are required for pharyngeal swallow function, male DTA-$Pax7^{CreERTM}$ heterozygous mice were given either vehicle or tamoxifen injections to induce ablation of *Pax7* expressing satellite cells *in vivo*, as outlined in Figure 5.4.6E. Tamoxifen treated DTA homozygotes were also used to control for tamoxifen-related effects. In collaboration with Dr. Lever's laboratory, VFSS was performed either at 12 months (Figure 6.11.4A-C) or 14 to 16 months (Figure

6.11.4D-H) following induction of satellite cell ablation. Multiple parameters of swallow function were used to assess swallow function during the oral phase (lick rates, number of licks per swallow), oropharyngeal phase (swallow rate, inter-swallow intervals) and the pharyngeal phase (pharyngeal transit time, and presence of residue remaining in pharynx post-swallow) of swallowing (Figure 6.11.4). No significant changes in swallow function were detected. These results may be confounded by the sensitivity of the technique, low numbers of mice per experimental groups, or the inability to ablate 100% of the resident satellite cell population. Considering the active myogenic nature of PSCs, pharyngeal muscle may only need 7-10% of its original satellite cell population to maintain swallow function. Whether impairment of 100% of the satellite cell population would affect swallow function remains unknown. These studies also do not rule out the potential contribution of other cell-types with myogenic potential (i.e. hematopoietic side-population cells, $PW1^{+}$ interstitial cells, mesangioblasts, and pericytes) in the maintenance of pharyngeal swallow function (Pannerec et al., 2012). In light of these caveats, our functional swallow studies provide inconclusive evidence for the necessity of satellite cells in pharyngeal swallowing. However, murine VFFS is a novel experimental tool with which to address pharyngeal swallow function in the context of multiple dysphagic disease models, paving the way for elucidating molecular and cellular mechanisms contributing to pharyngeal muscle pathology.

## 6.8 Implications of Regional Variation in Pharyngeal Muscle and Satellite Cell Biology

Regional variation in both pharyngeal muscle and PSC biology was a striking finding of our studies that could contribute to the muscle-specific sensitivities of various diseases, as summarized in Table 6.12.1. PSCs display differential phenotypes in population density, fusion incidence, and prevention of myonuclear loss, depending on the associated muscle and its location within the pharynx. Thus, pharyngeal muscles and PSCs provide us with a unique model system to delve deeper into basic mechanisms regulating satellite cell biology. For example, studies have shown that Type 1, slow-twitch myofibers are associated with larger numbers of satellite cells than Type 2, fast-twitch myofibers (Ontell et al., 1984; Reimann et al., 2000), but very little is known about the mechanisms that regulate satellite cell density on myofibers and within muscle tissue. The palatopharyngeus muscle and its satellite cells could provide a developmental system for identifying differential regulators and mechanisms that could be involved with determination of satellite cell population density as it is composed of only Type 2 myofibers in the mouse yet exhibits distinct regional differences in satellite cell number and biology.

## 6.9 Current Difficulties With Pharyngeal Muscle Model Systems

Our studies suggest that both spatial and functional anatomical differences of phayrngeal muscles can affect their biology. These differences could have a significant impact our ability to correlate spatial effects of murine models to human physiology. Mice and rats are quadripeds, hence, the entire pharynx, ranging from nasal to laryngeal,

is essentially parallel to the earth when standing. The pharyngeal anatomy of bipedal humans is unique in that the oral pharynx curves turn into the laryngopharynx, becoming almost perpendicular to the earth. The mechanical demands of altering the movement of food or liquid from a parallel to a perpendicular path is not recapitulated in either rat or mouse models, and is thus an inherent limitation to using mammalian models.

Additionally, anatomical difficulties associated with the murine model system as well as current limitations of OPMD mouse models make the study of pharyngeal skeletal muscle and PSC biology in the context of aging and muscular dystrophy challenging. As a model organism, mice are not ideal for studying pharyngeal skeletal muscle and satellite cell biology, as the dissections are technically difficult, the scale and size of the tissues makes reliable isolation of pharyngeal regions via dissection impossible, and digestion of murine pharyngeal muscles yield low numbers of satellite cells per animal. Rats could provide an alternative model for future studies of pharyngeal skeletal muscle and satellite cell biology for the following reasons: 1) the physiology of *Rattus norvegicus* has been extensively studied and commonly used as models of human disease (Jacob et al., 2010); 2) pharynxes of rats would be significantly larger allowing for increased reliability and precision with regional dissections of pharyngeal muscle tissue, as well as providing larger satellite cell yields per animal from muscle digests. However, the number of available mutant and transgenic rat models is significantly fewer when compared to mouse models (Jacob et al., 2010). New genetic techniques utilizing the CRISPR/Cas-9 nuclease system show promise for the rapid generation of site-directed mutagenic rat models (Shao et al., 2014). Generating and utilizing rat models of pharyngeal disease would enhance the experimental capability to directly test

mechanisms underlying pharyngeal skeletal muscle and satellite cell biology. The benefit to using mice is the ready availability of numerous mutant and transgenic mice. However, new genetic models of OPMD are needed. The OPMD mouse model system used in this dissertation overexpresses a 17 alanine-expanded mutant *PABPN1* allele under the muscle-specific human skeletal actin 1 promoter in the context of wild-type *PABPN1* expression from the endogenous alleles. However, this mouse model and others do not genetically recapitulate the genetic phenotype of OPMD patients who express either one or two mutant alleles under the endogenous *PABPN1* promoter (Davies et al., 2005; Dion et al., 2005; Hino et al., 2004). To specifically address the role of mutant PABPN1 in the context of pharyngeal skeletal muscle and PSC biology, genetic model systems which genocopy human OPMD need to be developed (Figure 6.11.5).

**6.10 Summary**

In summary, we provided fundamental insights into the biology of pharyngeal skeletal muscles and their associated satellite cell population. Thus expanding our knowledge as to why pharyngeal muscles are affected in some muscular dystrophies yet spared in others. We demonstrated that the fiber size of murine pharyngeal muscles is differentially affected by aging and muscular dystrophy depending on their location within the pharynx. Using a mouse model of an age-associated dysphagic disease, oculopharyngeal muscular dystrophy, we showed that overexpression of wild-type PABPN1 protein in muscle tissue prevents age-related dysphagia and age-related muscle atrophy of laryngopharyngeal muscles. The pronounced protective effects from muscle-specific wild-type A10 PABPN1 overexpression on pharyngeal muscle growth and

swallow function emphasize the integral role of pharyngeal muscles in swallow physiology. We also proposed a novel role for satellite cells in the maintenance of pharyngeal muscles (Figure 6.11.2). PSCs are transcriptionally distinct satellite cells that contribute new myonuclei to pharyngeal myofibers through constitutive myogenesis in the absence of injury. PSCs are required to maintain both pharyngeal myonuclear numbers and myofiber size, counteracting the results of active myonuclear turnover within pharyngeal muscles. Furthermore, new model organisms are needed to enhance the study of cellular and molecular mechanisms underlying the changes in pharyngeal muscle and satellite cell biology that occur with aging and disease. In particular, pharyngeal skeletal muscles could provide an excellent model system to address fundamental questions concerning the mechanisms of myonuclear turnover in multinucleated skeletal muscle.

Our studies provide new evidence for potential therapeutic approaches in treating patients with dysphagia or other pharyngeal myopathies. Differential pathology occurred in a regional-dependent manner with overexpression of mutant A17 PABPN1, suggesting that implementation of region-specific therapies may be necessary to address the pathologies between different pharyngeal regions. Additionally, these studies suggest that alleviating age- or OPMD-related PABPN1 loss with overexpression of wild-type A10 PABPN1 could potentially prevent muscle loss in the human laryngopharynx and ameliorate one of the most devastating symptoms of OPMD. Meanwhile, reversal of the OPMD-related growth impairment in the oropharyngeal region of the palatopharyngeus muscle may require a different therapeutic approach.

The findings reported in this dissertation significantly advance our understanding of pharyngeal skeletal muscle and satellite cell biology and the mechanisms underlying both their sensitivities and resistances to pathologic conditions. Importantly, our results provide insights into why pharyngeal muscles are affected in some muscular dystrophies yet spared in others. Further studies elucidating biological mechanisms in pharyngeal muscles, PSCs, and pharyngeal myonuclear loss could lead to new therapeutics for individuals suffering from pharyngeal myopathies or life-threatening dysphagia.

## 6.11 Figures

**Figure 6.11.1: Pharyngeal Myofiber Characterization**

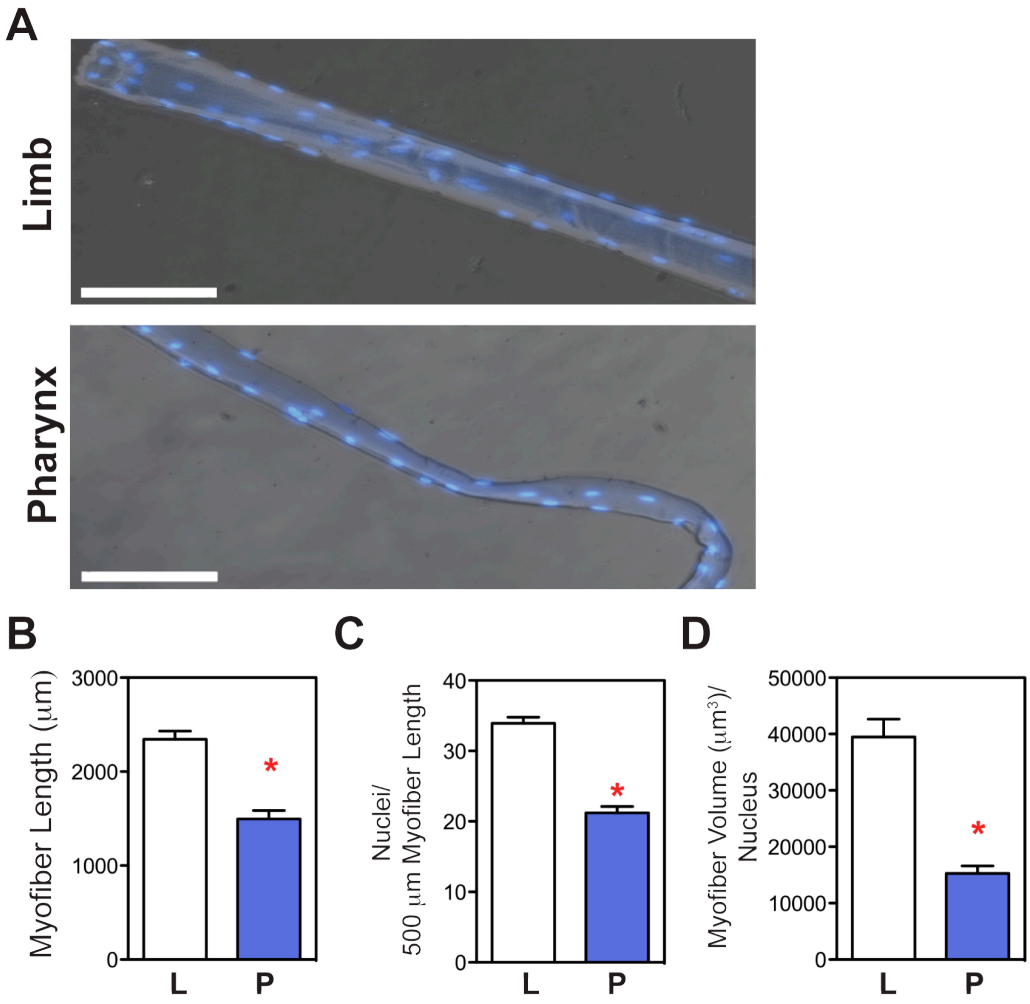

**Figure 6.11.1: Isolated pharyngeal myofibers differ from limb EDL myofibers** **(A)** Single myofibers were isolated from either limb extensor digitorum longus (EDL) muscles or pharyngeal muscles from 2-month-old C57BL/6 male mice. Nuclei were visualized with DAPI staining. Z stack images of single myofibers were obtained and merged. Bar=50 μm. **(B-D)** Image J was used to quantify (**B**) myofiber length, (**C**) myonuclei per unit length, and (**D**) cytoplasmic volume per nucleus. Pharyngeal myofibers are shorter and contain fewer myonuclei per unit length. Additionally, the volume of cytoplasm relative to each nucleus, quantified as myofiber volume ($\mu m^3$)/nucleus, is decreased in pharyngeal myofibers. Data are mean ± SEM. *P<0.05, n=26-35 myofibers.

**Figure 6.11.2: Potential mechanisms underlying basal pharyngeal satellite cell biology and maintenance of myofiber size**

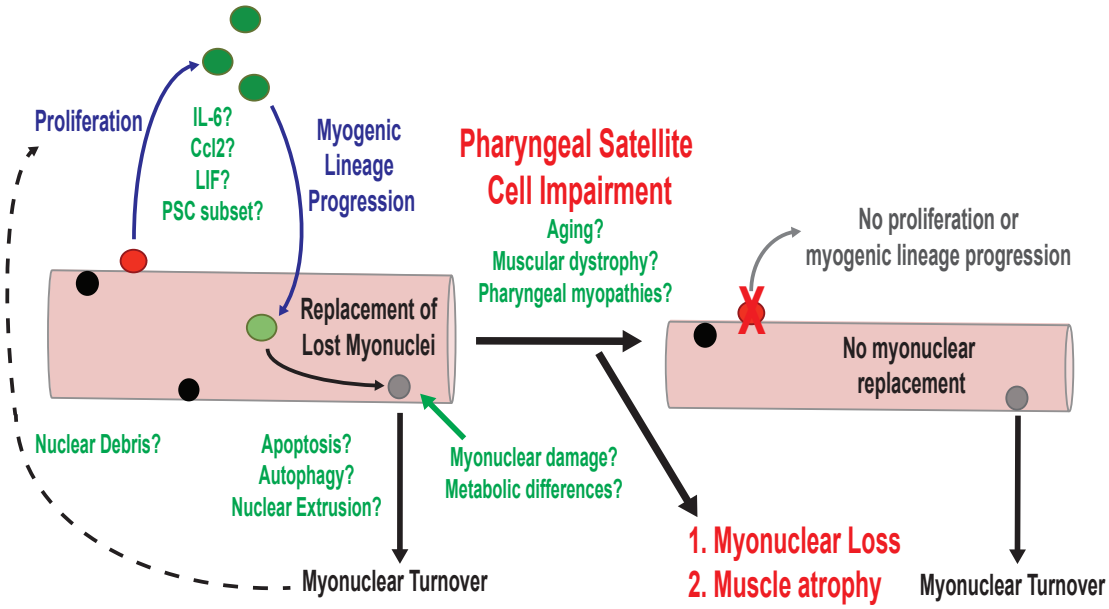

**Figure 6.11.2: Potential mechanisms underlying basal pharyngeal satellite cell biology and maintenance of myofiber size**

Pharyngeal satellite cells (red) proliferate, progress through myogenesis, and contribute myonuclei (black) to pharyngeal myofibers under basal conditions. The continual contribution of new myonuclei (light green) to pharyngeal myofibers counteracts the basal myonuclear loss (grey), preventing both loss of myonuclear numbers and myofiber size. Pharyngeal satellite cell impairment reduces myonuclear addition to pharyngeal myofibers resulting in both myonuclear loss and decreased myofiber size. Potential mechanisms contributing to this model, discussed in Chapter 6, still need to be elucidated (green font).

**Figure 6.11.3: Videofluoroscopic images depicting the distinct phases of swallowing in the mouse**

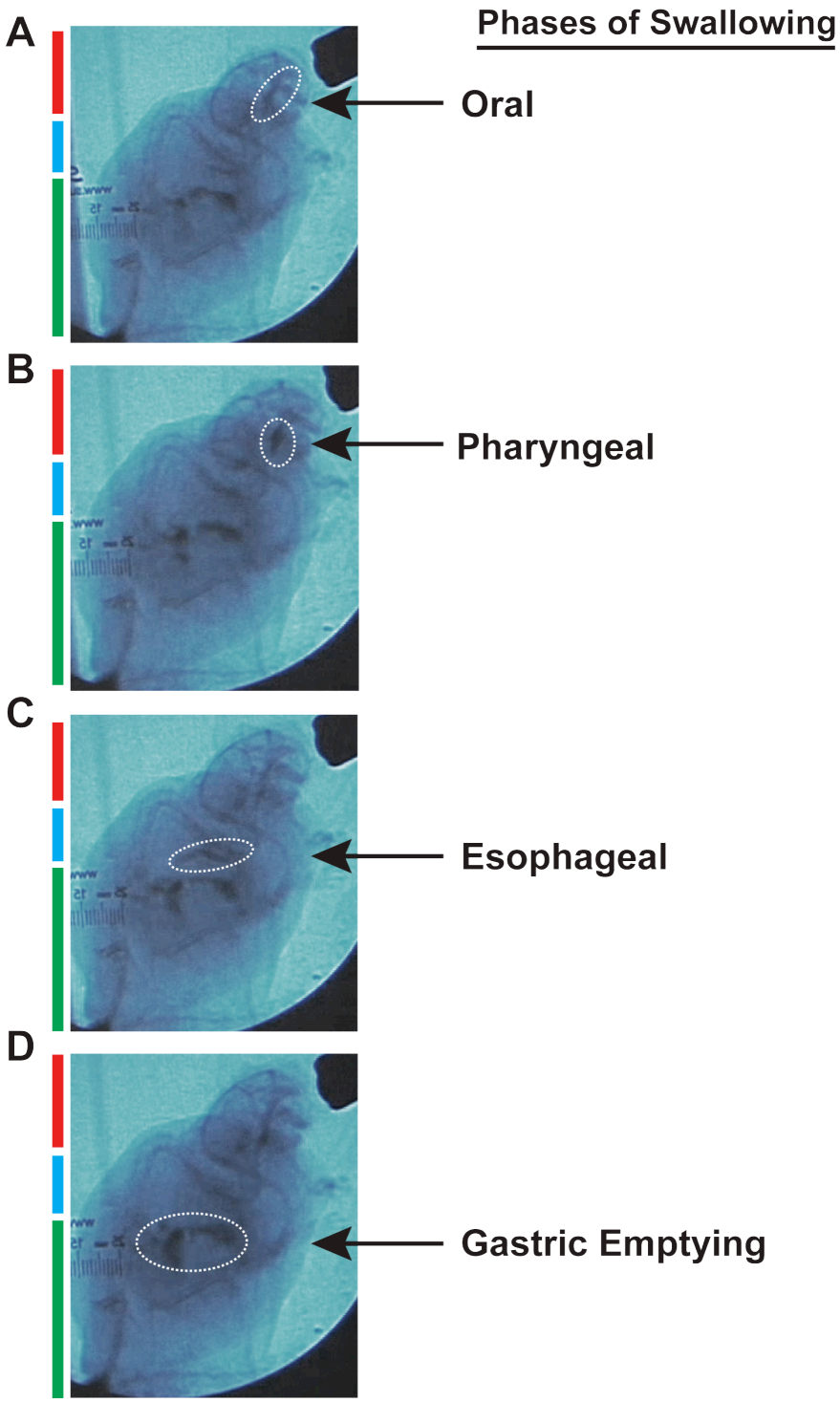

**Figure 6.11.3: Videofluoroscopic images depicting the distinct phases of swallowing in the mouse**

Videofluoroscopic images were taken of mice drinking flavored water containing 175 mg iodine/ml of water. (**A-D**) Bars on the left of each image demark the general regions of the head (red), thorax (blue), and abdomen (green). Dashed white circles outline a single radiopaque (black) fluid bolus as it moves from the oral cavity to the pharyngeal cavity to the esophagus and finally arriving at the gastric stomach. Representative images of (**A**) oral, (**B**) pharyngeal, (**C**) esophageal, and (**D**) gastric phases of swallowing are shown.

**Figure 6.11.4: Quantitative analysis of various parameters of swallow function in vehicle and tamoxifen treated DTA-Pax7$^{CreERTM}$ heterozygous mice**

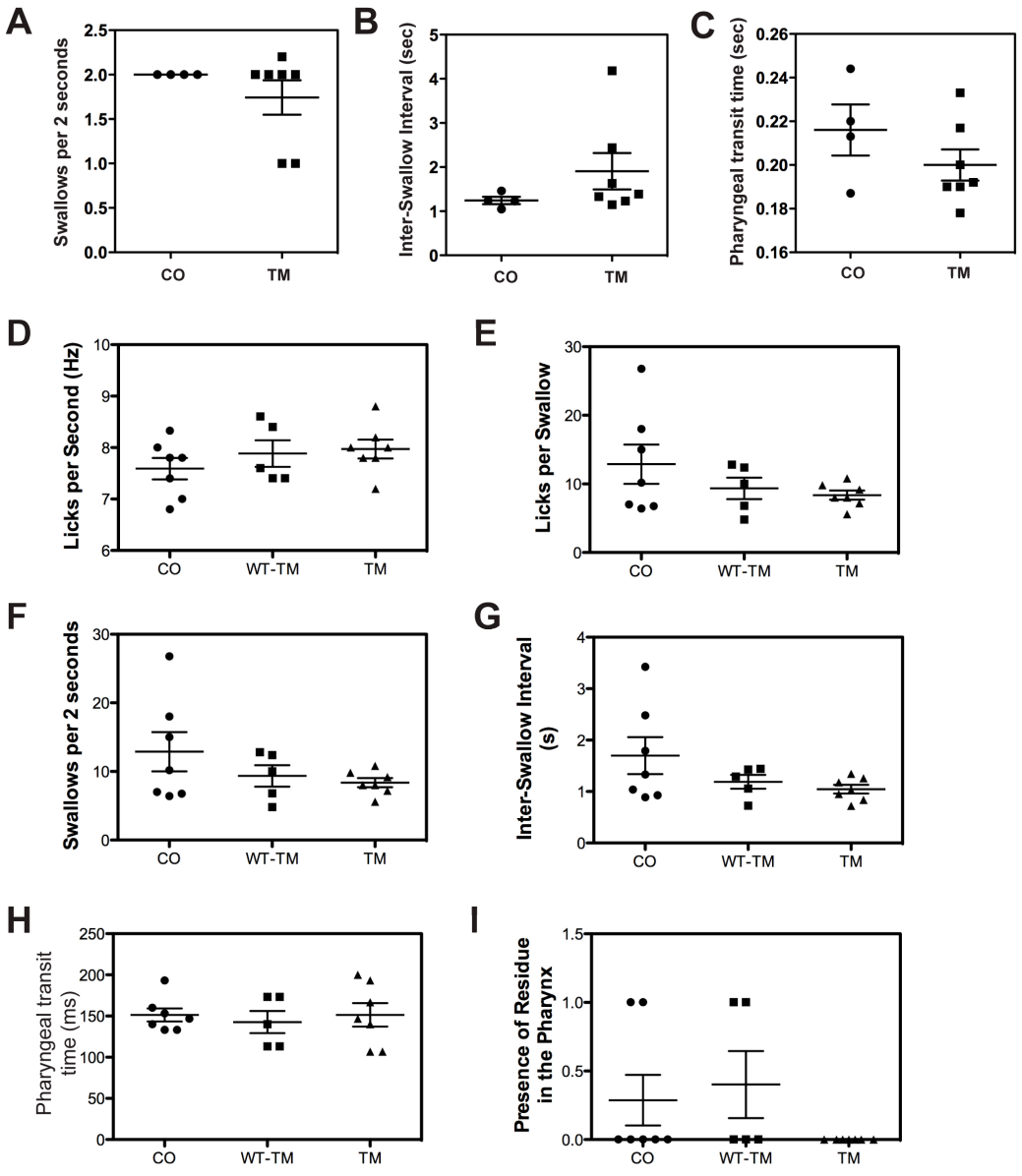

**Figure 6.11.4: Quantitative analysis of various parameters of swallow function in vehicle and tamoxifen treated DTA-Pax7$^{CreERTM}$ heterozygous mice**

Videofluoroscopic studies were performed on vehicle and tamoxifen treated DTA-Pax7$^{CreERTM}$ heterozygous or DTA homozygous mice at 12 months or 14-16 months post-treatment to quantify various metrics of swallow function. (**A-C**) Quantification of swallow function 12 months post-treatment. (**D-I**) Quantification of swallow function 14-16 months post-treatment. No significant changes were observed in any swallow metric at either time point.

**Figure 6.11.5: Current mouse models do not recapitulate the genotype or the protein expression of OPMD patients**

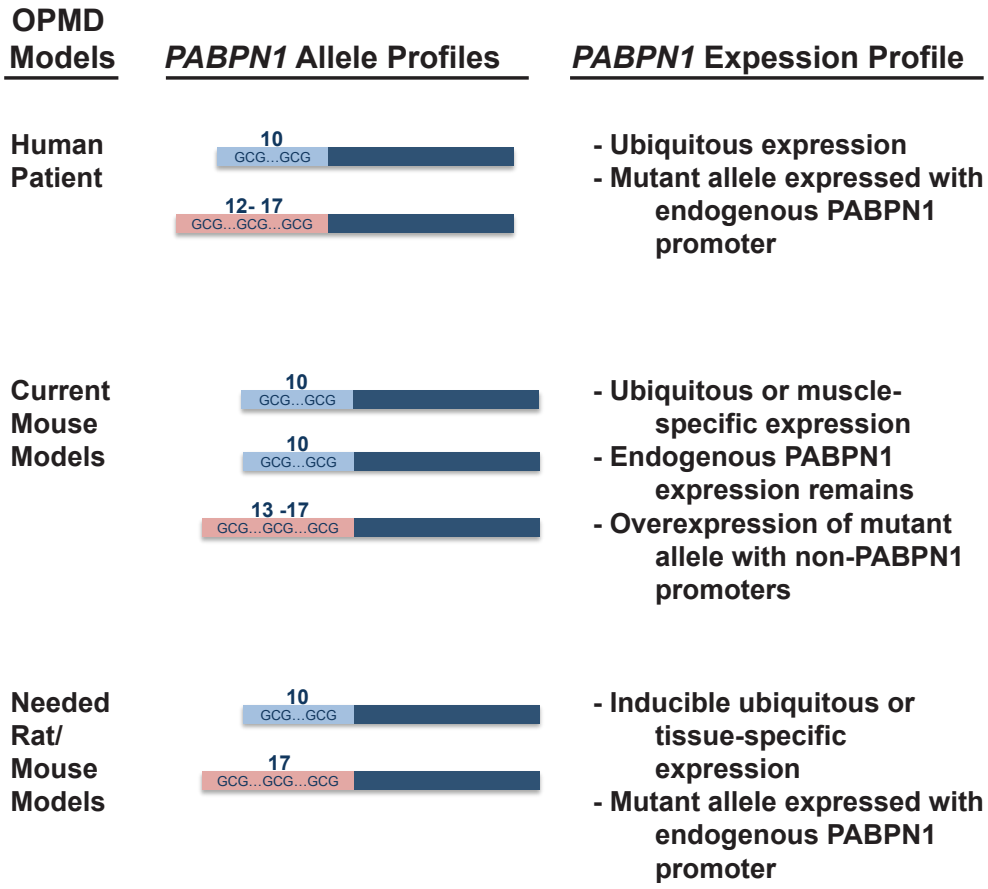

**Figure 6.11.5: Current mouse models do not recapitulate the genotype or the protein expression of OPMD patients**

Distinct differences in *PABPN1* alleles and protein expression exist between current mouse models and OPMD patients. Representative schematics of *PABPN1* alleles depict the presence of either wild-type with the endogenous trinucleotide run of $GCN_{10}$ (light blue) or a mutant-expanded run of $GCN_{12\text{-}17}$ (pink) for each OPMD model. We propose that new rat and mouse models, which genocopy human OPMD, need to be developed to reliably study the pathogenic mechanisms underlying this disease.

## 6.12 Table

### Table 6.12.1: Regional Variability of Pharyngeal Skeletal Muscle and Satellite Cells

| | Limb | Nasopharynx | Oropharynx | Laryngopharynx |
|---|---|---|---|---|
| Embryologic Origins | Somite-derived | Cranial paraxial mesoderm, 3rd and 4th brachial arches | Cranial paraxial mesoderm, 3rd and 4th brachial arches | Cranial paraxial mesoderm, 3rd and 4th brachial arches |
| Muscles | tibialis anterior; gastroc./ soleus; quadriceps; extensor digitorum longus | palatopharyngeal fold: stylopharyngeus, palatopharyngeus, salpingopharyngeus; superior pharyngeal constrictor | palatopharyngeal fold: stylopharyngeus, palatopharyngeus, salpingopharyngeus; middle pharyngeal constrictor | inferior pharyngeal constrictor: cricopharyngeus, thyropharyngeus |
| Myofiber Types | I, IIa, IIx, IIb | IIa, IIx, IIb | IIa, IIx, IIb | IIa, IIx, IIb, neonatal |
| Myonuclear Turnover | N/A | Yes | No | No |
| **Myofiber Size:** | | | | |
| Aging | N/A | Maximum size in mature adult mice | Maximum size in mature adult mice | Maximum size at 8 weeks-of-age |
| A10-PABPN1 | N/A | Increased only at 2 months-of-age | Increased only at 2 months-of-age | Increased at all studied ages |
| A17-PABPN1 | N/A | Minimally decreased | Significant impairment of myofiber growth | Moderately decreased |

**Table 6.12.1: Regional Variability of Pharyngeal Skeletal Muscle and Satellite Cells (continued)**

| Basal PSC Biology: | Limb | Nasopharynx | Oropharynx | Laryngopharynx |
|---|---|---|---|---|
| Numbers | Baseline | Mild increase | Moderate increase | Largest increase |
| Fusion | Baseline | Mild increase | Moderate increase | Largest increase |
| Centrally Localized Myonuclei | WT: Baseline | WT: 4-6 fold increase | WT: 4-6 fold increase | WT: 4-6 fold increase |
| | N/A | A10-PABPN1 OE: No change | A10-PABPN1 OE: No change | A10-PABPN1 OE: Increased above WT |
| | N/A | A17-PABPN1 OE: No change | A17-PABPN1 OE: No change | A17-PABPN1 OE: Decreased from A10 |

**Table 6.12.1: Regional Variability of Pharyngeal Skeletal Muscle and Satellite Cells**

Variable biological differences between skeletal muscles of the limb, nasopharynx, oropharynx, and laryngopharynx are summarized and highlighted in blue font. A10-PABPN1 OE = overexpression of wild-type polyadenylate binding nuclear protein 1; A17-PABPN1 OE = overexpression of mutant 17-alanine expanded polyadenylate binding nuclear protein 1; gastroc. = gastrocnemius; N/A = not assessed; WT = wild-type

## References

Abmayr, S.M., and G.K. Pavlath. 2012. Myoblast fusion: lessons from flies and mice. *Development*. 139:641-656.

Abu-Baker, A., and G.A. Rouleau. 2007. Oculopharyngeal muscular dystrophy: recent advances in the understanding of the molecular pathogenic mechanisms and treatment strategies. *Biochim Biophys Acta*. 1772:173-185.

Adhihetty, P.J., M.F. O'Leary, B. Chabi, K.L. Wicks, and D.A. Hood. 2007. Effect of denervation on mitochondrially mediated apoptosis in skeletal muscle. *Journal of applied physiology*. 102:1143-1151.

Aggarwal, V.S., and B.E. Morrow. 2008. Genetic modifiers of the physical malformations in velo-cardio-facial syndrome/DiGeorge syndrome. *Developmental disabilities research reviews*. 14:19-25.

Aherne, W., D.R. Ayyar, P.A. Clarke, and J.N. Walton. 1971. Muscle fibre size in normal infants, children and adolescents. An autopsy study. *In* J. Neurol. Sci. Vol. 14. 171-182.

Alfaro, L.A., S.A. Dick, A.L. Siegel, A.S. Anonuevo, K.M. McNagny, L.A. Megeney, D.D. Cornelison, and F.M. Rossi. 2011. CD34 promotes satellite cell motility and entry into proliferation to facilitate efficient skeletal muscle regeneration. *Stem cells*. 29:2030-2041.

Aloysius, A., P. Born, M. Kinali, T. Davis, M. Pane, and E. Mercuri. 2008. Swallowing difficulties in Duchenne muscular dystrophy: indications for feeding assessment

and outcome of videofluroscopic swallow studies. *Eur J Paediatr Neurol*. 12:239-245.

Altman, K.W. 2012. Oropharyngeal dysphagia pathophysiology, complications and science-based interventions. *Nestle Nutrition Institute workshop series*. 72:119-126.

Anvar, S.Y., Y. Raz, N. Verway, B. van der Sluijs, A. Venema, J.J. Goeman, J. Vissing, S.M. van der Maarel, P.A.C. t Hoen, B.G.M. van Engelen, and V. Raz. 2013. A decline in PABPN1 induces progressive muscle weakness in oculopharyngeal muscle dystrophy and in muscle aging. *In* Aging (Albany NY). Vol. 5. 412-426.

Apponi, L.H., A.H. Corbett, and G.K. Pavlath. 2011. RNA-binding proteins and gene regulation in myogenesis. *Trends in pharmacological sciences*. 32:652-658.

Apponi, L.H., A.H. Corbett, and G.K. Pavlath. 2013. Control of mRNA stability contributes to low levels of nuclear poly(A) binding protein 1 (PABPN1) in skeletal muscle. *Skeletal muscle*. 3:23.

Apponi, L.H., S.W. Leung, K.R. Williams, S.R. Valentini, A.H. Corbett, and G.K. Pavlath. 2010. Loss of nuclear poly(A)-binding protein 1 causes defects in myogenesis and mRNA biogenesis. *Human molecular genetics*.

Asakura, A., P. Seale, A. Girgis-Gabardo, and M.A. Rudnicki. 2002. Myogenic specification of side population cells in skeletal muscle. *The Journal of cell biology*. 159:123-134.

Attal, P., F. Lambert, S. Marchand-Adam, S. Bobin, J.C. Pourny, D. Chemla, Y. Lecarpentier, and C. Coirault. 2000. Severe mechanical dysfunction in pharyngeal muscle from adult mdx mice. *Am J Respir Crit Care Med*. 162:278-281.

Bachmann, G., M. Streppel, B. Krug, and E. Neuen-Jacob. 2001. Cricopharyngeal muscle hypertrophy associated with florid myositis. *In* Dysphagia. Vol. 16. 244-248.

Bajard, L., F. Relaix, M. Lagha, D. Rocancourt, P. Daubas, and M.E. Buckingham. 2006. A novel genetic hierarchy functions during hypaxial myogenesis: Pax3 directly activates Myf5 in muscle progenitor cells in the limb. *Genes Dev*. 20:2450-2464.

Banerjee, A., L.H. Apponi, G.K. Pavlath, and A.H. Corbett. 2013. PABPN1: molecular function and muscle disease. *The FEBS journal*. 280:4230-4250.

Barro, M., G. Carnac, S. Flavier, J. Mercier, Y. Vassetzky, and D. Laoudj-Chenivesse. 2010. Myoblasts from affected and non-affected FSHD muscles exhibit morphological differentiation defects. *Journal of cellular and molecular medicine*. 14:275-289.

Batten, F.E., & Gibb, H. P. . 1909. Myotonia Atrophica. *Brain : a journal of neurology*. 32:187–205.

Bayliss, L.M., and J.C. Sloper. 1971. Pre-irradiation and the regeneration of injured skeletal muscle. *The Journal of pathology*. 104:v-vi.

Beauchamp, J.R., L. Heslop, D.S. Yu, S. Tajbakhsh, R.G. Kelly, A. Wernig, M.E. Buckingham, T.A. Partridge, and P.S. Zammit. 2000. Expression of CD34 and Myf5 defines the majority of quiescent adult skeletal muscle satellite cells. *The Journal of cell biology*. 151:1221-1234.

Bentzinger, C.F., Y.X. Wang, N.A. Dumont, and M.A. Rudnicki. 2013. Cellular dynamics in the muscle satellite cell niche. *EMBO reports*. 14:1062-1072.

Bintliff, S., and B.E. Walker. 1960. Radioautographic study of skeletal muscle regeneration. *The American journal of anatomy*. 106: 233-245.

Bione, S., E. Maestrini, S. Rivella, M. Mancini, S. Regis, G. Romeo, and D. Toniolo. 1994. Identification of a novel X-linked gene responsible for Emery-Dreifuss muscular dystrophy. *Nat Genet*. 8:323-327.

Blakeley, W.R., E.J. Garety, and D.E. Smith. 1968. Section of the cricopharyngeus muscle for dysphagia. *Archives of surgery*. 96:745-762.

Blanco-Bose, W.E., C.C. Yao, R.H. Kramer, and H.M. Blau. 2001. Purification of mouse primary myoblasts based on alpha 7 integrin expression. *Exp Cell Res*. 265:212-220.

Blau, H.M., C. Webster, and G.K. Pavlath. 1983. Defective myoblasts identified in Duchenne muscular dystrophy. *Proceedings of the National Academy of Sciences of the United States of America*. 80:4856-4860.

Bloem, B.R., A.M. Lagaay, W. van Beek, J. Haan, R.A. Roos, and A.R. Wintzen. 1990. Prevalence of subjective dysphagia in community residents aged over 87. *Bmj*. 300:721-722.

Bondesen, B.A., S.T. Mills, K.M. Kegley, and G.K. Pavlath. 2004. The COX-2 pathway is essential during early stages of skeletal muscle regeneration. *American journal of physiology. Cell physiology*. 287:C475-483.

Bonne, G., M.R. Di Barletta, S. Varnous, H.M. Becane, E.H. Hammouda, L. Merlini, F. Muntoni, C.R. Greenberg, F. Gary, J.A. Urtizberea, D. Duboc, M. Fardeau, D. Toniolo, and K. Schwartz. 1999. Mutations in the gene encoding lamin A/C cause autosomal dominant Emery-Dreifuss muscular dystrophy. *Nat Genet*. 21:285-288.

Bosnakovski, D., S. Lamb, T. Simsek, Z. Xu, A. Belayew, R. Perlingeiro, and M. Kyba. 2008a. DUX4c, an FSHD candidate gene, interferes with myogenic regulators and abolishes myoblast differentiation. *Experimental neurology*. 214:87-96.

Bosnakovski, D., Z. Xu, E.J. Gang, C.L. Galindo, M. Liu, T. Simsek, H.R. Garner, S. Agha-Mohammadi, A. Tassin, F. Coppee, A. Belayew, R.R. Perlingeiro, and M. Kyba. 2008b. An isogenetic myoblast expression screen identifies DUX4-mediated FSHD-associated molecular pathologies. *The EMBO journal*. 27:2766-2779.

Brack, A.S., H. Bildsoe, and S.M. Hughes. 2005. Evidence that satellite cell decrement contributes to preferential decline in nuclear number from large fibres during murine age-related muscle atrophy. *J Cell Sci*. 118:4813-4821.

Brack, A.S., M.J. Conboy, S. Roy, M. Lee, C.J. Kuo, C. Keller, and T.A. Rando. 2007. Increased Wnt signaling during aging alters muscle stem cell fate and increases fibrosis. *Science*. 317:807-810.

Brack, A.S., and T.A. Rando. 2007. Intrinsic changes and extrinsic influences of myogenic stem cell function during aging. *Stem cell reviews*. 3:226-237.

Brais, B., J.P. Bouchard, Y.G. Xie, D.L. Rochefort, N. Chrétien, F.M. Tomé, R.G. Lafrenière, J.M. Rommens, E. Uyama, O. Nohira, S. Blumen, A.D. Korczyn, P. Heutink, J. Mathieu, A. Duranceau, F. Codère, M. Fardeau, G.A. Rouleau, and A.D. Korcyn. 1998. Short GCG expansions in the PABP2 gene cause oculopharyngeal muscular dystrophy. *Nat Genet*. 18:164-167.

Bredman, J.J., W.A. Weijs, H.A. Korfage, P. Brugman, and A.F. Moorman. 1992. Myosin heavy chain expression in rabbit masseter muscle during postnatal development. *Journal of anatomy*. 180 ( Pt 2):263-274.

Broglio, L., M. Tentorio, M.S. Cotelli, M. Mancuso, V. Vielmi, V. Gregorelli, A. Padovani, and M. Filosto. 2010. Limb-girdle muscular dystrophy-associated protein diseases. *The neurologist*. 16:340-352.

Broholm, C., M.J. Laye, C. Brandt, R. Vadalasetty, H. Pilegaard, B.K. Pedersen, and C. Scheele. 2011. LIF is a contraction-induced myokine stimulating human myocyte proliferation. *Journal of applied physiology*. 111:251-259.

Bulfield, G., W.G. Siller, P.A. Wight, and K.J. Moore. 1984. X chromosome-linked muscular dystrophy (mdx) in the mouse. *Proceedings of the National Academy of Sciences of the United States of America*. 81:1189-1192.

Bumm, K., M. Zenker, and A. Bozzato. 2009. Oculopharyngeal muscular dystrophy as a rare differential diagnosis for unexplained dysphagia: a case report. *Cases journal*. 2:94.

Butler-Browne, G.S., P.O. Eriksson, C. Laurent, and L.E. Thornell. 1988. Adult human masseter muscle fibers express myosin isozymes characteristic of development. *Muscle Nerve*. 11:610-620.

Calado, A., F.M. Tome, B. Brais, G.A. Rouleau, U. Kuhn, E. Wahle, and M. Carmo-Fonseca. 2000. Nuclear inclusions in oculopharyngeal muscular dystrophy consist of poly(A) binding protein 2 aggregates which sequester poly(A) RNA. *Hum Mol Genet*. 9:2321-2328.

Chang, N.C., and M.A. Rudnicki. 2014. Satellite cells: the architects of skeletal muscle. *Current topics in developmental biology*. 107:161-181.

Chazaud, B., C. Sonnet, P. Lafuste, G. Bassez, A.-C. Rimaniol, F. Poron, F.-J. Authier, P.A. Dreyfus, and R.K. Gherardi. 2003a. Satellite cells attract monocytes and use macrophages as a support to escape apoptosis and enhance muscle growth. *J Cell Biol*. 163:1133-1143.

Chazaud, B., C. Sonnet, P. Lafuste, G. Bassez, A.C. Rimaniol, F. Poron, F.J. Authier, P.A. Dreyfus, and R.K. Gherardi. 2003b. Satellite cells attract monocytes and use macrophages as a support to escape apoptosis and enhance muscle growth. *The Journal of cell biology*. 163:1133-1143.

Christiansen, S.P., and L.K. McLoon. 2006. The effect of resection on satellite cell activity in rabbit extraocular muscle. *Invest Ophthalmol Vis Sci*. 47:605-613.

Clark, W.E. 1946. An experimental study of the regeneration of mammalian striped muscle. *Journal of anatomy*. 80:24-36 24.

Collins, C.A., I. Olsen, P.S. Zammit, L. Heslop, A. Petrie, T.A. Partridge, and J.E. Morgan. 2005. Stem cell function, self-renewal, and behavioral heterogeneity of cells from the adult muscle satellite cell niche. *Cell*. 122:289-301.

Conboy, I.M., M.J. Conboy, A.J. Wagers, E.R. Girma, I.L. Weissman, and T.A. Rando. 2005. Rejuvenation of aged progenitor cells by exposure to a young systemic environment. *Nature*. 433:760-764.

Cooper, R.N., S. Tajbakhsh, V. Mouly, G. Cossu, M. Buckingham, and G.S. Butler-Browne. 1999. In vivo satellite cell activation via Myf5 and MyoD in regenerating mouse skeletal muscle. *J Cell Sci*. 112 ( Pt 17):2895-2901.

Cornelison, D.D., M.S. Filla, H.M. Stanley, A.C. Rapraeger, and B.B. Olwin. 2001. Syndecan-3 and syndecan-4 specifically mark skeletal muscle satellite cells and are implicated in satellite cell maintenance and muscle regeneration. *Dev Biol*. 239:79-94.

Couly, G.F., P.M. Coltey, and N.M. Le Douarin. 1992. The developmental fate of the cephalic mesoderm in quail-chick chimeras. *Development*. 114:1-15.

Czajkowski, M.T., C. Rassek, D.C. Lenhard, D. Brohl, and C. Birchmeier. 2014. Divergent and conserved roles of Dll1 signaling in development of craniofacial and trunk muscle. *Dev Biol*. 395:307-316.

Davies, J.E., S. Sarkar, and D.C. Rubinsztein. 2008. Wild-type PABPN1 is anti-apoptotic and reduces toxicity of the oculopharyngeal muscular dystrophy mutation. *In* Hum Mol Genet. Vol. 17. 1097-1108.

Davies, J.E., L. Wang, L. Garcia-Oroz, L.J. Cook, C. Vacher, D.G. O'Donovan, and D.C. Rubinsztein. 2005. Doxycycline attenuates and delays toxicity of the oculopharyngeal muscular dystrophy mutation in transgenic mice. *Nat Med*. 11:672-677.

Davis, M.V., A.L. Merati, S.S. Jaradeh, and J.H. Blumin. 2007. Myosin heavy chain composition and fiber size of the cricopharyngeus muscle in patients with achalasia and normal subjects. *In* The Annals of otology, rhinology, and laryngology. Vol. 116. 643-646.

Day, J.W., and L.P. Ranum. 2005. Genetics and molecular pathogenesis of the myotonic dystrophies. *Current neurology and neuroscience reports*. 5:55-59.

Dayal, V.S., and J. Freeman. 1976. Cricopharyngeal myotomy for dysphagia in oculopharyngeal muscular dystrophy. Report of a case. *Archives of otolaryngology*. 102:115-116.

Decary, S., C.B. Hamida, V. Mouly, J.P. Barbet, F. Hentati, and G.S. Butler-Browne. 2000. Shorter telomeres in dystrophic muscle consistent with extensive regeneration in young children. *Neuromuscul Disord*. 10:113-120.

Dimachkie, M.M., and R.J. Barohn. 2014. Distal myopathies. *Neurologic clinics*. 32:817-842, x.

Dion, P., V. Shanmugam, C. Gaspar, C. Messaed, I. Meijer, A. Toulouse, J. Laganiere, J. Roussel, D. Rochefort, S. Laganiere, C. Allen, G. Karpati, J.P. Bouchard, B. Brais, and G.A. Rouleau. 2005. Transgenic expression of an expanded (GCG)13 repeat PABPN1 leads to weakness and coordination defects in mice. *Neurobiol Dis*. 18:528-536.

Doherty, T.J. 2003. Invited review: Aging and sarcopenia. *In* J Appl Physiol. Vol. 95. 1717-1727.

Donner, M.W., J.F. Bosma, and D.L. Robertson. 1985. Anatomy and physiology of the pharynx. *In* Gastrointest Radiol. Vol. 10. 196-212.

Dreyer, H.C., C.E. Blanco, F.R. Sattler, E.T. Schroeder, and R.A. Wiswell. 2006. Satellite cell numbers in young and older men 24 hours after eccentric exercise. *Muscle Nerve*. 33:242-253.

Dupont-Versteegden, E.E., R.J. Murphy, J.D. Houle, C.M. Gurley, and C.A. Peterson. 1999. Activated satellite cells fail to restore myonuclear number in spinal cord transected and exercised rats. *The American journal of physiology*. 277:C589-597.

Durbeej, M., and K.P. Campbell. 2002. Muscular dystrophies involving the dystrophin-glycoprotein complex: an overview of current mouse models. *Current opinion in genetics & development*. 12:349-361.

Dutta, C.R., and J.V. Basmajian. 1960. Gross and histological structure of the pharyngeal constrictors in the rabbit. *In* The Anatomical record. Vol. 137. 127-134.

Edström, L., H. Larsson, and L. Larsson. 1992. Neurogenic effects on the palatopharyngeal muscle in patients with obstructive sleep apnoea: a muscle biopsy study. *In* J Neurol Neurosurg Psychiatr. Vol. 55. 916-920.

Eicher, P.S., D.M. McDonald-Mcginn, C.A. Fox, D.A. Driscoll, B.S. Emanuel, and E.H. Zackai. 2000. Dysphagia in children with a 22q11.2 deletion: unusual pattern found on modified barium swallow. *The Journal of pediatrics*. 137:158-164.

Ekberg, O., M. Ekman, L.I. Eriksson, R. Malm, E. Sundman, and A. Arner. 2009a. An in vitro model for studying neuromuscular transmission in the mouse pharynx. *In* Dysphagia. Vol. 24. 32-39.

Ekberg, O., M. Ekman, L.I. Eriksson, R. Malm, E. Sundman, and A. Arner. 2009b. An in vitro model for studying neuromuscular transmission in the mouse pharynx. *Dysphagia*. 24:32-39.

Emery, A.E.H. 2002. The muscular dystrophies. *Lancet*. 359:687-695.

Ertekin, C. 2002. Physiological and pathological aspects of oropharyngeal swallowing. *Mov Disord*. 17 Suppl 2:S86-89.

Ertekin, C., and I. Aydogdu. 2003. Neurophysiology of swallowing. *Clin Neurophysiol*. 114:2226-2244.

Ertekin, C., S. Tarlaci, I. Aydogdu, N. Kiylioglu, N. Yuceyar, A.B. Turman, Y. Secil, and F. Esmeli. 2002. Electrophysiological evaluation of pharyngeal phase of swallowing in patients with Parkinson's disease. *Mov Disord*. 17:942-949.

Ertekin, C., N. Yuceyar, and I. Aydogdu. 1998. Clinical and electrophysiological evaluation of dysphagia in myasthenia gravis. *J Neurol Neurosurg Psychiatry*. 65:848-856.

Eslick, G.D., and N.J. Talley. 2008. Dysphagia: epidemiology, risk factors and impact on quality of life--a population-based study. *Alimentary pharmacology & therapeutics*. 27:971-979.

Esteve-Altava, B., R. Diogo, C. Smith, J.C. Boughner, and D. Rasskin-Gutman. 2015. Anatomical networks reveal the musculoskeletal modularity of the human head. *Scientific reports*. 5:8298.

Favreau, C., D. Higuet, J.C. Courvalin, and B. Buendia. 2004. Expression of a mutant lamin A that causes Emery-Dreifuss muscular dystrophy inhibits in vitro differentiation of C2C12 myoblasts. *Molecular and cellular biology*. 24:1481-1492.

Frock, R.L., B.A. Kudlow, A.M. Evans, S.A. Jameson, S.D. Hauschka, and B.K. Kennedy. 2006. Lamin A/C and emerin are critical for skeletal muscle satellite cell differentiation. *Genes Dev*. 20:486-500.

Fry, C.S., J.D. Lee, J.R. Jackson, T.J. Kirby, S.A. Stasko, H. Liu, E.E. Dupont-Versteegden, J.J. McCarthy, and C.A. Peterson. 2014. Regulation of the muscle fiber microenvironment by activated satellite cells during hypertrophy. *FASEB J*. 28:1654-1665.

Fry, C.S., J.D. Lee, J. Mula, T.J. Kirby, J.R. Jackson, F. Liu, L. Yang, C.L. Mendias, E.E. Dupont-Versteegden, J.J. McCarthy, and C.A. Peterson. 2015. Inducible depletion of satellite cells in adult, sedentary mice impairs muscle regenerative capacity without affecting sarcopenia. *Nat Med*. 21:76-80.

Fukada, S., A. Uezumi, M. Ikemoto, S. Masuda, M. Segawa, N. Tanimura, H. Yamamoto, Y. Miyagoe-Suzuki, and S. Takeda. 2007. Molecular signature of quiescent satellite cells in adult skeletal muscle. *Stem cells*. 25:2448-2459.

Fukada, S., M. Yamaguchi, H. Kokubo, R. Ogawa, A. Uezumi, T. Yoneda, M.M. Matev, N. Motohashi, T. Ito, A. Zolkiewska, R.L. Johnson, Y. Saga, Y. Miyagoe-Suzuki, K. Tsujikawa, S. Takeda, and H. Yamamoto. 2011. Hesr1 and Hesr3 are essential to generate undifferentiated quiescent satellite cells and to maintain satellite cell numbers. *Development*. 138:4609-4619.

Furling, D., L. Coiffier, V. Mouly, J.P. Barbet, J.L. St Guily, K. Taneja, G. Gourdon, C. Junien, and G.S. Butler-Browne. 2001. Defective satellite cells in congenital myotonic dystrophy. *Hum Mol Genet*. 10:2079-2087.

Gidaro, T., E. Negroni, S. Périé, M. Mirabella, J. Lainé, J. Lacau St Guily, G. Butler-Browne, V. Mouly, and C. Trollet. 2013. Atrophy, fibrosis, and increased PAX7-positive cells in pharyngeal muscles of oculopharyngeal muscular dystrophy patients. *In* J. Neuropathol. Exp. Neurol. Vol. 72. 234-243.

Girgenrath, M., C.A. Kostek, and J.B. Miller. 2005. Diseased muscles that lack dystrophin or laminin-alpha2 have altered compositions and proliferation of mononuclear cell populations. *BMC neurology*. 5:7.

Godfrey, C., E. Clement, R. Mein, M. Brockington, J. Smith, B. Talim, V. Straub, S. Robb, R. Quinlivan, L. Feng, C. Jimenez-Mallebrera, E. Mercuri, A.Y. Manzur, M. Kinali, S. Torelli, S.C. Brown, C.A. Sewry, K. Bushby, H. Topaloglu, K. North, S. Abbs, and F. Muntoni. 2007. Refining genotype phenotype correlations in muscular dystrophies with defective glycosylation of dystroglycan. *Brain : a journal of neurology*. 130:2725-2735.

Gopinath, S.D., and T.A. Rando. 2008. Stem cell review series: aging of the skeletal muscle stem cell niche. *Aging Cell*. 7:590-598.

Grasl-Kraupp, B., B. Ruttkay-Nedecky, H. Koudelka, K. Bukowska, W. Bursch, and R. Schulte-Hermann. 1995. In situ detection of fragmented DNA (TUNEL assay) fails to discriminate among apoptosis, necrosis, and autolytic cell death: a cautionary note. *Hepatology*. 21:1465-1468.

Grenier, J., M.A. Teillet, R. Grifone, R.G. Kelly, and D. Duprez. 2009. Relationship between neural crest cells and cranial mesoderm during head muscle development. *PLoS One*. 4:e4381.

Griffin, C.A., L.H. Apponi, K.K. Long, and G.K. Pavlath. 2010. Chemokine expression and control of muscle cell migration during myogenesis. *J Cell Sci*. 123:3052-3060.

Harel, I., E. Nathan, L. Tirosh-Finkel, H. Zigdon, N. Guimarães-Camboa, S.M. Evans, and E. Tzahor. 2009. Distinct origins and genetic programs of head muscle satellite cells. *Dev Cell*. 16:822-832.

Helbling-Leclerc, A., G. Bonne, and K. Schwartz. 2002. Emery-Dreifuss muscular dystrophy. *European journal of human genetics : EJHG*. 10:157-161.

Henningsen, J., B.K. Pedersen, and I. Kratchmarova. 2011. Quantitative analysis of the secretion of the MCP family of chemokines by muscle cells. *Molecular bioSystems*. 7:311-321.

Hikida, R.S., S. Van Nostran, J.D. Murray, R.S. Staron, S.E. Gordon, and W.J. Kraemer. 1997. Myonuclear loss in atrophied soleus muscle fibers. *The Anatomical record*. 247:350-354.

Himmelreich, H.A. 1973. [The palatopharyngeal muscle of mammals]. *In* Gegenbaurs Morphol Jahrb. Vol. 119. 172-212.

Hino, H., K. Araki, E. Uyama, M. Takeya, M. Araki, K. Yoshinobu, K. Miike, Y. Kawazoe, Y. Maeda, M. Uchino, and K. Yamamura. 2004. Myopathy phenotype in transgenic mice expressing mutated PABPN1 as a model of oculopharyngeal muscular dystrophy. *Hum Mol Genet*. 13:181-190.

Hoffman, E.P., R.H. Brown, Jr., and L.M. Kunkel. 1987. Dystrophin: the protein product of the Duchenne muscular dystrophy locus. *Cell*. 51:919-928.

Holland, G., V. Jayasekeran, N. Pendleton, M. Horan, M. Jones, and S. Hamdy. 2011. Prevalence and symptom profiling of oropharyngeal dysphagia in a community dwelling of an elderly population: a self-reporting questionnaire survey. *Diseases of the esophagus : official journal of the International Society for Diseases of the Esophagus / I.S.D.E*. 24:476-480.

Hu, P., K.G. Geles, J.H. Paik, R.A. DePinho, and R. Tjian. 2008. Codependent activators direct myoblast-specific MyoD transcription. *Dev Cell*. 15:534-546.

Hyodo, M., E. Yumoto, S. Kawakita, and T. Yamagata. 1999. Postnatal changes in the types of muscle fibre in the canine inferior pharyngeal constrictor. *In* Acta Otolaryngol. Vol. 119. 843-846.

Ikemoto, M., S. Fukada, A. Uezumi, S. Masuda, H. Miyoshi, H. Yamamoto, M.R. Wada, N. Masubuchi, Y. Miyagoe-Suzuki, and S. Takeda. 2007. Autologous transplantation of SM/C-2.6(+) satellite cells transduced with micro-dystrophin CS1 cDNA by lentiviral vector into mdx mice. *Molecular therapy : the journal of the American Society of Gene Therapy*. 15:2178-2185.

Jackson, J.R., J. Mula, T.J. Kirby, C.S. Fry, J.D. Lee, M.F. Ubele, K.S. Campbell, J.J. McCarthy, C.A. Peterson, and E.E. Dupont-Versteegden. 2012. Satellite cell depletion does not inhibit adult skeletal muscle regrowth following unloading-induced atrophy. *American journal of physiology. Cell physiology*. 303:C854-861.

Jacob, H.J., J. Lazar, M.R. Dwinell, C. Moreno, and A.M. Geurts. 2010. Gene targeting in the rat: advances and opportunities. *Trends in genetics : TIG*. 26:510-518.

Janssen, I., S.B. Heymsfield, Z.M. Wang, and R. Ross. 2000. Skeletal muscle mass and distribution in 468 men and women aged 18-88 yr. *Journal of applied physiology*. 89:81-88.

Jerome, L.A., and V.E. Papaioannou. 2001. DiGeorge syndrome phenotype in mice mutant for the T-box gene, Tbx1. *Nat Genet*. 27:286-291.

Johnson, B.D., L.E. Wilson, W.Z. Zhan, J.F. Watchko, M.J. Daood, and G.C. Sieck. 1994. Contractile properties of the developing diaphragm correlate with myosin heavy chain phenotype. *Journal of applied physiology*. 77:481-487.

Kafadar, K.A., L. Yi, Y. Ahmad, L. So, F. Rossi, and G.K. Pavlath. 2009. Sca-1 expression is required for efficient remodeling of the extracellular matrix during skeletal muscle regeneration. *Dev Biol*. 326:47-59.

Kallestad, K.M., S.L. Hebert, A.A. McDonald, M.L. Daniel, S.R. Cu, and L.K. McLoon. 2011. Sparing of extraocular muscle in aging and muscular dystrophies: a myogenic precursor cell hypothesis. *Exp Cell Res*. 317:873-885.

Kaminski, H.J., M. al-Hakim, R.J. Leigh, M.B. Katirji, and R.L. Ruff. 1992. Extraocular muscles are spared in advanced Duchenne dystrophy. *Annals of neurology*. 32:586-588.

Katz, F.R.S. 1961. The termination of the afferent nerve fiber in the muscle spindle of the frog. . *Philos Trans R Soc Lond B Biol Sci*. 243:221-225.

Kawashima, K., Y. Motohashi, and I. Fujishima. 2004. Prevalence of dysphagia among community-dwelling elderly individuals as estimated using a questionnaire for dysphagia screening. *Dysphagia*. 19:266-271.

Kelly, R.G. 2010. Core issues in craniofacial myogenesis. *Experimental cell research*.

Kelly, R.G., L.A. Jerome-Majewska, and V.E. Papaioannou. 2004. The del22q11.2 candidate gene Tbx1 regulates branchiomeric myogenesis. *Hum Mol Genet*. 13:2829-2840.

Kirberger, R.M., G. Steenkamp, T.C. Spotswood, S.C. Boy, D.B. Miller, and M. van Zyl. 2006. Stenotic nasopharyngeal dysgenesis in the dachshund: seven cases (2002-2004). *In* J Am Anim Hosp Assoc. Vol. 119. 290-297.

Kuang, S., M.A. Gillespie, and M.A. Rudnicki. 2008. Niche regulation of muscle satellite cell self-renewal and differentiation. *Cell Stem Cell*. 2:22-31.

Kuang, S., K. Kuroda, F. Le Grand, and M.A. Rudnicki. 2007. Asymmetric self-renewal and commitment of satellite stem cells in muscle. *Cell*. 129:999-1010.

Kühn, U., M. Gündel, A. Knoth, Y. Kerwitz, S. Rüdel, and E. Wahle. 2009. Poly(A) tail length is controlled by the nuclear poly(A)-binding protein regulating the interaction between poly(A) polymerase and the cleavage and polyadenylation specificity factor. *J Biol Chem*. 284:22803-22814.

Kuhn, U., and E. Wahle. 2004. Structure and function of poly(A) binding proteins. *Biochim Biophys Acta*. 1678:67-84.

LaFramboise, W.A., R.D. Guthrie, D. Scalise, V. Elborne, K.L. Bombach, C.S. Armanious, and J.A. Magovern. 2003. Effect of muscle origin and phenotype on satellite cell muscle-specific gene expression. *Journal of molecular and cellular cardiology*. 35:1307-1318.

Lee, S.J., T.V. Huynh, Y.S. Lee, S.M. Sebald, S.A. Wilcox-Adelman, N. Iwamori, C. Lepper, M.M. Matzuk, and C.M. Fan. 2012. Role of satellite cells versus myofibers in muscle hypertrophy induced by inhibition of the myostatin/activin signaling pathway. *Proceedings of the National Academy of Sciences of the United States of America*. 109:E2353-2360.

Leese, G., and D. Hopwood. 1986. Muscle fibre typing in the human pharyngeal constrictors and oesophagus: the effect of ageing. *In* Acta Anat (Basel). Vol. 127. 77-80.

Lepper, C., S.J. Conway, and C.M. Fan. 2009. Adult satellite cells and embryonic muscle progenitors have distinct genetic requirements. *Nature*. 460:627-631.

Lepper, C., T.A. Partridge, and C.M. Fan. 2011. An absolute requirement for Pax7-positive satellite cells in acute injury-induced skeletal muscle regeneration. *Development*. 138:3639-3646.

Lescaudron, L., E. Peltekian, J. Fontaine-Perus, D. Paulin, M. Zampieri, L. Garcia, and E. Parrish. 1999. Blood borne macrophages are essential for the triggering of muscle regeneration following muscle transplant. *Neuromuscul Disord*. 9:72-80.

Lever, T.E., S.M. Braun, R.T. Brooks, R.A. Harris, L.L. Littrell, R.M. Neff, C.J. Hinkel, M.J. Allen, and M.A. Ulsas. 2015. Adapting Human Videofluoroscopic Swallow Study Methods to Detect and Characterize Dysphagia in Murine Disease Models. *J Vis Exp*. 97:e52319.

Lever, T.E., A. Gorsek, K.T. Cox, K.F. O'Brien, N.F. Capra, M.S. Hough, and A.K. Murashov. 2009. An animal model of oral dysphagia in amyotrophic lateral sclerosis. *Dysphagia*. 24:180-195.

Lever, T.E., E. Simon, K.T. Cox, N.F. Capra, K.F. O'Brien, M.S. Hough, and A.K. Murashov. 2010. A mouse model of pharyngeal dysphagia in amyotrophic lateral sclerosis. *Dysphagia*. 25:112-126.

Lexell, J., C.C. Taylor, and M. Sjöström. 1988. What is the cause of the ageing atrophy? Total number, size and proportion of different fiber types studied in whole vastus lateralis muscle from 15- to 83-year-old men. *In* J. Neurol. Sci. Vol. 84. 275-294.

Lindgren, S., and L. Janzon. 1991. Prevalence of swallowing complaints and clinical findings among 50-79-year-old men and women in an urban population. *Dysphagia*. 6:187-192.

Little, B.W., and D.P. Perl. 1982. Oculopharyngeal muscular dystrophy. An autopsied case from the French-Canadian kindred. *In* J. Neurol. Sci. Vol. 53. 145-158.

Livak, K.J., and T.D. Schmittgen. 2001. Analysis of relative gene expression data using real-time quantitative PCR and the 2(-Delta Delta C(T)) Method. *Methods*. 25:402-408.

Logemann, J.A. 2007. Swallowing disorders. *Best practice & research Clinical gastroenterology*. 21:563-573.

Lu, H., X. Luan, Y. Yuan, M. Dong, W. Sun, and C. Yan. 2008. The clinical and myopathological features of oculopharyngodistal myopathy in a Chinese family. *Neuropathology*. 28:599-603.

Lu, J.R., R. Bassel-Duby, A. Hawkins, P. Chang, R. Valdez, H. Wu, L. Gan, J.M. Shelton, J.A. Richardson, and E.N. Olson. 2002. Control of facial muscle development by MyoR and capsulin. *Science*. 298:2378-2381.

MacIntosh, B.R., P.F. Gardiner, and A.J. McComas. 2006. Skeletal muscle : form and function. Human Kinetics, Champaign, IL. viii, 423 p. pp.

Madisen, L., T.A. Zwingman, S.M. Sunkin, S.W. Oh, H.A. Zariwala, H. Gu, L.L. Ng, R.D. Palmiter, M.J. Hawrylycz, A.R. Jones, E.S. Lein, and H. Zeng. 2010. A robust and high-throughput Cre reporting and characterization system for the whole mouse brain. *Nature neuroscience*. 13:133-140.

Marques, M.J., R. Ferretti, V.U. Vomero, E. Minatel, and H.S. Neto. 2007. Intrinsic laryngeal muscles are spared from myonecrosis in the mdx mouse model of Duchenne muscular dystrophy. *Muscle Nerve*. 35:349-353.

Martin, B.J., M.M. Corlew, H. Wood, D. Olson, L.A. Golopol, M. Wingo, and N. Kirmani. 1994. The association of swallowing dysfunction and aspiration pneumonia. *Dysphagia*. 9:1-6.

Mauro, A. 1961. Satellite cell of skeletal muscle fibers. *The Journal of biophysical and biochemical cytology*. 9:493-495.

McCarthy, J.J., J. Mula, M. Miyazaki, R. Erfani, K. Garrison, A.B. Farooqui, R. Srikuea, B.A. Lawson, B. Grimes, C. Keller, G. Van Zant, K.S. Campbell, K.A. Esser, E.E. Dupont-Versteegden, and C.A. Peterson. 2011. Effective fiber hypertrophy in satellite cell-depleted skeletal muscle. *Development*. 138:3657-3666.

McGeachie, J., and D. Allbrook. 1978. Cell proliferation in skeletal muscle following denervation or tenotomy. A series of autoradiographic studies. *Cell and tissue research*. 193:259-267.

McLennan, I.S. 1996. Degenerating and regenerating skeletal muscles contain several subpopulations of macrophages with distinct spatial and temporal distributions. *Journal of anatomy*. 188 ( Pt 1):17-28.

McLoon, L.K. 1998. Muscle fiber type compartmentalization and expression of an immature myosin isoform in the sternocleidomastoid muscle of rabbits and primates. *In* J. Neurol. Sci. Vol. 156. 3-11.

McLoon, L.K., J. Rowe, J. Wirtschafter, and K.M. McCormick. 2004. Continuous myofiber remodeling in uninjured extraocular myofibers: myonuclear turnover and evidence for apoptosis. *Muscle Nerve*. 29:707-715.

McLoon, L.K., K.M. Thorstenson, A. Solomon, and M.P. Lewis. 2007. Myogenic precursor cells in craniofacial muscles. *Oral diseases*. 13:134-140.

McLoon, L.K., and J. Wirtschafter. 2002a. Activated satellite cells are present in uninjured extraocular muscles of mature mice. *Transactions of the American Ophthalmological Society*. 100:119-123; discussion 123-114.

McLoon, L.K., and J. Wirtschafter. 2003. Activated satellite cells in extraocular muscles of normal adult monkeys and humans. *Invest Ophthalmol Vis Sci*. 44:1927-1932.

McLoon, L.K., and J.D. Wirtschafter. 2002b. Continuous myonuclear addition to single extraocular myofibers in uninjured adult rabbits. *Muscle Nerve*. 25:348-358.

Messaed, C., and G.A. Rouleau. 2009. Molecular mechanisms underlying polyalanine diseases. *Neurobiol Dis*. 34:397-405.

Mijaljica, D., M. Prescott, and R.J. Devenish. 2010. The intricacy of nuclear membrane dynamics during nucleophagy. *Nucleus*. 1:213-223.

Miller, A.J. 2002. Oral and pharyngeal reflexes in the mammalian nervous system: their diverse range in complexity and the pivotal role of the tongue. *Crit Rev Oral Biol Med*. 13:409-425.

Miller, A.J. 2008. The neurobiology of swallowing and dysphagia. *Developmental disabilities research reviews*. 14:77-86.

Minetti, G.C., C. Colussi, R. Adami, C. Serra, C. Mozzetta, V. Parente, S. Fortuni, S. Straino, M. Sampaolesi, M. Di Padova, B. Illi, P. Gallinari, C. Steinkuhler, M.C. Capogrossi, V. Sartorelli, R. Bottinelli, C. Gaetano, and P.L. Puri. 2006. Functional and morphological recovery of dystrophic muscles in mice treated with deacetylase inhibitors. *Nat Med*. 12:1147-1150.

Mitchell, P.O., and G.K. Pavlath. 2001. A muscle precursor cell-dependent pathway contributes to muscle growth after atrophy. *American journal of physiology. Cell physiology*. 281:C1706-1715.

Mitchell, P.O., and G.K. Pavlath. 2004. Skeletal muscle atrophy leads to loss and dysfunction of muscle precursor cells. *American journal of physiology. Cell physiology*. 287:C1753-1762.

Mitsuhashi, S., and P.B. Kang. 2012. Update on the genetics of limb girdle muscular dystrophy. *Seminars in pediatric neurology*. 19:211-218.

Mittelbronn, M., T. Sullivan, C.L. Stewart, and A. Bornemann. 2008. Myonuclear degeneration in LMNA null mice. *Brain pathology*. 18:338-343.

Monaco, A.P., C.J. Bertelson, S. Liechti-Gallati, H. Moser, and L.M. Kunkel. 1988. An explanation for the phenotypic differences between patients bearing partial deletions of the DMD locus. *Genomics*. 2:90-95.

Montgomery, W.W., and J.P. Lynch. 1971. Oculopharyngeal muscular dystrophy treated by inferior constrictor myotomy. *Transactions - American Academy of Ophthalmology and Otolaryngology. American Academy of Ophthalmology and Otolaryngology*. 75:986-993.

Mootoosamy, R.C., and S. Dietrich. 2002. Distinct regulatory cascades for head and trunk myogenesis. *Development*. 129:573-583.

Morgan, J.E., and P.S. Zammit. 2010. Direct effects of the pathogenic mutation on satellite cell function in muscular dystrophy. *Experimental cell research*.

Mouly, V., F. Edom, J.P. Barbet, and G.S. Butler-Browne. 1993. Plasticity of human satellite cells. *Neuromuscul Disord*. 3:371-377.

Mu, L., and I. Sanders. 1998. Neuromuscular organization of the human upper esophageal sphincter. *In* The Annals of otology, rhinology, and laryngology. Vol. 107. 370-377.

Mu, L., and I. Sanders. 2002. Muscle fiber-type distribution pattern in the human cricopharyngeus muscle. *In* Dysphagia. Vol. 17. 87-96.

Mu, L., S. Sobotka, J. Chen, H. Su, I. Sanders, C.H. Adler, H.A. Shill, J.N. Caviness, J.E. Samanta, T.G. Beach, and A.P.a.s.D. Consortium. 2012. Altered pharyngeal muscles in Parkinson disease. *In* J. Neuropathol. Exp. Neurol. Vol. 71. 520-530.

Mu, L., H. Su, J. Wang, and I. Sanders. 2007. Myosin heavy chain-based fiber types in the adult human cricopharyngeus muscle. *In* Muscle Nerve. Vol. 35. 637-648.

Murphy, M.M., J.A. Lawson, S.J. Mathew, D.A. Hutcheson, and G. Kardon. 2011. Satellite cells, connective tissue fibroblasts and their interactions are crucial for muscle regeneration. *Development*. 138:3625-3637.

Nakano, T., and H. Muto. 1985. Anatomical observations in the pharynx of the mouse with special reference to the nasopharyngeal hiatus (Wood Jones). *In* Acta Anat (Basel). Vol. 121. 147-152.

Nigro, G., L.I. Comi, L. Politano, and R.J. Bain. 1990. The incidence and evolution of cardiomyopathy in Duchenne muscular dystrophy. *International journal of cardiology*. 26:271-277.

Nishijo, K., T. Hosoyama, C.R. Bjornson, B.S. Schaffer, S.I. Prajapati, A.N. Bahadur, M.S. Hansen, M.C. Blandford, A.T. McCleish, B.P. Rubin, J.A. Epstein, T.A. Rando, M.R. Capecchi, and C. Keller. 2009. Biomarker system for studying muscle, stem cells, and cancer in vivo. *FASEB J*. 23:2681-2690.

Noden, D.M., and P. Francis-West. 2006. The differentiation and morphogenesis of craniofacial muscles. *Dev Dyn*. 235:1194-1218.

Nonaka, I. 1999. Distal myopathies. *Current opinion in neurology*. 12:493-499.

Nozaki, S., Y. Umaki, S. Sugishita, K. Tatara, K. Adachi, and S. Shinno. 2007. Videofluorographic assessment of swallowing function in patients with Duchenne muscular dystrophy. *Rinsho shinkeigaku = Clinical neurology*. 47:407-412.

O'Connor, R.S., S.T. Mills, K.A. Jones, S.N. Ho, and G.K. Pavlath. 2007. A combinatorial role for NFAT5 in both myoblast migration and differentiation during skeletal muscle myogenesis. *J Cell Sci*. 120:149-159.

Olson, E.N., and W.H. Klein. 1994. bHLH factors in muscle development: dead lines and commitments, what to leave in and what to leave out. *Genes Dev*. 8:1-8.

Ono, Y., L. Boldrin, P. Knopp, J.E. Morgan, and P.S. Zammit. 2010. Muscle satellite cells are a functionally heterogeneous population in both somite-derived and branchiomeric muscles. *Dev Biol*. 337:29-41.

Ontell, M., K.C. Feng, K. Klueber, R.F. Dunn, and F. Taylor. 1984. Myosatellite cells, growth, and regeneration in murine dystrophic muscle: a quantitative study. *The Anatomical record*. 208:159-174.

Pacheco-Pinedo, E.C., M.T. Budak, U. Zeiger, L.H. Jørgensen, S. Bogdanovich, H.D. Schrøder, N.A. Rubinstein, and T.S. Khurana. 2009. Transcriptional and functional differences in stem cell populations isolated from extraocular and limb muscles. *Physiol Genomics*. 37:35-42.

Pallafacchina, G., B. Blaauw, and S. Schiaffino. 2013. Role of satellite cells in muscle growth and maintenance of muscle mass. *Nutrition, metabolism, and cardiovascular diseases : NMCD*. 23 Suppl 1:S12-18.

Pannerec, A., G. Marazzi, and D. Sassoon. 2012. Stem cells in the hood: the skeletal muscle niche. *Trends Mol Med*. 18:599-606.

Park, Y.E., Y.K. Hayashi, G. Bonne, T. Arimura, S. Noguchi, I. Nonaka, and I. Nishino. 2009. Autophagic degradation of nuclear components in mammalian cells. *Autophagy*. 5:795-804.

Pavlath, G.K., D. Thaloor, T.A. Rando, M. Cheong, A.W. English, and B. Zheng. 1998. Heterogeneity among muscle precursor cells in adult skeletal muscles with differing regenerative capacities. *Dev Dyn*. 212:495-508.

Périé, S., K. Mamchaoui, V. Mouly, S. Blot, B. Bouazza, L.-E. Thornell, J.L. St Guily, and G. Butler-Browne. 2006a. Premature proliferative arrest of cricopharyngeal myoblasts in oculo-pharyngeal muscular dystrophy: Therapeutic perspectives of autologous myoblast transplantation. *Neuromuscul Disord*. 16:770-781.

Périé, S., K. Mamchaoui, V. Mouly, S. Blot, B. Bouazza, L.-E. Thornell, J.L. St Guily, and G. Butler-Browne. 2006b. Premature proliferative arrest of cricopharyngeal myoblasts in oculo-pharyngeal muscular dystrophy: Therapeutic perspectives of autologous myoblast transplantation. *In* Neuromuscul Disord. Vol. 16. 770-781.

Perie, S., C. Trollet, V. Mouly, V. Vanneaux, K. Mamchaoui, B. Bouazza, J.P. Marolleau, P. Laforet, F. Chapon, B. Eymard, G. Butler-Browne, J. Larghero, and J.L. St Guily. 2014. Autologous myoblast transplantation for oculopharyngeal

muscular dystrophy: a phase I/IIa clinical study. *Molecular therapy : the journal of the American Society of Gene Therapy*. 22:219-225.

Petrof, B.J., J.B. Shrager, H.H. Stedman, A.M. Kelly, and H.L. Sweeney. 1993. Dystrophin protects the sarcolemma from stresses developed during muscle contraction. *Proceedings of the National Academy of Sciences of the United States of America*. 90:3710-3714.

Pisconti, A., D.D. Cornelison, H.C. Olguin, T.L. Antwine, and B.B. Olwin. 2010. Syndecan-3 and Notch cooperate in regulating adult myogenesis. *The Journal of cell biology*. 190:427-441.

Porter, J.D., and R.S. Baker. 1996. Muscles of a different 'color': the unusual properties of the extraocular muscles may predispose or protect them in neurogenic and myogenic disease. *Neurology*. 46:30-37.

Porter, J.D., J.A. Rafael, R.J. Ragusa, J.K. Brueckner, J.I. Trickett, and K.E. Davies. 1998. The sparing of extraocular muscle in dystrophinopathy is lost in mice lacking utrophin and dystrophin. *J Cell Sci*. 111 ( Pt 13):1801-1811.

Prasse, J.E., and G.E. Kikano. 2009. An overview of pediatric dysphagia. *Clinical pediatrics*. 48:247-251.

Rai, M., U. Nongthomba, and M.D. Grounds. 2014. Skeletal muscle degeneration and regeneration in mice and flies. *Current topics in developmental biology*. 108:247-281.

Randolph, M.E., Q. Luo, J. Ho, K.E. Vest, A.J. Sokoloff, and G.K. Pavlath. 2014. Ageing and muscular dystrophy differentially affect murine pharyngeal muscles in a region-dependent manner. *The Journal of physiology*. 592:5301-5315.

Raz, Y., and V. Raz. 2014. Oculopharyngeal muscular dystrophy as a paradigm for muscle aging. *Frontiers in aging neuroscience*. 6:317.

Reimann, J., A. Irintchev, and A. Wernig. 2000. Regenerative capacity and the number of satellite cells in soleus muscles of normal and mdx mice. *Neuromuscul Disord*. 10:276-282.

Reiser, P.J., R.L. Moss, G.G. Giulian, and M.L. Greaser. 1985a. Shortening velocity and myosin heavy chains of developing rabbit muscle fibers. *In* J Biol Chem. Vol. 260. 14403-14405.

Reiser, P.J., R.L. Moss, G.G. Giulian, and M.L. Greaser. 1985b. Shortening velocity in single fibers from adult rabbit soleus muscles is correlated with myosin heavy chain composition. *In* J Biol Chem. Vol. 260. 9077-9080.

Relaix, F., and P.S. Zammit. 2012. Satellite cells are essential for skeletal muscle regeneration: the cell on the edge returns centre stage. *Development*. 139:2845-2856.

Riuzzi, F., G. Sorci, R. Sagheddu, and R. Donato. 2012. HMGB1-RAGE regulates muscle satellite cell homeostasis through p38-MAPK- and myogenin-dependent repression of Pax7 transcription. *J Cell Sci*. 125:1440-1454.

Robbins, J., S. Langmore, J.A. Hind, and M. Erlichman. 2002. Dysphagia research in the 21st century and beyond: proceedings from Dysphagia Experts Meeting, August 21, 2001. *Journal of rehabilitation research and development*. 39:543-548.

Robinson, D.O., S.R. Hammans, S.P. Read, and J. Sillibourne. 2005. Oculopharyngeal muscular dystrophy (OPMD): analysis of the PABPN1 gene expansion sequence in 86 patients reveals 13 different expansion types and further evidence for

unequal recombination as the mutational mechanism. *In* Hum Genet. Vol. 116. 267-271.

Rocheteau, P., B. Gayraud-Morel, I. Siegl-Cachedenier, M.A. Blasco, and S. Tajbakhsh. 2012. A subpopulation of adult skeletal muscle stem cells retains all template DNA strands after cell division. *Cell*. 148:112-125.

Rodgers, J.T., K.Y. King, J.O. Brett, M.J. Cromie, G.W. Charville, K.K. Maguire, C. Brunson, N. Mastey, L. Liu, C.R. Tsai, M.A. Goodell, and T.A. Rando. 2014. mTORC1 controls the adaptive transition of quiescent stem cells from G0 to G(Alert). *Nature*. 510:393-396.

Rolfe, D.F., and G.C. Brown. 1997. Cellular energy utilization and molecular origin of standard metabolic rate in mammals. *Physiol Rev*. 77:731-758.

Rosenblatt, J.D., and R.I. Woods. 1992. Hypertrophy of rat extensor digitorum longus muscle injected with bupivacaine. A sequential histochemical, immunohistochemical, histological and morphometric study. *Journal of anatomy*. 181 ( Pt 1):11-27.

Rubesin, S.E., J. Jessurun, D. Robertson, B. Jones, J.F. Bosma, and M.W. Donner. 1987. Lines of the pharynx. *In* Radiographics. Vol. 7. 217-237.

Rudnicki, M.A., F. Le Grand, I. McKinnell, and S. Kuang. 2008. The molecular regulation of muscle stem cell function. *Cold Spring Harbor symposia on quantitative biology*. 73:323-331.

Runge, M.S., G.A. Stouffer, R.G. Sheahan, S. Yamamoto, V.G. Tsyplenkova, and T.N. James. 2000. Morphological patterns of death by myocytes in arrhythmogenic

right ventricular dysplasia. *The American journal of the medical sciences*. 320:310-319.

Sacco, A., F. Mourkioti, R. Tran, J. Choi, M. Llewellyn, P. Kraft, M. Shkreli, S. Delp, J.H. Pomerantz, S.E. Artandi, and H.M. Blau. 2010. Short telomeres and stem cell exhaustion model Duchenne muscular dystrophy in mdx/mTR mice. *Cell*. 143:1059-1071.

Salisbury, E., B. Schoser, C. Schneider-Gold, G.L. Wang, C. Huichalaf, B. Jin, M. Sirito, P. Sarkar, R. Krahe, N.A. Timchenko, and L.T. Timchenko. 2009. Expression of RNA CCUG repeats dysregulates translation and degradation of proteins in myotonic dystrophy 2 patients. *The American journal of pathology*. 175:748-762.

Sambasivan, R., B. Gayraud-Morel, G. Dumas, C. Cimper, S. Paisant, R. Kelly, and S. Tajbakhsh. 2009. Distinct regulatory cascades govern extraocular and pharyngeal arch muscle progenitor cell fates. *Dev Cell*. 16:810-821.

Sambasivan, R., and S. Tajbakhsh. 2007. Skeletal muscle stem cell birth and properties. *Semin Cell Dev Biol*. 18:870-882.

Scapolo, P.A., A. Rowlerson, F. Mascarello, and A. Veggetti. 1991. Neonatal myosin in bovine and pig tensor tympani muscle fibres. *Journal of anatomy*. 178:255-263.

Schiaffino, S., S.P. Bormioli, and M. Aloisi. 1976. The fate of newly formed satellite cells during compensatory muscle hypertrophy. *Virchows Archiv. B: Cell pathology*. 21:113-118.

Schiaffino, S., and C. Reggiani. 2011. Fiber types in mammalian skeletal muscles. *Physiol Rev*. 91:1447-1531.

Schmalbruch, H. 1976. The morphology of regeneration of skeletal muscles in the rat. *In* Tissue Cell. Vol. 8. 673-692.

Schoser, B., and L. Timchenko. 2010. Myotonic dystrophies 1 and 2: complex diseases with complex mechanisms. *Current genomics*. 11:77-90.

Schoser, B.G., and D. Pongratz. 2006. Extraocular mitochondrial myopathies and their differential diagnoses. *Strabismus*. 14:107-113.

Seale, P., L.A. Sabourin, A. Girgis-Gabardo, A. Mansouri, P. Gruss, and M.A. Rudnicki. 2000. Pax7 is required for the specification of myogenic satellite cells. *Cell*. 102:777-786.

Seiden, D. 1976. Quantitative analysis of muscle cell changes in compensatory hypertrophy and work-induced hypertrophy. *The American journal of anatomy*. 145:459-465.

Serrano, A.L., B. Baeza-Raja, E. Perdiguero, M. Jardi, and P. Munoz-Canoves. 2008. Interleukin-6 is an essential regulator of satellite cell-mediated skeletal muscle hypertrophy. *Cell metabolism*. 7:33-44.

Shao, Y., Y. Guan, L. Wang, Z. Qiu, M. Liu, Y. Chen, L. Wu, Y. Li, X. Ma, M. Liu, and D. Li. 2014. CRISPR/Cas-mediated genome editing in the rat via direct injection of one-cell embryos. *Nature protocols*. 9:2493-2512.

Sherwood, R.I., J.L. Christensen, I.M. Conboy, M.J. Conboy, T.A. Rando, I.L. Weissman, and A.J. Wagers. 2004. Isolation of adult mouse myogenic progenitors: functional heterogeneity of cells within and engrafting skeletal muscle. *Cell*. 119:543-554.

Shi, S., Y. Xia, S. Chen, M. Li, D. Chen, F. Liu, and H. Zheng. 2014. The relationship between structural/MHC changes in upper airway palatopharyngeal muscle morphology and obstructive sleep apnea/hypopnea syndrome. *European archives of oto-rhino-laryngology : official journal of the European Federation of Oto-Rhino-Laryngological Societies*. 271:109-116.

Shinin, V., B. Gayraud-Morel, D. Gomes, and S. Tajbakhsh. 2006. Asymmetric division and cosegregation of template DNA strands in adult muscle satellite cells. *Nat Cell Biol*. 8:677-687.

Shinonaga, C., M. Fukuda, Y. Suzuki, T. Higaki, Y. Ishida, E. Ishii, M. Hyodo, T. Morimoto, and N. Sano. 2008. Evaluation of swallowing function in Duchenne muscular dystrophy. *Developmental medicine and child neurology*. 50:478-480.

Shuler, C.F., and K.R. Dalrymple. 2001. Molecular regulation of tongue and craniofacial muscle differentiation. *Crit Rev Oral Biol Med*. 12:3-17.

Sims, G.P., D.C. Rowe, S.T. Rietdijk, R. Herbst, and A.J. Coyle. 2010. HMGB1 and RAGE in inflammation and cancer. *Annual review of immunology*. 28:367-388.

Spangenburg, E.E., and F.W. Booth. 2002. Multiple signaling pathways mediate LIF-induced skeletal muscle satellite cell proliferation. *American journal of physiology. Cell physiology*. 283:C204-211.

Stedman, H.H., H.L. Sweeney, J.B. Shrager, H.C. Maguire, R.A. Panettieri, B. Petrof, M. Narusawa, J.M. Leferovich, J.T. Sladky, and A.M. Kelly. 1991. The mdx mouse diaphragm reproduces the degenerative changes of Duchenne muscular dystrophy. *Nature*. 352:536-539.

Stuelsatz, P., A. Shearer, Y. Li, L.A. Muir, N. Ieronimakis, Q.W. Shen, I. Kirillova, and Z. Yablonka-Reuveni. 2015. Extraocular muscle satellite cells are high performance myo-engines retaining efficient regenerative capacity in dystrophin deficiency. *Dev Biol*. 397:31-44.

Tajbakhsh, S. 2003. Stem cells to tissue: molecular, cellular and anatomical heterogeneity in skeletal muscle. *Current opinion in genetics & development*. 13:413-422.

Tajbakhsh, S., E. Bober, C. Babinet, S. Pournin, H. Arnold, and M. Buckingham. 1996. Gene targeting the myf-5 locus with nlacZ reveals expression of this myogenic factor in mature skeletal muscle fibres as well as early embryonic muscle. *Dev Dyn*. 206:291-300.

Tamaki, T., A. Akatsuka, K. Ando, Y. Nakamura, H. Matsuzawa, T. Hotta, R.R. Roy, and V.R. Edgerton. 2002. Identification of myogenic-endothelial progenitor cells in the interstitial spaces of skeletal muscle. *The Journal of cell biology*. 157:571-577.

Tanaka, K.K., J.K. Hall, A.A. Troy, D.D. Cornelison, S.M. Majka, and B.B. Olwin. 2009. Syndecan-4-expressing muscle progenitor cells in the SP engraft as satellite cells during muscle regeneration. *Cell Stem Cell*. 4:217-225.

Tawil, R., and S.M. Van Der Maarel. 2006. Facioscapulohumeral muscular dystrophy. *Muscle Nerve*. 34:1-15.

Taylor, E.W. 1915. Progressive vagus-glossopharyngeal paralysis with ptosis: contribution to group of family diseases. *J Nerv Ment Dis*. 42:129-139.

Tedesco, F.S., A. Dellavalle, J. Diaz-Manera, G. Messina, and G. Cossu. 2010. Repairing skeletal muscle: regenerative potential of skeletal muscle stem cells. *The Journal of clinical investigation*. 120:11-19.

Ternaux, J.P., and P. Portalier. 1993. Influence of tongue myoblasts on rat dissociated hypoglossal motoneurons in culture. *International journal of developmental neuroscience : the official journal of the International Society for Developmental Neuroscience*. 11:33-48.

Thornell, L.E., M. Lindstom, V. Renault, A. Klein, V. Mouly, T. Ansved, G. Butler-Browne, and D. Furling. 2009. Satellite cell dysfunction contributes to the progressive muscle atrophy in myotonic dystrophy type 1. *Neuropathology and applied neurobiology*. 35:603-613.

Tieleman, A.A., S. Knuijt, J. van Vliet, B.J. de Swart, R. Ensink, and B.G. van Engelen. 2009. Dysphagia is present but mild in myotonic dystrophy type 2. *Neuromuscul Disord*. 19:196-198.

Tieleman, A.A., A. Vinke, N. van Alfen, J.P. van Dijk, S. Pillen, and B.G. van Engelen. 2012. Skeletal muscle involvement in myotonic dystrophy type 2. A comparative muscle ultrasound study. *Neuromuscul Disord*. 22:492-499.

Tome, F.M., and M. Fardeau. 1980. Nuclear inclusions in oculopharyngeal dystrophy. *Acta neuropathologica*. 49:85-87.

Toth, K.G., B.R. McKay, M. De Lisio, J.P. Little, M.A. Tarnopolsky, and G. Parise. 2011. IL-6 induced STAT3 signalling is associated with the proliferation of human muscle satellite cells following acute muscle damage. *PLoS One*. 6:e17392.

Trollet, C., S.Y. Anvar, A. Venema, I.P. Hargreaves, K. Foster, A. Vignaud, A. Ferry, E. Negroni, C. Hourde, M.A. Baraibar, P.A.C. 't Hoen, J.E. Davies, D.C. Rubinsztein, S.J. Heales, V. Mouly, S.M. van der Maarel, G. Butler-Browne, V. Raz, and G. Dickson. 2010. Molecular and phenotypic characterization of a mouse model of oculopharyngeal muscular dystrophy reveals severe muscular atrophy restricted to fast glycolytic fibres. *Human molecular genetics*. 19:2191-2207.

Valdez, M.R., J.A. Richardson, W.H. Klein, and E.N. Olson. 2000. Failure of Myf5 to support myogenic differentiation without myogenin, MyoD, and MRF4. *Dev Biol*. 219:287-298.

Van der Meer, S.F., R.T. Jaspers, and H. Degens. 2011. Is the myonuclear domain size fixed? *Journal of musculoskeletal & neuronal interactions*. 11:286-297.

Verdijk, L.B., R. Koopman, G. Schaart, K. Meijer, H.H. Savelberg, and L.J. van Loon. 2007. Satellite cell content is specifically reduced in type II skeletal muscle fibers in the elderly. *Am J Physiol Endocrinol Metab*. 292:E151-157.

Victor, M., R. Hayes, and R.D. Adams. 1962. Oculopharyngeal muscular dystrophy. A familial disease of late life characterized by dysphagia and progressive ptosis of the evelids. *The New England journal of medicine*. 267:1267-1272.

Vieira, N.M., M.S. Naslavsky, L. Licinio, F. Kok, D. Schlesinger, M. Vainzof, N. Sanchez, J.P. Kitajima, L. Gal, N. Cavacana, P.R. Serafini, S. Chuartzman, C. Vasquez, A. Mimbacas, V. Nigro, R.C. Pavanello, M. Schuldiner, L.M. Kunkel, and M. Zatz. 2014. A defect in the RNA-processing protein HNRPDL causes limb-girdle muscular dystrophy 1G (LGMD1G). *Hum Mol Genet*. 23:4103-4110.

Vohanka, S., M. Vytopil, J. Bednarik, Z. Lukas, Z. Kadanka, J. Schildberger, R. Ricotti, S. Bione, and D. Toniolo. 2001. A mutation in the X-linked Emery-Dreifuss muscular dystrophy gene in a patient affected with conduction cardiomyopathy. *Neuromuscul Disord*. 11:411-413.

Wada, K.I., S. Katsuta, and H. Soya. 2003. Natural occurrence of myofiber cytoplasmic enlargement accompanied by decrease in myonuclear number. *In* Jpn. J. Physiol. Vol. 53. 145-150.

Wallace, G.Q., K.A. Lapidos, J.S. Kenik, and E.M. McNally. 2008. Long-term survival of transplanted stem cells in immunocompetent mice with muscular dystrophy. *The American journal of pathology*. 173:792-802.

Webster, C., and H.M. Blau. 1990. Accelerated age-related decline in replicative life-span of Duchenne muscular dystrophy myoblasts: implications for cell and gene therapy. *Somat Cell Mol Genet*. 16:557-565.

Weintraub, H., V.J. Dwarki, I. Verma, R. Davis, S. Hollenberg, L. Snider, A. Lassar, and S.J. Tapscott. 1991. Muscle-specific transcriptional activation by MyoD. *Genes Dev*. 5:1377-1386.

White, R.B., A.S. Bierinx, V.F. Gnocchi, and P.S. Zammit. 2010. Dynamics of muscle fibre growth during postnatal mouse development. *BMC developmental biology*. 10:21.

Wieczorek, D.F., M. Periasamy, G.S. Butler-Browne, R.G. Whalen, and B. Nadal-Ginard. 1985. Co-expression of multiple myosin heavy chain genes, in addition to a tissue-specific one, in extraocular musculature. *The Journal of cell biology*. 101:618-629.

Winokur, S.T., Y.W. Chen, P.S. Masny, J.H. Martin, J.T. Ehmsen, S.J. Tapscott, S.M. van der Maarel, Y. Hayashi, and K.M. Flanigan. 2003. Expression profiling of FSHD muscle supports a defect in specific stages of myogenic differentiation. *Hum Mol Genet*. 12:2895-2907.

Wirtschafter, J.D., D.A. Ferrington, and L.K. McLoon. 2004a. Continuous remodeling of adult extraocular muscles as an explanation for selective craniofacial vulnerability in oculopharyngeal muscular dystrophy. *Journal of neuro-ophthalmology : the official journal of the North American Neuro-Ophthalmology Society*. 24:62-67.

Wirtschafter, J.D., D.A. Ferrington, and L.K. McLoon. 2004b. Continuous remodeling of adult extraocular muscles as an explanation for selective craniofacial vulnerability in oculopharyngeal muscular dystrophy. *Journal of neuro-ophthalmology : the official journal of the North American Neuro-Ophthalmology Society*. 24:62-67.

Wu, S., Y. Wu, and M.R. Capecchi. 2006. Motoneurons and oligodendrocytes are sequentially generated from neural stem cells but do not appear to share common lineage-restricted progenitors in vivo. *Development*. 133:581-590.

Yahiaoui, L., D. Gvozdic, G. Danialou, M. Mack, and B.J. Petrof. 2008. CC family chemokines directly regulate myoblast responses to skeletal muscle injury. *The Journal of physiology*. 586:3991-4004.

Zhang, J., Z. Xiao, C. Qu, W. Cui, X. Wang, and J. Du. 2014. CD8 T cells are involved in skeletal muscle regeneration through facilitating MCP-1 secretion and Gr1(high) macrophage infiltration. *Journal of immunology*. 193:5149-5160.

Zifko, U.A., A.F. Hahn, H. Remtulla, C.F. George, W. Wihlidal, and C.F. Bolton. 1996. Central and peripheral respiratory electrophysiological studies in myotonic dystrophy. *Brain : a journal of neurology*. 119 ( Pt 6):1911-1922.

# Appendix

**Appendix Table 1: Illumina transcriptome analysis comparing sorted pharyngeal satellite cells to sorted limb satellite cells**

| Illumina Probeset ID | Accession Number | Gene Name | Gene Symbol | Fold Change PSC to LSC | P-Value |
|---|---|---|---|---|---|
| 580685 | NM_009375.2 | thyroglobulin | *Tg* | 15.73 | 0.00068 |
| 3180356 | NM_001012392.1 | cDNA sequence U46068 , transcript variant 1 | *U46068* | 13.04 | 0.00001 |
| 1470619 | NM_016958.1 | keratin 14 | *Krt14* | 12.64 | 0.00123 |
| 7150326 | NM_027011.2 | keratin 5 | *Krt5* | 8.97 | 0.00632 |
| 670603 | NM_053200.2 | carboxylesterase 3 | *Ces3* | 7.25 | 0.00298 |
| 830333 | NM_001033131.1 | keratinocyte differentiation associated protein XM_923930 XM_923934 | *Krtdap* | 7.23 | 0.00720 |
| 670494 | NM_010662 | keratin 13 | *Krt1-13* | 7.18 | 0.00739 |
| 6270301 | NM_153418.2 | cDNA sequence U46068 , transcript variant 2 | *U46068* | 6.79 | 0.00052 |
| 70601 | NM_026323.2 | WAP four-disulfide core domain 2 | *Wfdc2* | 6.54 | 0.01116 |
| 4610414 | NM_010662.1 | keratin 13 | *Krt13* | 6.15 | 0.02733 |
| 610707 | NM_001033131.1 | keratinocyte differentiation-associated protein | *Krtdap* | 5.89 | 0.00997 |
| 6940037 | NM_008522.3 | lactotransferrin | *Ltf* | 5.83 | 0.01075 |
| 3060630 | NM_026334.1 | lipase, gastric | *Lipf* | 5.59 | 0.01316 |
| 1070630 | NM_009396.1 | tumor necrosis factor, alpha-induced protein 2 | *Tnfaip2* | 5.54 | 0.00015 |
| 4610674 | NM_009897.2 | creatine kinase, mitochondrial 1, ubiquitous, nuclear gene encoding mitochondrial protein | *Ckmt1* | 5.45 | 0.01448 |

| | | | | | |
|---|---|---|---|---|---|
| 3780386 | NM_009363.3 | trefoil factor 2 (spasmolytic protein 1) | *Tff2* | 5.40 | 0.00510 |
| 6040689 | NM_007817.2 | cytochrome P450, family 2, subfamily f, polypeptide 2 | *Cyp2f2* | 5.23 | 0.01935 |
| 4570278 | NM_008469.1 | keratin 15 | *Krt15* | 5.20 | 0.02010 |
| 4150750 | NM_009140 | chemokine (C-X-C motif) ligand 2 | *Cxcl2* | 5.12 | 0.00025 |
| 7050196 | NM_001039238.2 | demilune cell and parotid protein 2 | *Dcpp2* | 4.98 | 0.01677 |
| 5860427 | NM_001033233.1 | transmembrane protease, serine 11a | *Tmprss11a* | 4.86 | 0.01654 |
| 2630661 | XR_034363.1 | PREDICTED: similar to mucin 5, subtype B, tracheobronchial, misc RNA | *LOC640195* | 4.81 | 0.01032 |
| 1010435 | NM_010362.2 | glutathione S-transferase omega 1 | *Gsto1* | 4.78 | 0.01554 |
| 4180167 | NM_009335.1 | transcription factor AP-2, gamma | *Tcfap2c* | 4.70 | 0.00260 |
| 4920438 | NM_008475.2 | keratin 4 | *Krt4* | 4.67 | 0.01996 |
| 2650142 | AK075905 | spermine binding protein-like | *Sbpl* | 4.61 | 0.01132 |
| 620241 | NM_009626.3 | alcohol dehydrogenase 7 (class IV), mu or sigma polypeptide | *Adh7* | 4.21 | 0.04465 |
| 3370397 | NM_013800.2 | BarH-like homeobox 2 | *Barx2* | 4.09 | 0.00452 |
| 650392 | XM_001480745.1 | PREDICTED: RIKEN cDNA 5430433G21 gene | *5430433G21Rik* | 4.04 | 0.00560 |
| 70722 | NM_007969.4 | extracellular proteinase inhibitor | *Expi* | 3.82 | 0.00033 |
| 110112 | NM_011333.3 | chemokine (C-C motif) ligand 2 | *Ccl2* | 3.69 | 0.00006 |
| 7610646 | NM_007693.1 | chromogranin A | *Chga* | 3.65 | 0.03132 |
| 460682 | NM_183278.2 | RIKEN cDNA 2200001I15 gene | *2200001I15Rik* | 3.54 | 0.02698 |
| 6180202 | XM_001472699.1 | PREDICTED: similar to LPS-induced CXC chemokine | *LOC100044702* | 3.52 | 0.00040 |
| 1980603 | NM_009114.1 | S100 calcium binding protein A9 (calgranulin B) | *S100a9* | 3.47 | 0.03069 |
| 1450095 | NM_0104 | intercellular adhesion | *Icam1* | 3.35 | 0.00322 |

| | | | | | |
|---|---|---|---|---|---|
| | 93.2 | molecule 1 | | | |
| 4920470 | NM_0109 30.4 | nephroblastoma overexpressed gene | *Nov* | 3.34 | 0.01073 |
| 1450445 | NM_0118 24.1 | gremlin 1 | *Grem1* | 3.29 | 0.00074 |
| 7550500 | NM_0077 69.1 | deleted in malignant brain tumors 1 | *Dmbt1* | 3.26 | 0.00490 |
| 5860711 | NM_0010 39238.2 | demilune cell and parotid protein 2 | *Dcpp2* | 3.25 | 0.02915 |
| 5720609 | NM_0135 90.2 | lysozyme | *Lyz* | 3.18 | 0.01725 |
| 7650035 | NM_0279 71.1 | serine (or cysteine) peptidase inhibitor, clade B (ovalbumin), member 12 | *Serpinb 12* | 3.17 | 0.02660 |
| 2600600 | NM_1460 24.1 | ankyrin repeat domain 40 , transcript variant 2 | *Ankrd40* | 3.13 | 0.01387 |
| 7160307 | XM_0014 75459.1 | PREDICTED: similar to COUP-TFI | *LOC100 046044* | 3.09 | 0.00262 |
| 3830445 | NM_1940 55.1 | RNA binding motif protein 35A | *Rbm35a* | 3.08 | 0.01437 |
| 5910220 | NM_0110 19.1 | oncostatin M receptor | *Osmr* | 3.07 | 0.00054 |
| 7400601 | NM_0093 96.1 | tumor necrosis factor, alpha-induced protein 2 | *Tnfaip2* | 3.03 | 0.00370 |
| 4200605 | NM_0097 21.4 | ATPase, Na+/K+ transporting, beta 1 polypeptide | *Atp1b1* | 3.00 | 0.00030 |
| 6550035 | NM_0199 10.2 | demilune cell and parotid protein 1 | *Dcpp1* | 2.98 | 0.00767 |
| 630767 | NM_0010 77633.1 | demilune cell and parotid protein 3 | *Dcpp3* | 2.95 | 0.02635 |
| 6620368 | NM_1815 79.1 | premature ovarian failure 1B (Pof1b) | *Pof1b* | 2.93 | 0.00042 |
| 380717 | XM_9121 61.3 | PREDICTED: zinc finger protein 703 | *Zfp703* | 2.88 | 0.00214 |
| 20176 | NM_0098 51 | CD44 antigen | *Cd44* | 2.87 | 0.01104 |
| 2710347 | NM_1447 99.1 | LIM and cysteine-rich domains 1 | *Lmcd1* | 2.86 | 0.00134 |
| 130215 | NM_1383 14.2 | non-metastatic cells 7, protein expressed in (nucleoside-diphosphate kinase), transcript variant 1 | *Nme7* | 2.85 | 0.00450 |
| 5080725 | NM_0306 | myosin, heavy | *Myh1* | 2.84 | 0.00401 |

| | | | | | |
|---|---|---|---|---|---|
| | 79.1 | polypeptide 1, skeletal muscle, adult | | | |
| 5820184 | NM_009864.2 | cadherin 1 | *Cdh1* | 2.82 | 0.01005 |
| 610431 | NM_011580.3 | thrombospondin 1 | *Thbs1* | 2.81 | 0.01022 |
| 2260066 | NM_009405.2 | troponin I, skeletal, fast 2 | *Tnni2* | 2.80 | 0.00110 |
| 3120747 | NM_009285.3 | stanniocalcin 1 | *Stc1* | 2.78 | 0.00027 |
| 4260609 | NM_138314.2 | non-metastatic cells 7, protein expressed in (nucleoside-diphosphate kinase), transcript variant 1 | *Nme7* | 2.77 | 0.00351 |
| 2140136 | XM_001478074.1 | PREDICTED: hypothetical protein LOC100047934 | *LOC100047934* | 2.75 | 0.00127 |
| 4050014 | XM_001475821.1 | PREDICTED: similar to Demilune cell and parotid protein 1, transcript variant 1 | *LOC100046800* | 2.75 | 0.01409 |
| 1850487 | NM_008239.3 | forkhead box Q1 | *Foxq1* | 2.72 | 0.01039 |
| 4670674 | NM_013654.2 | chemokine (C-C motif) ligand 7 | *Ccl7* | 2.71 | 0.00080 |
| 5340044 | NM_019835.2 | UDP-Gal:betaGlcNAc beta 1,4-galactosyltransferase, polypeptide 5 | *B4galt5* | 2.69 | 0.00107 |
| 6980274 | NM_016660.2 | high mobility group AT-hook 1, transcript variant 1 | *Hmga1* | 2.66 | 0.00052 |
| 1940608 | NM_017372.2 | lysozyme | *Lyzs* | 2.66 | 0.03344 |
| 110079 | NM_001039150.1 | CD44 antigen, transcript variant 2 | *Cd44* | 2.63 | 0.00012 |
| 430025 | NM_031161.2 | cholecystokinin | *Cck* | 2.61 | 0.00081 |
| 270324 | NM_011607.2 | tenascin C | *Tnc* | 2.59 | 0.00175 |
| 4010019 | NM_026820.2 | interferon induced transmembrane protein 1 | *Ifitm1* | 2.58 | 0.00087 |
| 130593 | NM_011041.2 | paired box gene 9 | *Pax9* | 2.52 | 0.00223 |
| 830619 | NM_0112 | regenerating islet-derived | *Reg3g* | 2.49 | 0.04319 |

| | | | | | |
|---|---|---|---|---|---|
| | 60.1 | 3 gamma | | | |
| 1710754 | NM_0099 82.2 | cathepsin C | *Ctsc* | 2.49 | 0.00571 |
| 1070619 | XM_9821 44.1 | PREDICTED: similar to CYP4B1 | *LOC631 037* | 2.49 | 0.00165 |
| 830736 | NM_0074 17.2 | adrenergic receptor, alpha 2a | *Adra2a* | 2.48 | 0.00887 |
| 3840253 | NM_1986 16.2 | coiled-coil domain containing 85B | *Ccdc85b* | 2.47 | 0.00021 |
| 1300092 | NM_0296 39.2 | RIKEN cDNA 1600029D21 gene | *1600029 D21Rik* | 2.46 | 0.01512 |
| 1400632 | AK04002 0 | oncostatin M receptor | *Osmr* | 2.45 | 0.00590 |
| 630091 | NM_1721 42.3 | nuclear factor of kappa light polypeptide gene enhancer in B-cells inhibitor, delta | *Nfkbid* | 2.44 | 0.04494 |
| 6330482 | NM_0168 47.2 | arginine vasopressin receptor 1A | *Avpr1a* | 2.43 | 0.00024 |
| 160035 | NM_0167 67.2 | basic leucine zipper transcription factor, ATF-like | *Batf* | 2.42 | 0.00017 |
| 4780477 | XM_9109 11.3 | PREDICTED: RIKEN cDNA 2310039D24 gene | *2310039 D24Rik* | 2.42 | 0.01459 |
| 5550184 | NM_0200 36.4 | calmodulin 4 | *Calm4* | 2.41 | 0.01727 |
| 2760356 | NM_0253 93 | S100 calcium binding protein A14 | *S100a14* | 2.40 | 0.01944 |
| 2120687 | AK05451 6 | RIKEN cDNA A730049H05 gene | *A73004 9H05Rik* | 2.39 | 0.00107 |
| 7320202 | NM_0089 67.1 | prostaglandin I receptor (IP) | *Ptgir* | 2.39 | 0.00099 |
| 4150403 | NM_0098 73.2 | cyclin-dependent kinase 6 ( | *Cdk6* | 2.39 | 0.03591 |
| 4760180 | NM_0075 48.2 | PR domain containing 1, with ZNF domain | *Prdm1* | 2.38 | 0.00158 |
| 4880138 | NM_0010 39150.1 | CD44 antigen, transcript variant 2 | *Cd44* | 2.38 | 0.00010 |
| 7100685 | NM_0167 48.1 | cytidine 5'-triphosphate synthase | *Ctps* | 2.36 | 0.00956 |
| 2970615 | NM_0206 23.1 | parathyroid hormone | *Pth* | 2.35 | 0.00949 |
| 4210196 | NM_0079 04.3 | endothelin receptor type B | *Ednrb* | 2.33 | 0.00238 |
| 3420458 | XM_0014 75821.1 | PREDICTED: similar to Demilune cell and parotid | *LOC100 046800* | 2.33 | 0.01091 |

| | | | | | |
|---|---|---|---|---|---|
| | | protein 1, transcript variant 1 | | | |
| 4290706 | NM_016705.2 | kinesin family member 21A | *Kif21a* | 2.33 | 0.00325 |
| 2230538 | NM_001039150.1 | CD44 antigen, transcript variant 2 | *Cd44* | 2.32 | 0.00265 |
| 3890528 | NM_011267.2 | regulator of G-protein signaling 16 | *Rgs16* | 2.31 | 0.00228 |
| 4150471 | NM_145562.2 | RIKEN cDNA 9130213B05 gene | *9130213 B05Rik* | 2.31 | 0.00757 |
| 7570600 | NM_139307.2 | vasorin | *Vasn* | 2.29 | 0.00225 |
| 4610110 | NM_008046.2 | follistatin | *Fst* | 2.28 | 0.00192 |
| 4890440 | XM_894405.2 | PREDICTED: calpain, small subunit 2 | *Capns2* | 2.28 | 0.02702 |
| 6330332 | NM_011607.2 | tenascin C | *Tnc* | 2.28 | 0.00007 |
| 5670731 | NM_031168.1 | interleukin 6 | *Il6* | 2.28 | 0.00033 |
| 4200204 | NM_011893.2 | SH3-domain binding protein 2 | *Sh3bp2* | 2.26 | 0.00223 |
| 7210154 | NM_001039537.1 | leukemia inhibitory factor, transcript variant 2 | *Lif* | 2.26 | 0.00139 |
| 2970246 | AK051438 | early B cell factor 1 | *Ebf* | 2.26 | 0.02478 |
| 5420333 | NM_011607.1 | tenascin C | *Tnc* | 2.26 | 0.00313 |
| 2750692 | XM_621314.3 | PREDICTED: desmoplakin, transcript variant 1 (Dsp) | *Dsp* | 2.25 | 0.04978 |
| 5720064 | NM_172845.1 | a disintegrin-like and metallopeptidase (reprolysin type) with thrombospondin type 1 motif, 4 | *Adamts4* | 2.24 | 0.00033 |
| 2850451 | NM_133237.2 | adenomatosis polyposis coli down-regulated 1 | *Apcdd1* | 2.22 | 0.00937 |
| 3870670 | NM_011580.3 | thrombospondin 1 | *Thbs1* | 2.22 | 0.00140 |
| 2100358 | NM_008928.3 | mitogen activated protein kinase kinase 3 | *Map2k3* | 2.21 | 0.01956 |
| 2140148 | NM_007732.1 | collagen, type XVII, alpha 1 | *Col17a1* | 2.19 | 0.04612 |
| 3060180 | NM_018790.2 | activity regulated cytoskeletal-associated | *Arc* | 2.19 | 0.00816 |

| | | | | | |
|---|---|---|---|---|---|
| | | protein | | | |
| 5550291 | NM_027866.1 | collectin sub-family member 11 | *Colec11* | 2.18 | 0.00149 |
| 6020398 | NM_001038642.1 | E26 avian leukemia oncogene 1, 5' domain, transcript variant 2 | *Ets1* | 2.18 | 0.00044 |
| 1400041 | NM_010260.1 | guanylate binding protein 2 | *Gbp2* | 2.16 | 0.00643 |
| 3840750 | NM_009396.1 | tumor necrosis factor, alpha-induced protein 2 | *Tnfaip2* | 2.16 | 0.00018 |
| 2230373 | NM_001081412.1 | breakpoint cluster region homolog | *Bcr* | 2.15 | 0.00268 |
| 1580431 | NM_011627.3 | trophoblast glycoprotein | *Tpbg* | 2.14 | 0.00555 |
| 620372 | NM_011451.2 | sphingosine kinase 1, transcript variant 1 | *Sphk1* | 2.13 | 0.02586 |
| 2510632 | NM_007693.1 | chromogranin A | *Chga* | 2.13 | 0.00520 |
| 4780390 | NM_138314.2 | non-metastatic cells 7, protein expressed in (nucleoside-diphosphate kinase), transcript variant 1 | *Nme7* | 2.13 | 0.00515 |
| 50458 | AK048765 | tenascin C | *Tnc* | 2.12 | 0.01609 |
| 2060612 | NM_026145.3 | potassium channel tetramerisation domain containing 10 | *Kctd10* | 2.12 | 0.00033 |
| 1710242 | NM_007899.1 | extracellular matrix protein 1 | *Ecm1* | 2.11 | 0.03825 |
| 4860711 | NM_008241.1 | forkhead box G1 | *Foxg1* | 2.11 | 0.00092 |
| 7200519 | NM_007681.2 | centromere protein A | *Cenpa* | 2.11 | 0.00251 |
| 4250689 | NM_009834.1 | CCR4 carbon catabolite repression 4-like (S cerevisiae) | *Ccrn4l* | 2.10 | 0.00001 |
| 4070561 | NM_054049.2 | odd-skipped related 2 (Drosophila) | *Osr2* | 2.10 | 0.00534 |
| 5050463 | NM_010442.1 | heme oxygenase (decycling) 1 | *Hmox1* | 2.10 | 0.00036 |
| 2470392 | NM_009044.2 | reticuloendotheliosis oncogene | *Rel* | 2.09 | 0.00006 |
| 4210762 | NM_007609.1 | caspase 4, apoptosis-related cysteine peptidase | *Casp4* | 2.09 | 0.00085 |
| 540382 | NM_176811 | ubiquitin associated and | *Ubash3* | 2.08 | 0.00285 |

| | | | | | |
|---|---|---|---|---|---|
| | 60.5 | SH3 domain containing, B | *b* | | |
| 7160022 | NM_144799.1 | LIM and cysteine-rich domains 1 | *Lmcd1* | 2.08 | 0.01061 |
| 6350255 | NM_178920.3 | mal, T-cell differentiation protein 2 | *Mal2* | 2.08 | 0.02367 |
| 3360162 | NM_015744.1 | ectonucleotide pyrophosphatase/phosphodiesterase 2 | *Enpp2* | 2.06 | 0.00014 |
| 1780474 | AK031171 | moesin | *Msn* | 2.06 | 0.02441 |
| 2650162 | NM_011043.3 | protocadherin 10, transcript variant 4 | *Pcdh10* | 2.06 | 0.03180 |
| 7320661 | NM_008215.1 | hyaluronan synthase1 | *Has1* | 2.05 | 0.00395 |
| 2490537 | NM_011198.2 | prostaglandin-endoperoxide synthase 2 (prostaglandin G/H synthase and cyclooxygenase) | *Ptgs2* | 2.04 | 0.04777 |
| 4290180 | NM_007609.1 | caspase 4, apoptosis-related cysteine peptidase | *Casp4* | 2.04 | 0.00802 |
| 10446 | NM_015744 | ectonucleotide pyrophosphatase/phosphodiesterase 2 | *Enpp2* | 2.04 | 0.00136 |
| 6560204 | NM_178589.2 | tumor necrosis factor receptor superfamily, member 21 | *Tnfrsf21* | 2.04 | 0.01197 |
| 510707 | AK087179 | oncostatin M receptor | *Osmr* | 2.04 | 0.00956 |
| 3710730 | NM_148927.1 | pleckstrin homology domain containing, family A (phosphoinositide binding specific) member 4 | *Plekha4* | 2.03 | 0.04933 |
| 6590228 | NM_001039150.1 | CD44 antigen, transcript variant 2 | *Cd44* | 2.03 | 0.04785 |
| 4480180 | NM_009344.1 | pleckstrin homology-like domain, family A, member 1 | *Phlda1* | 2.03 | 0.00065 |
| 4220474 | NM_010855.2 | myosin, heavy polypeptide 4, skeletal muscle | *Myh4* | 2.02 | 0.04322 |
| 990767 | NM_007904.2 | endothelin receptor type B | *Ednrb* | 2.02 | 0.00394 |
| 5720164 | NM_144799.1 | LIM and cysteine-rich domains 1 | *Lmcd1* | 2.02 | 0.02409 |

| | | | | | |
|---|---|---|---|---|---|
| 4040189 | NM_010332.2 | endothelin receptor type A | *Ednra* | 2.02 | 0.00269 |
| 4920364 | XM_001480162.1 | PREDICTED: fer-1-like 3, myoferlin (C elegans), transcript variant 1 | *Fer1l3* | 2.02 | 0.00009 |
| 1980209 | NM_009610.1 | actin, gamma 2, smooth muscle, enteric | *Actg2* | 2.01 | 0.00354 |
| 430523 | NM_009397.2 | tumor necrosis factor, alpha-induced protein 3 | *Tnfaip3* | 2.01 | 0.00169 |
| 1300739 | AK028513 | dihydrolipoamide S-succinyltransferase (E2 component of 2-oxo-glutarate complex) | *Dlst* | 2.01 | 0.00850 |
| 1260689 | NM_054056.2 | PRKC, apoptosis, WT1, regulator | *Pawr* | 2.01 | 0.00005 |
| 670240 | NM_010730.2 | annexin A1 (Anxa1) | *Anxa1* | 2.01 | 0.00722 |
| 2970703 | NM_001039543.1 | myeloid leukemia factor 1, transcript variant 1 | *Mlf1* | 2.00 | 0.01414 |
| 2760561 | NM_008872 | plasminogen activator, tissue | *Plat* | 2.00 | 0.01046 |
| 5390639 | NM_009140.2 | chemokine (C-X-C motif) ligand 2 | *Cxcl2* | 2.00 | 0.00077 |
| 3140228 | NM_011607.2 | tenascin C | *Tnc* | 2.00 | 0.00144 |
| 60543 | XM_621314.3 | PREDICTED: desmoplakin, transcript variant 1 | *Dsp* | 1.99 | 0.03492 |
| 6450291 | NM_026145.3 | potassium channel tetramerisation domain containing 10 | *Kctd10* | 1.99 | 0.00093 |
| 4390333 | NM_029384.1 | RIKEN cDNA 2210411K11 gene | *2210411K11Rik* | 1.99 | 0.01194 |
| 150022 | NM_010907.1 | nuclear factor of kappa light polypeptide gene enhancer in B-cells inhibitor, alpha | *Nfkbia* | 1.97 | 0.00031 |
| 4060446 | AK042505 | sorting nexin 10 | *Snx10* | 1.96 | 0.01331 |
| 3120278 | NM_007426.3 | angiopoietin 2 | *Angpt2* | 1.96 | 0.00140 |
| 1820601 | NM_008343.2 | insulin-like growth factor binding protein 3 | *Igfbp3* | 1.95 | 0.04591 |
| 5360678 | NM_133836.1 | interleukin 15 receptor, alpha chain, transcript variant 2 | *Il15ra* | 1.95 | 0.02775 |

| | | | | | |
|---|---|---|---|---|---|
| 4880187 | NM_133362.2 | erythroid differentiation regulator 1 | *Erdr1* | 1.95 | 0.04460 |
| 4150370 | AK087259 | | *E030040G24Rik* | 1.94 | 0.01967 |
| 3170204 | NM_021327.1 | TNFAIP3 interacting protein 1 | *Tnip1* | 1.94 | 0.00345 |
| 1850411 | NM_025777.2 | dual oxidase maturation factor 2 | *Duoxa2* | 1.94 | 0.02054 |
| 1440286 | NM_172637.1 | HECT domain containing 2 | *Hectd2* | 1.94 | 0.01149 |
| 4220162 | XM_001472888.1 | PREDICTED: syntaxin 11 | *Stx11* | 1.94 | 0.00581 |
| 3390110 | NM_009846.2 | CD24a antigen | *Cd24a* | 1.93 | 0.01893 |
| 1260164 | NM_012055.3 | asparagine synthetase | *Asns* | 1.93 | 0.00020 |
| 3440021 | NM_007778.3 | colony stimulating factor 1 (macrophage) | *Csf1* | 1.93 | 0.00424 |
| 5290017 | NM_007609.1 | caspase 4, apoptosis-related cysteine peptidase | *Casp4* | 1.93 | 0.00075 |
| 3190047 | XM_358117.1 | | *LOC385205* | 1.93 | 0.02648 |
| 2000719 | NM_013885.2 | chloride intracellular channel 4 (mitochondrial), nuclear gene encoding mitochondrial protein | *Clic4* | 1.92 | 0.00623 |
| 2230026 | NM_145562.2 | RIKEN cDNA 9130213B05 gene | *9130213B05Rik* | 1.91 | 0.02115 |
| 5810767 | NM_011519.2 | syndecan 1 | *Sdc1* | 1.91 | 0.00872 |
| 7510243 | NM_009780.1 | complement component 4B (Childo blood group) XM_921663 XM_921673 XM_921676 XM_921678 | *C4b* | 1.91 | 0.00882 |
| 10674 | NM_028769.4 | synovial apoptosis inhibitor 1, synoviolin | *Syvn1* | 1.91 | 0.01691 |
| 4490639 | XM_148986.1 | uridine-cytidine kinase 2 | *Uck2* | 1.90 | 0.01692 |
| 3420273 | NM_175229.3 | serine/arginine repetitive matrix 2 | *Srrm2* | 1.90 | 0.01075 |
| 6350196 | NM_010825.2 | Meis homeobox 2, transcript variant 2 | *Meis2* | 1.90 | 0.00706 |
| 2630195 | NM_016847.2 | arginine vasopressin receptor 1A | *Avpr1a* | 1.89 | 0.04506 |
| 610100 | NM_001001488.3 | ATPase, class I, type 8B, member 1 | *Atp8b1* | 1.89 | 0.02298 |

| | | | | | |
|---|---|---|---|---|---|
| 1050358 | NM_021459.3 | ISL1 transcription factor, LIM/homeodomain | *Isl1* | 1.88 | 0.00155 |
| 5820168 | NM_207680.2 | BCL2-like 11 (apoptosis facilitator), transcript variant 1 | *Bcl2l11* | 1.88 | 0.01429 |
| 460156 | XM_358107.1 | | *LOC385187* | 1.88 | 0.04713 |
| 670328 | NM_212487.4 | keratin 78 | *Krt78* | 1.88 | 0.01383 |
| 2900131 | NM_177369.3 | myosin, heavy polypeptide 8, skeletal muscle, perinatal | *Myh8* | 1.87 | 0.03949 |
| 3610291 | NM_021318.3 | four and a half LIM domains 5 | *Fhl5* | 1.87 | 0.00636 |
| 1230148 | XM_195432.1 | | *LOC270552* | 1.87 | 0.04974 |
| 4900168 | NM_054049.1 | odd-skipped related 2 (Drosophila) | *Osr2* | 1.86 | 0.01559 |
| 3370377 | NM_008655.1 | growth arrest and DNA-damage-inducible 45 beta | *Gadd45b* | 1.86 | 0.00278 |
| 130010 | NM_138314.2 | non-metastatic cells 7, protein expressed in (nucleoside-diphosphate kinase), transcript variant 1 | *Nme7* | 1.85 | 0.03263 |
| 3400491 | NM_013885.2 | chloride intracellular channel 4 (mitochondrial), nuclear gene encoding mitochondrial protein | *Clic4* | 1.85 | 0.00002 |
| 7560673 | NM_016861.3 | PDZ and LIM domain 1 (elfin) | *Pdlim1* | 1.85 | 0.00201 |
| 4780711 | XM_358311 | zinc finger, SWIM-type containing 6 | *Zswim6* | 1.85 | 0.00275 |
| 990379 | NM_001037221.1 | sterile alpha motif domain containing 4, transcript variant 1 | *Samd4* | 1.85 | 0.01040 |
| 6770133 | NM_027418.1 | mitogen-activated protein kinase, transcript variant 2 | *Mapk6* | 1.85 | 0.00158 |
| 1010528 | XM_001474179.1 | PREDICTED: similar to Development and differentiation enhancing | *LOC100045359* | 1.84 | 0.02310 |
| 2900692 | NM_008216.2 | hyaluronan synthase 2 | *Has2* | 1.84 | 0.01969 |
| 6590154 | XM_147798.4 | solute carrier family 4, sodium bicarbonate cotransporter, member 7 | *Slc4a7* | 1.84 | 0.00803 |

| | | | | | |
|---|---|---|---|---|---|
| 990468 | NM_001001488.3 | ATPase, class I, type 8B, member 1 | *Atp8b1* | 1.84 | 0.01404 |
| 60626 | XM_916287.2 | PREDICTED: similar to TIFA, transcript variant 1 (LOC637082) | *LOC637082* | 1.83 | 0.00382 |
| 5290630 | NM_144900.1 | ATPase, Na+/K+ transporting, alpha 1 polypeptide | *Atp1a1* | 1.83 | 0.01471 |
| 3140646 | NM_012057.3 | interferon regulatory factor 5 | *Irf5* | 1.83 | 0.00974 |
| 4850470 | NM_030024.2 | proline rich 15 | *Prr15* | 1.83 | 0.01944 |
| 4050598 | NM_011607.2 | tenascin C | *Tnc* | 1.83 | 0.02262 |
| 1090139 | NM_008330.1 | interferon gamma inducible protein 47 | *Ifi47* | 1.82 | 0.03529 |
| 1410079 | XM_001476658.1 | PREDICTED: similar to serine (or cysteine) proteinase inhibitor, clade B (ovalbumin), member 12 | *LOC100046641* | 1.82 | 0.02222 |
| 670333 | NM_177708.5 | reticulon 4 receptor-like 1 | *Rtn4rl1* | 1.82 | 0.02269 |
| 160703 | NM_011589.1 | timeless homolog (Drosophila), transcript variant 2 | *Timeless* | 1.82 | 0.00010 |
| 6400348 | NM_009103.2 | ribonucleotide reductase M1 | *Rrm1* | 1.82 | 0.00040 |
| 4900370 | NM_145988.1 | La ribonucleoprotein domain family, member 1B | *Larp1b* | 1.81 | 0.00399 |
| 4150593 | NM_010751.2 | MAX dimerization protein 1 | *Mxd1* | 1.81 | 0.00451 |
| 5570113 | AK049856 | solute carrier family 11 (proton-coupled divalent metal ion transporters), member 2 | *Slc11a2* | 1.81 | 0.00348 |
| 5820068 | NM_026820.2 | interferon induced transmembrane protein 1 | *Ifitm1* | 1.81 | 0.01465 |
| 6650687 | NM_009821.1 | runt related transcription factor 1 | *Runx1* | 1.80 | 0.02403 |
| 940162 | NM_138314.2 | non-metastatic cells 7, protein expressed in (nucleoside-diphosphate kinase), transcript variant 1 | *Nme7* | 1.80 | 0.01990 |

| | | | | | |
|---|---|---|---|---|---|
| 1780091 | NM_021327.1 | TNFAIP3 interacting protein 1 | *Tnip1* | 1.80 | 0.00409 |
| 1660129 | NM_010050.2 | deiodinase, iodothyronine, type II | *Dio2* | 1.80 | 0.00789 |
| 4180669 | NM_008689.2 | nuclear factor of kappa light polypeptide gene enhancer in B-cells 1, p105 | *Nfkb1* | 1.80 | 0.00605 |
| 4780255 | NM_177603.1 | frequently rearranged in advanced T-cell lymphomas 2 | *Frat2* | 1.79 | 0.00004 |
| 4610722 | NM_023223.1 | cell division cycle 20 homolog (S cerevisiae) | *Cdc20* | 1.79 | 0.01906 |
| 1770634 | NM_201367.2 | G protein-coupled receptor 176 | *Gpr176* | 1.79 | 0.01085 |
| 1400398 | XM_001003622.2 | PREDICTED: RIKEN cDNA 2310014H01 gene, transcript variant 3 | *2310014H01Rik* | 1.79 | 0.01817 |
| 6180470 | NM_009126.2 | serine (or cysteine) peptidase inhibitor, clade B (ovalbumin), member 3A | *Serpinb3a* | 1.79 | 0.00521 |
| 4210121 | NM_008638 | methylenetetrahydrofolate dehydrogenase (NADP+ dependent) 2, methenyltetrahydrofolate cyclohydrolase | *Mthfd2* | 1.79 | 0.00031 |
| 6130328 | NM_011636.1 | phospholipid scramblase 1 | *Plscr1* | 1.78 | 0.00109 |
| 6040364 | NM_010415.1 | heparin-binding EGF-like growth factor | *Hbegf* | 1.78 | 0.00988 |
| 5080274 | NM_013906.2 | a disintegrin-like and metallopeptidase (reprolysin type) with thrombospondin type 1 motif, 8 | *Adamts8* | 1.78 | 0.00327 |
| 7040161 | NM_178907.1 | mitogen-activated protein kinase-activated protein kinase 3 | *Mapkapk3* | 1.78 | 0.02714 |
| 4880603 | NM_007526.1 | BarH-like homeobox 1 | *Barx1* | 1.78 | 0.00090 |
| 3710195 | NM_011127.1 | paired related homeobox 1 | *Prrx1* | 1.78 | 0.01093 |
| 2070594 | NM_198412.1 | DnaJ (Hsp40) homolog, subfamily C, member 6 | *Dnajc6* | 1.78 | 0.00000 |
| 5270743 | NM_1777 | potassium channel | *Kctd12* | 1.77 | 0.01020 |

| | | | | | |
|---|---|---|---|---|---|
| | 15.4 | tetramerisation domain containing 12 | | | |
| 7330767 | NM_175686.3 | paired related homeobox 1, transcript variant 2 | *Prrx1* | 1.77 | 0.00664 |
| 6760397 | NM_010333 | sphingosine-1-phosphate receptor 2 | *S1pr2* | 1.77 | 0.00578 |
| 1230767 | NM_009378.2 | thrombomodulin | *Thbd* | 1.77 | 0.00734 |
| 1510736 | NM_001004366.1 | signal peptide, CUB domain, EGF-like 3 | *Scube3* | 1.77 | 0.00433 |
| 1440192 | NM_173413.2 | RAB8B, member RAS oncogene family | *Rab8b* | 1.77 | 0.01400 |
| 4120296 | D13802 | runt-related transcription factor 1 | *Runx1* | 1.77 | 0.04099 |
| 7320619 | XM_358005.1 | | *LOC385032* | 1.77 | 0.04190 |
| 3830709 | NM_018861.2 | solute carrier family 1 (glutamate/neutral amino acid transporter), member 4 | *Slc1a4* | 1.77 | 0.01607 |
| 990528 | AK077713.1 | tropomyosin 1, alpha | *Tpm1* | 1.76 | 0.02239 |
| 5820056 | NM_011454.1 | serine (or cysteine) peptidase inhibitor, clade B, member 6b | *Serpinb6b* | 1.76 | 0.01266 |
| 5090017 | NM_010193.3 | feminization 1 homolog b (C elegans) | *Fem1b* | 1.76 | 0.00539 |
| 5260278 | NM_011808 | E26 avian leukemia oncogene 1, 5' domain | *Ets1* | 1.76 | 0.00465 |
| 3800240 | NM_018811.6 | abhydrolase domain containing 2 | *Abhd2* | 1.76 | 0.02501 |
| 1940477 | NM_028258.1 | DAZ interacting protein 1-like | *Dzip1l* | 1.75 | 0.00850 |
| 6020730 | NM_019983.2 | RAB guanine nucleotide exchange factor (GEF) 1 | *Rabgef1* | 1.75 | 0.00474 |
| 240438 | NM_031170.2 | keratin 8 | *Krt8* | 1.75 | 0.00135 |
| 4220717 | NM_011888.2 | chemokine (C-C motif) ligand 19 | *Ccl19* | 1.75 | 0.00472 |
| 7330719 | NM_029362.3 | chromatin modifying protein 4B | *Chmp4b* | 1.75 | 0.04543 |
| 1110414 | NM_199200.2 | family with sequence similarity 171, member A2 | *Fam171a2* | 1.75 | 0.00386 |
| 3850070 | NM_011589 | timeless circadian clock 1 | *Timeless* | 1.75 | 0.01285 |

| | | | | | |
|---|---|---|---|---|---|
| 6940176 | NM_013609.1 | nerve growth factor, beta | *Ngfb* | 1.75 | 0.00091 |
| 2600463 | NM_013529.2 | glutamine fructose-6-phosphate transaminase 2 | *Gfpt2* | 1.75 | 0.01132 |
| 6180411 | NM_019821.2 | glycolipid transfer protein | *Gltp* | 1.75 | 0.04949 |
| 6420450 | NM_008690.3 | nuclear factor of kappa light polypeptide gene enhancer in B-cells inhibitor, epsilon | *Nfkbie* | 1.75 | 0.00581 |
| 6590402 | NM_001081053.1 | integrin, alpha 10 | *Itga10* | 1.75 | 0.03273 |
| 4540162 | NM_018811.4 | abhydrolase domain containing 2 | *Abhd2* | 1.74 | 0.00513 |
| 770725 | NM_007395.3 | activin A receptor, type 1B | *Acvr1b* | 1.74 | 0.00432 |
| 7040491 | NM_007669.2 | cyclin-dependent kinase inhibitor 1A (P21) | *Cdkn1a* | 1.74 | 0.01020 |
| 5420605 | NM_011607.2 | tenascin C | *Tnc* | 1.73 | 0.02788 |
| 1510349 | NM_009890.1 | cholesterol 25-hydroxylase | *Ch25h* | 1.73 | 0.00536 |
| 4250246 | NM_009994.1 | cytochrome P450, family 1, subfamily b, polypeptide 1 | *Cyp1b1* | 1.73 | 0.00570 |
| 6770379 | NM_011170.1 | prion protein | *Prnp* | 1.73 | 0.00544 |
| 3120358 | NM_021327.1 | TNFAIP3 interacting protein 1 | *Tnip1* | 1.73 | 0.00622 |
| 6940221 | NM_011595.2 | tissue inhibitor of metalloproteinase 3 | *Timp3* | 1.73 | 0.00094 |
| 1090471 | NM_133915.2 | paxillin, transcript variant beta | *Pxn* | 1.73 | 0.01445 |
| 1580678 | NM_139143.2 | solute carrier family 39 (metal ion transporter), member 6 | *Slc39a6* | 1.72 | 0.01191 |
| 6560477 | NM_009289.2 | STE20-like kinase (yeast) | *Slk* | 1.72 | 0.01555 |
| 7050370 | NM_030724.1 | uridine-cytidine kinase 2 | *Uck2* | 1.72 | 0.01132 |
| 2230504 | NM_001134829.1 | lysophosphatidylglycerol acyltransferase 1 | *Lpgat1* | 1.72 | 0.01346 |
| 520148 | AK029434 | IQ motif containing GTPase activating protein 1 | *Iqgap1* | 1.72 | 0.01947 |
| 2750209 | NM_1786 | anoctamin 1, calcium | *Ano1* | 1.72 | 0.01909 |

| | | | | | |
|---|---|---|---|---|---|
| | 42.4 | activated chloride channel | | | |
| 4150148 | NM_0194 | | *Panx1* | 1.71 | 0.00468 |
| | 82.2 | pannexin 1 | | | |
| 10121 | NM_0105 | interleukin 6 receptor, | *Il6ra* | 1.71 | 0.01171 |
| | 59.2 | alpha | | | |
| 7650731 | NM_0083 | interleukin 1 receptor, | *Il1r1* | 1.71 | 0.00189 |
| | 62.1 | type I | | | |
| 6510470 | NM_0095 | | *Zfp46* | 1.71 | 0.00194 |
| | 57.3 | zinc finger protein 46 | | | |
| 2320403 | NM_0081 | | *Gch1* | 1.71 | 0.00184 |
| | 02.3 | GTP cyclohydrolase 1 | | | |
| 2450474 | AK05066 | | *Tpm3* | 1.71 | 0.02591 |
| | 5.1 | tropomyosin 3, gamma | | | |
| 1450056 | NM_1748 | | *Micall2* | 1.71 | 0.00339 |
| | 50.2 | MICAL-like 2 | | | |
| 6350386 | NM_0273 | asparaginyl-tRNA | *Nars* | 1.70 | 0.00993 |
| | 50.2 | synthetase | | | |
| 7210274 | XM_1271 | | *Cep170 b* | 1.70 | 0.00311 |
| | 32.3 | centrosomal protein 170B | | | |
| 1660309 | NM_0085 | MAD homolog 1 | *Smad1* | 1.70 | 0.00011 |
| | 39.3 | (Drosophila) | | | |
| 5360608 | NM_0115 | | *Tjp2* | 1.70 | 0.00040 |
| | 97.2 | tight junction protein 2 | | | |
| 2070014 | NM_0194 | nuclear factor of kappa | *Nfkb2* | 1.70 | 0.00085 |
| | 08.1 | light polypeptide gene enhancer in B-cells 2 (p49/p100) | | | |
| 1070152 | NM_0115 | | *Stxbp2* | 1.69 | 0.02981 |
| | 03.2 | syntaxin binding protein 2 | | | |
| 6330543 | NM_0531 | | *Glrx1* | 1.69 | 0.03926 |
| | 08 | Glutaredoxin | | | |
| 3850333 | NM_0111 | protein C receptor, | *Procr* | 1.69 | 0.00074 |
| | 71.1 | endothelial | | | |
| 7040619 | NM_0138 | chloride intracellular | *Clic4* | 1.69 | 0.00048 |
| | 85.2 | channel 4 (mitochondrial), nuclear gene encoding mitochondrial protein | | | |
| 6270131 | NM_0258 | PQ loop repeat containing | *Pqlc1* | 1.69 | 0.00771 |
| | 61.2 | 1 | | | |
| 6840112 | NM_1338 | UDP-N- | *Uap1* | 1.69 | 0.03130 |
| | 06.4 | acetylglucosamine pyrophosphorylase 1 | | | |
| 7000112 | NM_0256 | | *Zwint* | 1.68 | 0.04393 |
| | 35.3 | ZW10 interactor | | | |
| 830273 | NM_0113 | small chemokine (C-C | *Ccl11* | 1.68 | 0.00122 |
| | 30.1 | motif) ligand 11 | | | |

| | | | | | |
|---|---|---|---|---|---|
| 2100424 | NM_001289606.1 | bromodomain containing 8 | *Brd8* | 1.68 | 0.01573 |
| 2850326 | NM_013760.3 | DnaJ (Hsp40) homolog, subfamily B, member 9 | *Dnajb9* | 1.68 | 0.00293 |
| 6940537 | NM_198412 | DnaJ (Hsp40) homolog, subfamily C, member 6 | *Dnajc6* | 1.68 | 0.00008 |
| 460594 | NM_030704.1 | heat shock protein 8 | *Hspb8* | 1.68 | 0.02984 |
| 4920288 | NM_008343.2 | insulin-like growth factor binding protein 3 | *Igfbp3* | 1.68 | 0.02804 |
| 6270739 | NM_133219.1 | glucosaminyl (N-acetyl) transferase 2, I-branching enzyme, transcript variant 3 | *Gcnt2* | 1.68 | 0.00172 |
| 7160167 | NM_010128.4 | epithelial membrane protein 1 | *Emp1* | 1.68 | 0.00294 |
| 1010347 | NM_178589.3 | tumor necrosis factor receptor superfamily, member 21 | *Tnfrsf21* | 1.67 | 0.00221 |
| 2190025 | AK051669 | polypyrimidine tract binding protein 1 | *Ptbp1* | 1.67 | 0.01285 |
| 1400689 | NM_019535.2 | SH3-domain GRB2-like 2 | *Sh3gl2* | 1.67 | 0.00802 |
| 6060520 | NM_011330.2 | small chemokine (C-C motif) ligand 11 | *Ccl11* | 1.67 | 0.01315 |
| 4560246 | NM_010225.1 | forkhead box F2 | *Foxf2* | 1.67 | 0.03491 |
| 2030632 | NM_028800.2 | serine/threonine kinase 40 | *Stk40* | 1.67 | 0.00253 |
| 5960475 | NM_001033352.3 | kelch-like 21 (Drosophila) | *Klhl21* | 1.66 | 0.03923 |
| 1770541 | NM_013749.1 | tumor necrosis factor receptor superfamily, member 12a (Tnfrsf12a) | *Tnfrsf12a* | 1.66 | 0.01082 |
| 7160021 | NM_153537.3 | pleckstrin homology-like domain, family B, member 1 | *Phldb1* | 1.66 | 0.02588 |
| 3840446 | NM_010807.3 | MARCKS-like 1 | *Marcksl1* | 1.66 | 0.00538 |
| 6660176 | NM_213659.2 | signal transducer and activator of transcription 3, transcript variant 1 | *Stat3* | 1.66 | 0.00057 |
| 7150575 | XM_110498 | expressed sequence C77080 | *C77080* | 1.65 | 0.04816 |
| 3400014 | NM_009289.1 | STE20-like kinase (yeast) | *Slk* | 1.65 | 0.00927 |

| | | | | | |
|---|---|---|---|---|---|
| 2680414 | NM_010801.1 | myeloid leukemia factor 1 | *Mlf1* | 1.65 | 0.00097 |
| 4050619 | NM_011488.2 | signal transducer and activator of transcription 5A | *Stat5a* | 1.65 | 0.00467 |
| 6660626 | NM_183140.1 | zinc finger protein 691 | *Zfp691* | 1.65 | 0.01954 |
| 4210193 | NM_133252.2 | translocating chain-associating membrane protein 2 | *Tram2* | 1.65 | 0.03809 |
| 6480273 | NM_013838 | transient receptor potential cation channel, subfamily C, member 6 | *Trpc6* | 1.65 | 0.00171 |
| 4860224 | NM_013671.2 | superoxide dismutase 2, mitochondrial | *Sod2* | 1.64 | 0.00682 |
| 5390239 | NM_008465.4 | karyopherin (importin) alpha 1 | *Kpna1* | 1.64 | 0.01552 |
| 7510240 | NM_172503.3 | zinc finger, SWIM domain containing 4 | *Zswim4* | 1.64 | 0.00466 |
| 4150014 | NM_001039150.1 | CD44 antigen, transcript variant 2 | *Cd44* | 1.64 | 0.02688 |
| 3310068 | NM_019514.3 | astrotactin 2, transcript variant 1 | *Astn2* | 1.64 | 0.00310 |
| 7330008 | NM_029457.2 | SUMO/sentrin specific peptidase 2 | *Senp2* | 1.64 | 0.02836 |
| 2760097 | XM_001481214.1 | PREDICTED: similar to nuclear pore-targeting complex component of 58 kDa, transcript variant 1 | *LOC100043906* | 1.64 | 0.02354 |
| 5130156 | NM_017466.4 | chemokine (C-C motif) receptor-like 2 | *Ccrl2* | 1.64 | 0.00896 |
| 3710598 | NM_030249.3 | CTTNBP2 N-terminal like | *Cttnbp2nl* | 1.64 | 0.00353 |
| 1820551 | NM_001077696.1 | histone deacetylase 5, transcript variant 1 | *Hdac5* | 1.64 | 0.04410 |
| 2970598 | NM_007746.2 | mitogen-activated protein kinase kinase kinase 8 | *Map3k8* | 1.63 | 0.00907 |
| 2630162 | AK045190 | serpine1 mRNA binding protein 1 | *Serbp1* | 1.63 | 0.00314 |
| 6040753 | NM_001005865.2 | mitochondrial tumor suppressor 1, nuclear gene encoding mitochondrial protein, transcript variant 4 | *Mtus1* | 1.63 | 0.00506 |
| 630543 | XM_355170.1 | | *LOC381234* | 1.63 | 0.02928 |

| | | | | | |
|---|---|---|---|---|---|
| 1780735 | NM_009754.2 | BCL2-like 11 (apoptosis facilitator) | *Bcl2l11* | 1.63 | 0.00723 |
| 1710193 | NM_010288.2 | gap junction membrane channel protein alpha 1 | *Gja1* | 1.63 | 0.03994 |
| 4070681 | NM_009644.2 | aryl-hydrocarbon receptor repressor | *Ahrr* | 1.63 | 0.00344 |
| 3400521 | AK037075 | | *9930108O06Rik* | 1.63 | 0.00146 |
| 6480201 | NM_026779.1 | molybdenum cofactor sulfurase | *Mocos* | 1.63 | 0.01828 |
| 4040563 | AK028452 | lectin, mannose-binding 2 | *Lman2* | 1.62 | 0.01120 |
| 4010162 | NM_007823.2 | cytochrome P450, family 4, subfamily b, polypeptide 1 | *Cyp4b1* | 1.62 | 0.00023 |
| 2450259 | NM_025782 | tetratricopeptide repeat domain 39B | *Ttc39b* | 1.62 | 0.00374 |
| 6840600 | NM_133626.2 | ribosome binding protein 1, transcript variant 2 | *Rrbp1* | 1.62 | 0.03213 |
| 2340242 | NM_008013.3 | fibrinogen-like protein 2 | *Fgl2* | 1.62 | 0.00530 |
| 7150541 | NM_007487.3 | ADP-ribosylation factor-like 4A, transcript variant 1 | *Arl4a* | 1.62 | 0.00108 |
| 7570050 | NM_001077696.1 | histone deacetylase 5, transcript variant 1 | *Hdac5* | 1.62 | 0.00236 |
| 4830050 | NM_001080929.1 | cerebellar degeneration-related protein 2-like | *Cdr2l* | 1.62 | 0.00168 |
| 4880494 | NM_026950.3 | OCIA domain containing 2 | *Ociad2* | 1.61 | 0.00257 |
| 4810437 | | protein kinase, cAMP dependent regulatory, type I beta, related sequence | *Prkar1b-rs* | 1.61 | 0.00427 |
| 150019 | NM_019980.1 | LPS-induced TN factor | *Litaf* | 1.61 | 0.00010 |
| 1440739 | NM_013923.2 | ring finger protein 19A | *Rnf19a* | 1.61 | 0.00169 |
| 6550647 | NM_146191.3 | leucine-rich repeat kinase 1 | *Lrrk1* | 1.61 | 0.00789 |
| 1940307 | NM_010720.2 | lipase, endothelial | *Lipg* | 1.60 | 0.00018 |
| 2450553 | NM_025789.4 | radial spokehead-like 2A | *Rshl2a* | 1.60 | 0.04261 |
| 6060349 | NM_153159.1 | zinc finger CCCH type containing 12A | *Zc3h12a* | 1.60 | 0.00905 |
| 6650435 | NM_1773 | myosin, heavy | *Myh8* | 1.60 | 0.04391 |

| | | | | | |
|---|---|---|---|---|---|
| | 69.3 | polypeptide 8, skeletal muscle, perinatal | | | |
| 360014 | NM_201394.1 | plectin 1, transcript variant 11 | *Plec1* | 1.60 | 0.00302 |
| 6270528 | NM_173370.3 | CDP-diacylglycerol synthase 1 | *Cds1* | 1.60 | 0.00195 |
| 430131 | NM_013654 | chemokine (C-C motif) ligand 7 | *Ccl7* | 1.60 | 0.03344 |
| 1500703 | XM_357532.1 | | *LOC384273* | 1.60 | 0.03006 |
| 6020196 | NM_008362.2 | interleukin 1 receptor, type I, transcript variant 1 | *Il1r1* | 1.60 | 0.00068 |
| 3360553 | NM_009834.1 | CCR4 carbon catabolite repression 4-like (S cerevisiae) | *Ccrn4l* | 1.60 | 0.00051 |
| 5260095 | NM_008301.4 | heat shock protein 2, transcript variant 1 | *Hspa2* | 1.59 | 0.01418 |
| 1980411 | NM_178917.2 | arrestin domain containing 3 | *Arrdc3* | 1.59 | 0.00212 |
| 6100719 | NM_030249 | CTTNBP2 N-terminal like | *Cttnbp2nl* | 1.59 | 0.00588 |
| 7400358 | NM_016807.1 | syndecan binding protein | *Sdcbp* | 1.59 | 0.00206 |
| 6840521 | AK011851 | guanine nucleotide binding protein (G protein), alpha 13 | *Gna13* | 1.59 | 0.01384 |
| 4760224 | NM_010217 | connective tissue growth factor | *Ctgf* | 1.59 | 0.02145 |
| 3290044 | NM_021478.1 | tubby like protein 1 | *Tulp1* | 1.59 | 0.04532 |
| 5820070 | NM_008956.2 | polypyrimidine tract binding protein 1, transcript variant 2 | *Ptbp1* | 1.59 | 0.00046 |
| 6370204 | NM_178598.2 | transgelin 2 | *Tagln2* | 1.59 | 0.01839 |
| 1070709 | NM_017464.2 | neural precursor cell expressed, developmentally down-regulated gene 9 | *Nedd9* | 1.59 | 0.00471 |
| 3610082 | NM_008176.1 | chemokine (C-X-C motif) ligand 1 | *Cxcl1* | 1.59 | 0.00173 |
| 6900504 | XR_032036.1 | PREDICTED: similar to protein tyrosine phosphatase-like protein PTPLB, misc RNA | *LOC666053* | 1.59 | 0.00113 |
| 1070632 | NM_0010 | sperm associated antigen | *Spag9* | 1.59 | 0.02409 |

| | | | | | |
|---|---|---|---|---|---|
| | 25429.1 | 9, transcript variant 3 | | | |
| 3140220 | NM_0167 48.1 | cytidine 5'-triphosphate synthase | *Ctps* | 1.59 | 0.00243 |
| 3130669 | NM_0299 26.3 | interleukin-1 receptor-associated kinase 4 | *Irak4* | 1.59 | 0.02830 |
| 6020040 | NM_0086 55.1 | growth arrest and DNA-damage-inducible 45 beta | *Gadd45 b* | 1.58 | 0.00024 |
| 10167 | NM_0010 81015.1 | predicted gene, EG630499 | *EG6304 99* | 1.58 | 0.00072 |
| 5050577 | NM_0167 48.1 | cytidine 5'-triphosphate synthase | *Ctps* | 1.58 | 0.01313 |
| 2100068 | NM_0102 60.1 | guanylate binding protein 2 | *Gbp2* | 1.58 | 0.01374 |
| 4260195 | NM_1337 54.3 | filamin binding LIM protein 1 | *Fblim1* | 1.58 | 0.04326 |
| 1990376 | NM_0235 98.2 | AT rich interactive domain 5B (MRF1-like) | *Arid5b* | 1.58 | 0.02059 |
| 450110 | NM_0109 07 | nuclear factor of kappa light polypeptide gene enhancer in B-cells inhibitor, alpha | *Nfkbia* | 1.58 | 0.01069 |
| 4150133 | NM_0088 08 | latelet-derived growth factor alpha polypeptide | *Pdgfa* | 1.58 | 0.00182 |
| 2070360 | NM_1752 56.4 | HEG homolog 1 (zebrafish) | *Heg1* | 1.57 | 0.00753 |
| 5130041 | NM_0297 87.2 | cytochrome b5 reductase 3 | *Cyb5r3* | 1.57 | 0.01192 |
| 610463 | NM_0296 88.2 | sulfiredoxin 1 homolog (S cerevisiae) | *Srxn1* | 1.57 | 0.01527 |
| 2230707 | AK01831 3 | eukaryotic translation initiation factor 6 | *Itgb4bp* | 1.57 | 0.00796 |
| 4670372 | NM_0111 73.2 | protein S (alpha) | *Pros1* | 1.57 | 0.00624 |
| 1980348 | NM_0288 00 | *s*erine/threonine kinase 40 | *Stk40* | 1.57 | 0.00294 |
| 4250605 | AK04292 5 | early B cell factor 1 | *Ebf1* | 1.56 | 0.03483 |
| 5550092 | NM_0010 81214.1 | peroxisome proliferative activated receptor, gamma, coactivator-related 1 | *Pprc1* | 1.56 | 0.02237 |
| 4920615 | NM_0307 24.1 | uridine-cytidine kinase 2 | *Uck2* | 1.56 | 0.00317 |
| 6650349 | NM_1748 50.2 | MICAL-like 2 | *Micall2* | 1.56 | 0.00362 |
| 5960152 | NM_0263 | brix domain containing 2 | *Bxdc2* | 1.56 | 0.02437 |

| | | | | | |
|---|---|---|---|---|---|
| | 96.2 | | | | |
| 430360 | NM_028943.3 | sphingomyelin synthase 2 | *Sgms2* | 1.56 | 0.03750 |
| 3930114 | NM_080846.1 | HIG1 domain family, member 1B | *Higd1b* | 1.56 | 0.00383 |
| 4250670 | NM_026908.3 | calcium binding protein 39-like | *Cab39l* | 1.56 | 0.00209 |
| 6520044 | NM_009595.2 | v-abl Abelson murine leukemia viral oncogene homolog 2 (arg, Abelson-related gene) | *Abl2* | 1.56 | 0.00738 |
| 2570440 | NM_017464.2 | neural precursor cell expressed, developmentally down-regulated gene 9 | *Nedd9* | 1.55 | 0.00885 |
| 7200133 | NM_010295.1 | glutamate-cysteine ligase, catalytic subunit | *Gclc* | 1.55 | 0.04470 |
| 2320626 | NM_012055.1 | asparagine synthetase | *Asns* | 1.55 | 0.00069 |
| 5550035 | NM_019662.1 | Ras-related associated with diabetes | *Rrad* | 1.55 | 0.01338 |
| 1570139 | NM_181650.2 | PR domain containing 4 | *Prdm4* | 1.55 | 0.01723 |
| 5220259 | NM_010451.1 | homeo box A2 | *Hoxa2* | 1.55 | 0.03891 |
| 6380255 | NM_153457.6 | reticulon 1, transcript variant 1 | *Rtn1* | 1.55 | 0.00055 |
| 6650021 | NM_008524 | Lumican | *Lum* | 1.55 | 0.04865 |
| 2570689 | AK017390.1 | RIKEN cDNA 5430434G16 gene | *5430434G16Rik* | 1.55 | 0.02099 |
| 3420242 | XM_980150.1 | PREDICTED: similar to Su48, transcript variant 3 | *LOC674611* | 1.55 | 0.01249 |
| 3460669 | NM_001025429.1 | sperm associated antigen 9, transcript variant 3 | *Spag9* | 1.55 | 0.01701 |
| 4490537 | NM_175155.4 | SAM and SH3 domain containing 1 | *Sash1* | 1.55 | 0.00589 |
| 5560100 | NM_028186.3 | naked cuticle 2 homolog (Drosophila) | *Nkd2* | 1.54 | 0.02281 |
| 3180215 | NM_013613.1 | nuclear receptor subfamily 4, group A, member 2 | *Nr4a2* | 1.54 | 0.01866 |
| 2000139 | NM_027429.1 | centromere protein L | *Cenpl* | 1.54 | 0.00491 |
| 5690327 | NM_029478.3 | transmembrane protein 49 | *Tmem49* | 1.54 | 0.00844 |
| 3440615 | NM_0194 | regulator of calcineurin 1 | *Rcan1* | 1.54 | 0.00059 |

| | | | | | |
|---|---|---|---|---|---|
| | 66.2 | | | | |
| 5490114 | NM_173363.4 | eukaryotic translation initiation factor 5, transcript variant 1 | *Eif5* | 1.54 | 0.00654 |
| 5130100 | NM_153387.2 | tubulin, gamma complex associated protein 4 | *Tubgcp4* | 1.54 | 0.04146 |
| 3990438 | NM_008667.2 | Ngfi-A binding protein 1 | *Nab1* | 1.54 | 0.01940 |
| 4830528 | NM_011241 | Ran GTPase activating protein 1 | *Rangap1* | 1.54 | 0.01027 |
| 1470070 | NM_027366.1 | lymphocyte antigen 6 complex, locus G6E | *Ly6g6e* | 1.54 | 0.00707 |
| 5090056 | NM_001005510.2 | synaptic nuclear envelope 2 | *Syne2* | 1.54 | 0.02180 |
| 1580209 | NM_178684.3 | RIKEN cDNA C130032J12 gene | *C130032J12Rik* | 1.53 | 0.00486 |
| 4560670 | NM_015817.2 | phosphatidic acid phosphatase type 2c | *Ppap2c* | 1.53 | 0.00939 |
| 1190088 | NM_008390.1 | interferon regulatory factor 1 | *Irf1* | 1.53 | 0.04622 |
| 1400309 | NM_011595.2 | tissue inhibitor of metalloproteinase 3 | *Timp3* | 1.53 | 0.00265 |
| 4070184 | NM_007465.1 | baculoviral IAP repeat-containing 2 | *Birc2* | 1.53 | 0.01825 |
| 2690142 | NM_022314.2 | tropomyosin 3, gamma | *Tpm3* | 1.53 | 0.02338 |
| 6420088 | NM_025626.3 | RIKEN cDNA 3110001A13 gene | *3110001A13Rik* | 1.53 | 0.01120 |
| 6960630 | NM_009781.2 | calcium channel, voltage-dependent, L type, alpha 1C subunit XM_925104 XM_925108 XM_925111 | *Cacna1c* | 1.53 | 0.02772 |
| 870246 | NM_010431.1 | hypoxia inducible factor 1, alpha subunit | *Hif1a* | 1.53 | 0.01841 |
| 6620164 | AK076298 | RIKEN cDNA 2010111I01 gene | *2010111I01Rik* | 1.53 | 0.02768 |
| 6900091 | NM_019765 | CAP-GLY domain containing linker protein 1 | *Clip1* | 1.53 | 0.03466 |
| 6290152 | NM_053202.1 | forkhead box P1 | *Foxp1* | 1.53 | 0.03904 |
| 7610603 | NM_011552 | Treacher Collins-Franceschetti syndrome 1 | *Tcof1* | 1.52 | 0.04120 |
| 5220600 | NM_001039185.1 | carcinoembryonic antigen-related cell adhesion molecule 1, transcript variant 1 | *Ceacam1* | 1.52 | 0.03337 |

| | | | | | |
|---|---|---|---|---|---|
| 520544 | NM_007666.3 | cadherin 6 | *Cdh6* | 1.52 | 0.03961 |
| 4180088 | NM_027460.2 | solute carrier family 25, member 33 | *Slc25a33* | 1.52 | 0.04059 |
| 6350767 | AK045838 | AE binding protein 2 | *Aebp2* | 1.52 | 0.00473 |
| 3830747 | AK016549 | predicted gene, 16982 | *Gm16982* | 1.52 | 0.01122 |
| 6020768 | NM_013760.4 | DnaJ (Hsp40) homolog, subfamily B, member 9 | *Dnajb9* | 1.52 | 0.00124 |
| 2750114 | NM_178113.2 | non-SMC condensin II complex, subunit D3 | *Ncapd3* | 1.52 | 0.00093 |
| 4050333 | NM_011534.1 | T-box 15 | *Tbx15* | 1.52 | 0.04021 |
| 450309 | NM_173413.2 | RAB8B, member RAS oncogene family | *Rab8b* | 1.51 | 0.01481 |
| 3450164 | NM_018811.6 | abhydrolase domain containing 2 | *Abhd2* | 1.51 | 0.01014 |
| 7100674 | NM_016923.1 | lymphocyte antigen 96 | *Ly96* | 1.51 | 0.04414 |
| 5820685 | NM_007426.3 | angiopoietin 2 | *Angpt2* | 1.51 | 0.03391 |
| 3420110 | NM_009394.2 | troponin C2, fast | *Tnnc2* | 1.51 | 0.01753 |
| 7380019 | NM_001077404.1 | neuropilin 2, transcript variant 2 | *Nrp2* | 1.51 | 0.02599 |
| 2070474 | NM_010577.2 | integrin alpha 5 (fibronectin receptor alpha) | *Itga5* | 1.51 | 0.01044 |
| 2600484 | XM_358311.5 | PREDICTED: zinc finger, SWIM domain containing 6 | *Zswim6* | 1.51 | 0.00001 |
| 5890221 | NM_007987.1 | Fas (TNF receptor superfamily member 6) | *Fas* | 1.51 | 0.01053 |
| 380014 | NM_008539.3 | MAD homolog 1 (Drosophila) | *Smad1* | 1.51 | 0.02035 |
| 2260184 | XM_356123.1 | | *LOC382050* | 1.51 | 0.00689 |
| 5340609 | NM_153178.4 | argonaute RISC catalytic subunit 2 | *Ago2* | 1.51 | 0.02310 |
| 870309 | AK045954 | serine (or cysteine) peptidase inhibitor, clade E, member 2 | *Serpine2* | 1.51 | 0.02756 |
| 6840154 | NM_010509.1 | interferon (alpha and beta) receptor 2 | *Ifnar2* | 1.51 | 0.03164 |
| 2140338 | NM_0197 | CAP-GLY domain | *Clip1* | 1.51 | 0.03722 |

| | | | | | |
|---|---|---|---|---|---|
| | 65.2 | containing linker protein 1 | | | |
| 3800022 | NM_175937 | cytoplasmic polyadenylation element binding protein 2 | *Cpeb2* | 1.51 | 0.03067 |
| 5810079 | NM_011835.1 | katanin p60 (ATPase-containing) subunit A1 | *Katna1* | 1.51 | 0.01136 |
| 4880300 | NM_029614.3 | protease, serine, 23 | *Prss23* | 1.51 | 0.00033 |
| 6250731 | XM_001472777.1 | PREDICTED: pappalysin 2 | *Pappa2* | 1.50 | 0.00922 |
| 4780373 | NM_011278.3 | ring finger protein 4 | *Rnf4* | 1.50 | 0.00369 |
| 7610477 | NM_008536.2 | transmembrane 4 L six family member 1 | *Tm4sf1* | 1.50 | 0.00533 |
| 5490678 | XM_001001363.1 | PREDICTED: centaurin, delta 1, transcript variant 5 | *Centd1* | 1.50 | 0.00412 |
| 7400468 | NM_080558 | sperm specific antigen 2 | *Ssfa2* | 1.50 | 0.01089 |
| 2630189 | NM_001047159.1 | neuroepithelial cell transforming gene 1, transcript variant 2 | *Net1* | 1.50 | 0.00686 |
| 270671 | NM_030888.2 | C1q and tumor necrosis factor related protein 3 | *C1qtnf3* | -1.50 | 0.03736 |
| 3520020 | XM_001476583.1 | PREDICTED: similar to Bcl2-like protein | *LOC100046608* | -1.50 | 0.02119 |
| 6620670 | NM_023202.3 | NADH dehydrogenase (ubiquinone) 1 alpha subcomplex, 7 (B145a) | *Ndufa7* | -1.50 | 0.01736 |
| 4210128 | NM_007389.4 | cholinergic receptor, nicotinic, alpha polypeptide 1 (muscle) | *Chrna1* | -1.51 | 0.03924 |
| 7050719 | NM_144519.2 | zinc finger protein 639 | *Zfp639* | -1.51 | 0.04616 |
| 1770672 | NM_012019.2 | apoptosis-inducing factor, mitochondrion-associated 1, nuclear gene encoding mitochondrial protein | *Aifm1* | -1.51 | 0.00124 |
| 5690242 | NM_001081041.1 | RIKEN cDNA 1110014N23 gene | *1110014N23Rik* | -1.51 | 0.02458 |
| 2900338 | NM_011491.3 | stanniocalcin 2 | *Stc2* | -1.51 | 0.01209 |
| 6900328 | XM_001003712.1 | PREDICTED: similar to neuron navigator 3, transcript variant 5 | *LOC676640* | -1.51 | 0.00650 |
| 6370079 | NM_1531 | zinc finger, CCHC | *Zcchc17* | -1.51 | 0.00280 |

| | | | | | |
|---|---|---|---|---|---|
| | 60.3 | domain containing 17 (Zcchc17) | | | |
| 5090372 | NM_207655.1 | epidermal growth factor receptor | *Egfr* | -1.51 | 0.02675 |
| 1940215 | XR_035347.1 | PREDICTED: RIKEN cDNA 2700046G09 gene, misc RNA | *2700046G09Rik* | -1.51 | 0.00998 |
| 4390634 | NM_008121.2 | gap junction membrane channel protein alpha 5 | *Gja5* | -1.51 | 0.01027 |
| 3120240 | NM_001033770.1 | gene model 904, (NCBI) | *Gm904* | -1.51 | 0.00025 |
| 5720669 | NM_007588.2 | calcitonin receptor, transcript variant a | *Calcr* | -1.51 | 0.00135 |
| 70504 | NM_025917.3 | unconventional SNARE in the ER 1 homolog (S cerevisiae), transcript variant 1 | *Use1* | -1.51 | 0.00370 |
| 2900327 | NM_173019.5 | 6-phosphofructo-2-kinase/fructose-2,6-biphosphatase 4 | *Pfkfb4* | -1.52 | 0.03342 |
| 1300554 | NM_134033.1 | coiled-coil domain containing 117 | *Ccdc117* | -1.52 | 0.02678 |
| 4610451 | NM_010284.2 | growth hormone receptor, transcript variant 1 | *Ghr* | -1.52 | 0.04554 |
| 130544 | NM_177176.2 | nuclear factor I/A | *Nfia* | -1.52 | 0.00449 |
| 160255 | NM_173451.1 | arylsulfatase J | *Arsj* | -1.52 | 0.00248 |
| 3460056 | NM_148930.2 | RNA binding motif protein 5 | *Rbm5* | -1.52 | 0.02480 |
| 4860435 | NM_010209 | fumarate hydratase 1 | *Fh1* | -1.52 | 0.04430 |
| 650403 | NM_145471.2 | leucine rich repeat containing 14 | *Lrrc14* | -1.52 | 0.04447 |
| 1260747 | NM_007473.4 | aquaporin 7 | *Aqp7* | -1.52 | 0.00598 |
| 6200494 | NM_009161.3 | sarcoglycan, alpha (dystrophin-associated glycoprotein) | *Sgca* | -1.52 | 0.01110 |
| 4570181 | NM_153594.2 | protein-L-isoaspartate (D-aspartate) O-methyltransferase domain containing 2 | *Pcmtd2* | -1.52 | 0.02140 |
| 1090669 | NM_175310.5 | androgen-induced proliferation inhibitor | *Aprin* | -1.52 | 0.02761 |
| 6100215 | NM_0255 | coiled-coil domain | *Ccdc90b* | -1.52 | 0.01593 |

| | | | | | |
|---|---|---|---|---|---|
| | 15.2 | containing 90B | | | |
| 360228 | XM_0014 74305.1 | PREDICTED: hypothetical protein LOC100040159 | *LOC100 040159* | -1.52 | 0.00047 |
| 6620142 | NM_0531 42.3 | protocadherin beta 17 | *Pcdhb17* | -1.52 | 0.00716 |
| 1690035 | NM_0194 44.2 | receptor (calcitonin) activity modifying protein 2 | *Ramp2* | -1.52 | 0.03661 |
| 6420672 | NM_0256 77.2 | tRNA splicing endonuclease 15 homolog (S cerevisiae) | *Tsen15* | -1.52 | 0.01162 |
| 6840379 | NM_0283 72.1 | RIKEN cDNA 2900024O10 gene | *2900024 O10Rik* | -1.53 | 0.02020 |
| 840437 | NM_0205 77.2 | arsenic (+3 oxidation state) methyltransferase | *As3mt* | -1.53 | 0.01242 |
| 2140605 | NM_1338 50.1 | COMM domain containing 7 | *Commd 7* | -1.53 | 0.02240 |
| 650131 | NM_1385 90.2 | DNA segment, Chr 4, Wayne State University 132, expressed | *D4Wsu1 32e* | -1.53 | 0.03129 |
| 70379 | NM_1455 50.2 | Yip1 domain family, member 1 | *Yipf1* | -1.53 | 0.04037 |
| 7160603 | NM_0091 55.3 | selenoprotein P, plasma, 1, transcript variant 1 | *Sepp1* | -1.53 | 0.01414 |
| 6860524 | NM_0078 72.4 | DNA methyltransferase 3A, transcript variant 1 | *Dnmt3a* | -1.53 | 0.01622 |
| 5960343 | NM_0081 97.3 | H1 histone family, member 0 | *H1f0* | -1.53 | 0.00356 |
| 7330026 | NM_0101 18.1 | early growth response 2 | *Egr2* | -1.53 | 0.01494 |
| 6760653 | NM_0215 13.1 | THAP domain containing 11 | *Thap11* | -1.53 | 0.02194 |
| 580189 | NM_0254 34.2 | mitochondrial ribosomal protein S28, nuclear gene encoding mitochondrial protein | *Mrps28* | -1.53 | 0.00136 |
| 2970327 | AK03873 1 | zinc finger and BTB domain containing 20 | *Zbtb20* | -1.53 | 0.01636 |
| 2810450 | NM_0134 68.3 | ankyrin repeat domain 1 (cardiac muscle) | *Ankrd1* | -1.53 | 0.04450 |
| 7380474 | NM_0087 48.3 | dual specificity phosphatase 8 | *Dusp8* | -1.53 | 0.01028 |
| 4540382 | NM_0079 12.4 | epidermal growth factor receptor, transcript variant 2 | *Egfr* | -1.54 | 0.00195 |

| | | | | | |
|---|---|---|---|---|---|
| 4920382 | NM_152806.3 | DEAD (Asp-Glu-Ala-Asp) box polypeptide 17, transcript variant 3 | *Ddx17* | -1.54 | 0.01700 |
| 4880132 | NM_025831.3 | RIKEN cDNA 1300014I06 gene | *1300014I06Rik* | -1.54 | 0.01857 |
| 2450427 | NM_025677.1 | RIKEN cDNA 5730449L18 gene | *5730449L18Rik* | -1.54 | 0.02186 |
| 290048 | NM_177344.3 | RIKEN cDNA C730025P13 gene | *C730025P13Rik* | -1.54 | 0.02164 |
| 380035 | NR_040721.1 | small nucleolar RNA host gene 5 | *Snhg5* | -1.54 | 0.00062 |
| 5810470 | NM_013467.3 | aldehyde dehydrogenase family 1, subfamily A1 | *Aldh1a1* | -1.54 | 0.04414 |
| 5870739 | NM_007406.1 | adenylate cyclase 7, transcript variant 1 | *Adcy7* | -1.54 | 0.01262 |
| 3390731 | NM_010875.3 | neural cell adhesion molecule 1, transcript variant 2 | *Ncam1* | -1.54 | 0.00008 |
| 2450315 | XM_905813.3 | PREDICTED: hypothetical LOC627985 | *LOC627985* | -1.54 | 0.03996 |
| 6860519 | NM_008786.1 | protein-L-isoaspartate (D-aspartate) O-methyltransferase 1 | *Pcmt1* | -1.54 | 0.03843 |
| 2370113 | XM_358848.1 | | *LOC385653* | -1.54 | 0.00089 |
| 4570468 | NM_146236.1 | transcription elongation factor A (SII)-like 1 | *Tceal1* | -1.54 | 0.03042 |
| 2850079 | NM_133835.1 | ubiquitin associated domain containing 1 | *Ubac1* | -1.54 | 0.04834 |
| 6290041 | NM_029272.3 | NADH dehydrogenase (ubiquinone) Fe-S protein 7, nuclear gene encoding mitochondrial protein | *Ndufs7* | -1.54 | 0.00502 |
| 650400 | NM_028543.3 | RIKEN cDNA 1700065O13 gene (1700065O13Rik) | *1700065O13Rik* | -1.55 | 0.02488 |
| 2350092 | NM_016806.2 | heterogeneous nuclear ribonucleoprotein A2/B1, transcript variant 1 | *Hnrnpa2b1* | -1.55 | 0.00894 |
| 4860491 | NM_001083906.1 | nuclear receptor subfamily 3, group C, member 2 | *Nr3c2* | -1.55 | 0.01019 |
| 130239 | NM_018865.2 | WNT1 inducible signaling pathway protein 1 | *Wisp1* | -1.55 | 0.03854 |
| 4070215 | NM_133670.1 | sulfotransferase family 1A, phenol-preferring, member 1 | *Sult1a1* | -1.55 | 0.03374 |

| | | | | | |
|---|---|---|---|---|---|
| 2480397 | NM_001013786.1 | zinc finger protein 187 | *Zfp187* | -1.55 | 0.02808 |
| 830491 | NM_009057.2 | recombination activating gene 1 activating protein 1 | *Rag1ap1* | -1.55 | 0.02176 |
| 5860138 | NM_019565.3 | zinc finger protein 386 (Kruppel-like), transcript variant 2 | *Zfp386* | -1.55 | 0.00723 |
| 1110440 | NM_026840.2 | platelet-derived growth factor receptor-like | *Pdgfrl* | -1.55 | 0.00530 |
| 4070121 | NM_001081044.1 | myosin, light polypeptide kinase 2, skeletal muscle | *Mylk2* | -1.55 | 0.01160 |
| 2750521 | NM_026526.2 | N-6 adenine-specific DNA methyltransferase 2 (putative) | *N6amt2* | -1.55 | 0.00606 |
| 3610356 | NM_001081242.1 | talin 2 | *Tln2* | -1.56 | 0.00437 |
| 3890288 | NM_010473.2 | histidine rich calcium binding protein | *Hrc* | -1.56 | 0.02863 |
| 2900301 | NM_025597.2 | NADH dehydrogenase (ubiquinone) 1 beta subcomplex 3 | *Ndufb3* | -1.56 | 0.03587 |
| 290041 | NM_026756.2 | nuclear factor I/C, transcript variant 2 | *Nfic* | -1.56 | 0.02868 |
| 2490243 | AK087605 | | *E23002 4B12Rik* | -1.56 | 0.00393 |
| 3450300 | NM_016674.2 | claudin 1 | *Cldn1* | -1.56 | 0.02002 |
| 4150482 | NM_028543.1 | RIKEN cDNA 1700065O13 gene | *1700065 O13Rik* | -1.56 | 0.00965 |
| 5810010 | NM_019772.2 | RIKEN cDNA 1110004F10 gene | *1110004 F10Rik* | -1.56 | 0.00156 |
| 4280193 | NM_016849.3 | interferon regulatory factor 3 | *Irf3* | -1.56 | 0.04793 |
| 110630 | NM_026598.2 | emopamil binding protein-like | *Ebpl* | -1.56 | 0.00369 |
| 6860475 | NM_175206.2 | F-box and leucine-rich repeat protein 22 | *Fbxl22* | -1.57 | 0.00023 |
| 840189 | NM_019919.2 | latent transforming growth factor beta binding protein 1, transcript variant 1 | *Ltbp1* | -1.57 | 0.00372 |
| 5290367 | XM_001477963.1 | PREDICTED: similar to myocardial vascular inhibition factor | *LOC100 047353* | -1.57 | 0.04469 |
| 2100521 | NM_023689.2 | sparc/osteonectin, cwcv and kazal-like domains proteoglycan 3 | *Spock3* | -1.57 | 0.00081 |

| | | | | | |
|---|---|---|---|---|---|
| 510102 | NM_010206.2 | fibroblast growth factor receptor 1, transcript variant 1 | *Fgfr1* | -1.57 | 0.01053 |
| 4050603 | NM_023240.2 | eukaryotic translation elongation factor 1 delta (guanine nucleotide exchange protein), transcript variant 2 | *Eef1d* | -1.57 | 0.00230 |
| 3130040 | NM_178667.3 | transcription factor Dp 2 | *Tfdp2* | -1.57 | 0.03698 |
| 6130411 | NM_011526.4 | transgelin | *Tagln* | -1.57 | 0.04598 |
| 3190670 | NM_147220.1 | ATP-binding cassette transporter sub-family A member 9 | *Abca9* | -1.57 | 0.01810 |
| 5310048 | NM_199032.2 | centrosomal protein 135 | *Cep135* | -1.57 | 0.01684 |
| 2480475 | NM_001013370.1 | sestrin 1 | *Sesn1* | -1.58 | 0.02375 |
| 10309 | NM_153526.2 | insulin induced gene 1 ( | *Insig1* | -1.58 | 0.00616 |
| 2650538 | NM_019880.3 | mitochondrial carrier homolog 1 (C elegans), nuclear gene encoding mitochondrial protein | *Mtch1* | -1.58 | 0.01196 |
| 6980576 | NM_007705.2 | cold inducible RNA binding protein | *Cirbp* | -1.58 | 0.00544 |
| 7050682 | NM_022000.2 | GNAS (guanine nucleotide binding protein, alpha stimulating) complex locus, transcript variant 3 | *Gnas* | -1.58 | 0.00479 |
| 4280402 | NM_010145.2 | epoxide hydrolase 1, microsomal | *Ephx1* | -1.58 | 0.00425 |
| 1440022 | NM_134189.2 | UDP-N-acetyl-alpha-D-galactosamine:polypeptide N-acetylgalactosaminyltransferase 10 | *Galnt10* | -1.58 | 0.00800 |
| 3450706 | NM_027633.1 | RIKEN cDNA 4931417G12 gene | *4931417G12Rik* | -1.58 | 0.00052 |
| 5050280 | NM_001081335.1 | p53-associated parkin-like cytoplasmic protein | *Parc* | -1.58 | 0.01339 |
| 4290142 | NM_172294.1 | sulfatase 1 | *Sulf1* | -1.58 | 0.00123 |
| 7560674 | NM_001 | lectin, mannose-binding | *Lman2l* | -1.58 | 0.00992 |

| | | | | | |
|---|---|---|---|---|---|
| | 13374.1 | 2-like | | | |
| 6380201 | NM_173437 | neuron navigator 1 | *Nav1* | -1.58 | 0.00606 |
| 2760382 | NM_010017.1 | dystroglycan 1 | *Dag1* | -1.58 | 0.01139 |
| 3610435 | NM_028314.1 | RIKEN cDNA 2700097O09 gene | *2700097O09Rik* | -1.59 | 0.02617 |
| 3420544 | NM_022995.3 | prostate transmembrane protein, androgen induced 1 | *Pmepa1* | -1.59 | 0.00575 |
| 3780609 | NM_011489.2 | signal transducer and activator of transcription 5B | *Stat5b* | -1.59 | 0.01341 |
| 4070253 | NM_009601.3 | cholinergic receptor, nicotinic, beta polypeptide 1 (muscle) (Chrnb1) | *Chrnb1* | -1.59 | 0.00773 |
| 4230138 | XM_001480474.1 | PREDICTED: RIKEN cDNA 2810055G20 gene | *2810055G20Rik* | -1.59 | 0.00901 |
| 2900220 | NM_144808.4 | solute carrier family 39 (zinc transporter), member 14, transcript variant 3 | *Slc39a14* | -1.59 | 0.02204 |
| 3390088 | NM_001033140.3 | RIKEN cDNA 0610010E21 gene | *0610010E21Rik* | -1.59 | 0.00769 |
| 6620025 | NM_026072.1 | serologically defined colon cancer antigen 10 XM_980999 XM_981042 XM_981078 | *Sdccag10* | -1.59 | 0.00566 |
| 3890050 | AK031063 | Chondrolectin | *Chodl* | -1.59 | 0.00168 |
| 3170358 | NM_009211.2 | SWI/SNF related, matrix associated, actin dependent regulator of chromatin, subfamily c, member 1 | *Smarcc1* | -1.59 | 0.00652 |
| 2360114 | NM_010549.2 | interleukin 11 receptor, alpha chain 1 | *Il11ra1* | -1.59 | 0.00149 |
| 2470465 | NM_001012336.1 | midkine, transcript variant 3 | *Mdk* | -1.59 | 0.00000 |
| 2370037 | XM_001480824.1 | PREDICTED: similar to regulatory factor X domain containing 2 homolog | *LOC100048616* | -1.59 | 0.04892 |
| 2350162 | AK089127 | nuclear factor I/B | *Nfib* | -1.59 | 0.00741 |
| 1440215 | NM_177124.3 | trinucleotide repeat containing 6b, transcript | *Tnrc6b* | -1.59 | 0.02481 |

| | | | | | |
|---|---|---|---|---|---|
| | | variant 2 | | | |
| 4260594 | NM_181728.1 | ADP-ribosyltransferase 3 | *Art3* | -1.59 | 0.00005 |
| 2450128 | XM_001474412.1 | PREDICTED: similar to Skullin | *LOC100045502* | -1.59 | 0.00242 |
| 7100538 | NM_019998 | asparagine-linked glycosylation 2 (alpha-1,3-mannosyltransferase) | *Alg2* | -1.60 | 0.02189 |
| 7400110 | NM_148930.2 | RNA binding motif protein 5 | *Rbm5* | -1.60 | 0.02418 |
| 5290379 | NM_001037863.1 | ATPase, class VI, type 11C, transcript variant 1 | *Atp11c* | -1.60 | 0.00079 |
| 4900719 | NM_172768 | GRAM domain containing 1B | *Gramd1b* | -1.60 | 0.02416 |
| 4920092 | NM_019988.3 | G protein beta subunit-like | *Gbl* | -1.60 | 0.03112 |
| 3180754 | NM_025988.2 | acyl-Coenzyme A binding domain containing 4, transcript variant 1 | *Acbd4* | -1.60 | 0.02152 |
| 1510041 | NM_001081417.1 | chromodomain helicase DNA binding protein 7 | *Chd7* | -1.60 | 0.01509 |
| 360524 | NM_027422.1 | mesoderm induction early response 1, family member 2 | *Mier2* | -1.60 | 0.00808 |
| 60646 | NM_001083906.1 | nuclear receptor subfamily 3, group C, member 2 | *Nr3c2* | -1.60 | 0.00735 |
| 150240 | NM_031397.2 | bicaudal C homolog 1 (Drosophila) | *Bicc1* | -1.60 | 0.01976 |
| 160091 | NM_144920.3 | pleckstrin homology domain containing, family A member 5 | *Plekha5* | -1.60 | 0.00271 |
| 1850349 | NM_172700.2 | zinc metallopeptidase, STE24 homolog (S cerevisiae) | *Zmpste24* | -1.60 | 0.00961 |
| 3370176 | XM_978742.1 | PREDICTED: RIKEN cDNA 2810409K11 gene | *2810409K11Rik* | -1.60 | 0.00297 |
| 610717 | NM_007632.2 | cyclin D3, transcript variant 1 | *Ccnd3* | -1.60 | 0.00014 |
| 580379 | NM_009441.2 | tetratricopeptide repeat domain 3 | *Ttc3* | -1.60 | 0.02300 |
| 6510463 | NM_133738.1 | anthrax toxin receptor 2 | *Antxr2* | -1.60 | 0.01322 |
| 6270564 | NM_198033.2 | senataxin | *Setx* | -1.61 | 0.01592 |
| 7050612 | NM_008254.1 | 3-hydroxy-3-methylglutaryl-Coenzyme | *Hmgcl* | -1.61 | 0.00851 |

| | | | | | |
|---|---|---|---|---|---|
| | | A lyase | | | |
| 6940278 | NM_0097 55.2 | bone morphogenetic protein 1 | *Bmp1* | -1.61 | 0.03303 |
| 1510435 | NM_0272 30.3 | protein kinase C binding protein 1 | *Prkcbp1* | -1.61 | 0.01507 |
| 4120017 | NM_0253 63.2 | RIKEN cDNA 1110001J03 gene | *1110001 J03Rik* | -1.61 | 0.02566 |
| 6420296 | NM_0274 23.1 | polymerase (RNA) III (DNA directed) polypeptide B | *Polr3b* | -1.61 | 0.02824 |
| 1090093 | NM_0094 41.1 | tetratricopeptide repeat domain 3 | *Ttc3* | -1.61 | 0.02307 |
| 3170372 | NM_0298 49.2 | RIKEN cDNA 4632433K11 gene | *4632433 K11Rik* | -1.61 | 0.00753 |
| 3180750 | NM_0169 74.1 | D site albumin promoter binding protein | *Dbp* | -1.61 | 0.00730 |
| 6520561 | NM_0293 20.2 | progesterone immunomodulatory binding factor 1, transcript variant 1 | *Pibf1* | -1.61 | 0.00422 |
| 2320653 | NM_1725 88.2 | serine incorporator 5 | *Serinc5* | -1.62 | 0.00799 |
| 360400 | NM_0113 07.2 | ubiquitin interaction motif containing 1 | *Uimc1* | -1.62 | 0.02369 |
| 6560594 | NM_1531 45.3 | ATP-binding cassette, sub-family A (ABC1), member 8a | *Abca8a* | -1.62 | 0.00673 |
| 3170041 | NM_0111 62.2 | mitogen activated protein kinase 8 interacting protein 1 | *Mapk8ip 1* | -1.62 | 0.03862 |
| 2030546 | NM_0100 17.3 | dystroglycan 1 | *Dag1* | -1.62 | 0.02331 |
| 6480113 | NR_0460 06.1 | RIKEN cDNA 2310010J17 gene | *2310010 J17Rik* | -1.62 | 0.03560 |
| 2680360 | XM_9041 20.2 | PREDICTED: similar to putative serine/threonine protein kinase MAK-V | *LOC630 567* | -1.62 | 0.01139 |
| 610746 | NM_0010 10937.1 | gap junction protein, beta 6, transcript variant 2 | *Gjb6* | -1.62 | 0.00670 |
| 6180619 | NM_0187 44.2 | sema domain, transmembrane domain (TM), and cytoplasmic domain, (semaphorin) 6A | *Sema6a* | -1.62 | 0.00388 |
| 4260433 | NM_0103 45 | growth factor receptor bound protein 10 | *Grb10* | -1.62 | 0.00454 |
| 7160543 | NM_0254 | coiled coil domain | *Ccdc28b* | -1.62 | 0.00695 |

| | | | | | |
|---|---|---|---|---|---|
| | 55.2 | containing 28B | | | |
| 4730148 | NM_028636.2 | mannosidase, alpha, class 2C, member 1 | *Man2c1* | -1.62 | 0.03515 |
| 3610465 | NM_178600.2 | vitamin K epoxide reductase complex, subunit 1 | *Vkorc1* | -1.62 | 0.01231 |
| 7510356 | NM_133748.1 | insulin induced gene 2 | *Insig2* | -1.62 | 0.02981 |
| 780292 | XR_031489.1 | PREDICTED: similar to chloride channel 5, misc RNA | *LOC100045272* | -1.62 | 0.00136 |
| 1050348 | NM_001037937.2 | DEP domain containing 6, transcript variant 2 | *Depdc6* | -1.63 | 0.00087 |
| 6840382 | NM_001077364.1 | TSC22 domain family, member 3, transcript variant 1 | *Tsc22d3* | -1.63 | 0.00069 |
| 6100523 | NM_010160.2 | CUG triplet repeat, RNA binding protein 2, transcript variant 6 | *Cugbp2* | -1.63 | 0.00204 |
| 5900577 | NM_013703.1 | very low density lipoprotein receptor | *Vldlr* | -1.63 | 0.00354 |
| 3850196 | NM_001081225.1 | family with sequence similarity 178, member A | *Fam178a* | -1.63 | 0.01106 |
| 2760343 | NM_019413.2 | roundabout homolog 1 (Drosophila) | *Robo1* | -1.63 | 0.00034 |
| 60670 | NM_026551.3 | dephospho-CoA kinase domain containing | *Dcakd* | -1.63 | 0.02783 |
| 2490593 | NM_001048267.1 | transportin 1, transcript variant 2 | *Tnpo1* | -1.63 | 0.02711 |
| 4280300 | NM_146061.4 | proline rich 5 (renal) | *Prr5* | -1.63 | 0.00114 |
| 4490730 | NM_178790.3 | ABI gene family, member 3 (NESH) binding protein, transcript variant 1 | *Abi3bp* | -1.63 | 0.01697 |
| 7050215 | XM_001478166.1 | PREDICTED: similar to LSM7 homolog, U6 small nuclear RNA associated | *LOC100041500* | -1.63 | 0.02791 |
| 5270082 | NM_017376.2 | thyrotroph embryonic factor, transcript variant 1 | *Tef* | -1.64 | 0.01227 |
| 380132 | NM_145447.2 | major facilitator superfamily domain containing 7C | *Mfsd7c* | -1.64 | 0.01531 |
| 2850575 | NM_011693.2 | vascular cell adhesion molecule 1 | *Vcam1* | -1.64 | 0.03029 |
| 1980446 | NM_023203.1 | RIKEN cDNA 2410015N17 gene | *2410015N17Rik* | -1.64 | 0.01874 |

| | | | | | |
|---|---|---|---|---|---|
| 4150367 | NM_021446.2 | RIKEN cDNA 0610007P14 gene | *0610007P14Rik* | -1.64 | 0.03262 |
| 6770497 | NM_010096.2 | early B-cell factor 3 | *Ebf3* | -1.64 | 0.00234 |
| 2060246 | NM_007570.2 | B-cell translocation gene 2, anti-proliferative | *Btg2* | -1.65 | 0.00168 |
| 6420253 | NM_025436.1 | sterol-C4-methyl oxidase-like | *Sc4mol* | -1.65 | 0.03727 |
| 5690475 | NM_026490.1 | mitochondrial ribosomal protein L19 | *Mrpl19* | -1.65 | 0.03509 |
| 1470731 | XM_130497.2 | ryanodine receptor 3 | *Ryr3* | -1.65 | 0.02108 |
| 7200348 | NM_009023.1 | receptor-associated protein of the synapse | *Rapsn* | -1.65 | 0.00277 |
| 5390128 | NM_010023.3 | dodecenoyl-Coenzyme A delta isomerase (3,2 trans-enoyl-Coenyme A isomerase), nuclear gene encoding mitochondrial protein | *Dci* | -1.65 | 0.00689 |
| 5050689 | XM_977814.1 | PREDICTED: similar to Probable ubiquitin carboxyl-terminal hydrolase FAF-X (Ubiquitin thiolesterase FAF-X) (Ubiquitin-specific-processing protease FAF-X) (Deubiquitinating enzyme FAF-X) (Fat facets protein-related, X-linked) (Ubiquitin-specific protease 9, X | *LOC665566* | -1.65 | 0.00003 |
| 6370181 | NM_023041.2 | peroxisome biogenesis factor 19 | *Pex19* | -1.65 | 0.01731 |
| 630717 | NM_133823.3 | methylmalonic aciduria (cobalamin deficiency) type A, nuclear gene encoding mitochondrial protein | *Mmaa* | -1.65 | 0.01102 |
| 5090133 | NM_007689.4 | chondroadherin | *Chad* | -1.65 | 0.02368 |
| 3800603 | NM_011395.2 | solute carrier family 22 (organic cation transporter), member 3 | *Slc22a3* | -1.65 | 0.01193 |
| 7610608 | NM_0010 | family with sequence | *Fam178* | -1.66 | 0.01593 |

| | | | | | |
|---|---|---|---|---|---|
| | 81225.1 | similarity 178, member A | *a* | | |
| 940678 | XM_3567 31.1 | | *LOC382 885* | -1.66 | 0.02191 |
| 2340066 | NM_1751 37.3 | valyl-tRNA synthetase 2, mitochondrial (putative) | *Vars2* | -1.66 | 0.03482 |
| 5900598 | NM_0158 19.3 | heparan sulfate 6-O-sulfotransferase 2, transcript variant 2 | *Hs6st2* | -1.66 | 0.00920 |
| 2260324 | NM_0195 10 | transient receptor potential cation channel, subfamily C, member 3 | *Trpc3* | -1.66 | 0.01891 |
| 5670424 | NM_0110 66.1 | period homolog 2 (Drosophila) | *Per2* | -1.67 | 0.00099 |
| 2570204 | NM_0213 39.1 | cell adhesion molecule-related/down-regulated by oncogenes | *Cdon* | -1.67 | 0.00392 |
| 7610703 | NM_1387 43.2 | RIKEN cDNA 1190017O12 gene | *1190017 O12Rik* | -1.67 | 0.01224 |
| 430170 | NM_0214 32.2 | nucleosome assembly protein 1-like 5 | *Nap1l5* | -1.67 | 0.00004 |
| 270129 | NM_0010 81256.1 | jumonji domain containing 1B | *Jmjd1b* | -1.67 | 0.00122 |
| 1570669 | NM_1456 26.1 | RIKEN cDNA 2610208M17 gene | *2610208 M17Rik* | -1.67 | 0.00446 |
| 2100253 | NM_1772 63.3 | zinc fingers and homeoboxes 3 | *Zhx3* | -1.67 | 0.00660 |
| 3370427 | XM_1370 17.3 | RIKEN cDNA 9330159F19 gene | *9330159 F19Rik* | -1.67 | 0.01330 |
| 10767 | NM_0261 67.3 | kelch-like 13 (Drosophila) | *Klhl13* | -1.68 | 0.03195 |
| 6840347 | NM_0259 31.2 | RAB, member of RAS oncogene family-like 4 | *Rabl4* | -1.68 | 0.00236 |
| 3120215 | NM_0139 05.3 | hairy/enhancer-of-split related with YRPW motif-like | *Heyl* | -1.68 | 0.02134 |
| 5820129 | NM_1814 04.5 | KN motif and ankyrin repeat domains 1 | *Kank1* | -1.68 | 0.00897 |
| 780491 | NM_0244 74.2 | EMI domain containing 2 | *Emid2* | -1.68 | 0.01876 |
| 2070025 | NM_0199 19.2 | latent transforming growth factor beta binding protein 1 (Ltbp1), transcript variant 1 | *Ltbp1* | -1.68 | 0.00014 |
| 4780113 | NM_0106 87.1 | like-glycosyltransferase | *Large* | -1.68 | 0.00943 |
| 5490561 | NM_0260 | solute carrier family 25 | *Slc25a1* | -1.68 | 0.03160 |

| | | | | | |
|---|---|---|---|---|---|
| | 71.2 | (mitochondrial thiamine pyrophosphate carrier), member 19, nuclear gene encoding mitochondrial protein | *9* | | |
| 5860609 | NM_134094.3 XM_921409 XM_921419 XM_921424 | neurocalcin delta | *Ncald* | -1.68 | 0.04757 |
| 4540450 | NM_010582.2 | inter-alpha trypsin inhibitor, heavy chain 2 | *Itih2* | -1.68 | 0.01748 |
| 4850338 | XM_130011.5 | ankyrin repeat domain 16 | *Ankrd16* | -1.69 | 0.00887 |
| 1740767 | XM_130951.1 | dolichyl-phosphate mannosyltransferase polypeptide 3 | *Dpm3* | -1.69 | 0.03456 |
| 670685 | NM_178615.3 | RGM domain family, member B | *Rgmb* | -1.70 | 0.00048 |
| 5700301 | NM_001025568.1 | phosphodiesterase 1C, transcript variant 2 | *Pde1c* | -1.70 | 0.01606 |
| 3390672 | NM_181048.2 | RIKEN cDNA A130010J15 gene | *A13001 0J15Rik* | -1.70 | 0.00026 |
| 2650301 | NM_013555.2 | homeo box D9 | *Hoxd9* | -1.70 | 0.02580 |
| 2970072 | NM_001025568.1 | phosphodiesterase 1C, transcript variant 2 | *Pde1c* | -1.70 | 0.02723 |
| 6550672 | NM_001014288.2 | protein tyrosine phosphatase, receptor type, D, transcript variant a | *Ptprd* | -1.70 | 0.02138 |
| 7160209 | NM_001033140.3 | RIKEN cDNA 0610010E21 gene | *0610010 E21Rik* | -1.70 | 0.00235 |
| 2120110 | NM_008502.1 | lethal giant larvae homolog 1 (Drosophila) | *Llgl1* | -1.70 | 0.00969 |
| 6180168 | NM_011581.1 | thrombospondin 2 | *Thbs2* | -1.71 | 0.01727 |
| 4540598 | NM_023395.1 | WAP four-disulfide core domain 1 | *Wfdc1* | -1.71 | 0.00296 |
| 5890338 | NM_181728.1 | ADP-ribosyltransferase 3 | *Art3* | -1.71 | 0.00005 |
| 4670280 | XM_147215.1 | zinc finger and BTB domain containing 20 | *Zbtb20* | -1.71 | 0.00255 |
| 1820296 | NM_025695.4 | structural maintenance of chromosomes 6 | *Smc6* | -1.71 | 0.00403 |
| 3400184 | NM_013543.1 | H2-K region expressed gene 6 | *H2-Ke6* | -1.72 | 0.01193 |
| 3120546 | NM_1753 | solute carrier organic | *Slco2b1* | -1.72 | 0.00078 |

| | | | | | |
|---|---|---|---|---|---|
| | 16.3 | anion transporter family, member 2b1 | | | |
| 3190364 | NM_015787.2 | histone cluster 1, H1e | *Hist1h1e* | -1.72 | 0.01394 |
| 6110053 | NM_026366.1 | N-6 adenine-specific DNA methyltransferase 1 (putative) | *N6amt1* | -1.72 | 0.00352 |
| 3390152 | NM_026894.1 | RIKEN cDNA 1500001M20 gene | *1500001M20Rik* | -1.72 | 0.02401 |
| 3520148 | NM_199195.1 | branched chain ketoacid dehydrogenase E1, beta polypeptide, nuclear gene encoding mitochondrial protein | *Bckdhb* | -1.72 | 0.00495 |
| 770086 | NM_025650.2 | ubiquinol-cytochrome c reductase (64kD) subunit | *Uqcr* | -1.73 | 0.01491 |
| 5340224 | NM_021463.3 | phosphoribosyl pyrophosphate synthetase 1 | *Prps1* | -1.73 | 0.01100 |
| 70414 | XM_486197 | zinc finger protein 266 | *Zfp266* | -1.73 | 0.00410 |
| 510280 | NM_007956.4 | estrogen receptor 1 (alpha) | *Esr1* | -1.73 | 0.02998 |
| 1990477 | NM_018744.2 | sema domain, transmembrane domain (TM), and cytoplasmic domain, (semaphorin) 6A | *Sema6a* | -1.73 | 0.00233 |
| 5360300 | NM_008509.2 | lipoprotein lipase | *Lpl* | -1.73 | 0.01084 |
| 1980427 | NM_008882.2 | plexin A2 | *Plxna2* | -1.73 | 0.01849 |
| 5080279 | NM_023245.2 | Palmdelphin | *Palmd* | -1.73 | 0.01956 |
| 4490192 | NM_198619.2 | RIKEN cDNA 2810408P10 gene | *2810408P10Rik* | -1.73 | 0.00069 |
| 5910241 | NM_008817.2 | paternally expressed 3 | *Peg3* | -1.73 | 0.00425 |
| 1740521 | XM_357880 | claudin 22 | *Cldn22* | -1.73 | 0.00404 |
| 6520164 | NM_020510.2 | frizzled homolog 2 (Drosophila) | *Fzd2* | -1.73 | 0.00431 |
| 3610768 | NM_013792.1 | alpha-N-acetylglucosaminidase (Sanfilippo disease IIIB) | *Naglu* | -1.74 | 0.03386 |
| 2360519 | NM_013690.2 | endothelial-specific receptor tyrosine kinase | *Tek* | -1.74 | 0.04265 |

| | | | | | |
|---|---|---|---|---|---|
| 380397 | XM_001476775.1 | PREDICTED: hypothetical protein LOC100046690 | *LOC100046690* | -1.74 | 0.00056 |
| 4920647 | NM_026054.2 | RIKEN cDNA 2810474O19 gene | *2810474O19Rik* | -1.75 | 0.01557 |
| 7550445 | NM_025988.2 | acyl-Coenzyme A binding domain containing 4, transcript variant 1 | *Acbd4* | -1.75 | 0.01080 |
| 6520446 | XM_126043.3 | H2A histone family, member V | *H2afv* | -1.75 | 0.01775 |
| 360053 | NM_001003948.1 | RIKEN cDNA 5033414K04 gene | *5033414K04Rik* | -1.75 | 0.03167 |
| 4280113 | NM_133952.2 | unc-45 homolog A (C. elegans) | *Unc45a* | -1.75 | 0.04335 |
| 580463 | NM_001081225.1 | family with sequence similarity 178, member A | *Fam178a* | -1.76 | 0.01113 |
| 6280474 | NM_026324.2 | kin of IRRE like 3 (Drosophila) XM_922973 XM_922987 XM_922995 XM_923006 XM_923014 | *Kirrel3* | -1.76 | 0.00136 |
| 4570070 | NM_011915.1 | Wnt inhibitory factor 1 | *Wif1* | -1.76 | 0.02705 |
| 1740139 | NM_172428.2 | coiled-coil domain containing 134 | *Ccdc134* | -1.76 | 0.00977 |
| 4610431 | NM_021324.4 | tweety homolog 1 (Drosophila), transcript variant 2 | *Ttyh1* | -1.76 | 0.02031 |
| 630053 | NM_010058.1 | dystrophia myotonica-containing WD repeat motif | *Dmwd* | -1.76 | 0.03221 |
| 4060075 | NM_008687.2 | nuclear factor I/B | *Nfib* | -1.76 | 0.00030 |
| 1090142 | NM_009672.2 | acidic (leucine-rich) nuclear phosphoprotein 32 family, member A | *Anp32a* | -1.77 | 0.02148 |
| 150544 | NM_013468.2 | ankyrin repeat domain 1 (cardiac muscle) | *Ankrd1* | -1.77 | 0.02922 |
| 4260661 | XM_001476559.1 | PREDICTED: similar to sprouty 1, transcript variant 1 | *LOC100046643* | -1.77 | 0.00032 |
| 4640446 | NM_010231.2 | flavin containing monooxygenase 1 | *Fmo1* | -1.77 | 0.00942 |
| 6130014 | NM_027711.1 | IQ motif containing GTPase activating protein 2 | *Iqgap2* | -1.77 | 0.00033 |
| 6550309 | NM_0220 | FXYD domain-containing | *Fxyd6* | -1.78 | 0.00378 |

| | | | | | |
|---|---|---|---|---|---|
| | 04.6 | ion transport regulator 6 | | | |
| 2450500 | NM_028199.2 | plexin domain containing 1 | *Plxdc1* | -1.78 | 0.01948 |
| 6580563 | NM_023041.2 | peroxisome biogenesis factor 19 | *Pex19* | -1.78 | 0.00199 |
| 5900368 | NM_153581.2 | glycoprotein m6a | *Gpm6a* | -1.78 | 0.02432 |
| 2030239 | AK082711 | sema domain, transmembrane domain (TM), and cytoplasmic domain, (semaphorin) 6A | *Sema6a* | -1.79 | 0.00044 |
| 1190537 | AK035513 | PDZ and LIM domain 4 | *Pdlim4* | -1.79 | 0.01563 |
| 3370279 | NM_175553 | nuclear factor I/B | *Nfib* | -1.79 | 0.03255 |
| 1400053 | XM_001479138.1 | PREDICTED: similar to apolipoprotein D | *LOC100047583* | -1.79 | 0.00227 |
| 1240095 | NM_029394.3 | sorting nexing 24 | *Snx24* | -1.79 | 0.01586 |
| 7160070 | NM_172286 | RIKEN cDNA 6430548M08 gene | *6430548M08Rik* | -1.79 | 0.00383 |
| 6770184 | NM_008067.3 | gamma-aminobutyric acid (GABA-A) receptor, subunit alpha 3 | *Gabra3* | -1.79 | 0.00070 |
| 2450220 | NM_031394.1 | synaptotagmin-like 2 | *Sytl2* | -1.80 | 0.02671 |
| 3140164 | NM_013456.1 | actinin alpha 3 | *Actn3* | -1.80 | 0.00919 |
| 6040379 | NM_001025373.1 | RIKEN cDNA 4930432O21 gene | *4930432O21Rik* | -1.80 | 0.03469 |
| 1710477 | NM_011769.3 | zinc finger, imprinted 1 | *Zim1* | -1.80 | 0.03068 |
| 2690446 | NM_144882.3 | RIKEN cDNA 2810022L02 gene | *2810022L02Rik* | -1.81 | 0.00083 |
| 450300 | XM_001472574.1 | PREDICTED: similar to Nuclear receptor coactivator 1 (NCoA-1) (Steroid receptor coactivator 1) (SRC-1) (Nuclear receptor coactivator protein 1) (mNRC-1) | *LOC100044566* | -1.81 | 0.00360 |
| 1300274 | NM_010222.1 | FK506 binding protein 7 | *Fkbp7* | -1.81 | 0.00069 |
| 3890273 | NM_022318.2 | popeye domain containing 2, transcript variant 2 | *Popdc2* | -1.81 | 0.00456 |

| | | | | | |
|---|---|---|---|---|---|
| 2320189 | NM_022000.2 | GNAS (guanine nucleotide binding protein, alpha stimulating) complex locus, transcript variant 3 | *Gnas* | -1.81 | 0.00273 |
| 6960180 | NM_024220.1 | NADH dehydrogenase (ubiquinone) 1, subcomplex unknown, 2 | *Ndufc2* | -1.81 | 0.01542 |
| 540138 | NM_001081005.1 | RIKEN cDNA 1500012F01 gene | *1500012F01Rik* | -1.81 | 0.04933 |
| 1500524 | NM_019919 | latent transforming growth factor beta binding protein 1 | *Ltbp1* | -1.81 | 0.00811 |
| 6380370 | NM_009088.2 | polymerase (RNA) I polypeptide A | *Polr1a* | -1.82 | 0.03416 |
| 4570376 | NM_173395.2 | family with sequence similarity 132, member B | *Fam132b* | -1.82 | 0.00447 |
| 2340608 | NM_019823.3 | cytochrome P450, family 2, subfamily d, polypeptide 22 | *Cyp2d22* | -1.82 | 0.00053 |
| 5870601 | NM_001014288.2 | protein tyrosine phosphatase, receptor type, D, transcript variant a | *Ptprd* | -1.82 | 0.00037 |
| 2360685 | NM_001025568.1 | phosphodiesterase 1C, transcript variant 2 | *Pde1c* | -1.82 | 0.00582 |
| 1850327 | NM_026063.1 | RIKEN cDNA 2900010M23 gene | *2900010M23Rik* | -1.82 | 0.04885 |
| 3850039 | NM_172993.1 | zinc finger protein 512 | *Zfp512* | -1.82 | 0.04576 |
| 2000647 | NM_010512.3 | insulin-like growth factor 1, transcript variant 1 | *Igf1* | -1.82 | 0.01083 |
| 6590451 | NM_172274.1 | coiled-coil and C2 domain containing 2A | *Cc2d2a* | -1.82 | 0.00961 |
| 1660358 | NM_144804.1 | DEP domain containing 7 | *Depdc7* | -1.83 | 0.02014 |
| 610392 | NM_025366.2 | coiled-coil-helix-coiled-coil-helix domain containing 1 | *Chchd1* | -1.83 | 0.00177 |
| 160392 | NM_009911.2 | chemokine (C-X-C motif) receptor 4 (Cxcr4) | *Cxcr4* | -1.84 | 0.01839 |
| 6220360 | NM_008771.2 | purinergic receptor P2X, ligand-gated ion channel, 1 | *P2rx1* | -1.84 | 0.02066 |
| 4860577 | NM_013456.1 | actinin alpha 3 | *Actn3* | -1.84 | 0.03920 |

| | | | | | |
|---|---|---|---|---|---|
| 6220612 | NM_177583.4 | anterior pharynx defective 1b homolog (C elegans) | *Aph1b* | -1.84 | 0.00970 |
| 780356 | NM_007504.2 | ATPase, Ca++ transporting, cardiac muscle, fast twitch 1 | *Atp2a1* | -1.84 | 0.00193 |
| 5090348 | XM_907370.3 | PREDICTED: collagen, type XXII, alpha 1, transcript variant 3 | *Col22a1* | -1.85 | 0.00406 |
| 3170196 | XM_354921.1 | nuclear receptor binding protein 2 | *Nrbp2* | -1.85 | 0.01220 |
| 2650685 | XR_002058.1 | PREDICTED: predicted gene, EG667190, misc RNA | *EG667190* | -1.85 | 0.01455 |
| 1850161 | NM_183100.1 | RIKEN cDNA 5430414B19 gene | *5430414B19Rik* | -1.85 | 0.00279 |
| 1400747 | NM_144854.1 | open reading frame 63 | *ORF63* | -1.86 | 0.01677 |
| 2450523 | NM_207655.2 | epidermal growth factor receptor | *Egfr* | -1.87 | 0.00022 |
| 650280 | NM_011380.1 | sine oculis-related homeobox 2 homolog (Drosophila) | *Six2* | -1.87 | 0.02175 |
| 830524 | NM_027560.1 | arrestin domain containing 2 | *Arrdc2* | -1.87 | 0.00258 |
| 5670735 | NM_175418.3 | RIKEN cDNA 8030451F13 gene | *8030451F13Rik* | -1.88 | 0.00288 |
| 270139 | NM_010818.3 | CD200 antigen | *Cd200* | -1.88 | 0.00370 |
| 450537 | NM_008760.4 | osteoglycin | *Ogn* | -1.88 | 0.00215 |
| 4230086 | NM_026721.2 | solute carrier family 39 (metal ion transporter), member 13 | *Slc39a13* | -1.89 | 0.00416 |
| 7380450 | NM_133738.1 | anthrax toxin receptor 2 | *Antxr2* | -1.89 | 0.00161 |
| 7320053 | NM_008161.2 | glutathione peroxidase 3, transcript variant 2 | *Gpx3* | -1.89 | 0.01050 |
| 3990053 | NM_010169.3 | coagulation factor II (thrombin) receptor | *F2r* | -1.90 | 0.00124 |
| 3310338 | NM_026828.2 | DNA segment, Chr 2, Brigham & Women's Genetics 1335 expressed | *D2Bwg1335e* | -1.90 | 0.00508 |
| 4540669 | NM_008263.1 | homeo box A10 | *Hoxa10* | -1.90 | 0.00129 |
| 7320551 | NM_178615.3 | RGM domain family, member B | *Rgmb* | -1.90 | 0.00319 |

| | | | | | |
|---|---|---|---|---|---|
| 870279 | NM_022021.1 | CDK5 and Abl enzyme substrate 1 | *Cables1* | -1.90 | 0.00058 |
| 6560022 | NM_173419.1 | deleted in lymphocytic leukemia, 7 | *Dleu7* | -1.90 | 0.01744 |
| 540202 | NM_009441.1 | tetratricopeptide repeat domain 3 | *Ttc3* | -1.90 | 0.00184 |
| 2060142 | NM_027711.1 | IQ motif containing GTPase activating protein 2 | *Iqgap2* | -1.91 | 0.04146 |
| 4290343 | NM_001033355.2 XM_899378 XM_899382 XM_899389 XM_899395 | zinc finger protein 568 | *Zfp568* | -1.91 | 0.00079 |
| 3850438 | NM_009928.3 | collagen, type XV, alpha 1 | *Col15a1* | -1.91 | 0.00472 |
| 3120014 | NM_008416.1 | Jun-B oncogene | *Junb* | -1.92 | 0.00488 |
| 2750035 | NM_007643.3 | CD36 antigen | *Cd36* | -1.92 | 0.00074 |
| 1090576 | NM_010078.2 | dystrophin related protein 2 | *Drp2* | -1.92 | 0.00563 |
| 1300300 | NM_172442.2 | deltex 4 homolog (Drosophila) XM_001000490 | *Dtx4* | -1.92 | 0.02203 |
| 4060626 | XM_001474897.1 | PREDICTED: TRAF2 and NCK interacting kinase, transcript variant 1 | *Tnik* | -1.93 | 0.00134 |
| 5910750 | NM_001040682.1 | calmin, transcript variant 2 | *Clmn* | -1.93 | 0.00097 |
| 1440300 | NM_023245.3 | palmdelphin | *Palmd* | -1.94 | 0.02288 |
| 2480050 | NM_053155.1 | calmin (calponin-like, transmembrane) | *Clmn* | -1.95 | 0.00004 |
| 7040044 | NM_133977.2 | transferrin | *Trf* | -1.95 | 0.00002 |
| 2100689 | NM_019449.1 | unc-93 homolog B1 (C elegans) | *Unc93b1* | -1.95 | 0.00047 |
| 1440204 | | RIKEN cDNA 6330509M05 gene | *6330509M05Rik* | -1.96 | 0.01886 |
| 1660187 | NM_007554.2 | bone morphogenetic protein 4 | *Bmp4* | -1.96 | 0.00006 |
| 4070746 | NM_183285.2 | potassium channel tetramerisation domain containing 2 | *Kctd2* | -1.96 | 0.00533 |
| 5390524 | NM_001083809.1 | solute carrier family 43, member 1, transcript variant 3 | *Slc43a1* | -1.96 | 0.00003 |

| | | | | | |
|---|---|---|---|---|---|
| 4560603 | NM_021567.2 | poly(rC) binding protein 4 | *Pcbp4* | -1.97 | 0.00813 |
| 4290424 | NM_001017983.1 | FAD-dependent oxidoreductase domain containing 2 | *Foxred2* | -1.97 | 0.00031 |
| 6840707 | NM_001039122.1 | defensin beta 25 | *Defb25* | -1.98 | 0.00082 |
| 4390538 | NM_008409.2 | integral membrane protein 2A | *Itm2a* | -1.99 | 0.00778 |
| 7380524 | NM_054077.3 | proline arginine-rich end leucine-rich repeat | *Prelp* | -1.99 | 0.00109 |
| 5270307 | NM_133709.2 | chordin-like 2 | *Chrdl2* | -1.99 | 0.00660 |
| 2190056 | NM_175088.3 | MyoD family inhibitor domain containing | *Mdfic* | -1.99 | 0.01071 |
| 2510390 | NM_173011.1 | isocitrate dehydrogenase 2 (NADP+), mitochondrial, nuclear gene encoding mitochondrial protein | *Idh2* | -2.00 | 0.01379 |
| 4290544 | NM_173437.1 | neuron navigator 1 | *Nav1* | -2.00 | 0.00109 |
| 7210687 | NM_009696.2 | apolipoprotein E | *Apoe* | -2.01 | 0.02223 |
| 5820470 | NM_013875.2 | phosphodiesterase 7B | *Pde7b* | -2.01 | 0.00225 |
| 7160343 | NM_001077510.1 | GNAS (guanine nucleotide binding protein, alpha stimulating) complex locus, transcript variant 8 | *Gnas* | -2.02 | 0.00048 |
| 7380603 | NM_008344.2 | insulin-like growth factor binding protein 6 | *Igfbp6* | -2.02 | 0.01892 |
| 1300630 | AK021409.1 | matrix-remodelling associated 7 | *Mxra7* | -2.02 | 0.00090 |
| 240433 | NM_027208.1 | 3-hydroxybutyrate dehydrogenase, type 2 | *Bdh2* | -2.02 | 0.01973 |
| 5960228 | NM_028001.2 | junctional sarcoplasmic reticulum protein 1 | *Jsrp1* | -2.02 | 0.00204 |
| 2070376 | NM_133213.2 | X-prolyl aminopeptidase (aminopeptidase P) 2, membrane-bound, transcript variant 1 | *Xpnpep2* | -2.03 | 0.00153 |
| 7570537 | NM_008505.3 | LIM domain only 2 | *Lmo2* | -2.04 | 0.00693 |
| 2480546 | NM_008011.2 | fibroblast growth factor receptor 4 | *Fgfr4* | -2.05 | 0.00799 |

| | | | | | |
|---|---|---|---|---|---|
| 4860753 | NM_026358.2 | RIKEN cDNA 4930583H14 gene | *4930583H14Rik* | -2.05 | 0.00214 |
| 610491 | NM_029758.3 | DNA segment, Chr 12, ERATO Doi 553, expressed | *D12Ertd553e* | -2.05 | 0.03395 |
| 4880537 | NM_025347.1 | yippee-like 3 (Drosophila) | *Ypel3* | -2.05 | 0.00111 |
| 3890066 | NM_026840.2 | platelet-derived growth factor receptor-like (Pdgfrl) | *Pdgfrl* | -2.07 | 0.00431 |
| 2760411 | NM_010450.2 | homeo box A11 | *Hoxa11* | -2.07 | 0.00257 |
| 4070706 | NM_011056.2 | phosphodiesterase 4D, cAMP specific | *Pde4d* | -2.07 | 0.00100 |
| 630215 | NM_019727.2 | sorting nexin 1 | *Snx1* | -2.07 | 0.02546 |
| 4850731 | NM_173437.1 | neuron navigator 1 | *Nav1* | -2.07 | 0.00050 |
| 6520324 | NM_172778.1 | monoamine oxidase B, nuclear gene encoding mitochondrial protein | *Maob* | -2.08 | 0.00108 |
| 2680463 | NM_011054 | phosphodiesterase 1C | *Pde1c* | -2.08 | 0.00748 |
| 5090343 | NM_021455.3 | MLX interacting protein-like | *Mlxipl* | -2.08 | 0.00004 |
| 6760445 | XM_131572.4 | eukaryotic translation initiation factor 2B, subunit 3 | *Eif2b3* | -2.09 | 0.02980 |
| 3180543 | NM_138741.1 | serum deprivation response | *Sdpr* | -2.09 | 0.00002 |
| 1740541 | NM_153534.2 | adenylate cyclase 2 | *Adcy2* | -2.09 | 0.00144 |
| 1070010 | NM_030180.2 | ubiquitin specific peptidase 54 | *Usp54* | -2.09 | 0.02471 |
| 6020609 | NM_001013370.1 | sestrin 1 | *Sesn1* | -2.09 | 0.01405 |
| 7570598 | NM_010423.2 | hairy/enhancer-of-split related with YRPW motif 1 | *Hey1* | -2.10 | 0.00820 |
| 1050259 | NM_001040397.1 | RIKEN cDNA 4631422O05 gene | *4631422O05Rik* | -2.10 | 0.00043 |
| 2750196 | NM_177159.3 | RIKEN cDNA 9530091C08 gene | *9530091C08Rik* | -2.10 | 0.00016 |
| 2490575 | NM_011340.3 | serine (or cysteine) peptidase inhibitor, clade F, member 1 | *Serpinf1* | -2.10 | 0.04190 |

| | | | | | |
|---|---|---|---|---|---|
| 4040088 | NM_025355.2 | transcription elongation factor A (SII)-like 6 | *Tceal6* | -2.11 | 0.00415 |
| 2360594 | XM_906862.3 | PREDICTED: similar to PNG protein | *LOC632667* | -2.11 | 0.00600 |
| 2900132 | XM_001476775.1 | PREDICTED: hypothetical protein LOC100046690 | *LOC100046690* | -2.11 | 0.03232 |
| 2260402 | NM_008889.1 | protein phosphatase 1, regulatory (inhibitor) subunit 14B | *Ppp1r14b* | -2.12 | 0.01872 |
| 6550470 | NM_029270.1 | Rho GTPase activating protein 24, transcript variant 1 | *Arhgap24* | -2.12 | 0.00998 |
| 6270521 | NM_001081445.1 | neural cell adhesion molecule 1, transcript variant 1 | *Ncam1* | -2.12 | 0.00199 |
| 7100561 | NM_018780.2 | secreted frizzled-related sequence protein 5 | *Sfrp5* | -2.12 | 0.02934 |
| 2230324 | NM_025514.2 | DNA segment, Chr 10, ERATO Doi 641, expressed | *D10Ertd641e* | -2.12 | 0.00042 |
| 770441 | NM_008760.2 | osteoglycin | *Ogn* | -2.14 | 0.00281 |
| 7400441 | NM_153786.1 | vestigial like 2 homolog (Drosophila) | *Vgll2* | -2.15 | 0.00293 |
| 2030168 | NR_002452.1 | non-coding transcript 1, non-coding RNA | *Nctc1* | -2.15 | 0.00059 |
| 5670612 | NM_177649.3 | cDNA sequence BC034076 | *BC034076* | -2.15 | 0.00032 |
| 2650019 | NM_027519.3 | RIKEN cDNA 6330406I15 gene | *6330406I15Rik* | -2.15 | 0.00072 |
| 1190202 | NM_133859.2 | olfactomedin-like 3 | *Olfml3* | -2.16 | 0.00161 |
| 840209 | NM_027519.1 | RIKEN cDNA 6330406I15 gene | *6330406I15Rik* | -2.16 | 0.00159 |
| 5310497 | NM_011858.3 | odd Oz/ten-m homolog 4 (Drosophila) | *Odz4* | -2.16 | 0.00402 |
| 3370482 | NM_009023.2 | receptor-associated protein of the synapse | *Rapsn* | -2.17 | 0.00225 |
| 3870072 | NM_008610.2 | matrix metallopeptidase 2 | *Mmp2* | -2.17 | 0.00945 |
| 7400463 | NM_010865.2 | myocilin | *Myoc* | -2.17 | 0.00220 |
| 7560543 | NM_010456.2 | homeo box A9 | *Hoxa9* | -2.18 | 0.00028 |
| 6180148 | NM_181076 | tetratricopeptide repeat, | *Tanc2* | -2.18 | 0.00020 |

| | | | | | |
|---|---|---|---|---|---|
| | 71.3 | ankyrin repeat and coiled-coil containing 2 XM_001000900 XM_001000913 XM_001000922 XM_001004226 XM_001004229 XM_001004235 XM_001004240 XM_903099 XM_903101 XM_903102 XM_911892 XM_922187 XM_922195 XM_922205 XM_922212 XM_922217 XM_922223 XM_984944 | | | |
| 2940615 | NM_019417.2 | PDZ and LIM domain 4 | *Pdlim4* | -2.18 | 0.00199 |
| 780520 | XM_357585.1 | | *LOC384338* | -2.19 | 0.01514 |
| 4120300 | NM_001001979.1 | multiple EGF-like-domains 10 | *Megf10* | -2.20 | 0.00643 |
| 4560634 | NM_023326.2 | brain expressed myelocytomatosis oncogene | *Bmyc* | -2.20 | 0.00044 |
| 7040243 | NM_053078.3 | DNA segment, human D4S114 | *D0H4S114* | -2.21 | 0.00000 |
| 450632 | NM_010512.3 | insulin-like growth factor 1, transcript variant 1 | *Igf1* | -2.22 | 0.01042 |
| 5270450 | NC_000068.7 | GNAS (guanine nucleotide binding protein, alpha stimulating) complex locus | *Gnas* | -2.23 | 0.00196 |
| 1500328 | NM_010456.1 | homeobox A9 | *Hoxa9* | -2.23 | 0.00031 |
| 580433 | NM_008276.2 | homeo box D8 | *Hoxd8* | -2.25 | 0.00055 |
| 3290523 | NM_019521.2 | growth arrest specific 6 | *Gas6* | -2.27 | 0.00491 |
| 670554 | NM_009601.3 | cholinergic receptor, nicotinic, beta polypeptide 1 (muscle) | *Chrnb1* | -2.27 | 0.00000 |
| 5810021 | AK040711 | cell adhesion molecule-related/down-regulated by oncogenes | *Cdon* | -2.28 | 0.01878 |
| 1450364 | NM_009189.1 | sine oculis-related homeobox 1 homolog | *Six1* | -2.28 | 0.03880 |

| | | | | | |
|---|---|---|---|---|---|
| | | (Drosophila) | | | |
| 6520451 | NM_0010 39554.1 | angiopoietin-like 7 | *Angptl7* | -2.28 | 0.01370 |
| 3140576 | NM_0301 80.2 | ubiquitin specific peptidase 54 | *Usp54* | -2.30 | 0.00098 |
| 1110301 | NM_0113 75.2 | ST3 beta-galactoside alpha-2,3-sialyltransferase 5, transcript variant 2 | *St3gal5* | -2.31 | 0.04825 |
| 3890332 | NM_0078 36.1 | growth arrest and DNA-damage-inducible 45 alpha | *Gadd45a* | -2.33 | 0.00061 |
| 430037 | NM_0279 50.1 | oxidative stress induced growth inhibitor 1 | *Osgin1* | -2.33 | 0.00413 |
| 3890176 | NM_1751 50.3 | thioredoxin domain containing 15 | *Txndc15* | -2.33 | 0.02004 |
| 7400037 | AK04982 6 | expressed sequence AU015687 | *Au015687* | -2.34 | 0.00101 |
| 4640239 | NM_0090 79.2 | ribosomal protein L22 | *Rpl22* | -2.34 | 0.02518 |
| 6060523 | NM_0136 48.5 | reticulon 2 (Z-band associated protein), transcript variant B | *Rtn2* | -2.35 | 0.00612 |
| 3710167 | NM_0158 19.3 | heparan sulfate 6-O-sulfotransferase 2, transcript variant 2 | *Hs6st2* | -2.37 | 0.00051 |
| 4810735 | NM_0104 62.2 | homeo box C10 | *Hoxc10* | -2.38 | 0.00046 |
| 5720112 | NM_0104 55.2 | homeo box A7 | *Hoxa7* | -2.38 | 0.00077 |
| 580609 | NM_0078 36.1 | growth arrest and DNA-damage-inducible 45 alpha | *Gadd45a* | -2.39 | 0.00415 |
| 160402 | NM_0087 60.2 | osteoglycin | *Ogn* | -2.39 | 0.00143 |
| 4280184 | NM_1770 23.2 | RIKEN cDNA E130114P18 gene | *E13011 4P18Rik* | -2.39 | 0.00953 |
| 3800348 | NM_0075 56.2 | bone morphogenetic protein 6 | *Bmp6* | -2.40 | 0.00095 |
| 6770438 | NM_0075 88 | calcitonin receptor | *Calcr* | -2.41 | 0.00133 |
| 6060546 | NM_0302 29.4 | polymerase (RNA) III (DNA directed) polypeptide H | *Polr3h* | -2.41 | 0.01793 |
| 6290278 | NM_1770 13.3 | RIKEN cDNA 6332401O19 gene | *6332401 O19Rik* | -2.42 | 0.00236 |
| 4290722 | NM_1454 | integrin, beta-like 1 | *Itgbl1* | -2.46 | 0.01051 |

| | | | | | |
|---|---|---|---|---|---|
| | 67 | | | | |
| 4390288 | NM_0102 53.3 | galanin | *Gal* | -2.46 | 0.00560 |
| 6290471 | NM_0079 56.4 | estrogen receptor 1 (alpha) | *Esr1* | -2.48 | 0.02200 |
| 3710168 | NM_0110 39.2 | paired box gene 7 | *Pax7* | -2.48 | 0.00144 |
| 6280010 | | RIKEN cDNA 5730409N16 gene | *5730409 N16Rik* | -2.48 | 0.00343 |
| 4290521 | NM_0231 25.2 | kininogen 1 | *Kng1* | -2.54 | 0.00173 |
| 130102 | NM_1724 42.2 | deltex 4 homolog (Drosophila) | *Dtx4* | -2.58 | 0.00431 |
| 4480373 | XM_001000490 NM_0010 01979.1 | multiple EGF-like-domains 10 | *Megf10* | -2.59 | 0.02118 |
| 2100162 | XM_1315 38.1 | 24-dehydrocholesterol reductase | *Dhcr24* | -2.64 | 0.00568 |
| 4250228 | NM_0532 72.2 | 24-dehydrocholesterol reductase | *Dhcr24* | -2.65 | 0.00337 |
| 20360 | AK03559 1 | | *9530073 A13Rik* | -2.66 | 0.00128 |
| 6560382 | NM_0532 72.2 | 24-dehydrocholesterol reductase | *Dhcr24* | -2.66 | 0.00294 |
| 2260561 | NM_0235 23.4 | peroxisomal trans-2-enoyl-CoA reductase | *Pecr* | -2.68 | 0.01641 |
| 4060100 | NM_0294 15.2 | solute carrier family 10 (sodium/bile acid cotransporter family), member 6 | *Slc10a6* | -2.76 | 0.00219 |
| 780253 | NM_0294 15.1 | solute carrier family 10 (sodium/bile acid cotransporter family), member 6 | *Slc10a6* | -2.77 | 0.00917 |
| 3450626 | NM_0109 33.4 | natriuretic peptide precursor type C | *Nppc* | -2.79 | 0.00011 |
| 4670082 | NM_1332 29.1 | Down syndrome critical region homolog 6 (human) | *Dscr6* | -2.87 | 0.00640 |
| 3140706 | NM_0089 37.2 | prospero-related homeobox 1 | *Prox1* | -2.90 | 0.00008 |
| 7000687 | NM_0010 17983.2 | FAD-dependent oxidoreductase domain containing 2 | *Foxred2* | -2.91 | 0.00015 |
| 5700044 | NM_0075 54.2 | bone morphogenetic protein 4 | *Bmp4* | -2.92 | 0.00509 |

| | | | | | |
|---|---|---|---|---|---|
| 6590630 | NM_175271.2 | G protein-coupled receptor 23 | *Gpr23* | -2.93 | 0.00006 |
| 6200689 | NM_153786.1 | vestigial like 2 homolog (Drosophila) | *Vgll2* | -2.93 | 0.00166 |
| 7650370 | NM_007662.2 | cadherin 15 | *Cdh15* | -2.95 | 0.00245 |
| 3800139 | NM_145467.1 | integrin, beta-like 1 | *Itgbl1* | -2.97 | 0.01802 |
| 4810358 | NM_010286.3 | TSC22 domain family, member 3, transcript variant 2 | *Tsc22d3* | -2.98 | 0.00052 |
| 1110154 | NM_008656.4 | myogenic factor 5 | *Myf5* | -3.00 | 0.00274 |
| 780546 | NM_030127.1 | HtrA serine peptidase 3 | *Htra3* | -3.08 | 0.00346 |
| 7320739 | NM_175271 | lysophosphatidic acid receptor 4 | *Gpr23* | -3.08 | 0.00014 |
| 2100053 | NM_011582.2 | thrombospondin 4 | *Thbs4* | -3.08 | 0.00355 |
| 5820725 | XM_907184.2 | PREDICTED: RIKEN cDNA 2310015B20 gene | *2310015 B20Rik* | -3.09 | 0.00340 |
| 830170 | NM_008086.1 | growth arrest specific 1 | *Gas1* | -3.24 | 0.00006 |
| 6280672 | NM_015750.2 | neuraminidase 2 | *Neu2* | -3.32 | 0.00649 |
| 4540528 | AK076523 | Chondrolectin | *Chodl* | -3.42 | 0.00005 |
| 3780450 | NM_018827.2 | cytokine receptor-like factor 1 | *Crlf1* | -3.56 | 0.00004 |
| 3850301 | NM_139134.3 | chondrolectin | *Chodl* | -3.63 | 0.00029 |
| 4900242 | NM_016685.1 | cartilage oligomeric matrix protein | *Comp* | -3.86 | 0.01784 |
| 6270192 | NM_001033356.2 | gene model 484, (NCBI) | *Gm484* | -3.94 | 0.00813 |
| 6110520 | NM_021355.3 | fibromodulin | *Fmod* | -4.16 | 0.00210 |
| 6620435 | NM_010691.2 | ladybird homeobox homolog 1 (Drosophila) (Lbx1h) | *Lbx1h* | -4.27 | 0.00058 |
| 5080358 | NM_021355.2 | fibromodulin (Fmod) | *Fmod* | -4.37 | 0.00355 |
| 4570564 | NM_008438.1 | keratocan (Holland et al.) | *Kera* | -4.44 | 0.00145 |
| 4570196 | NM_008288.1 | hydroxysteroid (11-beta) dehydrogenase 1 | *Hsd11b 1* | -4.48 | 0.00027 |

| | | | | | |
|---|---|---|---|---|---|
| | | (Hsd11b1) | | | |
| 2340301 | NM_0082 88.1 | hydroxysteroid (11-beta) dehydrogenase 1 (Hsd11b1) | *Hsd11b 1* | -4.63 | 0.00055 |
| 5700189 | NM_1729 28.3 | doublecortin-like kinase 3 | *Dclk3* | -4.70 | 0.00013 |
| 4730551 | NM_0104 62.2 | homeo box C10 | *Hoxc10* | -4.98 | 0.00000 |
| 5550343 | NM_0104 65.2 | homeo box C6 | *Hoxc6* | -5.33 | 0.00001 |
| 4050369 | NM_0082 88.2 | hydroxysteroid 11-beta dehydrogenase 1, transcript variant 1 | *Hsd11b 1* | -5.47 | 0.00064 |
| 7380215 | NM_0101 33 | engrailed homeobox 1 | *En1* | -7.28 | 0.00001 |
| 3400368 | NM_0082 72.3 | homeo box C9 | *Hoxc9* | -7.49 | 0.00000 |